

AD-A140 797

ENGINEERING AND TECHNICAL SERVICES TO IMPROVE
RELIABILITY AND MAINTAINABILITY (U) OHIO UNIV ATHENS
AVIONICS ENGINEERING CENTER J D LONGWORTH ET AL

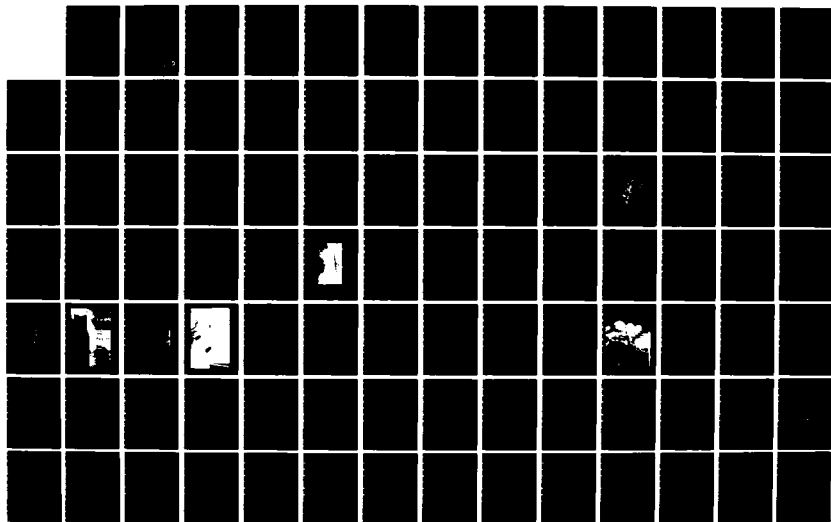
1/4

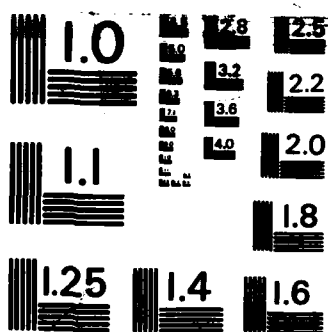
UNCLASSIFIED

JAN 83 OU/REC/EER-62-1 DOT/FAA/PM-84/7

F/G 17/7

NL





MICROCOPY RESOLUTION TEST CHART
NATIONAL BUREAU OF STANDARDS-1963-A

DOT/FAA/PM-84/7

Program Engineering &
Maintenance Service
Washington, D.C. 20591

Engineering and Technical Services to Improve Reliability and Maintainability of Instrument Landing System Components

Avionics Engineering Center
Department of Electrical and Computer Engineering
Ohio University
Athens, OH 45701

AD-A140 797

DTIC FILE COPY

January 1983

Final Report

This document is available to the U.S. public
through the National Technical Information
Service, Springfield, Virginia 22161.

DTIC
ELECTE
MAY 04 1984
S E D



US Department of Transportation
Federal Aviation Administration

84 05 04 002

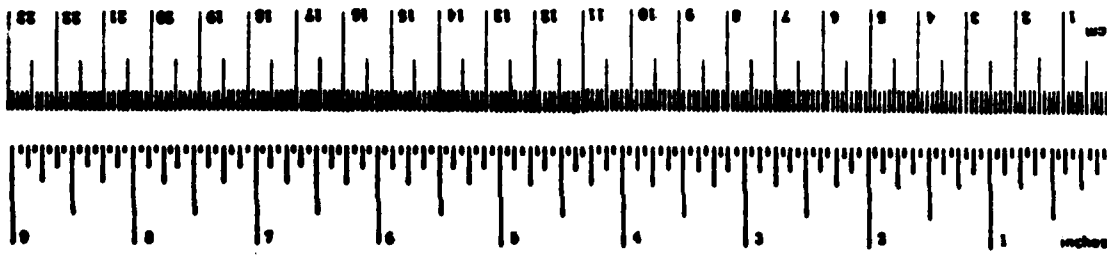
NOTICE

This document is disseminated under the sponsorship of the Department of Transportation in the interest of information exchange. The United States Government assumes no liability for the contents or use thereof.

1. Report No. DOT/FAA/PM-84/7		2. Government Accession No. AD-A140 797		3. Recipient's Catalog No.	
4. Title and Subtitle ENGINEERING AND TECHNICAL SERVICES TO IMPROVE RELIABILITY AND MAINTAINABILITY OF ILS COMPONENTS				5. Report Date January 1983	
				6. Performing Organization Code	
7. Author(s) Joe D. Longworth, R. H. McFarland, Walter Chippis, Thierry d'Estaintot, M. Jamil				8. Performing Organization Report No. OU/AEC/EER 62-1	
9. Performing Organization Name and Address Avionics Engineering Center Department of Electrical and Computer Engineering Ohio University Athens, Ohio 45701				10. Work Unit No. (TRAIS)	
				11. Contract or Grant No. DTFA01-81-C-20101	
12. Sponsoring Agency Name and Address U.S. Department of Transportation Federal Aviation Administration Systems Research and Development Service Washington, D.C. 20591				13. Type of Report and Period Covered Final Report Sept. 1981 - April 1983	
				14. Sponsoring Agency Code	
15. Supplementary Notes					
16. Abstract Results of ILS anomaly investigation conducted at Buffalo, NY, Los Angeles, CA., International Falls, MN., and San Francisco, CA. are documented. In addition, an anomalous performance of the FA5723 and FA8633 ILS clearance transmitter was investigated. Studies into the feasibility of ground check procedures for the capture effect glide slope systems and an investigation of maximum allowable audio harmonic content are also presented.					
17. Key Words ILS, localizer, glide slope, parabolic localizer, CAT III, AMD, capture effect			18. Distribution Statement This document is available to the U.S. public through the National Technical Information Service, Springfield, Virginia 22161.		
19. Security Classif. (of this report) Unclassified		20. Security Classif. (of this page) Unclassified		21. No. of Pages 291	
				22. Price	

METRIC CONVERSION FACTORS

Approximate Conversions from Metric Measures			
Symbol	What You Have	Multiply by	To Find
LENGTH			
m	meters	3.28	feet
cm	centimeters	0.39	inches
mm	millimeters	0.04	inches
km	kilometers	0.62	miles
AREA			
m ²	square meters	1.10	square feet
cm ²	square centimeters	1.55	square inches
ha	hectares (10,000 m ²)	2.47	acres
MASS (weight)			
kg	kilograms	2.20	pounds
g	grams	0.035	ounces
tonne	metric tons (1,000 kg)	2,205	short tons
VOLUME			
m ³	cubic meters	35.3	cubic feet
l	liters	1.06	quarts
ml	milliliters	0.034	fluid ounces
TEMPERATURE (exact)			
°C	Celsius temperature	9/5 (then add 32)	Fahrenheit temperature



*1 m = 2.54 exactly. For other exact conversions and more detailed tables, see NIST Spec. Publ. 280, Guide for Weight and Measures, NIST 85-375, 50 Centing No. C13.10-250.

TABLE OF CONTENTS

	<table><tr><td colspan="2">Accession For</td></tr><tr><td>NTIS GRA&I</td><td><input checked="" type="checkbox"/></td></tr><tr><td>DTIC TAB</td><td><input type="checkbox"/></td></tr><tr><td>Unannounced</td><td><input type="checkbox"/></td></tr><tr><td colspan="2">Justification</td></tr><tr><td colspan="2">By _____</td></tr><tr><td colspan="2">Distribution/_____</td></tr><tr><td colspan="2">Availability Codes</td></tr><tr><td>Dist</td><td>Avail and/or Special</td></tr><tr><td>A-1</td><td></td></tr></table>	Accession For		NTIS GRA&I	<input checked="" type="checkbox"/>	DTIC TAB	<input type="checkbox"/>	Unannounced	<input type="checkbox"/>	Justification		By _____		Distribution/_____		Availability Codes		Dist	Avail and/or Special	A-1		PAGE
Accession For																						
NTIS GRA&I	<input checked="" type="checkbox"/>																					
DTIC TAB	<input type="checkbox"/>																					
Unannounced	<input type="checkbox"/>																					
Justification																						
By _____																						
Distribution/_____																						
Availability Codes																						
Dist	Avail and/or Special																					
A-1																						
List of Figures		v																				
List of Tables		xiv																				
INTRODUCTION																						
Purpose.		1																				
Background.		1																				
Pertinent Sections.		1																				
ILS ANOMALY INVESTIGATIONS		3																				
Evaluation of Waveguide Glide Slope Performance, Runway 23, Buffalo, New York.		3																				
Introduction and Background.		3																				
Determination of Reference Location.		4																				
Discussion of Measurements and Data.		5																				
Investigation of the Problem of Excess Roughness in the CAT III Localizer Course Structure for Runway 24R at Los Angeles International Airport.		17																				
Summary and Conclusions.		17																				
Introduction and Background.		19																				
Approaches to Identify the Cause of the Localizer Course Structure Problem.		21																				
Discussion of Possible Solutions.		31																				
Measurements and Discussion of Data.		33																				
Recommendations.		34																				
Investigation of Anomalous Performance of the International Falls Null Reference Glide Slope.		35																				
Summary and Conclusions.		35																				
Introduction and Background.		37																				
Data Collection and Discussion.		43																				
Recommendations.		56																				
An Evaluation of Localizer Performance and Causes of Dero- gation at San Francisco International Airport.		57																				
Introduction and Background.		57																				
Approach.		59																				
Analysis.		61																				
SBO Energy Distribution.		67																				
Calculational Approach.		70																				
Conclusions.		79																				
Recommendations.		81																				

TABLE OF CONTENTS (CONTINUED)

	PAGE
A Demonstration of Two Solutions to the Category III Localizer Problem on Runway 28R at San Francisco International Airport.	82
Summary and Conclusions.	82
Introduction and Statement of the Problem.	84
Approaches.	86
Data Collection and Discussion.	87
Recommendations.	101
Modification to the FA-5723 and FA-8633 Clearance Transmitters.	102
Conclusions.	102
Summary.	103
ILS SETUP PROCEDURES	105
Investigation of Ground-check Procedures for ILS Glide Slopes.	105
Introduction and Background.	105
Near-field Model (TGCSG) Description.	107
Data (Measured and Modeled).	126
Conclusions.	139
Recommendations.	140
Investigation of ILS Transmitter Carrier Output Modulation Components	141
Introduction.	141
Theoretical Background.	142
Preliminary Measurements.	146
ILS Receiver Model Calculations.	155
Conclusions and Recommendations.	205
INVESTIGATORS AND ACKNOWLEDGEMENTS	206
BIBLIOGRAPHY	207
APPENDICES	208
A. Additional Figures for Los Angeles, CA., Runway 24R Investigation.	208
B. Model Analysis.	212
C. Parameters Modeled By TGCSG.	227
D. General Data for Tamiami Airport CEGS.	228
E. Program Listings.	229
F. Harmonics Analyser Program Listing.	248
G. Tests.	251
H. Experimental Results.	258

LIST OF FIGURES

Figure		PAGE
2-1	Flight Record of Differential Amplifier Output for Waveguide Glide Slope Conditions as Originally Found Without Auxiliary Radiators.	7
2-2	Flight Record of Differential Amplifier Output for Waveguide Glide Slope Conditions of a Lower Auxiliary Radiator with Screen.	8
2-3	Flight Record of Differential Amplifier Output for Waveguide Glide Slope Conditions with Two Auxiliary Radiators Mounted Either Side of Waveguide 26 Feet Above Ground.	9
2-4	Flight Record of Differential Amplifier Output for Waveguide Glide Slope Conditions as in Figure 2-3, but with Attenuation Increased 4 dB.	10
2-5	Flight Record of Differential Amplifier Output for Waveguide Glide Slope Conditions as in Figure 2-3, but with Upper Waveguide Feed Attenuation Decreased 1 dB to Change Coning.	11
2-6	Flight Record of Differential Amplifier Output for Waveguide Glide Slope Conditions as in Figure 2-3, but with Antenna Made More Perpendicular by Moving the Base Back One Inch.	12
2-7	Flight Record of Differential Amplifier Output for Waveguide Glide Slope Conditions of a Lower Auxiliary Antenna Only.	13
2-8	Flight Record of Differential Amplifier Output for Waveguide Glide Slope Conditions as Originally Found Except with an Increase in Sideband Power.	14
2-9	Recording of CDI Made During Level Flight 1000 Feet Above the Localizer Centerline Extended for Original Antenna Conditions.	15
2-10	Los Angeles Airport Layout.	20
2-11	Calculated Side-Band Only Pattern for the Wilcox Category-III Localizer.	22

LIST OF FIGURES (CONTINUED)

Figure		PAGE
2-12	Calculated Pattern Showing 1.2 db Reduction in Side-band Signal at 5° Azimuth When 60° of Phase Delay Has Been Inserted In Feed Lines to Antennas, #4, #5, #6 and #7 On the 90 Hz Side.	23
2-13	Three Flight Recordings Revealing the Small but Significant Path Perturbation Between ILS Points B and the Threshold.	25
2-14	Layout Configuration of Runway 24R at Los Angeles International Airport.	26
2-15	Geometries Associated with Calculation to Determine a Location of the Hypothetical Reflector.	27
2-16	Photograph of Embankment 600 to 700 feet from the Runway On the North Side Approximately 6300 feet from the Stop End of Runway 24R.	29
2-17	Calculated Course Structure Produced With A Wilcox Category III Array With a Reflector 500 feet long, 40 feet high, 608 feet North of the Centerline of the Runway, 6362 feet from the Array.	30
2-18	Photograph of Lower Bay (Carrier Antennas) for the International Falls, Null-reference Glide Slope Array.	38
2-19	View of Terrain Forming the Reflecting Plane for the Null Reference Glide Slope at International Falls.	39
2-20	Aerial View of the Glide Slope Site Looking Southwest.	40
2-21	Aerial View which Illustrates the Nearly Linear Northeast Boundary of the Woods.	41
2-22	Flight Recording of the Structure Produced by the International Falls Glide Slope in the As-found, Normal Condition.	44
2-23	Flight Recording Showing the Vertical Structure of the International Falls Glide Slope Under Normal Conditions.	45
2-24	Flight Recording Showing the Differential Amplifier Trace Representative of the Structure Produced When the Azimuthal Directivity of the Carrier and Sideband Antenna is Reduced.	46
2-25	Photograph of Antennas Being Cocked Approximately 20 Degrees Towards the Runway and Away from the Woods.	48

LIST OF FIGURES (CONTINUED)

Figure		PAGE
2-26	Flight Recording of Path Structure Produced when Antennas are Aimed Away from the Woods and Towards the Runway.	49
2-27	Flight Recording Showing Differential Amplifier Trace for the Path which has been Lowered by Raising the Sideband Antenna 18 inches.	51
2-28	Flight Recording of the Differential Amplifier Output Mode when Flying Approximately 400 feet to the Left of the Localizer Centerline.	52
2-29	Flight Recording of Differential Amplifier Output made When Flying 400 feet to the Right of the Localizer Centerline.	53
2-30	FAA Flight Recording Made of the Localizer Structure in Zones 3, 4, and 5 for Runway 28R at San Francisco International Airport.	62
2-31	FAA Recording of Localizer Structure Made During a Taxi from One End of the Runway to the Other.	63
2-32	Airport Layout Indicating the Tanks, and UAL Maintenance Complex Along with the Localizer.	64
2-33	FAA Flight Recording Made of the Localizer Structure for Runway 28L at San Francisco.	65
2-34	Plots of Measured SBO Energy Distributions for the Parabolic Antenna and for the 14-element, Wide-aperture Array.	68
2-35	Calculated Path Perturbation Produced by American Airlines Hangar Using Measured SBO Distribution.	71
2-36	Calculated Path Structure Produced by Fuel Storage Tanks with Measured SBO Energy Distribution.	72
2-37	Calculated Path Structure Produced by Fuel Storage Tanks with SBO Energy Distribution Skewed One Degree to Account for Possible Error in Azimuth Angle Determination Accomplished by Dividing the Region Between the Front and Back Course into 180 Equal Segments.	73
2-38	Calculated Path Structure Produced by Reflecting Surface in the United Airlines Maintenance Complex with measured Asymmetrical SBO Energy Distribution.	74

LIST OF FIGURES (CONTINUED)

Figure		PAGE
2-39	Calculated Path Structure Produced by Reflecting Surface in the United Airlines Maintenance Complex but with an SBO Energy Distribution that is Symmetrical and Consistent with the South-side Distribution.	75
2-40	Calculated Path Structure Produced by the Wide-aperture, 14-Discrete-Element Array Designed by R. W. Redlich and Having Undergone tests at the Ohio University Test Site at Tamiami Airport in Florida.	76
2-41	Calculated Path Structure Produced by the Wide-aperture Array. The SBO pattern used was measured.	77
2-42	Calculated Path Structure Produced by the Wide-aperture Array. The SBO pattern used was derived from measurements made at Tamiami.	78
2-43	Flight Recording Showing the As-found, Out-of-tolerance Structure in ILS Zone 4.	88
2-44	Sideband Only Radiation Pattern of the San Francisco Parabolic Localizer.	89
2-45	Flight Recording of the Structure Produced When Additional Course SBO Energy Is Directed to the United Airlines Maintenance Complex.	90
2-46	Flight Recording of the Course Structure Produced for Normal Conditions Except the Height of the Parabolic Screen Has Been Lowered by 8 Horizontal Wire Elements.	92
2-47	Flight Recording With Conditions Similar to Figure 2-46 Except that 16 Wire Elements Have Been Removed Thus Lowering the Height of the Screen Approximately 24 Inches.	93
2-48	Flight Recording With Conditions Similar to Figure 2-46 Except that 23 Wire Elements Have Been Removed Thus Lowering the Height of the Reflecting Screen by Approximately 3 Feet.	94
2-49	Flight Recording Showing the Improvement Obtained in the Structure When the Parabolic Reflecting Screen is Raised 6 Feet.	95
2-50	Photograph of Parabolic Antenna Array With 6-foot Extension In Place.	96
2-51	Another Photograph of the 6-foot Extension Constructed At the Top of the Existing Parabolic Reflecting Screen.	97

LIST OF FIGURES (CONTINUED)

Figure		PAGE
2-52	Photograph of the 14-element, Log-periodic, Wide-aperture Array in Place in Front of the Existing Parabolic Antenna System.	99
2-53	Flight Recording of Course Structure Produced With the 14-element, Log-periodic, Wide-aperture Array.	100
3-1	Geometry Illustrating a Possible Deficiency in Ground Measurements Caused by Terrain Irregularities Beyond the Measuring Point.	106
3-2	Theoretical Airport Geometry with Grid Used for Primary TGCGS Tests.	109
3-3	CDI vs. Receiving Antenna Height for Grid Line $x=30.5m$.	110
3-4	CDI vs. Receiving Antenna Height for Grid Line $x=61m$.	111
3-5	CDI vs. Receiving Antenna Height for Grid Line $x=91.5m$.	112
3-6	CDI vs. Receiving Antenna Height for Grid Line $x=122m$ (in front of the antenna mast).	113
3-7	Effect of Faults in CEGS System on Glide Path Performances.	115
3-8	Modeled CDI vs. Receiving Antenna Height for Normal System and for Broad and Narrow Alarms.	116
3-9	Modeled CDI vs. Receiving Antenna Height with $\pm 15^\circ$ Dephasing of the Middle Antenna.	117
3-10	Modeled CDI vs. Receiving Antenna Height with $\pm 15^\circ$ Dephasing of the Lower Antenna.	118
3-11	Modeled CDI vs. Receiving Antenna Height with $\pm 15^\circ$ Dephasing of the Upper Antenna.	119
3-12	Modeled CDI vs. Receiving Antenna Height. Effect of attenuation in antenna currents.	120
3-13	Modeled CDI vs. Receiving Antenna Height for Various Reflecting Ground Electric Constants.	121
3-13a	Magnitude of the Horizontally-Polarized Reflection Coefficient vs. Incidence Angle for Various Ground Plane Electrical Constants (modeled).	122
3-14	Modeled CDI vs. Receiving Antenna Height for Various Snow Depths.	123

LIST OF FIGURES (CONTINUED)

Figure		PAGE
3-15	Clearance Signal Relative Strength for Normal and Fault Conditions.	125
3-16	Control Points for ILS Site at New Tamiami Airport, Florida.	127
3-17	CEGS Transmitter Mast Equipped with Three FA8976 Antennas.	128
3-18	Ground Measurement Equipment (foreground) and CEGS Array (background).	129
3-19	Electronic Equipment Used in Collecting Ground Measurements Data; Only the PIR is Required for the Measurements.	130
3-20	Measured and Modeled CDI vs. Elevation Angle for the 360° Phase Proximity Point Located Directly in Front of the Antenna Mast.	132
3-21	Modeled CDI vs. Receiving Antenna Height at the 122244 Ground Check Point for a Normal System.	133
3-22	Measured and Modeled CDI vs. Receiving Antenna Height (244m in front of the antenna mast). Normal system (first test).	134
3-23	Measured and Modeled CDI vs. Receiving Antenna Height (244m in front of the antenna mast). Dephasing -15° of the middle antenna (first test).	135
3-24	Measured and Modeled CDI vs. Receiving Antenna Height (244m in front of the antenna mast). Normal system (second test).	136
3-25	Measured and Modeled CDI vs. Receiving Antenna Height (244m in front of the antenna mast). Narrow alarm (second test).	137
3-26	Measured and Modeled CDI vs. Receiving Antenna Height (244m in front of the antenna mast). Broad alarm (second test).	138
3-27	Combined 90 Hz and 150 Hz Tones Summed Together in Equal Amplitude.	143
3-28	Measured Collins Localizer Receiver, 90 Hz Filter Response, Measured Q = 3.	147
3-29	Measured Collins Localizer Receiver, 150 Hz Filter Response, Measured Q = 4.72.	148
3-30	Measured Collins Glide Slope Receiver, 90 Hz Filter Response, Measured Q = 2.9.	149

LIST OF FIGURES (CONTINUED)

Figure		PAGE
3-31	Measured Collins Glide Slope Receiver, 150 Hz Filter Response, Measured $Q = 5$.	150
3-32	Measured NARCO Glide Slope Receiver, 150 Hz Filter Response, Measured $Q = 4.8$.	151
3-33	NARCO Glide Slope Receiver, 90 Hz Response, Measured $Q = 3$.	152
3-34	NARCO Localizer Receiver, 90 Hz Response, Measured $Q = 2.88$.	153
3-35	Measured NARCO Localizer Receiver, 150 Hz Filter Response, Measured $Q = 4.9$.	154
3-36	Comparison of Measured and Calculated 180 Hz Harmonic Effect on the Collins 51RV4B Receiver CDI.	156
3-37	Calculated Response for NARCO Localizer with 30 Hz Harmonic.	181
3-38	Calculated Response for NARCO Localizer with 60 Hz Harmonic.	182
3-39	Calculated Response for NARCO Localizer with 180 Hz Harmonic.	183
3-40	Calculated Response for NARCO Localizer with 240 Hz Harmonic.	184
3-41	Calculated Response for NARCO Localizer with 300 Hz Harmonic.	185
3-42	Calculated Response for NARCO Localizer with 540 Hz Harmonic.	186
3-43	Calculated Response for NARCO Glide Slope with 30 Hz Harmonic.	187
3-44	Calculated Response for NARCO Glide Slope with 60 Hz Harmonic.	188
3-45	Calculated Response for NARCO Glide Slope with 180 Hz Harmonic.	189
3-46	Calculated Response for NARCO Glide Slope with 240 Hz Harmonic.	190
3-47	Calculated Response for NARCO Glide Slope with 300 Hz Harmonic.	191
3-48	Calculated Response for NARCO Glide Slope with 540 Hz Harmonic.	192
3-49	Calculated Response for Collins Localizer with 30 Hz Harmonic.	193
3-50	Calculated Response for Collins Localizer with 60 Hz Harmonic.	194
3-51	Calculated Response for Collins Localizer with 180 Hz Harmonic.	195
3-52	Calculated Response for Collins Localizer with 240 Hz Harmonic.	196
3-53	Calculated Response for Collins Localizer with 300 Hz Harmonic.	197

LIST OF FIGURES (CONTINUED)

Figure		PAGE
3-54	Calculated Response for Collins Localizer with 540 Hz Harmonic.	198
3-55	Calculated Response for Collins Glide Slope with 30 Hz Harmonic.	199
3-56	Calculated Response for Collins Glide Slope with 60 Hz Harmonic.	200
3-57	Calculated Response for Collins Glide Slope with 180 Hz Harmonic.	201
3-58	Calculated Response for Collins Glide Slope with 240 Hz Harmonic.	202
3-59	Calculated Response for Collins Glide Slope with 300 Hz Harmonic.	203
3-60	Calculated Response for Collins Glide Slope with 540 Hz Harmonic.	204
A-1	Recommended Cut and Fill Operation on Embankment Centered 6400 Feet from the Array, 650 Feet North of the Runway to Give Acceptable Category III Localizer Performance.	208
A-2	Calculated Localizer Course Structure Resulting from 60-Degree Phase Delays Inserted in Antenna Feeds #4, #5, #6, and #7 on the 90 Hz Side.	209
A-3	Calculated Course Structure for 60-Degree Phase Delay Placed in Lines #6 and #7 of the 90 Hz Side.	210
A-4	Calculated Localizer Course Structure Resulting From Reflections from the Wall that has been Lowered from 40 to 30 Feet in Height but still 500 Feet Long.	211
B-1	Reference Coordinate System for TCGS Model.	213
B-2	Image Theory for Reflected Field.	214
B-3	Magnitude of the Horizontally-polarized Reflection Coefficient vs. Incidence Angle for Various Ground Plane Electrical Constants (Modeled).	216
B-4	Geometry Illustrating How to Reduce Spherical Wave Incidence into Infinite Series of Plane Wave Reflections.	217
B-5	Spherical Wave Propagation Effect on Reflection Coefficient (angle of incidence=80°, $\alpha=1 \times 10^{-4}$ s/m, $\epsilon_r=3$).	219
B-6	Antenna Products Company FA8976.	220
B-7	Three-Element Colinear Antenna Array.	221
B-8	Modeled Array Factor vs. Azimuth Angle for Normal and Faulty System.	223

LIST OF FIGURES (Continued)

	PAGE
B-9 Image Theory Applied to Corner Reflector.	224
B-10 Modeled Reflector Factor Magnitude vs. Elevation Angle.	225
B-11 Modeled Magnitude of the Roughness Coefficient vs. Angle of Incidence for Various Roughness Parameters (roughness parameter=h).	226
G-1 Set Up to Obtain 90 Hz or 150 Hz Filter Response Data.	252
G-2 Set Up for Obtaining the Change in CDI Current Readings Due to the Change in Amplitude of Subharmonics.	253
G-3 Set Up for Total Harmonic Distortion Measurements.	254
G-4 Summing Amplifier.	255
G-5 General View of Bench Test Area.	256
G-6 General View of Bench Test Area.	257

LIST OF TABLES

Table	PAGE
2-1 Numerical Values Derived from Flight Records to Summarize the Glide Path Conditions with Respect to Tolerance Limits.	6
2-2 Comparison of Path Structure Values for Three Antenna Conditions.	50
2-3 Summary of Data.	54
2-4 FAA Data with PIR.	67
3-1 Calculated Response for Narco Localizer with 30 Hz Harmonic.	157
3-2 Calculated Response for Narco Localizer with 60 Hz Harmonic.	158
3-3 Calculated Response for Narco Localizer with 180 Hz Harmonic.	159
3-4 Calculated Response for Narco Localizer with 240 Hz Harmonic.	160
3-5 Calculated Response for Narco Localizer with 300 Hz Harmonic.	161
3-6 Calculated Response for Narco Localizer with 540 Hz Harmonic.	162
3-7 Calculated Response for Narco Glide Slope with 30 Hz Harmonic.	163
3-8 Calculated Response for Narco Glide Slope with 60 Hz Harmonic.	164
3-9 Calculated Response for Narco Glide Slope with 180 Hz Harmonic.	165
3-10 Calculated Response for Narco Glide Slope with 240 Hz Harmonic.	166
3-11 Calculated Response for Narco Glide Slope with 300 Hz Harmonic.	167
3-12 Calculated Response for Narco Glide Slope with 540 Hz Harmonic.	168
3-13 Calculated Response for Collins Localizer with 30 Hz Harmonic.	169
3-14 Calculated Response for Collins Localizer with 60 Hz Harmonic.	170
3-15 Calculated Response for Collins Localizer with 180 Hz Harmonic.	171
3-16 Calculated Response for Collins Localizer with 240 Hz Harmonic.	172
3-17 Calculated Response for Collins Localizer with 300 Hz Harmonic.	173
3-18 Calculated Response for Collins Localizer with 540 Hz Harmonic.	174
3-19 Calculated Response for Collins Glide Slope with 30 Hz Harmonic.	175
3-20 Calculated Response for Collins Glide Slope with 60 Hz Harmonic.	176

LIST OF TABLES (CONTINUED)

Table	PAGE
3-21 Calculated Response for Collins Glide Slope with 180 Hz Harmonic.	177
3-22 Calculated Response for Collins Glide Slope with 240 Hz Harmonic.	178
3-23 Calculated Response for Collins Glide Slope with 300 Hz Harmonic.	179
3-24 Calculated Response for Collins Glide Slope with 540 Hz Harmonic.	180
H-1a Collins Localizer Receiver, 0 DDM.	259
H-1b Collins Localizer Receiver, 0.115 DDM (90>150).	260
H-1c Collins Localizer Receiver, 0.155 DDM (150>90).	261
H-2a Collins Glide Slope Receiver, 0 DDM.	262
H-2b Collins Glide Slope Receiver, 0.175 DDM (90>150).	263
H-2c Collins Glide Slope Receiver, 0.175 DDM (150>90).	264
H-3a Narco Glide Slope Receiver, 0 DDM.	265
H-3b Narco Glide Slope Receiver, 0.175 DDM (90>150).	266
H-3c Narco Glide Slope Receiver, 0.175 DDM (150>90).	267
H-4 Narco Localizer Receiver, 0 DDM.	268
H-5a Collins Localizer Receiver, 90 Hz Triangular Wave.	269
H-5b Collins Localizer Receiver, 150 Hz Triangular Wave.	270
H-6a Collins Glide Slope Receiver, 90 Hz Triangular Wave.	271
H-6b Collins Glide Slope Receiver, 150 Hz Triangular Wave.	272
H-7a Narco Glide Slope Receiver, 90 Hz Triangular Wave.	273
H-7b Narco Glide Slope Receiver, 150 Hz Triangular Wave.	274
H-8a Narco Localizer Receiver, 90 Hz Triangular Wave.	275
H-8b Narco Localizer Receiver, 150 Hz Triangular Wave.	276

INTRODUCTION

PURPOSE.

This report documents the results of engineering and technical services provided to the the Airways Facilities Division of the Federal Aviation Administration during the period of September 24, 1981 to January 22, 1983. These technical services consisted of ILS anomaly investigations conducted at Buffalo (New York), Los Angeles (California), International Falls (Minnesota), and San Francisco (California). In addition to these on-site investigations, an anomalous performance of auxiliary monitor detectors for the FA-5723 and FA-8633 clearance transmitters was investigated.

Studies to provide a means for developing maintenance standards and tolerances were also conducted. These consisted of investigations into the feasibility and reliability of ground checking the capture effect and side-band reference glide slope systems and an investigation of the maximum allowable 90 and 150 Hz audio harmonic content for ILS systems.

BACKGROUND.

Much of the information contained herein has been previously published in Ohio University Technical Memoranda B-1 through B-7. These individual memoranda were intended to provide a more timely reporting basis on the individual efforts. This document is ostensibly to compile the previously published work and to complete the documentation of data which may have been in a preliminary form until this date.

This report is organized into discrete sections presenting information and pertinent results aligned with specific portions of the contractual tasks. As such, the conclusions and other pertinent data are contained in the applicable sections and are not repeated in a separate section. In addition, some repetition in the introductory material may appear.

PERTINENT SECTIONS.

Section II of this report discusses the individual anomaly investigations. First, the results of flight measurements of the Buffalo waveguide glide-slope system with 7 different configurations are presented. Next, an investigation of an excess roughness problem in the Los Angeles International runway 24R localizer is documented. An anomalous performance of the International Falls null reference glide slope and the San Francisco International Airport parabolic localizer are documented. In addition to these specific on-site investigations a modification to the FA-5723 and FA-8633 clearance transmitters to improve load termination monitoring circuitry is presented.

Section III contains the documentation of studies to develop maintenance standards and tolerances, and certification procedures for special types of ILS systems. These consist of an investigation of whether or not it is

feasible to ground check the capture-effect, glide-slope system. Also included is an evaluation of the sideband reference, 360-degree ground-checking point and an investigation of new ground-check locations, if required and/or feasible. In addition, a study to determine the maximum allowable audio harmonic content for the 90 Hz and 150 Hz audio navigation tones is presented.

ILS ANOMALY INVESTIGATIONS

EVALUATION OF WAVEGUIDE GLIDESLOPE PERFORMANCE RUNWAY 23, BUFFALO, NEW YORK.

INTRODUCTION AND BACKGROUND.

The terrain available for an image glide slope which would serve Runway 23 at the Buffalo International Airport is seriously deficient. The runway forms a pedestal with the berm extending only 75 feet from the hard surface. Beyond this distance there is a dropoff of 28 feet with a grade of approximately 28%, this feature extending parallel to the runway from the threshold back nearly 1500 feet.

In 1965 a waveguide glide slope was installed by the FAA beyond the dropoff at the lower level and with the help of the Westinghouse Corporation was commissioned Category II. A review of that work is contained in FAA Report FAA-RD 76-9 (reference 1).

Measurements by the FAA Flight Inspection in early 1981 resulted in the glide slope being downgraded to Category I. Since that time, regional engineers have worked on modifications to the system to improve the quality of the path structure produced by the waveguide. Limited availability of flight time prevented final determinations from being reached. The objective of the work reported here has been to obtain flight-check data which will allow a careful evaluation of performance and determination of the effectiveness of various modifications that were performed.

On October 13, 1981, a flight-check team from Ohio University travelled to Buffalo to perform necessary measurements. The equipment used was the Ohio University Mark III Minilab flown in a Model 36 Beechcraft. A tracking reference was established on the ground northwest of Runway 23 by using a Warren Knight Model WK-83 Radio Telemetry Theodolite with a Reaction Instruments telemetry transmitter. Approximately 12 hours of flight time were required to acquire 51 records documenting the performance of 7 different antenna and transmission line conditions. Calibration was performed using an IFR 401L signal standard carried on board the aircraft and traceable to the National Bureau of Standards.

Since the three-dimensional on-course surface from the waveguide is conical downwards (due to deliberate coning by means of feed adjustments), it cannot be expected to be congruent with the 3°-upward oriented theodolite reference cone. As a result, the location of the theodolite at Buffalo is a compromise to give minimum error for a real-time, direct readout with a differential amplifier operating on the telemetry signal. The maximum error introduced is calculated to be less than 2 microamperes assuming the aircraft is tracking the on-course within 30 microamperes. The reference on-course departs less than one-foot from a reference straight line extending through the 55-foot threshold-crossing-height point and making a 3.00°-angle with the horizontal. Elaboration on this concept is provided in the next section.

DETERMINATION OF REFERENCE LOCATION.

Because the waveguide is a non-image system the procedure for locating the reference prescribed in U.S. Flight Inspection Manual OA P 8200.1 217.25 is not appropriate. Instead, the location is established consistent with those for the non-image endfire and consistent with the recommendations presented in FAA Report FAA-R-6750.3 AAF-420 (reference 2).

The determination of the reference coordinate origin is determined as follows. The TCH (Threshold Crossing Height) is given as 55 feet for runway 23 at Buffalo. Further, the commissioned path angle is 3.00 degrees and the existing runway gradient is 0.5 feet per 850 feet along the runway. These numbers uniquely fix the runway point of intercept at 1038 feet back from the threshold which is 188 feet back of the existing waveguide antenna structure. For practical reasons, the tracking theodolite location was located 125 feet from the runway centerline and 25 feet from the hard surface edge. A measurement of the theodolite indicated that the terrain below the theodolite location would be 34 inches lower than the runway centerline at the RPI. Calculations using this number placed the theodolite 54 feet back of a position should the terrain be flat. This position assuming flat terrain calculated with an eyepiece height of 62 inches divided by the tangent of the path angle to give 98 feet. Taking this all into account placed the theodolite 993 feet from the threshold, i.e., 143 feet¹ to the rear of the waveguide antenna.

The phase center of the waveguide is reported to be 42.5 feet above the ground which makes it 12.5 feet above the runway. With a 500-foot offset from the centerline this means that a discrepancy between the small angular change, say 0.1°, as seen from the phase center and the theodolite reference location is only 2 percent; thus for reasonable aircraft tracks into the threshold the microampere error introduced is on the order of one microampere and is not significant.

$$^1 \frac{55}{\tan 3^\circ + .5/850} - \frac{62/12}{\tan 3^\circ} + \frac{34/12}{\tan 3^\circ} - 850' = 143'$$

DISCUSSION OF MEASUREMENTS AND DATA.

Seven discrete conditions of the radiating system were established by the FAA Regional Engineer and flight measurements made of the signal in space. Particular interest was given to the location of the auxiliary radiators. In general, all the parameters specified in the U.S. Flight Inspection Handbook OA P 8200.1 217 3101g were considered. Special attention was given to path structure in ILS Zone 3 angle, width, symmetry and below path clearance.

The seven different conditions measured were:

1. As found, operating Category I. This is the main waveguide but with no auxiliary radiators operating.
2. Lower auxiliary antenna added, directed towards the runway area abeam and with a screen immediately to its side (to the rear considering the direction of radiation of the main array).
3. Two auxiliary radiators separated 6 feet, located each side of the main array, 26 feet above the ground, aligned with the main array. Attenuation 20 dB.
4. Configuration of No. 3 but with attenuation increased to 24 dB.
5. Configuration of No. 3 but with coning produced with 7 dB instead of 8 dB of attenuation in the upper feed.
6. Configuration of No. 3 but with antenna made more nearly perpendicular by a one-inch movement of the base to the rear.
7. Feed removed from one auxiliary antenna and the other auxiliary antenna moved to the original position of No. 2 but with no side (back) screen.
8. Configuration of No. 1 for restoration.

Table 2-1 is provided to summarize the critical items important to judgment as to whether Category II specification can be met.

Figures 2-1 through 2-8 are the differential amplifier traces (course deviation indicator current value minus telemetered position of the aircraft as indicated by the radio telemetering theodolite). From these one can assess the quality of the glide slope structure including the reversals that were present in some of the traces. A typical recording of CDI during a level run is shown in figure 2-9. Other than random noise there are no pronounced features. The cross over is not particularly smooth.

After reviewing the records one can recognize that at best marginal Category II conditions can be produced. The resulting path characteristics

CONDITION	ANGLE	WIDTH	STRUCTURE	SYMMETRY	MINIMUM CLEARANCE μ A	REVERSALS μ A/1000'
Tolerance	2.77-3.23°	.5°-.9°	% of Tol.	58:42	180	25
1	2.97	.65	99	57:43	x	48
2	3.10	.76	<u>115</u>	<u>66:34</u>	x	-
3	3.00	.71	73	<u>59:41</u>	200	20
4	3.01	.67	26	<u>61:39</u>	<u>170</u>	<u>26</u>
5	3.05	.79	85	<u>61:39</u>	<u>170</u>	15
6	2.97	.66	80	<u>59:41</u>	<u>175</u>	<u>74</u>
7	3.15	.75	<u>165</u>	<u>61:39</u>	<u>130</u>	20
8	2.97	.82	85	<u>61:39</u>	<u>160</u>	<u>30</u>

x = NOT MEASURED

- = NOT PRESENT

Table 2-1. Numerical Values Derived from Flight Records to Summarize the Glide Path Conditions with Respect to Tolerance Limits. Underline indicates out-of-tolerance values.

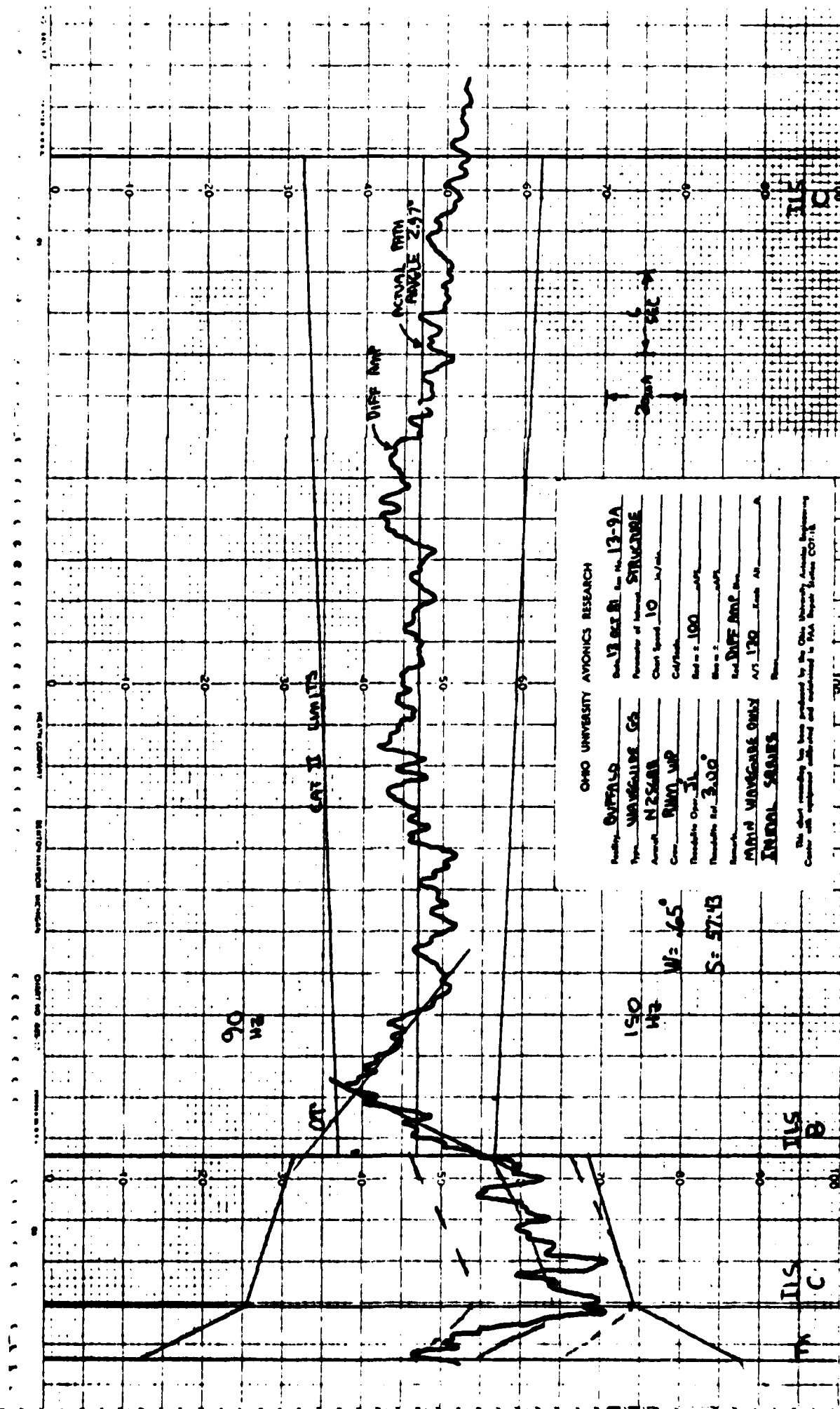


Figure 2-1. Flight Record of Differential Amplifier Output for Waveguide Glide Slope Conditions as Originally Found Without Auxilliary Radiators.

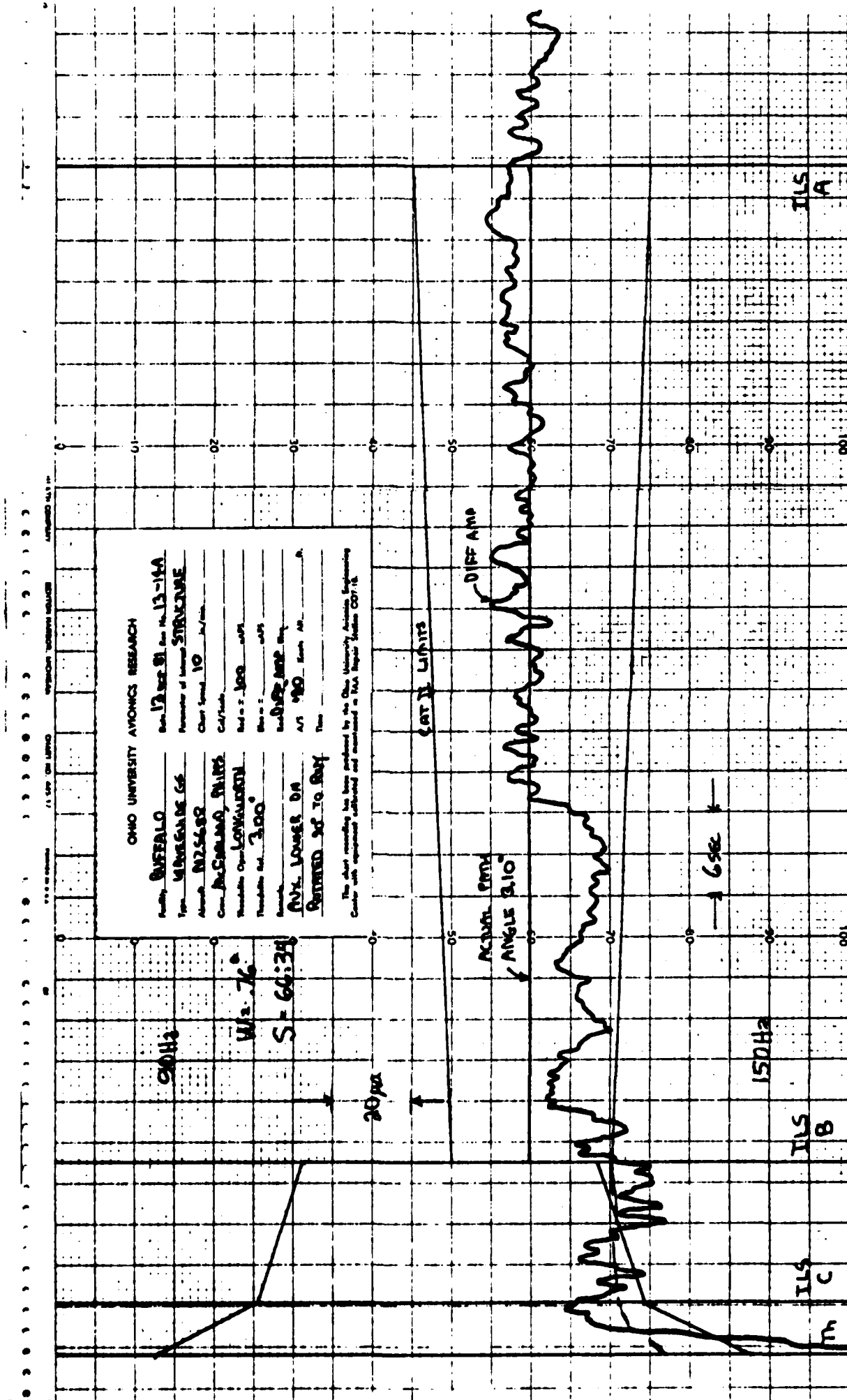


Figure 2-2. Flight Record of Differential Amplifier Output for Waveguide Glide Slope Conditions of a Lower Auxiliary Radiator with Screen.

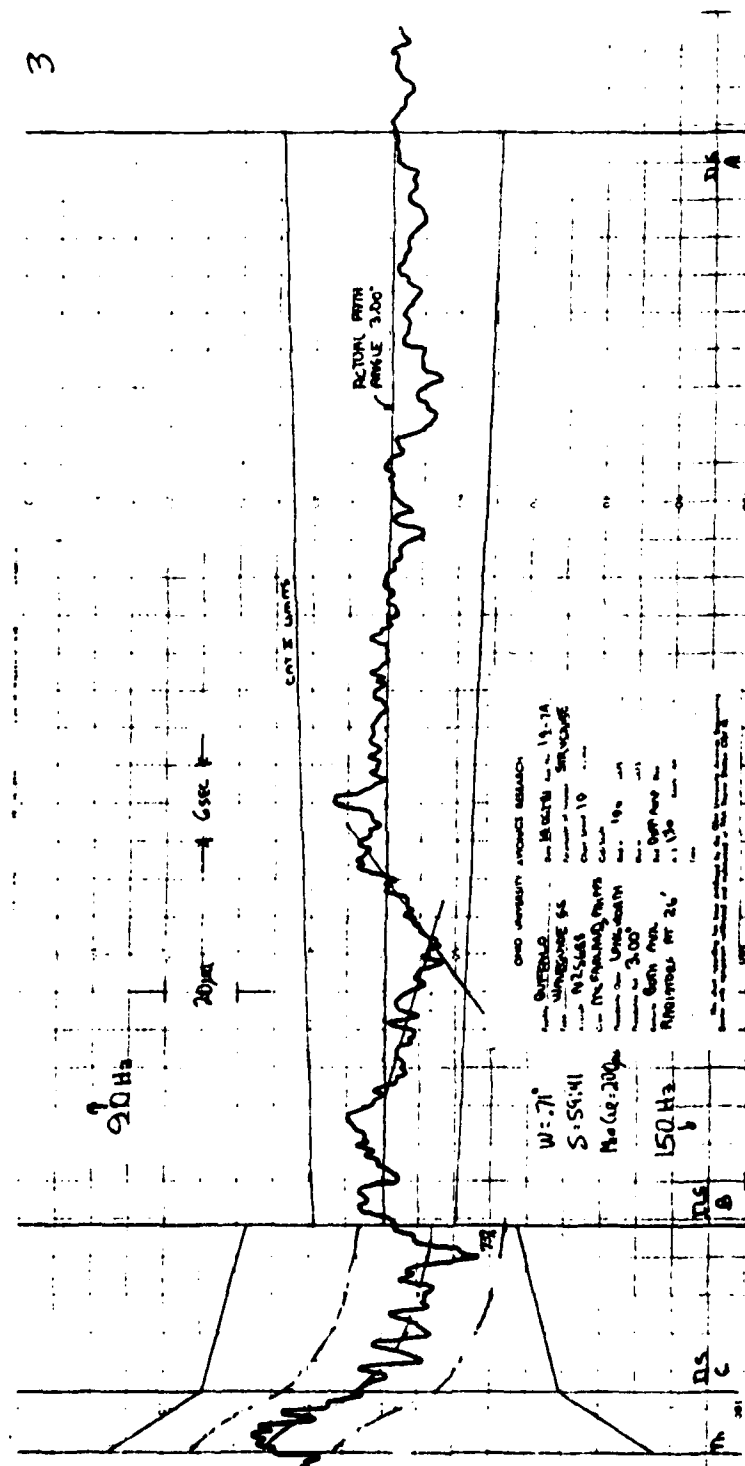


Figure 2-3. Flight Record of Differential Amplifier Output for Waveguide Glide Slope Conditions With Two Auxiliary Radiators Mounted Either Side of Waveguide 26 Feet Above Ground.

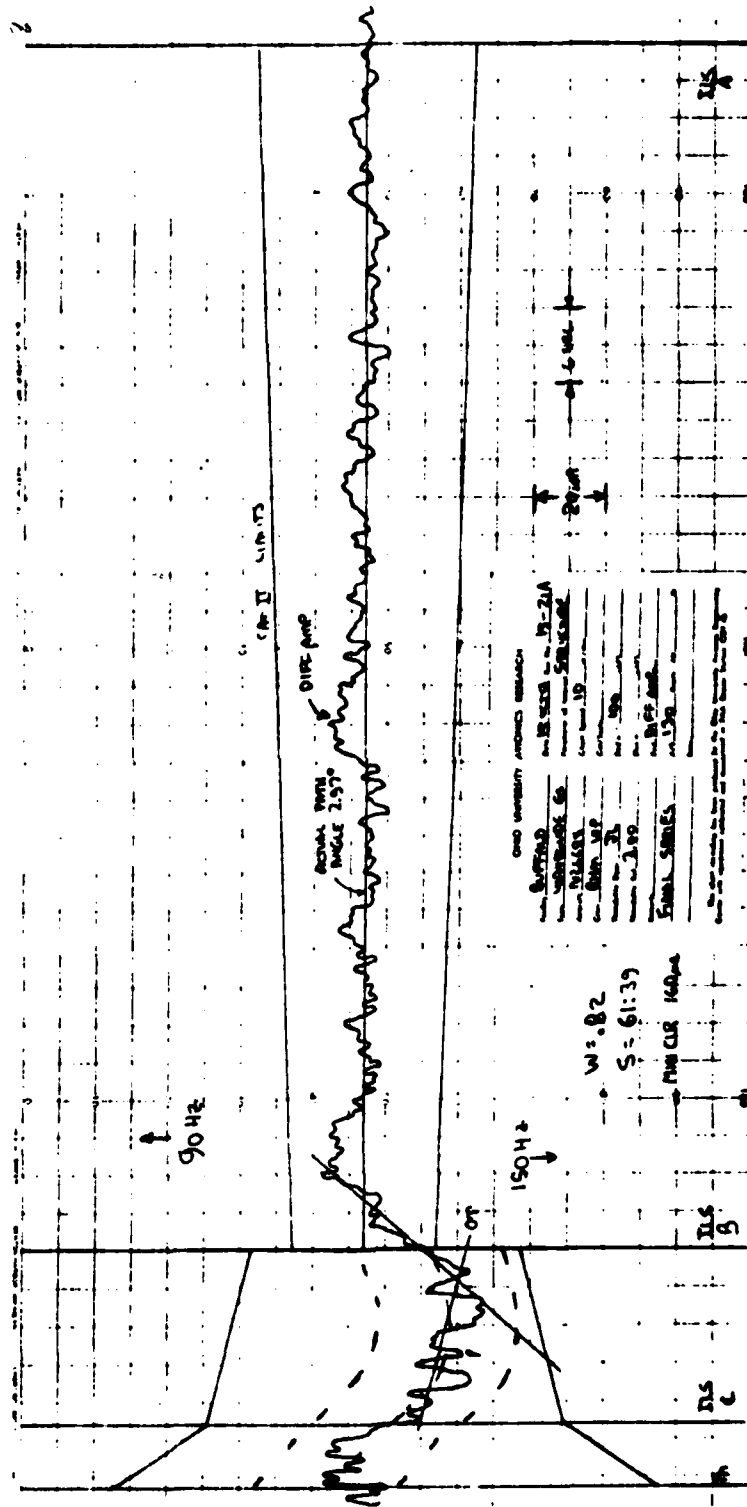


Figure 2-8. Flight Record of Differential Amplifier Output for Waveguide Glide Slope Conditions As Originally Found Except With An Increase in Sideband Power.

which are of greatest concern are the structure roughness, the symmetry, path reversals, and the minimum clearance values.

INVESTIGATION OF THE PROBLEM OF EXCESS ROUGHNESS IN THE CAT III LOCALIZER
COURSE STRUCTURE FOR RUNWAY 24R AT LOS ANGELES INTERNATIONAL AIRPORT

This section documents only the portion of the investigations performed under this contract. An additional effort was conducted under a separate contract with the FAA Western Region and is reported in OU/AEC/EER Report No. 55-1.

SUMMARY AND CONCLUSIONS.

An investigation of localizer course structure roughness which is preventing Category II and III criteria from being met for Runway 24R at Los Angeles International Airport has been completed. The results obtained from calculations, analyses, and measurements of path conditions indicate that there is a reflecting object 600 feet from the centerline, approximately abeam the midpoint of the runway, which is contributing multipath signals that roughen the course between the threshold and the middle marker. A visual inspection reveals there is an embankment in the precise area of concern north of the runway. This embankment is approximately 40 feet high and extends parallel to the runway for over 300 feet, approximately 650 feet from centerline. The upper portion of the embankment surface, which is illuminated greatest, is smooth and nearly vertical thus providing good reflection characteristics.

Conclusions reached as a result of this work, which included going to Los Angeles to inspect the site and make special flight measurements, are:

1. The roughness in the Runway 24R localizer course structure is regular and repeatable in character, thus indicating that there is an interfering multipath signal coming from a single reflector arriving at the aircraft when it is between the middle marker and the threshold.
2. The analyses indicate that the reflector is approximately 600 feet from the runway centerline and 6400 feet from the antenna array.
3. Visual inspection of the possible areas north and south of the runway reveal only one possibility as the reflector, that being a 40-foot high embankment north of the runway midpoint region.
4. Seven different methods have been conceived for correcting the problem. The most immediate and reliable is to cut the upper portion of the embankment away thus removing the nearly vertical, nearly planar surface which receives the greatest illumination resulting in multipath.
5. There are a number of trees at the foot of the embankment that have raised concern about their contributing to the roughness problem. The tree line-air interface is irregular in terms of wavelength and do not present a condition which would support coherent reflections. The trees visually obscure much of the embankment and thus what might be an obvious reflector otherwise is overlooked. Further, the trees are not dense and do

not contain much moisture thus making them poor absorbers of 100-MHz radiation. All things considered the trees are an asset, albeit not a great one, and they should not be cut.

6. The Wilcox Category III localizer system now in place is performing well based on the design.

7. The 5-microampere tolerance for Category II and III appears to be overly restrictive. This conclusion is based on the fact that over 5 microamperes of roughness existed for years on the path with no known complaints. A cursory investigation of one report concerning potential complaints revealed that some autopilots disconnected at 5 microamperes which is, of course, unsatisfactory, thus provoking the comment that 5 microamperes was an appropriate tolerance. It turned out, however, that the disconnect occurred at five simply because the electrical adjustment on the autopilot was set at five and this was set because five was the FAA tolerance.

8. When the aircraft is descending to land, it migrates into a region of very low localizer signal strength. If there is multipath coming from an omnidirectional reflector that is well illuminated, then considerable vulnerability to multipath exists. It is in this particular region of low signal level that the most critical localizer tolerances are applied. It is important, considering this vulnerability, that they be no tighter than necessary; otherwise, frequent denial of the facility to the user will occur due to unwarranted shutdowns.

INTRODUCTION AND BACKGROUND.

The Los Angeles International Airport is one of the largest and busiest airports in the world. It consists of four parallel runways 25L, 25R, 24L and 24R with the terminal area being located between the two sets of runways (i.e. between the 24's and 25's). See figure 2-10. Hangars border the south edge of the airport, and to the north, houses have been removed leaving a relatively unoccupied area. This unoccupied area is elevated approximately 30 feet above the airport level, and the transition from the airdrome surface to this vacated area is by means of an abrupt slope or escarpment-type surface, steep in places, which is screened by eucalyptus trees and therefore appears visually to be quite benign.

Runway 24R at Los Angeles International Airport is considered by some to be the principal instrument runway at the airport. The intent by the FAA is to furnish the lowest possible landing minima for this runway relative to the other seven instrument-landing-system-equipped runways on the airdrome. Unfortunately, FAA Flight Inspection reported that the desired Category III criteria cannot be met because of localizer course structure roughness found between the middle marker and the runway threshold.

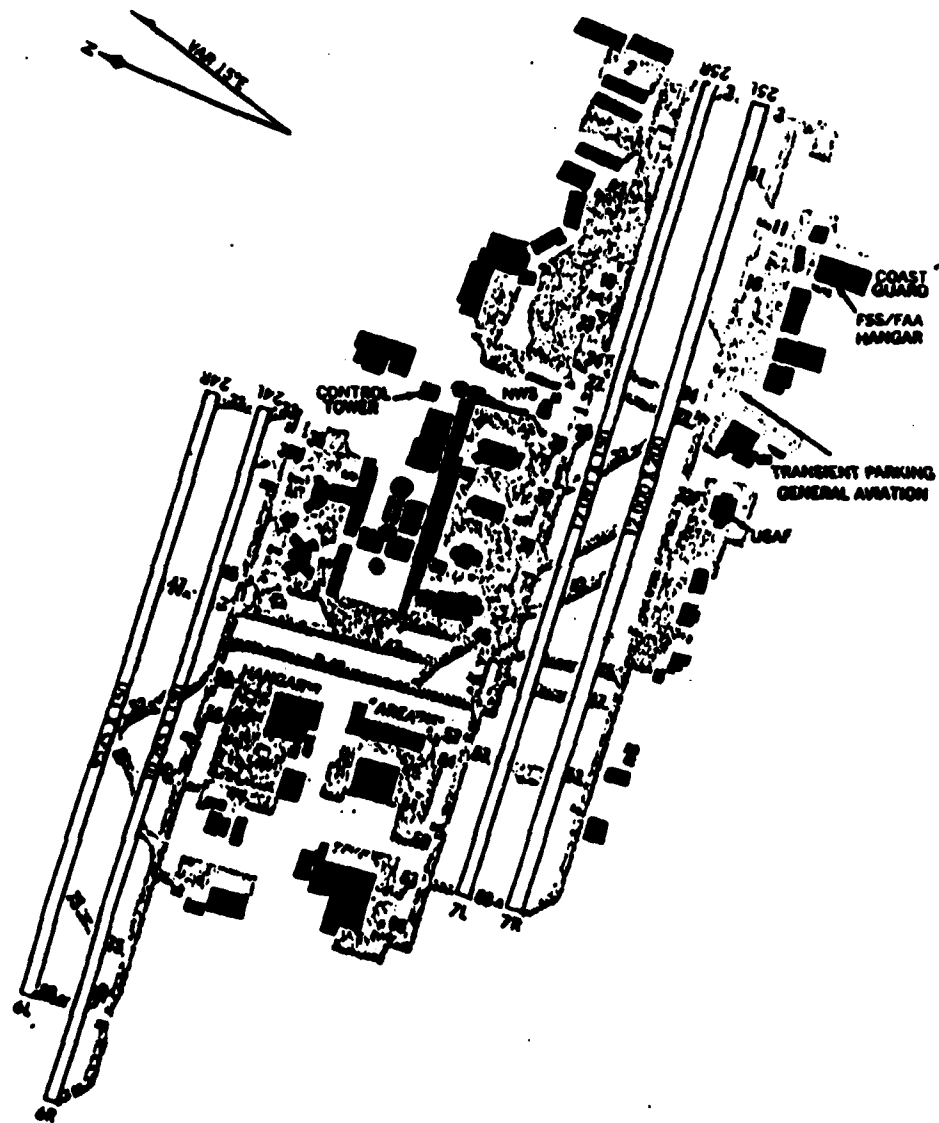
Ohio University was asked to investigate and evaluate the localizer performance. If the localizer was indeed found to be out-of-tolerance then the cause should be identified and recommendations formulated to solve the problem.

The work reported here was directed to these ends. Some history of the facility was gathered. This indicated that the ILS on Runway 24R was originally a Category-II, Texas Instrument System which was replaced by the FAA in 1981 with a Wilcox, Category-III type. The intent was to move the facility status from a Category II to a III. Reports obtained from FAA Flight Inspection indicated that the original Category II commissioning was with a DC-3 manually-operated system, whereas, the current measurements are made with the AFIS (Automatic Flight Inspection System) flying in a Sabreliner. Opinions expressed by flight inspection personnel indicate that there has been no degradation of localizer performance with the Wilcox Category III but has been no improvement either. This statement is consistent with what one would expect considering the designs and the relative performance capabilities of the two arrays. Both are 86-foot aperture, two-frequency arrays nominally at 108.5 MHz.

Occasional fog conditions with low visibilities and the numerous flight operations at Los Angeles airport make the Category II/III requirement meaningful and significant. The tight structure tolerances for Category III, viz 5 microamperes of course deviation current (CDI) peak deviation for Category III operations, essentially mandate directional arrays with no reflecting objects in the beam areas of the sideband radiation patterns.

AIRPORT TAXI CHART

178 LOS ANGELES INTERNATIONAL AIRPORT (LAX)
AL-237 (FAA)
LOS ANGELES, CALIFORNIA



ELEV 126

Figure 2-10. Los Angeles Airport Layout.

APPROACHES TO IDENTIFY THE CAUSE OF THE LOCALIZER COURSE STRUCTURE PROBLEM.

The first step taken to obtain a solution to the Los Angeles problem was to obtain the history of the work done with the 24R (OSS) localizer facility. The impression was quickly obtained that, indeed, the problem was formidable and important as evidenced by the attention given by the city, the FAA sector, region, and Aeronautical Center. Each had performed work on the problem and a review of this history was accomplished. Documents on this are given (references 3 and 4).

A review of the available materials and reports indicated that there was a high probability of existing reflecting object or objects in the environment. An effort was, therefore, made using the available Ohio University mathematical models to determine if there were reflectors, was there any convenient, practical means to alter the shape of the course SBO radiation pattern to reduce incident radiation on the reflectors located in the specific directions?

Evidence from the FAA's work indicated that the course array was at fault since the structure problem persisted even when the clearance transmitter was shut down.

Only a few calculations were possible in the few days available from the time the request was made until departure of the team for Los Angeles. However, sufficient calculations were made to give encouragement that if reflectors were found at 5 to 10° azimuth angles, inserting phase delays in 2 or 4 of the feed lines would shift the SBO patterns making them asymmetrical and reducing radiations on one side. Calculations did show that derogation in course symmetry and adverse course shift was small enough such that compensations could be provided.

Figure 2-11 shows a plot of the normal SBO pattern for a Wilcox, Category-III localizer system. Figure 2-12 shows the results of introducing 60 degrees phase delays in the #4, #5, #6 and #7 lines on the 90 Hz side of the array. From the drawing approximately 1.2 db of course SBO reduction appears to result. This is sufficient to make this approach worthy of a practical test. Of particular interest are the tradeoffs and penalties associated with the asymmetry.

Armed with the results of the calculations the Ohio University team with the Mark III Minilab flew to Los Angeles in a Beechcraft Model 36 to investigate further a solution to the localizer problem. Tracking equipment, viz, a Warren-Knight Radio telemetering theodolite and a Reaction Instruments telemetry transmitter were taken along for providing the ground-based references. An IFR 401-L signal generator was carried on board each flight and used as a transfer standard traceable to the National Bureau of Standards.

A review of FAA flight check data was accomplished for Runways 6L and 24L localizer course structures. The fortuitous existence of these localizers permitted examination of effects of the critical reflectors on these

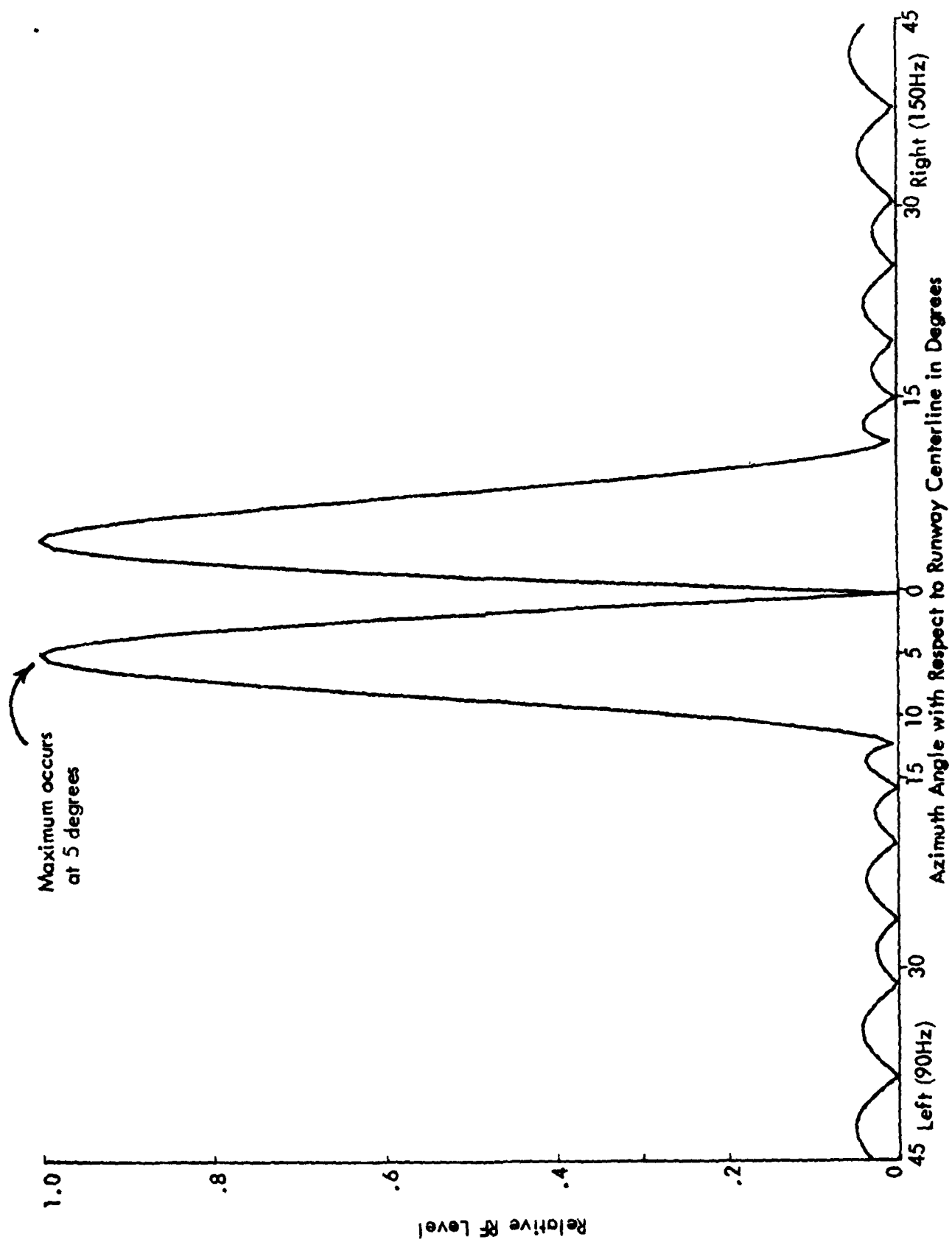


Figure 2-11. Calculated Side-Band Only Pattern for the Wilcox Category III Localizer.

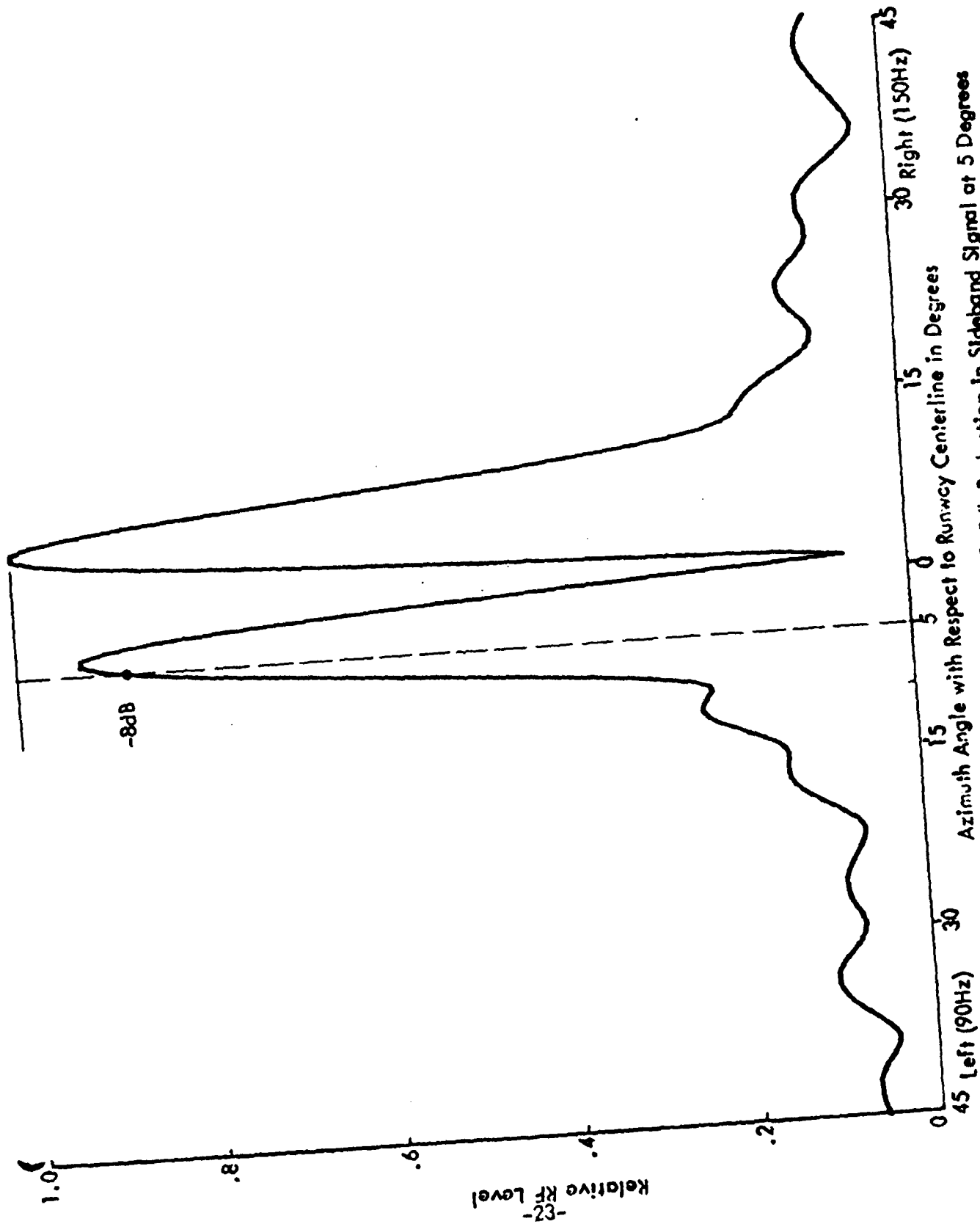


Figure 2-12. Calculated Pattern Showing 1.2db Reduction in Sideband Signal at 5 Degrees Azimuth when 60 Degrees of Phase Delay has been Inserted in Feed Lines to Antennas #4, #5, #6, and #7 on the 90 Hz Side

signals. The reflector which is suspected as causing the problem for 24R certainly must exist for the opposite runway. The records for the localizer course structure for runway 6L show a 5-microampere scalloping between the middle marker and the threshold which has a similar character to that observed on the other end. Because it serves only Category I requirements, this roughness is of no concern for operational purposes; however, it does support the hypothesis that the hill surface approximately directly across from the transmissometers is the problem. The localizer for 6L is a 14-element, log periodic, dipole array.

The localizer array serving runway 24L, 700 feet to the south is a V-ring type. This system is closer to the complex of hangars, fuel storage tanks, and miscellaneous buildings. The significant finding from analyzing the record of course structure for this localizer is that there is 6 to 7 microamperes of incoherent course noise suggesting that there are multiple sources of the reflection and that they are illuminated to a greater extent than is the hill north of the runway complex.

Initially, measurements of localizer antennas impedance were made and all antennas were found to be well within tolerance. All transmitter and feed parameters were found to be very close to nominal.

Flight measurements were then made of the course structure and of the array pattern for the sidebands (SBO) of the course array. The SBO pattern was found to be normal, whereas, the course roughness in Zone 3 was found to ± 5 microamperes (see figure 2-13).

This information, in effect, confirmed what had already been reported by the FAA. The data were repeatable; signal strength recordings gave evidence that the array was performing according to the design.

The next step was to make some calculations to locate the position of a hypothetical, secondary source which could give reflections to produce the course roughness that was observed. As can be seen from figure 2-13, the roughness is regular in character. The period was measured to be 2000 feet and centered 12,725 feet² from the transmitting antennas. See figure 2-14.

The energy coming to the central region of the reflector, which must be regarded as in the far field, can be depicted as shown in figure 2-15. From this the path lengths to produce one wavelength of phase difference may be calculated as follows:

$$d = (R_2 - R_1) - (R_2 - R_1) \cos \alpha$$

This must be equal to one wavelength, viz λ .

²Calculated by adding 2800 feet from array to stop end of runway 24R, 8925 feet as length of runway, to $\frac{1}{2}$ the 2000-foot period.

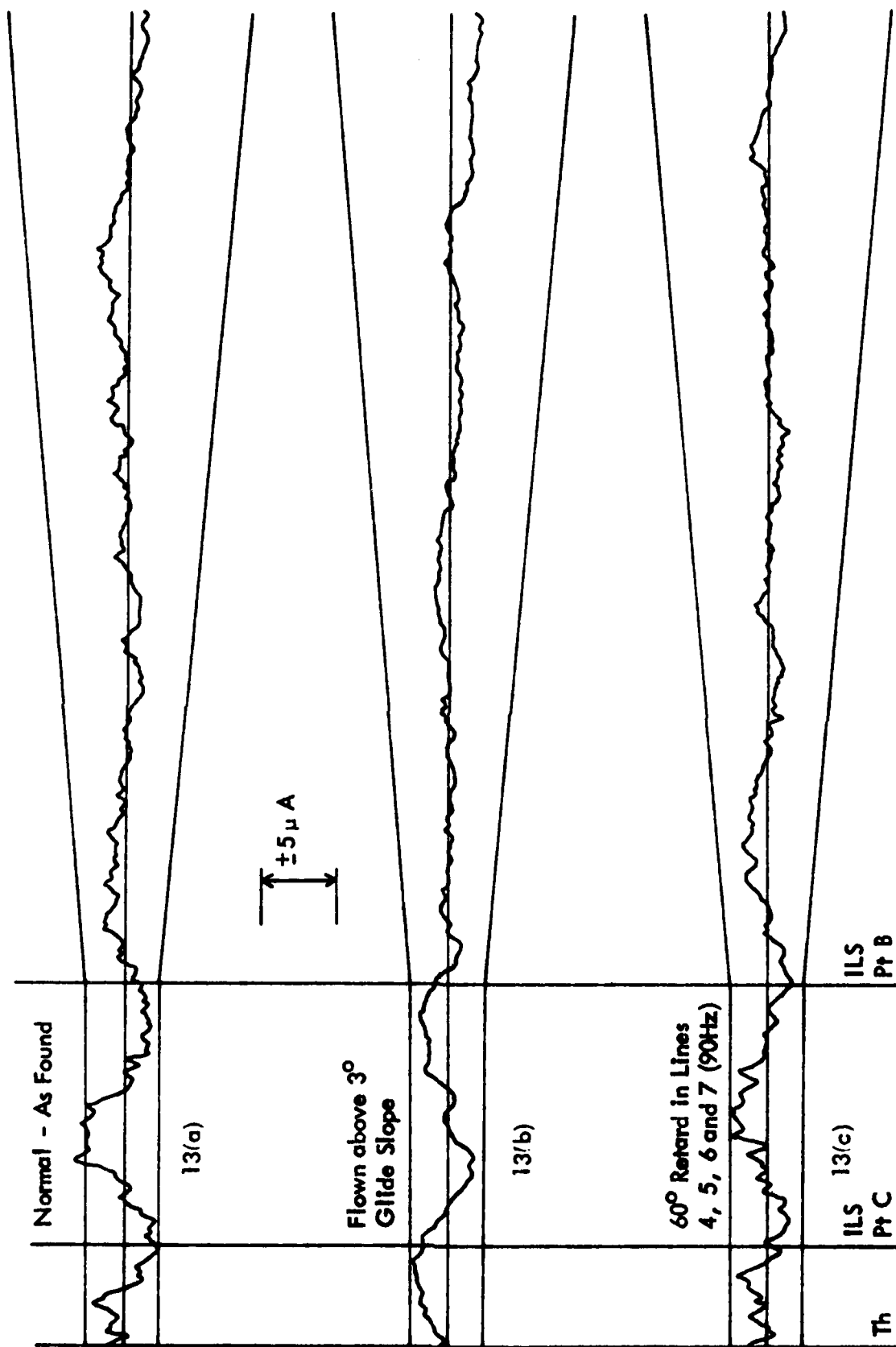


Figure 2-13. Three Flight Recordings Revealing the Small but Significant Path Perturbation Between ILS Points B and the Threshold. A small reduction in amplitude is found if the approach is above the glide path or if delays are introduced into 4 of the feed lines to antennas.

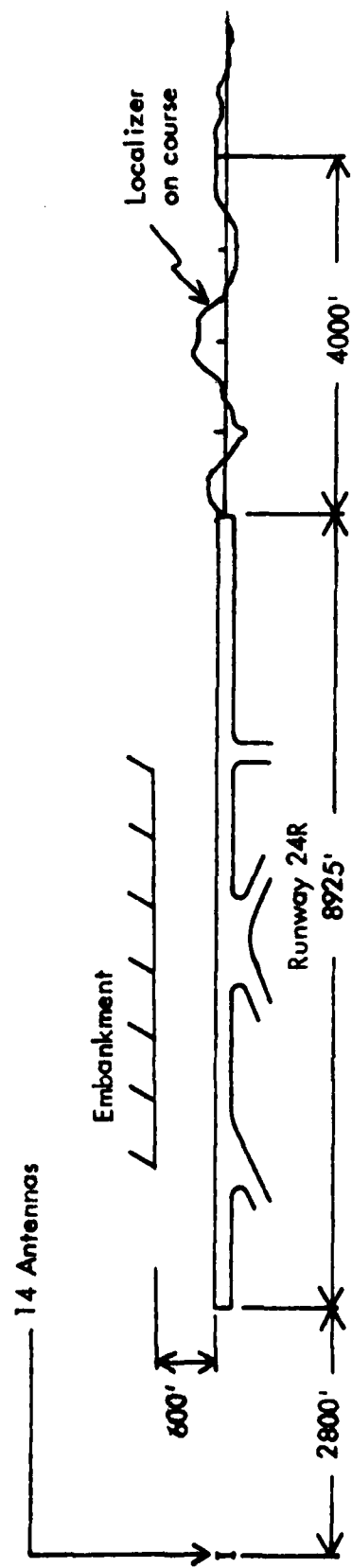


Figure 2-14. Layout Configuration of Runway 24R at Los Angeles International Airport. A pictorial representation has been provided to show the location of the roughness in the course structure.

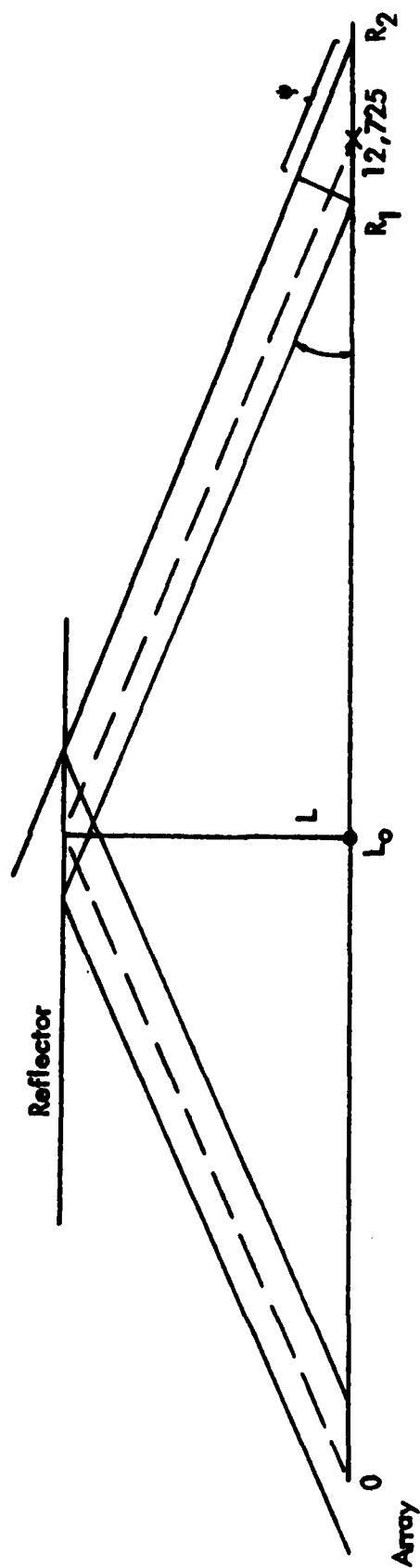


Figure 2-15. Geometries Associated with Calculation to Determine a Location of the Hypothetical Reflector.

Noting that $R_2 - R_1 = 2000'$, the spatial period, this becomes

$$\lambda = 2000(1 - \cos \alpha)$$

Solving for α with an operating frequency of 108.5 MHz gives

$$\alpha = \cos^{-1} \frac{2000 - 985/108.5}{2000} = 5.46^\circ$$

This means that the grazing angle is 5.46° . To find how far the central portion of the reflecting area is displaced from the runway centerline the following calculation is made. Noting figure 2-15 again,

$$L = L_0 \tan \alpha$$

$$= \frac{12725}{2} \tan 5.46 = 608 \text{ feet, the displacement from centerline}$$

These calculations indicate that the hypothetical, reflecting object producing the course roughness observed is 6362 feet down the runway from the array (3562 feet from the stop end) and 608 feet to the side. The character of the roughness, i.e., the rather uniform sine wave indicates that there is a high probability that it is a single, specular-type reflector. The low value of the magnitude of the sine wave indicates that the quantity of the reflected energy is not great since the direct signal being received at the elevation angle of 0.47° is of low magnitude. It should be recalled that the ratio of the magnitudes of the reflected and direct signals determine the amplitude of the scallop.

A visual inspection of areas 600 feet either side of the runways, approximately 6362 feet from the localizer antenna array revealed only transmissometers and taxiways on the south side but a 20- to 30-foot high earth embankment 600 to 650 feet from centerline exists on the north side with a bare, nearly vertical, smooth surface. Figure 2-16 shows this terrain feature.

To aid in confirming the cause of the course roughness, a calculation was made using the mathematical model of the localizer which was originally developed for determination of critical areas. These are defined to be areas where, if reflecting objects such as large aircraft exist, course perturbations will be produced. Based on the observed roughness and the previous calculations for location of the reflector, a hypothetical vertical planar reflector, 40 feet high, 500 feet long, was positioned with its center 608 feet north of the runway centerline point, 6362 feet from the array. Figure 2-17 shows the results of the calculations. The scalloping can be seen to be in precisely the same location as that measured and has an identical period. The amplitude is about 3 db smaller but this is not significant since the reflector is not intended to be a precise replica of the earth embankment.



Figure 2-16. Photograph of Embankment 600 to 700 Feet From the Runway On the North Side
Approximately 6300 Feet from the Stop End of Runway 24R.

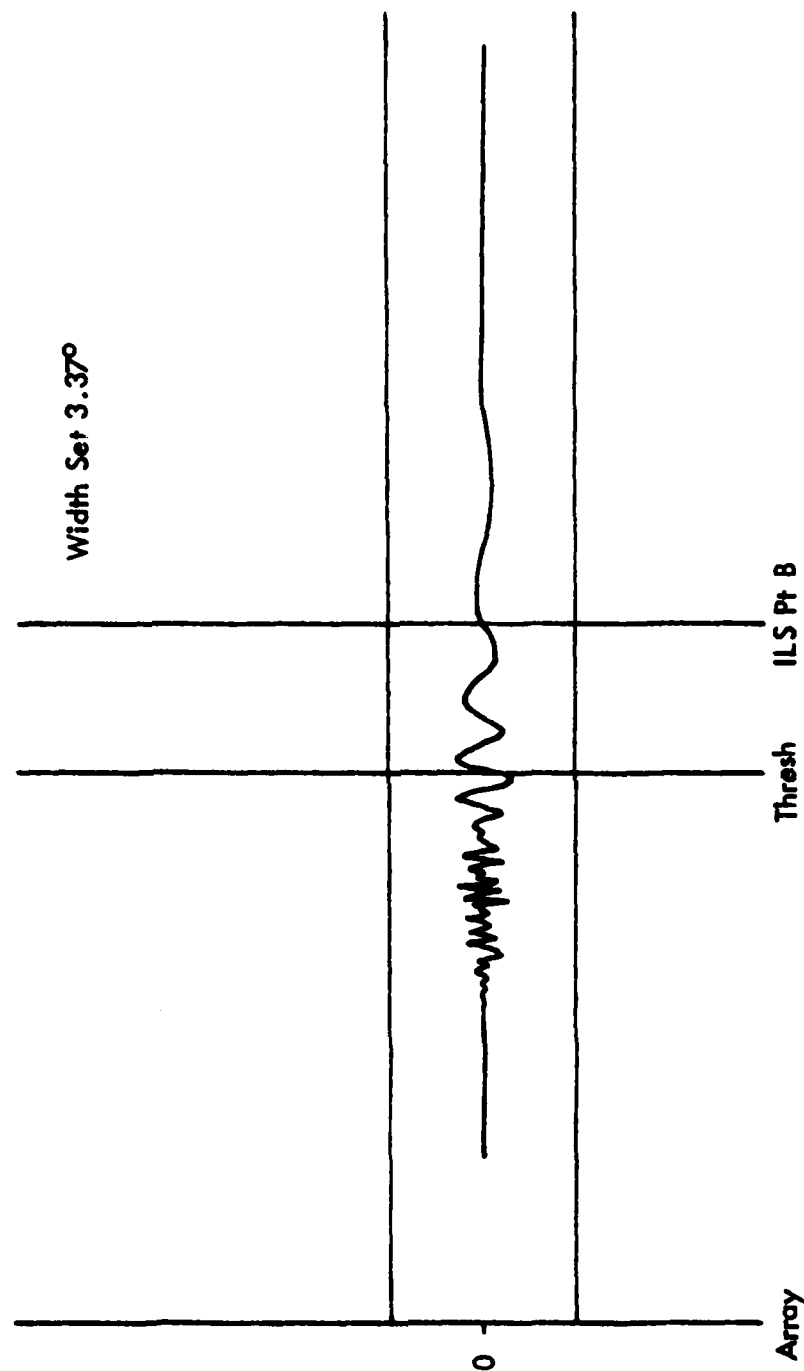


Figure 2-17. Calculated Course Structure produced with a Willcox Category III Array with a Reflector 500 Feet Long, 40 Feet High, 608 Feet North of the Centerline of the Runway, 6362 Feet from the Array. Peak excursions are 2.5 microamperes located in Zone 3. The period is precisely the same as measured and shown in Figure 2-13a.

DISCUSSION OF POSSIBLE SOLUTIONS.

Having identified there is a high probability that the earth embankment is the cause of the localizer course roughness problem, consideration was given to means for eliminating the problem. Following is a listing of possible solutions with comments concerning desirability and practicality.

A. Alter Array Radiation Patterns. The crucial radiation pattern to be considered is the sideband-only pattern for the course array. Both theory and measurements support this. Calculations were made using the IBM 370 computer at Ohio University to determine if significant reduction in the energy incident on the embankment could be made by changing the phase of the excitation of the course portion of the two-frequency array. Calculations indicated that when 60° electrical phase delay was introduced in the lines feeding antennas numbers 4, 5, 6 and 7 on the 90 Hz side, an asymmetrical pattern was produced with a net reduction in energy on the north (150 Hz) side. Side effects on path symmetry and course shift were of concern; however, from the calculations it appeared that compensation with tone balance could be provided for the course shift and the symmetry remained satisfactory. This solution was considered as sufficiently viable that the array feeds were modified and flight measurements made.

B. Increase Amount of Vegetation. Certain types of vegetation can be effective as absorbers of electromagnetic energy. Some trees exist but very little vegetation in the form of shrubs exist principally because of the lack of moisture. Apparently, only eucalyptus trees thrive. They contain very little moisture; consequently, they are not effective absorbers. Existing trees should be retained for what benefit they do provide. Increasing the amount of vegetation to shield the hill is not considered practical because of the time and expense required, and further, the lack of rainfall would permit only poor absorbers to survive in that region.

C. Install Electromagnetic Absorbing Material. Ten years ago the FAA supported an investigation of development of electromagnetic absorbers that were produced by the Avco Corporation. Consideration of these was given, but cost, availability, and installation provided rather overwhelming factors such that the penalties are too great.

D. Install A More Directive Array. Currently, the FAA has under development a wide-aperture array. This is follow-on work that was begun by the Alford Company in the early 1970's and was known then as a 22-8, two-frequency array system. Ohio University participated then in the two-frequency array development and is currently involved in the evaluation of two arrays, one designed by the Wilcox Electric Company and the other by Dr. R. W. Redlich of Athens, Ohio. Measured patterns, especially with the Redlich array, indicate that SBO (sideband only) radiation would be reduced by 3 db on the hill and this would produce sufficient improvement to bring the course roughness within tolerance. Fortunately, the new arrays make use of the same number and type of antennas (14-log periodic antennas) that exist with the Los Angeles Category III site. The aperture, however, is extended from 86 feet to 121 feet. Unfortunately, the monitor development

has not been completed and an immediate solution, therefore, is not available with the wide-aperture array.

E. Installation of Screens. Historically, the FAA has used screening methods to improve ILS course quality. Screens in principal can be placed on a reflecting surface to reflect and refract the signals and thus, hopefully, minimize the magnitude and coherence of the original multipath signal. Screens have the advantage that they can be fabricated locally and usually installed in a straightforward manner. The disadvantages are that they must be maintained, they are not monitored except by visual inspection and they do not perform in the manner that is predicted easily by simple ray techniques. As a result, intuition does not work well. Diffracted signal must be taken into account for any accurate prediction. In the case of 24R, the measurements show the reflecting object must be singular in nature and regular. The addition of a sufficient area of screens will tend to reduce the regularity of the principal reflecting surface. The results should reduce peak amplitudes. Screens for the near-vertical surface north of Runway 24R may be hard to install and stabilize simply because of the steep slopes. Screening appears to be more art than science unless a major modeling effort is accomplished.

F. Earth Contour Change. The calculation has permitted identification with high probability an area which is serving as a reflector. A good approach is to change the contour of the earth reflector located in the identified area. (See figure 2-14.) This modification can be done in a straightforward manner using common earth-moving techniques. Because an irregular surface is desired, no particular care is needed to produce the desired contour. The objective is to make the surface rough (in terms of wavelength which is approximately 9 feet) and make the general slope at an angle that is not parallel to the localizer on-course plane. It is unfortunate that the course roughness that is now present occurs in the region of tightest tolerance; however, a change in the general slope of the reflecting surface may move roughness to another region of the course which will not be as critical with respect to tolerances. Roughness will make the reflection less coherent and will tend to reduce peak amplitudes of the roughness that presently exists. A drawing is provided in appendix A which suggests a specific contour modification.

G. Scarify the Reflecting Surface. The signal that is being reflected is apparently coming from a singular smooth surface as evidenced by all of the flight recordings. Scarifying the surface, i.e., cutting grooves running approximately 3 feet deep vertically on the slope and spaced 6 to 9 feet apart would destroy the coherence of the reflected signal and permit a reduction in peak amplitudes of the scalloping seen in the course structures.

MEASUREMENTS AND DISCUSSION OF DATA.

As mentioned earlier, the initial measurements were expressly for the purpose of confirming FAA flight checks but using a ground-based reference instead of an inertial platform. These were completed successfully (figure 2-13a) to show that the course roughness did indeed repeat and the radiation patterns were as predicted by array design. Lacking other information, a logical suspect for a source of course problems was deficient performance of the array such that obstacle reflectors were unintentionally illuminated. This was found certainly not to be the case.

The course structure was measured with the flight track above the glide slope by approximately 0.7° . The expectation was that the path roughness would decrease because the direct signal would increase with altitude due to the transmitter array (with image) pattern; whereas, the reflected signal could be expected to have rather uniform signal strength with altitude. The change in the ratio of reflected to direct signal from normal would be expected to decrease. The roughness was found, in fact, to decrease. (See figure 2-13b.) A below-glide-slope run was made, and this showed an increase in roughness, again consistent with the hypothesis.

A measurement was made to determine if reducing sideband power, which takes place in going to broad alarm condition, would result in reduced structure roughness. The measurement by Ohio University showed a very slight reduction but FAA measurements had documented that roughness decreased and was within tolerance at broad alarm.

Measurements were made of the condition of the array when four of the feed lines on the 90 Hz side (#4, #5, #6, and #7) were delayed 60° . This was motivated by the calculations; the results of which were produced in figure A-2 (appendix). Improvement was noted in the course roughness. Specifically, the peak amplitudes that were measured dropped to 3.5 microamperes as revealed in figure 2-13c. Although this reduced the roughness within tolerances, the margin was only slightly more than one microampere, and to achieve nominal course alignment, modulation percentages had to be moved to approximately 19 and 21 percent which is at the tolerance limits for Cat III operation. Calculations for this condition made after the flight indicated that there was only a 10% improvement (reduction available); whereas, the measurement had shown 30%. This discrepancy points to an important issue of the ability to measure or resolve one microampere in a DDM space pattern. Clearly, it is difficult to repeat precisely such measurements.

Plots of AGC values representing signal strength for normal and for an asymmetrical condition using delays in lines #6 and #7 are shown for reference purposes. See figure A-3 (appendix). An AGC trace is not available for the condition with the 4 lines delayed.

RECOMMENDATIONS.

Some recommendations are in order which, if followed, are intended to provide for a solution to the localizer course roughness problem on Runway 24R.

1. The upper 18 feet (2 wavelengths) should be cut from the face of the reflecting wall of the earth which extends critically some 300 feet parallel to Runway 24R, 650 feet north. This can be expected to reduce the magnitude of roughness to less than 50% of previous values and provide an in-tolerance condition which can be maintained.

2. Scarifying the remaining surfaces with 36-inch grooves spaced 6 to 10 feet apart will provide additional insurance for minimizing multipath problems.

3. Trees now existing at the foot of the embankment north of the runway should be allowed to remain. Although they are dry in character, they are more of an absorber than they are a coherent scatterer and therefore, provide a net benefit to localizer operation.

4. Additional recommendations are contained in reference OU/AEC/EER 55-1.

INVESTIGATION OF ANOMALOUS PERFORMANCE OF THE INTERNATIONAL FALLS NULL
REFERENCE GLIDE SLOPE.

SUMMARY AND CONCLUSIONS.

Over the past few years the glide slope at International Falls, Minnesota, has been found by FAA Flight Inspection to be in and out of tolerance from one flight check to the next, thus requiring restrictions. An evaluation was performed by Ohio University to determine why a change/reversal in the slope of the glide path in Zone 2 does not meet tolerances. Further, a review of FAA flight-check data was performed with the end objective of all work being to identify the problems and make recommendations as to possible solutions. Sufficiently detailed topographic data was not available for a thorough mathematical analysis; however, complete flight data was obtained for several system configurations, these data being obtained using an optical reference system and equipment calibrated with traceability to the National Bureau of Standards.

The conclusions reached are as follows:

1. The glide slope structure at INL is indeed marginal with respect to established FAA flight-check tolerance limits. Only by applying the allowable exception of 354 feet out of 7089 feet can the structure be considered marginally within tolerance.
2. There are two distinct structure problems with the path. First, there is a 0.16° , rather rapid change in the path angle in the Zone 2 interval. Second, on top of this aberration is some high-frequency scalloping. When additive, these produce a marginally in-tolerance condition at best. When made subtractive by lowering the path angle to shift the angle transition point closer to the threshold, the path is in tolerance limits.
3. Measurements show a lower path angle of 2.8° gives a structure which is 83% of tolerance limits.
4. The large scale aberration in the path structure is logically a result of a multi-level ground plane. Both theory and flight measurements support the concept that an effective two-level ground is present in forming the path. The farther level would be the lower. Also, both theory and measurements indicate that the path-angle transition zone migrates closer to the antennas when the path is lowered. Measurements of the vertical structure reveal reversals which are a typical result of a multi-level, path-forming ground.
5. Small-scale scalloping, most probably, is coming from the woods approximately 800 feet southwest of the approach path, 1000 to 2000 feet out from the glide slope.
6. There is a reasonable probability that the small scrub-tree growth in the area directly in front of, and 1000 feet beyond, the transmitting antennas contributes to path roughness.

7. In addition to the scrub growth, the trees in the woods have grown taller over the past 10 years, and these subtend a 2.0-degree angle from the glide-slope site. This elevation angle of the woods interface has increased in size over the past years which allows for greater reflection of signals to degrade the path structure.

8. FAA flight data from periodic checks do not show consistently an effect which could be ascribed to the trees. There is no good seasonal correlation.

9. Runway widening was accomplished by adding only to the southwest (glide slope side) thus moving the new centerline southwest. As a result, the flight measurements are now being made closer to the woods (reflector). These tracks tend to produce greater perturbational effects.

10. From flight data obtained on this mission, reversals in the structure are not an issue in meeting tolerances. The shift from one path angle to another gives, initially, a prime concern for a reversal but the necessary second portion of the trace to form the reversal is not inherently forthcoming due to the ground plane. Roughness from a secondary source may contribute somewhat to an appearance of a reversal but traces do not meet the criteria specified in FAA Flight Inspection Manual 8200.1 217.42 (reference 6).

INTRODUCTION AND BACKGROUND.

Falls International Airport, International Falls, Minnesota has had an ILS glide slope serving Runway 31 for approximately 10 years (reference 7). In the last several years, FAA flight checks have placed restrictions on use below 1640 feet MSL, 456 feet above the airdrome, because of structure roughness which has shown variability from flight check to flight check. Ohio University was asked to examine the path characteristics through special measurements using optical tracking references and evaluate the performance of the facility. Specific interest was expressed in an observed change/reversal in the shape of the glide slope in Zone 2. On June 7 and 8, 1982, an Ohio University team traveled to International Falls and made a series of measurements. Low ceilings hampered measurements the first day; however, conditions improved to near-perfect conditions on the second.

Topographic charts (reference 8) were available and the Ohio University Math Model was used for calculations. Unfortunately, the detail on these was insufficient to allow useful predictions to be made. The investigation, therefore, was principally experimental in nature.

The glide slope at International Falls is a null-reference type operating on a carrier frequency of 331.4 MHz. The transmitting equipment is a Mark I-A with original antennas having been replaced with bays of three Meridian-type, curved-dipole antennas with one-half egg-shaped radomes. Figure 2-18 shows the bay of antennas serving as the carrier antenna.

As a part of the work effort, a review of the history of glide slope performance was accomplished through the use of a series of flight check recordings which were furnished by the Great Lakes Region. This history was particularly important because of some environmental changes, one being the temporary location of a batch plant relatively near the threshold. By the time the measurements were made by Ohio University, this plant had been removed and, except for a small shelter for approach lighting power, the general area was free from man-made obstructions.

When considering environmental changes which have taken place with time, one immediately recognizes that the earth from 1000 to 2000 feet in front of the glide slope, which was formerly scraped clean, now has considerable scrub growth appearing. In addition, a boundary with a woods has become much more pronounced because some of the trees have grown to an estimated height of 100 feet and subtend an angle from the glide slope of approximately 2° .

Some of the described conditions are illustrated in the figures. Figure 2-19 shows the apparently relatively good terrain extending outward from the glide slope mast to provide the reflecting plane. Figure 2-20 is an aerial view of the site looking southwest and reveals the obvious discontinuity near the reflecting zone caused by the wooded area just to the southwest of the approach path. Figure 2-21 best illustrates the nearly linear (planar) interface the large woods makes with the space on the northeast side. From this figure also can be seen the area of scrub growth

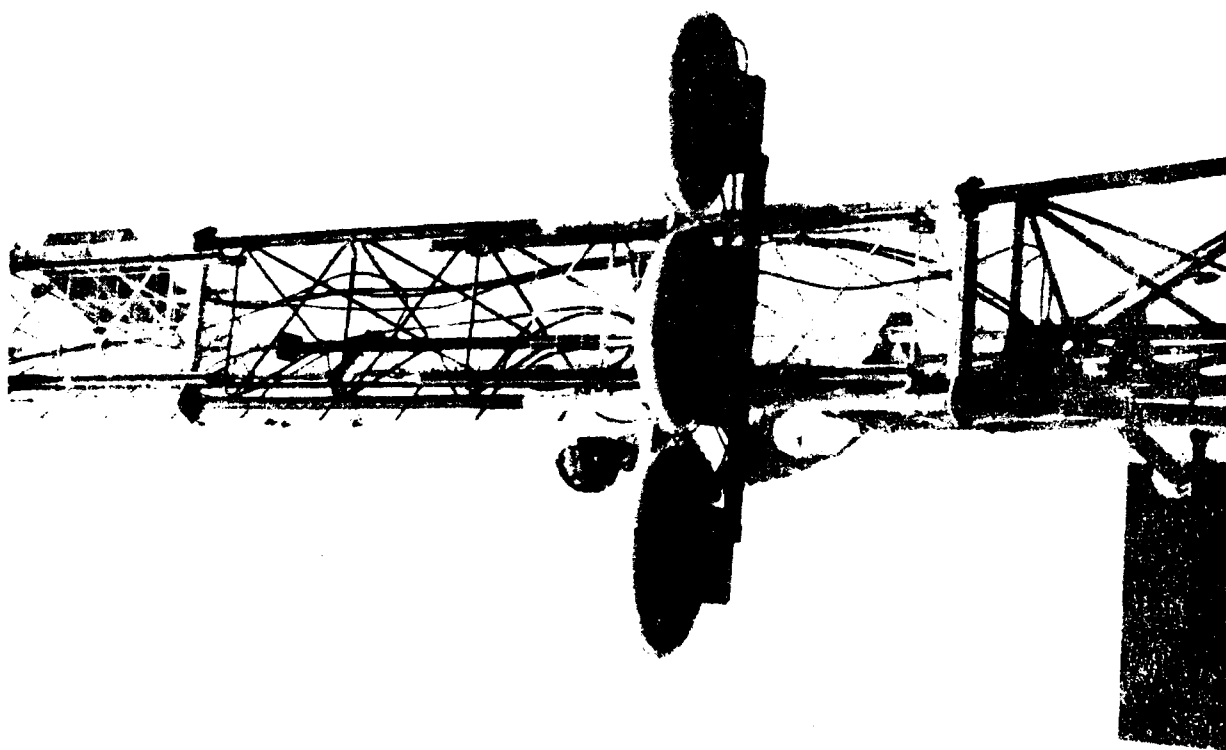


Figure 2-18. Photograph of Lower Bay (Carrier Antennas) for the International Falls,
Null-Reference Glide Slope Array.

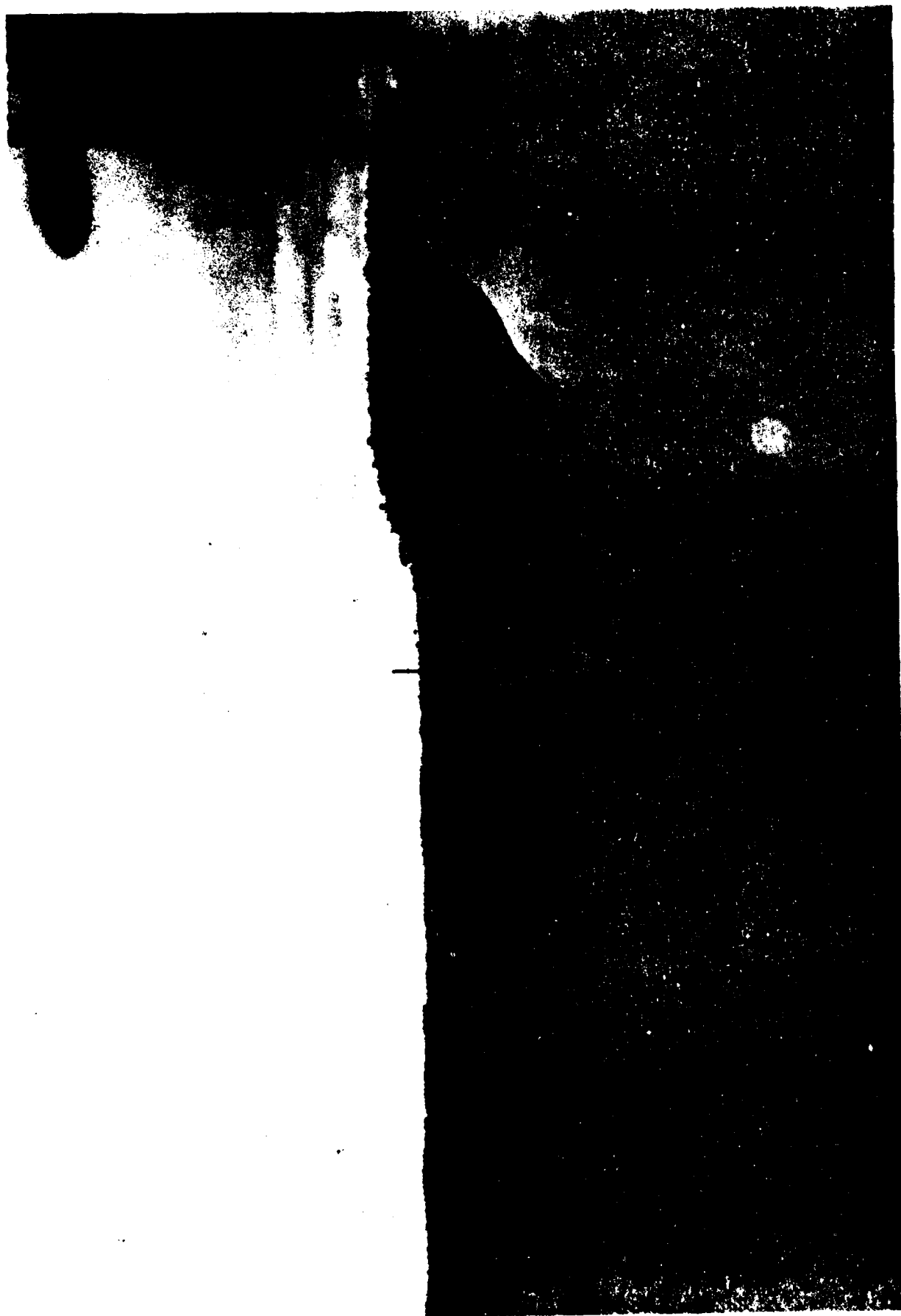


Figure 2-19. View of Terrain Forming the Reflecting Plane for the Null Reference
Glide Slope at International Falls. The wooded areas can be seen
in the right hand section of the photograph.



Figure 2-20. Aerial View of the Glide Slope Site Looking Southwest. The photograph was taken when the aircraft was directly abeam the wooded area which is believed to be the source of some of the spurious multipath signal.

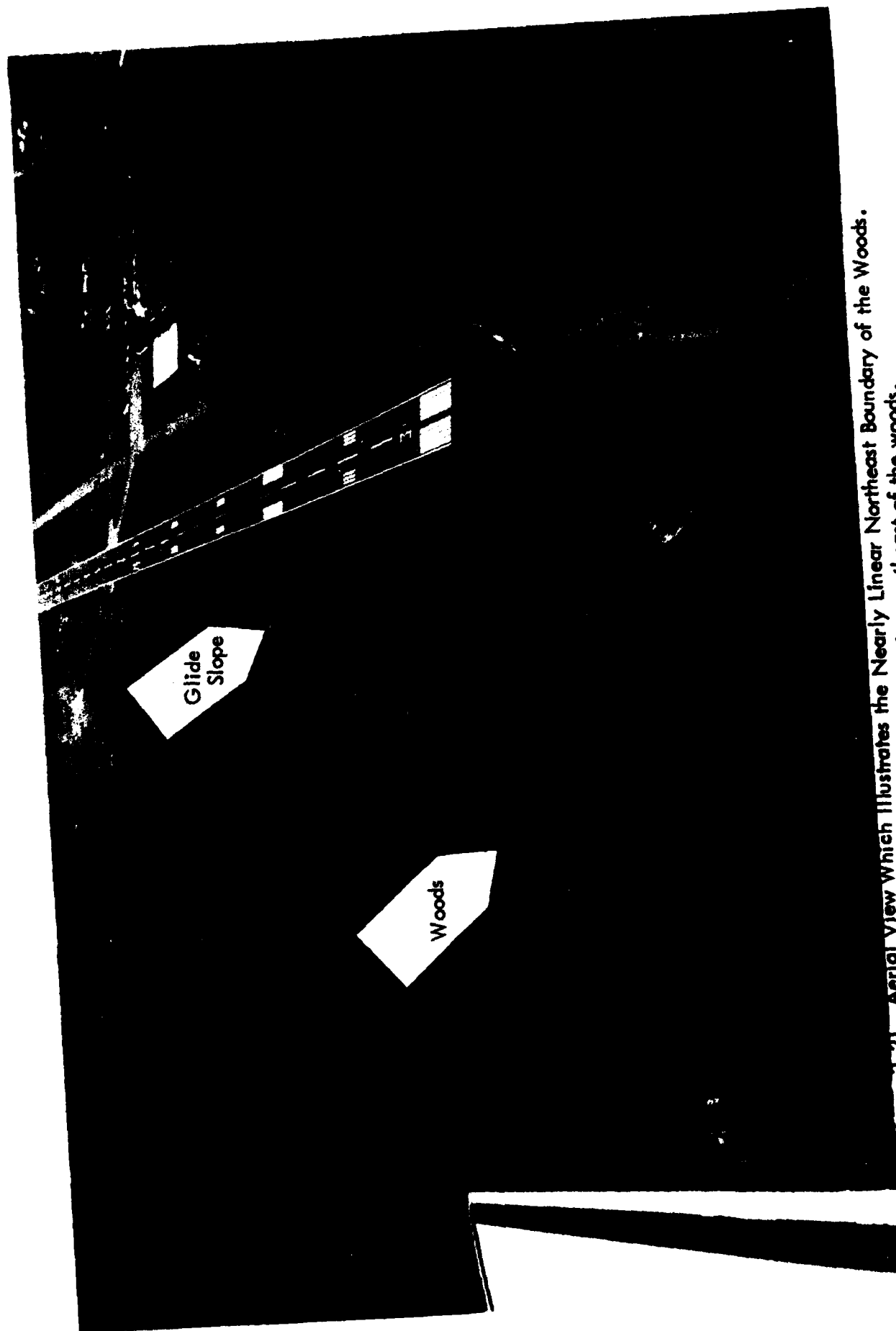


Figure 2-21. Aerial View Which Illustrates the Nearly Linear Northeast Boundary of the Woods.
Shown also is the scrub growth appearing northeast of the woods.

which has appeared over the years. Personnel acquainted with the site during its entire history tell that these scrub trees were not present at commissioning.

The principal objective of the work effort was to determine the problem or problems which were preventing the ILS glide slope from being unrestricted and to recommend changes which could be implemented to give a quality facility. The experiments performed dealt with changes which were intended to yield data that would help identify sources of the structure problem.

DATA COLLECTION AND DISCUSSION.

A major part of the work effort was the flight data collection involving four different glide-slope configurations (one being the original). All airborne data collected was accomplished using the Ohio University Minilab Mark III flown in a Beechcraft Model 36 aircraft. The equipment was calibrated by an on-board IFR 401-L signal generator standard traceable to the National Bureau of Standards through the Ohio University FAA-Approved Repair Station C07-10. Ground references were obtained through the use of a Warren-Knight Model WK83 theodolite radio telemetering at a location surveyed consistent with FAA Flight Inspection Handbook 8200.1 217.25. A Reaction Instruments telemetry transmitter was used to uplink the angular reference. A total of 26 flight records were obtained during 5 hours of flight time over a 2-day period.

The data taken represents 4 different configurations of the glide slope. These are as follows:

1. NORMAL - This is the system as commissioned with a 3° angle. Figure 2-22 is a representative structure obtained with the glide slope in normal configuration. All differential amplifier traces for normal conditions exceeded tolerance limits in Zone 2 with high frequency oscillations superimposed on a major path angle shift of $.15^\circ$. The excess-of-tolerance conditions are very brief and occur at a distance of 6500-7000 feet from threshold. The tolerance values given in the U. S. Flight Inspection Handbook 8200.1-217.5-10 are mitigated by section 217.41 to allow marginally acceptable structure conditions to be evident.

Figure 2-23 shows the vertical structure with three reversals. These suggest the existence of distinctly different ground levels in the reflecting plane (reference 9).

2. OUTER ANTENNAS DUMMIED - The two outer elements on both the lower and upper antennas' bays were dummiied, only the center element radiating. The rationale for implementing these antenna conditions was to eliminate the azimuthal directivity produced by the three-element arrays thus providing greater illumination in the direction of possible reflecting objects, in this case, specifically the woods interface.³ If the woods, for example, were providing for spurious multipath, the path structure should worsen. The results shown in Figure 2-24 clearly show a worse structure. In fact, it is the worst structure recorded at International Falls.

3. ANTENNAS COCKED - The upper and lower antennas were shifted

³Using the method outlined in Appendix 2-4 of FAA Order 6750.16A dated August 18, 1973, calculations show an offset of a reflecting surface 600 to 725 feet from centerline depending on the length of the spatial period used. The uncertainty in determining the short period of the scallops was due simply to available precision in determining range using overflight of check points.

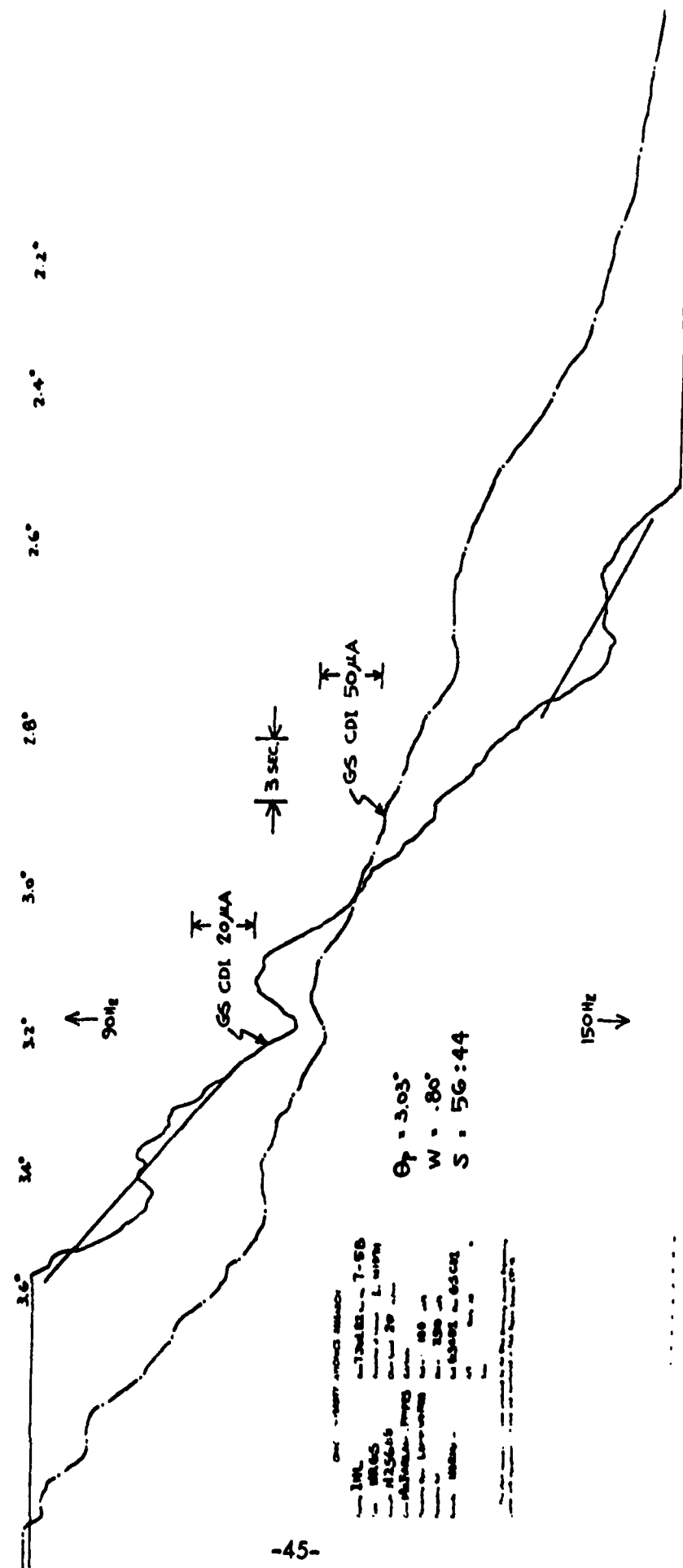


Figure 2-23. Flight recording showing the vertical structure of the International Falls glide slope under normal conditions. Normal operating width has been reported historically as being left broad. The reversals shown suggest a ground plane which has effectively two different levels. They appear consistently above the on-course structure for the runs made at 1000 feet AGL.



Figure 2-24. Flight recording showing the differential amplifier trace representative of the structure produced when the azimuthal directivity of the carrier and sideband antennas is reduced. The outer antenna elements of the three element bays were dummed thus allowing for greater illumination of the woods area. An out-of-tolerance, unacceptable condition is evident late in Zone 2. The vertical path width was maintained at 0.78° to be consistent with the other conditions measured in this series of experiments.

forward 7 inches away from the mast on the side farthest from the runway. This is shown in figure 2-25. This cocked the antennas to approximately a 20° angle away from the woods. If the woods are a source of reflection, then the magnitude of roughness should decrease. Figure 2-26 shows the structure that has reduced high frequency oscillations, and this further supports the hypothesis of the woods being a contributing factor. Table 2-2 allows a quick comparison of the three-antenna conditions, viz, normal, reduced directivity and different direction of aiming. Peak-to-peak numbers refer to high frequency oscillations; whereas, the microampere values for the excursion relate to the long period path shifts.

4. LOW PATH ANGLE - The upper antenna was moved up 19" to lower the path angle to 2.80° . Because good path conditions were obtained at commissioning when a 2.8° path was established, a return to this lower path angle was accomplished in order to determine the path angle effects on structure with environment conditions constant. The long period oscillation is changed which, in effect, gives path-angle change at a different location along the approach path. This is consistent with theoretical considerations. Importantly, the high frequency path disturbance does not change appreciably in space, thus producing its effect in a different portion of the long wave pattern. The result is that tolerance limits are not exceeded; in fact, only 83% of the limit is reached. Figure 2-27 demonstrates the results. While in this configuration, a structure run was made several hundred feet from centerline on both the left and right sides of the runway. From fundamental electromagnetic theory dealing with multipath signals, it is known that the frequency of the scalloping or oscillation caused by multipath is directly related to the spacing of the reflector from the line joining the observer and the source. Accordingly, flights were made approximately 400 feet either side of the centerline to check the effects of the multipath glide-slope indications obtained on those tracks. Figures 2-28 and 2-29 show the results of these two measurements respectively.

Clearly, the character of the path perturbations are changed. Flying closer to the woods increases the spatial period and increases the magnitude with a peak-to-peak value of nearly 80 microamperes; whereas, flying farther away decreases the period to the point of indicating high frequency scalloping. This is consistent with the hypothesis of the woods being the source of reflections.

A summary of the structure characteristics for each configuration of the glide slope along with the nominal path data as measured on a level run is presented in Table 2-3. The numbers are taken from the average of all level runs made in each configuration.

In summary, the facility shows the most improvement with respect to tolerance limits when the path is lowered to 2.8° . This is mostly due to the region of path angle change shifting towards the threshold. The benefit is somewhat counter-balanced by the path shift that is introduced near ILS Point A which reaches 90% of tolerance. Similar reduction in the peak-to-peak amplitude of the path deviation is obtained by decreasing the



Figure 2-25. Photograph of Antennas Being Cocked Approximately 20 Degrees Towards the Runway and Away From the Woods.

REF. FIG.	CONDITION	RUN NUMBER	PEAK- TO-PEAK	EXCURSION
2-22	NORMAL	7-6A	28 μ a	52 μ a
2-24	DUMMIED Reduced Azimuth Directivity	8-2A	37 μ a	66 μ a
2-25	COCKED Change in Aiming	8-8A	21 μ a	47 μ a

Table 2-2. Comparison of Path Structure Values
for Three Antenna Conditions.

Run No.	Zone 2 Excursion	Zone 2 % of Tolerance Structure	Zone 2 Average Path Angle	Path Angle	Width	Symmetry	Structure Angle	Condition
7-6A	52 μ A	113%	3.01					Normal
7-7A	50 μ A	110%	3.01	3.02°	.79°	60:40	2.26°	Normal
7-8A	53 μ A	110%	3.01					Normal
8-2A	66 μ A	150%	3.04	3.00°	.78°	62:38	2.16°	Dummy Outer Antennas
8-3A	56 μ A	130%	3.01					Dummy Outer Antennas
8-8A	47 μ A	103%	3.07	3.02°	.68°	66:34	2.36°	Antennas Cocked
8-9A	48 μ A	100%	3.04					Antennas Cocked
8-14A	53 μ A	100%	2.81					Low Path Angle
8-15A	48 μ A	80%	2.80	2.81°	.73°	53:47	2.08°	Low Path Angle
8-17A	63 μ A	123%	3.06					Left Side Rwy
8-18A	47 μ A	123%	3.06					Right Side Rwy

Table 2-3. Summary of Data.

contribution or concentration of energy from the tree line area such as cocking the antennas, using the far edge of the glide path, or using the normal directional configuration of the antennas.

RECOMMENDATIONS.

The following recommendations are made based on a review of the historical data for International Falls, discussions with involved technical personnel, theoretical considerations, flight data obtained during a site visit in June 1982, and inspection of the glide-slope site and environment.

Scrub-tree growth should be removed from the area serving as the first fresnel zone for the glide slope.

To correct the fundamental path problem, i.e., the two-angle path, the recommendation is either to convert to a capture-effect system to minimize dependence on vast expanses of ground plane or to grade the earth in the first fresnel zone such that a uniform slope exists.

To correct the problem of high frequency scalloping, the height of the trees in the woods should be reduced, the antennas should be cocked towards the runway, or more directional antennas used. A more irregular interface on the wooded area would also aid in minimizing scalloping effect.

AN EVALUATION OF LOCALIZER PERFORMANCE AND CAUSES OF DEROGATION AT SAN FRANCISCO INTERNATIONAL AIRPORT.

INTRODUCTION AND BACKGROUND.

In 1973-74 the FAA installed one of the first Category-III, Texas Instruments ILSs on Runway 28R at San Francisco International Airport. This system produced localizer and glide slope course structures that were not ideal but were within tolerances. The engineering report by TI written in 1973 prior to the installation indicated that the system might not meet tolerances. Flight check records are not any longer available but obviously tolerances were met and commissioning as Category-III was accomplished; however, in July 1981 FAA flight check found the system marginal and initiated downgrading action. This motivated a review of details and after inter-group consultations in the FAA, the use of averaging techniques specified in USFIM 8200.1 allowed Category-III status to be maintained.

Continuing construction on the airport has, during the past two years, increased the number of potential reflecting surfaces, some of which may be affecting localizer performance adversely. In November 1982 FAA flight inspection officially downgraded the system to Category-I based principally on glide slope performance. A careful study of localizer records following change out of transmission line components in November also indicated that the localizer was at best marginal and at times recorded out of tolerance. The localizer was downgraded to Category-II status with the ILS being down to Category I because of the glide slope.

Work has progressed on a change from the original null reference glide slope to a sideband reference type, and indications are that it will pass Category-II requirements, thus permitting the ILS to be established as Category-II. This is expected to be accomplished by early 1983.

The Texas Instruments parabolic-type localizer antenna has a 178-foot aperture and is designed specifically for airports having the potential of multipath interference. San Francisco International Airport has two parallel east-west runways. Fortunately, the one of interest in this study/evaluation is 28R and is the one farthest from the terminal complex. This means that a large number of buildings associated with the terminal are farther removed from the most critical areas. The terminal is located on the south side of the 28 runways.

On the north side of the runways there are few buildings. Unfortunately, however, one of these is very large. The American Airlines hangar is 550 feet wide, 450 feet long and approximately 120 feet high. It subtends the angle in azimuth from the localizer of 12.5 to 18 degrees on the north side. It is the obvious contributor to path derogation, and calculations do indeed show this to be true.

The objective of this work is to reduce the localizer course structure roughness to well below the tolerance limits of 5 microamperes for zones 3 and 4. Marginal conditions appear to have prevailed too long at San Francisco and patchwork measures are not considered the most desirable. A variety of measures are, nevertheless, addressed. Long experience permits the generation of concepts which could be beneficial but the tradeoffs must also be considered. In some cases, these tradeoffs are unacceptable and do motivate against the use of the particular approach. All of these are discussed in the following pages.

APPROACH.

Several discrete actions were taken to accomplish the evaluation of the anomalous course structure produced by the localizer serving runway 28R at San Francisco. For documentation purposes, this localizer is identified with the three letters GWQ operating with a carrier frequency of 111.7 MHz (nominal).

1. Available information was collected. Solicitations were made to FAA Headquarters and the Western Pacific Region to obtain historical data concerning operation of the GWQ localizer. Flight check recordings were obtained along with a report by Texas Instruments engineers who had planned installation of the parabolic-type localizer at San Francisco. This report, titled "Site Survey Report, Proposed Mark II San Francisco International Airport", is dated May 1973 and contains results of math modeling which took into account 19 cases involving various obstructions and combinations of obstructions which could be expected to affect localizer performance. Additionally, charts and photographs were collected to aid in the analyses.

2. Initiation of mathematical modeling programs was accomplished. Preparations for running the mathematical models on the Ohio University IBM 370 computer was accomplished. Special consideration had to be given for the San Francisco work since the calculations would have to take into account a large aperture antenna that was not comprised of a number of discrete elements.

3. An analysis of existing data was accomplished.

4. A site visit was performed. One purpose was to confirm existence of the various obstructions.

5. Participation in collection of special data not already available was accomplished. A radiation pattern representative of the SBO from the course array was critically needed to use in the math modeling effort. Experience shows that use of a measured pattern from the specific array being investigated gives superior results to those obtained when purely theoretical or generalized patterns are applied.

6. Interviews of involved personnel in the regional office and in San Francisco were accomplished. Considerable time was spent interrogating technical personnel involved with the GWQ localizer problem. Specifically, FAA regional and sector personnel along with flight inspection workers were questioned.

7. Needs for additional data were identified.

8. Plans of obtaining needed additional data were prepared.

9. Math modeling using measured SBO pattern was implemented.

10. Analysis of all data was accomplished synoptically.

11. Conclusions and recommendations were prepared.

The time period for execution of this work did not permit completion of all the exploration that would be desirable. Sufficient work was accomplished, however, to allow some firm plans to be laid and firm conclusions to be drawn. The process which led to the conclusions presented in this report is described in the following pages.

In a preliminary way, certain modifications to the existing antenna system can be considered. For example, creating a larger aperture will provide more directivity which is almost universally beneficial in correcting problems such as exist at San Francisco. Restructuring the parabolic antenna system is not a trivial task and certainly cannot be considered as a prime possibility for implementation.

Beams can be shifted and compensated electrically but this results in non-standard modulation balances. If the SBO patterns are shifted so that the look angles together with the on-course minimum are moved to provide less illumination on a reflector, it is mandatory that compensation be provided by a tone unbalance to maintain the on-course over the centerline of the runway. This unbalance is considered generally undesirable, especially for a Category-III operation.

Once reflecting objects have been identified, cosmetic changes can sometimes be introduced so that incident signal is scattered in a region of no interest or be made incoherent. A strong negative factor against recommendation of this type of solution is that unless major construction efforts are made to secure any surface modifications, there will be an uncertainty that the change will remain effective. Wind, for example, can change locations of reflecting materials such as screens, and these changes will likely go undetected because there is no monitoring present to observe them.

Signal cancellation techniques using auxiliary signals radiated directly to the reflector suffer the same problems of consistency and monitoring. The far field, in general, is not monitored; therefore, a minimum of dependency upon equipment outside the array proper is an important consideration, especially for Category III-type operations.

ANALYSIS.

The principal problem area for structure of the GWQ localizer is in Zone 4 with marginal conditions sometimes appearing in Zone 3. The path structure exhibiting the oscillations is given in figure 2-30. Figure 2-31 shows a more pronounced, regular pattern during a measurement made while taxiing down the runway.

Equation 1 taken from the report, titled "Investigation of Array Changes and Terrain Modifications to Provide for Category-III-Quality Localizer Course Structure at Los Angeles International Airport", allows determination of the grazing angle of the incident signal.

$$\alpha = \cos^{-1} \frac{P-\lambda}{P} \quad (\text{Eq. 1})$$

where α is the grazing angle

P is the spatial period in feet

and λ is the operating wavelength in feet.

Applying this analysis to the reflected radiation covering over the first two-thirds of the runway (in the approach direction) suggests a source in the United Airlines complex. This area contains a hangar with a surface facing the terminal area that must be considered as a candidate for the source of the problem.

Clearly, the possibility of more than one source must be considered. There are certainly many apparent reflectors, and there are sufficient irregularities in the records to suggest a multi-source hypothesis. Possibilities of sources can be obtained from a review of a record that was taken for the localizer serving 28L. This localizer is 14-element, single frequency system operating much closer to the terminal area complex. Figure 2-32 also shows the relative positions of the two localizer transmitting systems.

Figure 2-33 shows a record of the structure of the 28L localizer. Clearly evident is the larger quantity of noise, i.e., roughness and the more irregular patterns, thus indicating multiple sources of reflections.

Another deduction can be made after studying the recording of the 28L localizer structure, and that is, if the reflector or reflectors of concern for 28R operation were south of the runways, then their effects should be more prominent in the 28L localizer recording. This is not the case; therefore, the highest probability is that the reflectors are north of the 28 runways. There are no obstructions between the runways that would reflect localizer signals.

Referring again to figure 2-30, one can appreciate the regularity of this noise pattern by comparison. The slower motion of the aircraft is obviously not aggravating the case. More regularity suggests that, at least at the altitude of the antenna during taxi, the multipath signal is principally

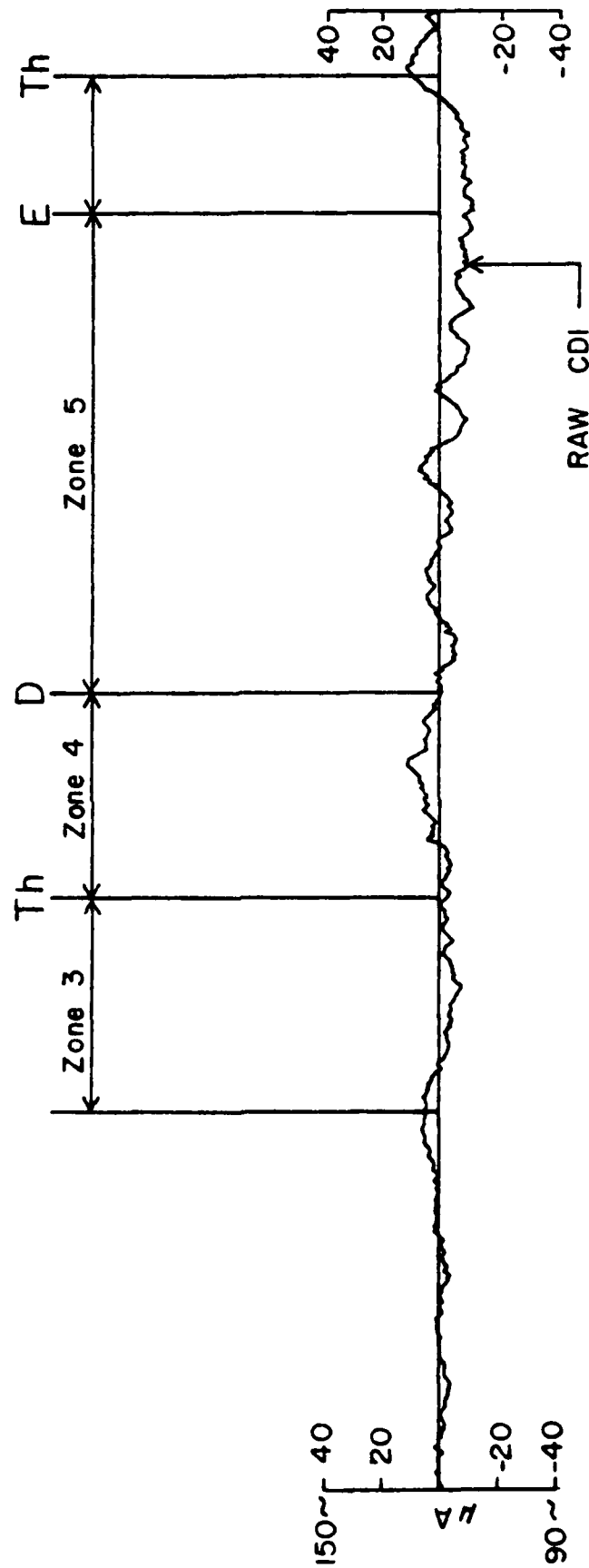


Figure 2-30. FAA flight recording made of the localizer structure in Zones 3, 4, and 5 for Runway 28R at San Francisco International Airport. A major area of concern obviously must be Zone 4.

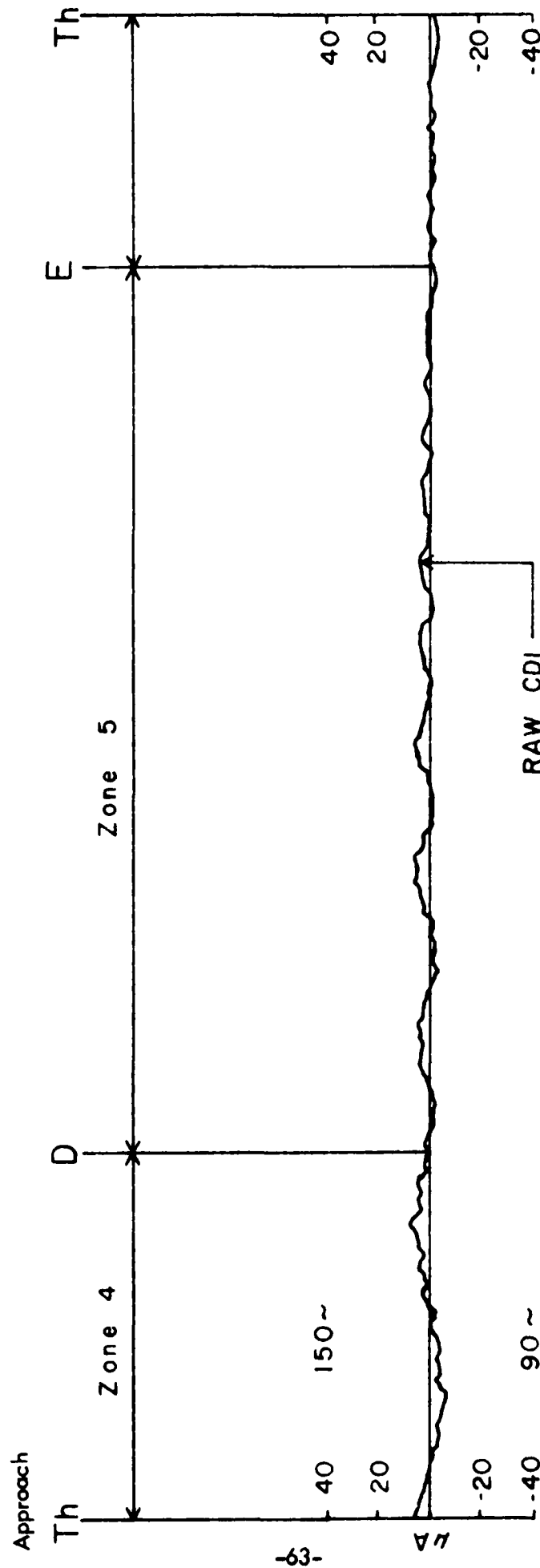


Figure 2-31. FAA recording of localizer structure made during a taxi from one end of the runway to the other. The pattern of oscillations is more regular and effectively vanish over the last 2000 feet of runway. Calculations based on this pattern indicated a source in the area of the United Airlines Maintenance Complex, San Francisco International.

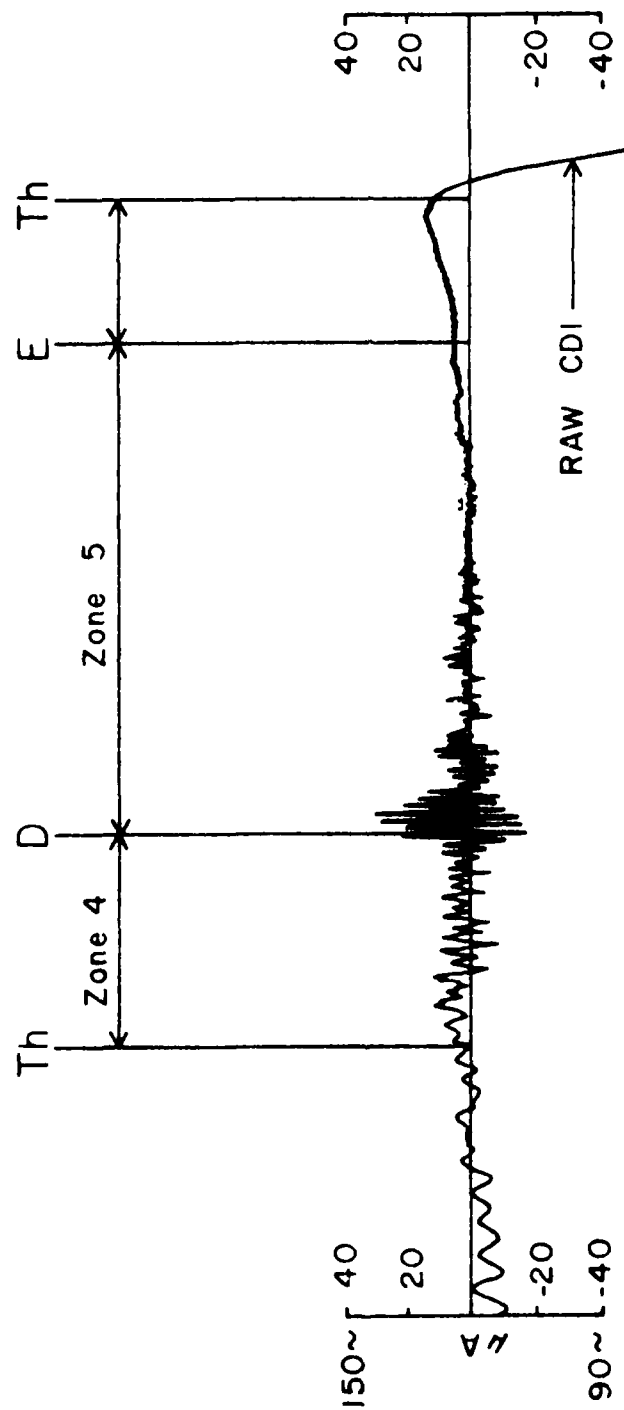


Figure 2-33. FAA flight recording made of the localizer structure for Runway 28L at San Francisco. The character of this structure is dramatically different from that of Runway 28R. The structure exhibits a high frequency, larger magnitude noise than that for 28R thus indicating that more SBO energy was reflecting from objects at a greater distance from the runway centerline. The larger amount of energy is undoubtedly due to the less directive radiation pattern of the localizer antenna array used on 28L.

from a single source. Low altitude flight measurements over the runway (i.e., 50 to 100 feet) reveal a greater quantity of noise and less regularity. This indicates that the vertical radiation patterns of the transmitting array and the reflector are probably not similar.

Inquiries concerning the availability of design data for the parabolic antenna system yielded that the information is either in France where the design originated or that it is in deep files at Texas Instruments Co. The handicap this produces is that a major effort must be undertaken to construct a math model for this specific parabolic type antenna or that an aperture distribution be assumed which produces the observed field patterns in space. This latter is what has been done because of time constraints. Unfortunately, with this approach, flexibility is lost, particularly when perturbations to the feed are of interest for changing the energy distribution in space. When considering the course array, it is quickly observed that two of the three feed antennas for the parabola are not at the focus simply because it is physically impossible to have three antennas at one location. Consequently, the two sideband antennas are displaced from the focus and, therefore, must have some defocusing present, some of which is desirable to broaden the energy distribution in the course area. The extent of this is not easily known, particularly in terms of phase front deformation.

Lacking precise calculational capability for the parabolic antenna, considerable hesitancy exists for experimenting with the feed elements of the array. Experience with previous work with this type of array and comments from others with considerable experience both suggest caution when physical movements are involved. Considerable precision of placement must be achieved. Following any experimentation, restoration could very well be a problem. For these reasons, experiments involving antenna movements will be undertaken only after other methods have been proved unsuccessful.

The question of whether the clearance array is involved in any way with the derogation of the course signal must be considered. The FAA did look at this earlier by obtaining a flight recording of the course structure without the clearance transmitter operating. The result was that there was no significant change in the structure with or without the clearance transmitter operating. Having this information allows narrowing the problem to that of dealing with the course generation only. This does not mean, of course, that the presence of the clearance transmitting antennas located near the course antennas can be ignored. Parasitic effects remain possibilities and will be investigated.

SBO ENERGY DISTRIBUTIONS.

A necessary condition for structure roughness to be created is the illumination of a reflecting object with sideband-only energy. It is this energy that provides for the space modulation, and with a source to the side of the approach path, the irregularity is in the form of oscillations, sometimes called scallops. These possess a varied frequency as the recording progresses. Of interest, consequently, is the SBO radiation as a function of azimuth. Two approaches were used to obtain this information. The first approach was to make a request for FAA flight inspection to fly an orbit of the localizer while recording AGC voltage with the array configured to feed carrier energy into the system where SBO normally exists. (This is necessary because the receiver will not operate properly with SBO and no carrier.) Figure 2-34 shows the data taken from the flight recordings. Two items are noteworthy. There is an asymmetrical condition which indicates that there is more SBO energy being radiated by the parabolic system to the north of the runway than to the south. Clearly, the design for the array would not call for this, and this, therefore, must be considered an anomaly. Unfortunately, this energy is radiating into an area which contains possible reflectors, especially in the United Airlines maintenance complex.

Two interesting but probably unimportant features of the SBO pattern are the two rather sharp minimums occurring just south of the front course areas. If these caused problems, then they would be in the clearance pattern.

The second approach to obtaining information on SBO distribution was a request to Airway Facilities personnel to make ground readings with a PIR (Portable ILS Receiver) in the areas near the reflectors. FAA data from these readings are shown in table 2-4.

<u>LOCATION</u>	
Centerline of R/W	8
Runway Edge	40
50 ft N. of Edge	42 (max)
First tank	20
Second tank	23
AAL Hgr South	12
AAL Hgr West	22
Range for all readings approximately 5000 feet from localizer.	

TABLE 2-4. FAA data with PIR.

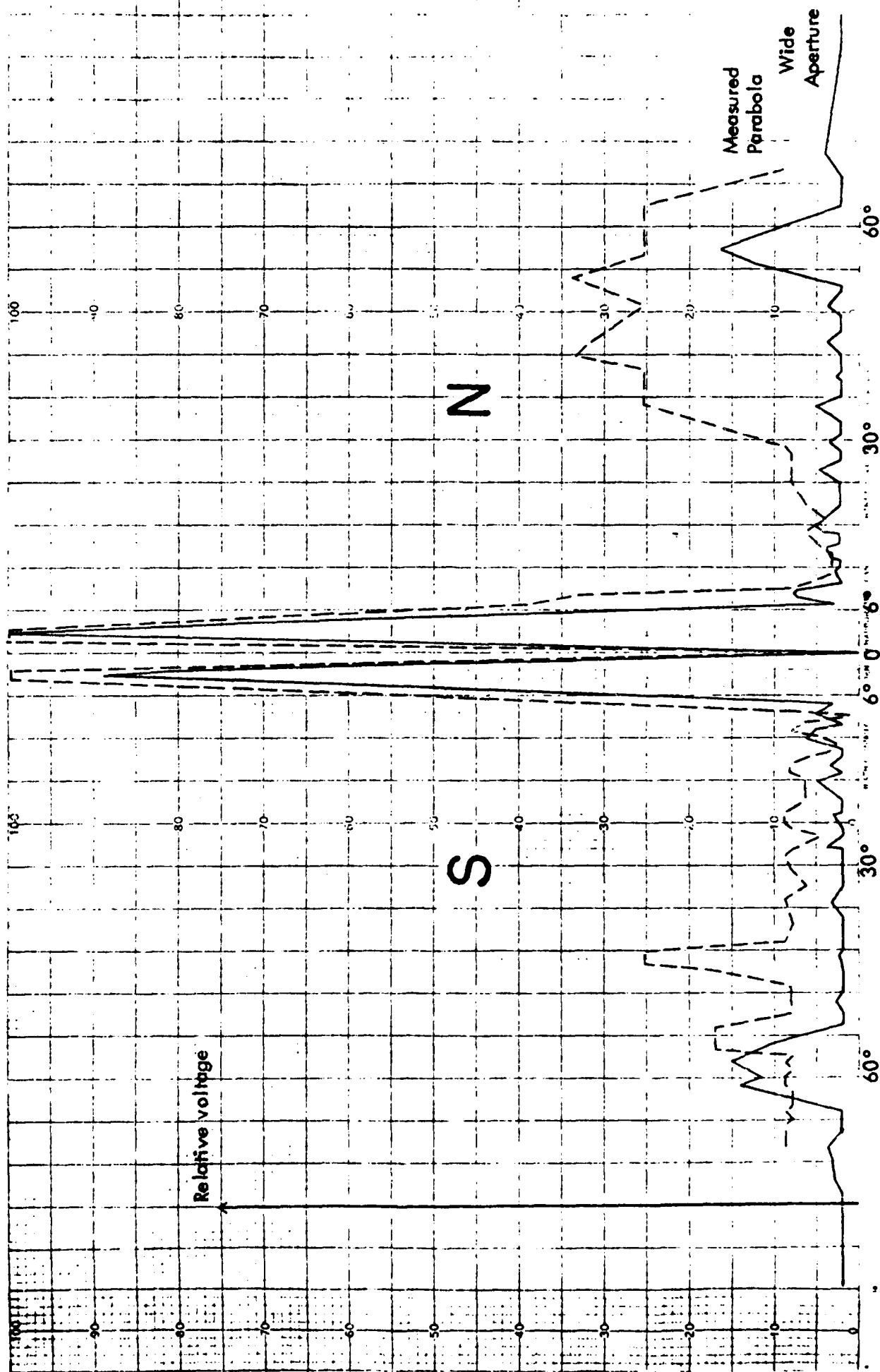


Figure 2-34. Plots of measured SBO energy distributions for the parabolic antenna and for the 14-element, wide-aperture array. The parabolic antenna produces slightly broader main lobes and certainly an anomalous high level of energy on the north side.

Information from this table indicates that SBO illumination of the tanks is only 6.4 db down from the peak. This is not consistent with the theoretical pattern and varies with that shown in figure 2-34 produced with the aircraft. These ground measurements, nevertheless, suggest that the tanks could be a cause of the undesirable reflections.

CALCULATIONAL APPROACH.

Having a measured SBO pattern and a previously measured carrier (CSB) pattern, a powerful calculational, investigative approach to identifying the principal derogative factor in the GWQ localizer operation is possible. Calculations assuming the existence of reflectors at locations indicated by locations of hangars, buildings and tanks are practical. A major objective is to assess the correspondence between the periods and amplitudes of calculated patterns against those produced in the measurements. Fortunately, the repeatability of the irregularities in the measured path is quite good, thus making this job of correlation much more practical and meaningful. Accordingly, a great number of calculations have been performed. Following, in figures 2-35 through 2-42, are some of the results. Detailed information is carried in the captions.

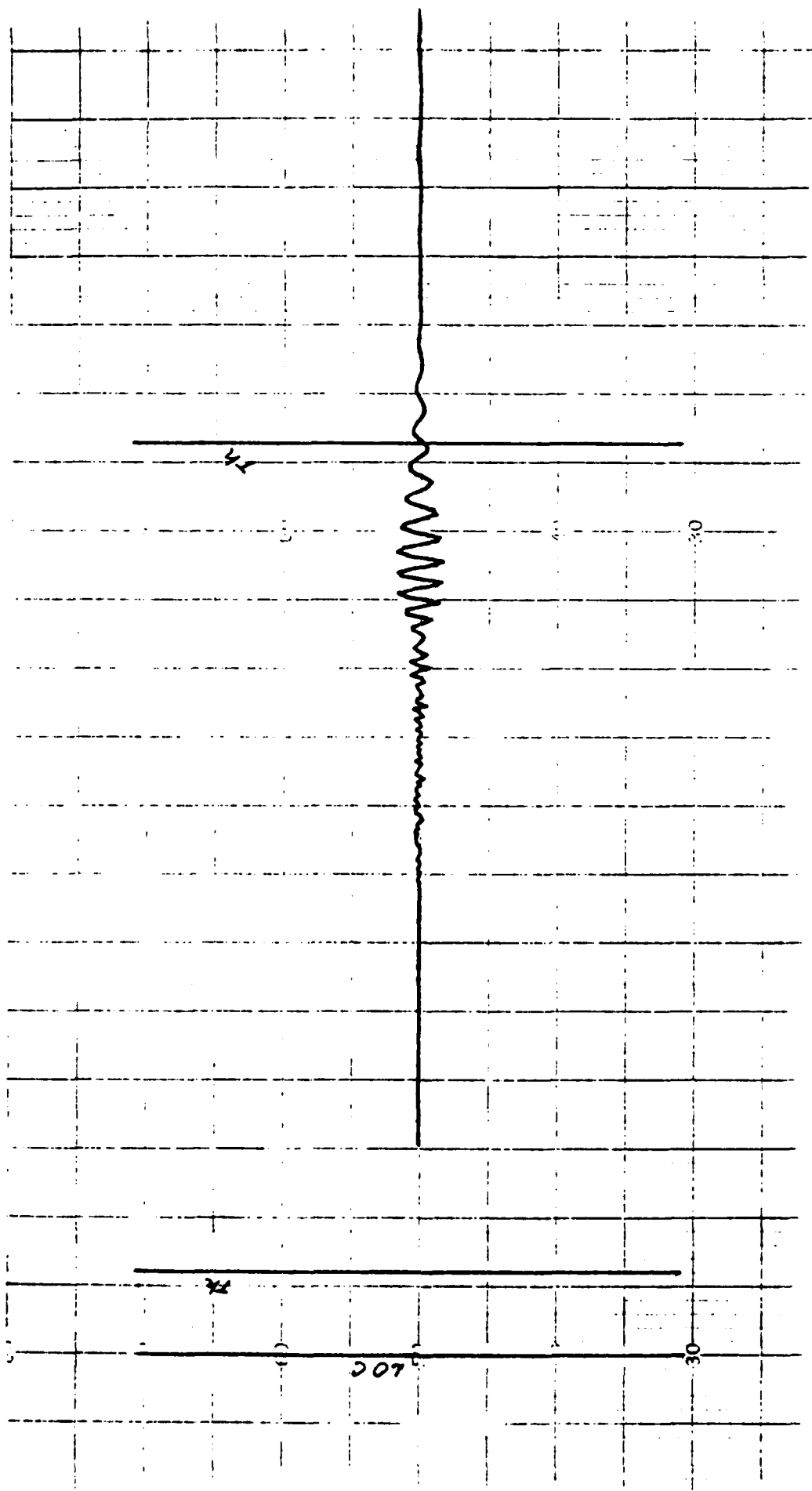


Figure 2-35. Calculated Path Perturbation Produced by American Airlines Hangar Using Measured SBO Distribution.

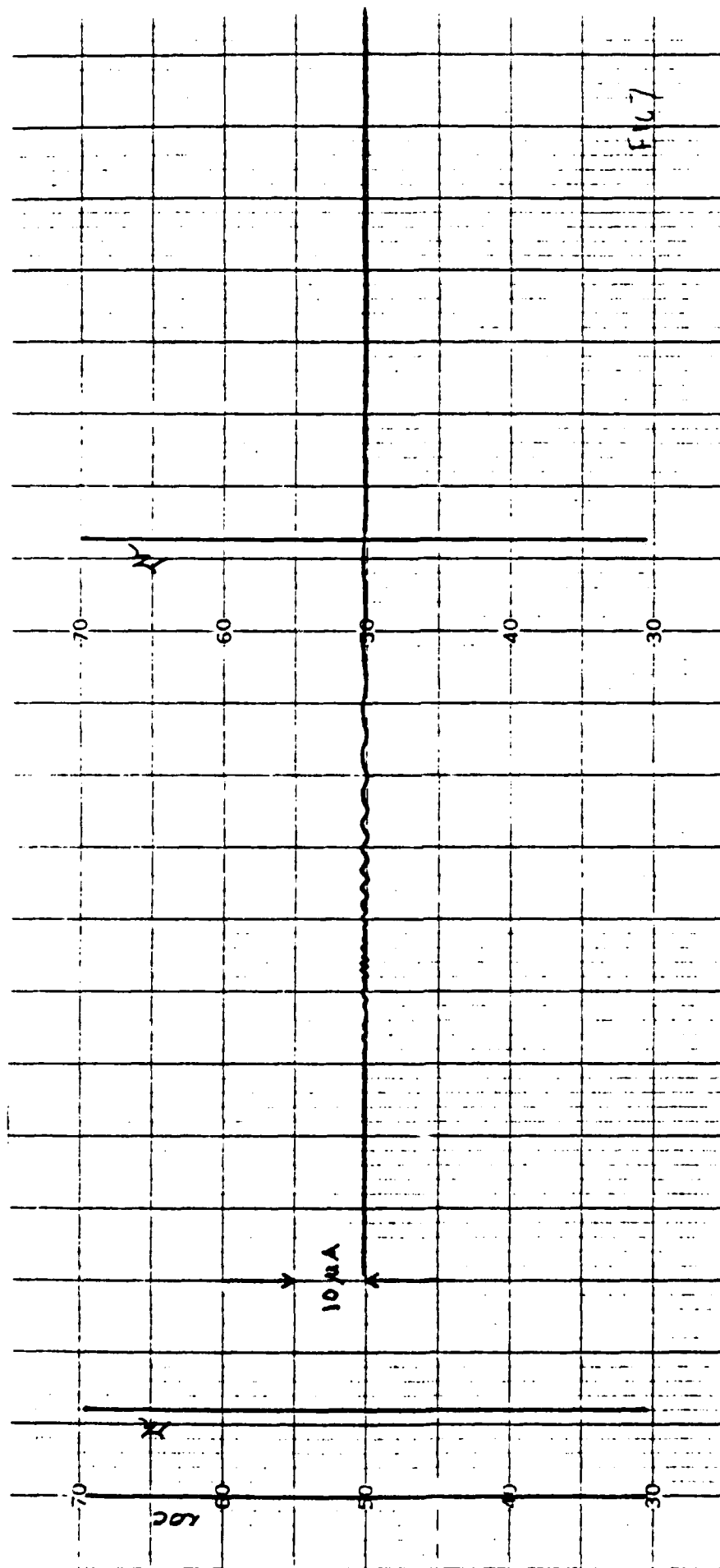


Figure 2-36. Calculated Path Structure Produced by Fuel Storage Tanks with Measured SBO Energy Distribution.

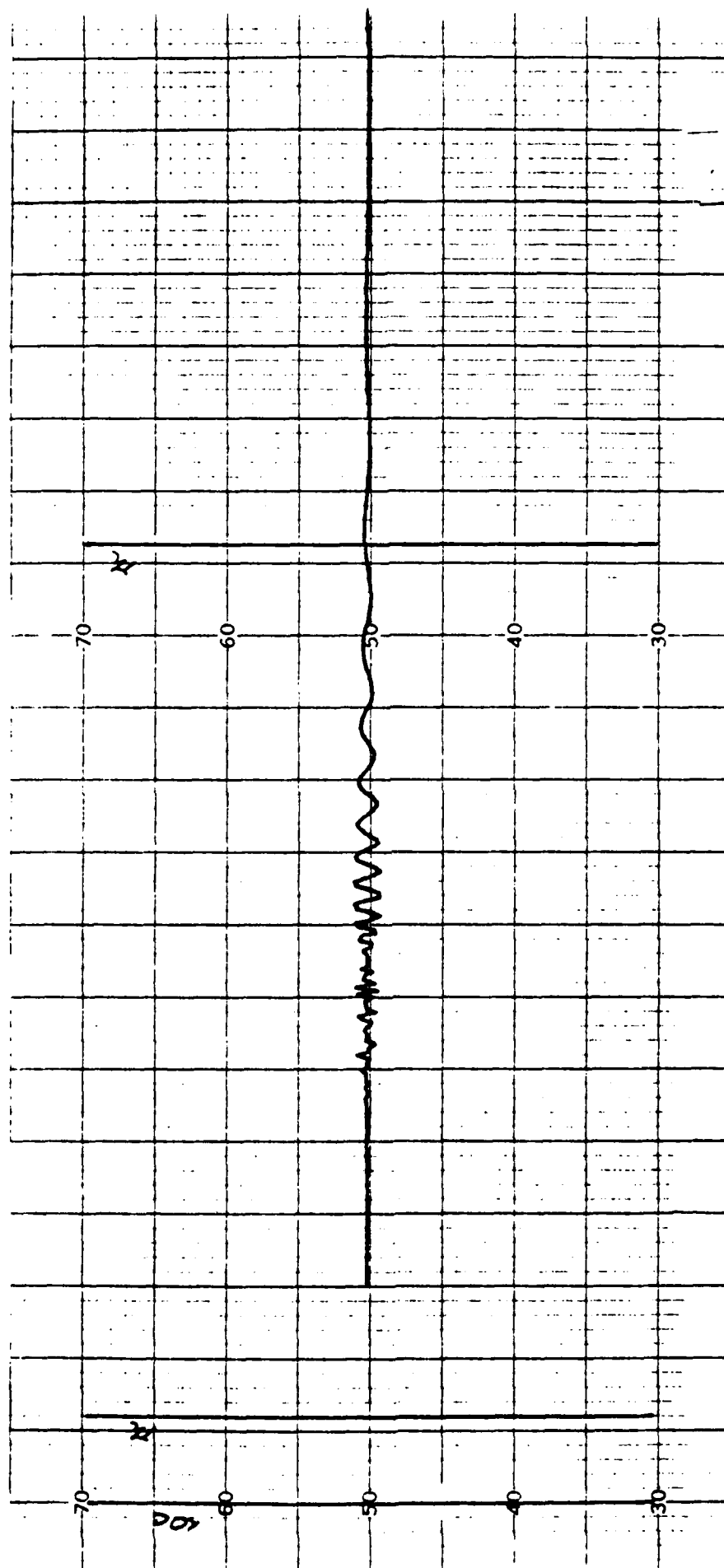


Figure 2-37. Calculated Path Structure Produced by Fuel Storage Tanks with SBO Energy Distribution Skewed One Degree to Account for Possible Error in Azimuth Angle Determination Accomplished by Dividing the Region Between the Front and Back Course into 180 Equal Segments. Because of the steep slope of the SBO pattern at the angle of the tanks this is a method of exploring a possible worst case.

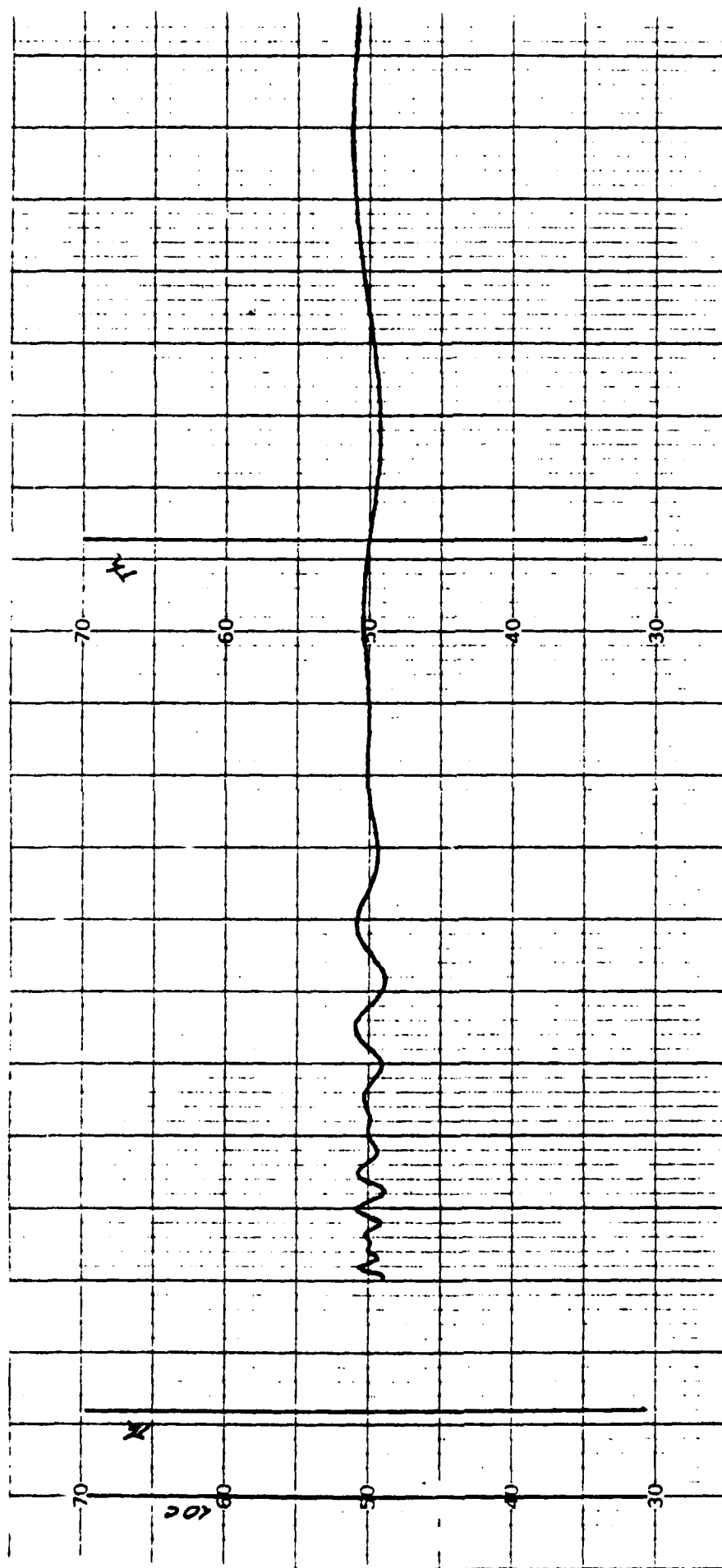


Figure 2-38. Calculated Path Structure Produced by Reflecting Surface in the United Airlines Maintenance Complex with Measured Asymmetrical SBO Energy Distribution.

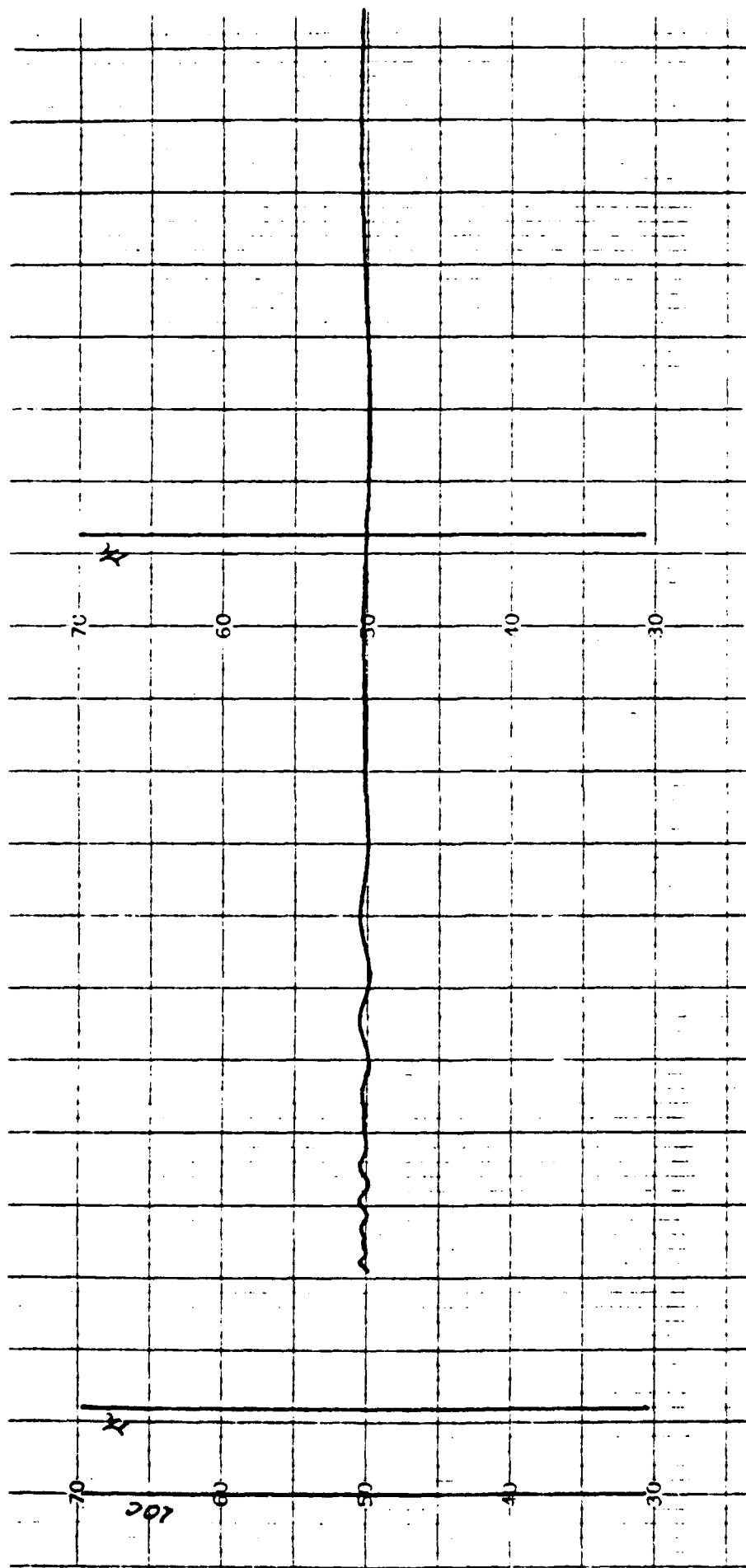


Figure 2-39. Calculated Path Structure Produced by Reflecting Surface in the United Airlines Maintenance Complex but with an SBO energy distribution that is symmetrical and consistent with the south side distribution. In other words, the SBO pattern is assumed for this calculation to be optimum in that it is low in amplitude in both the north and south sectors near 60 degrees.

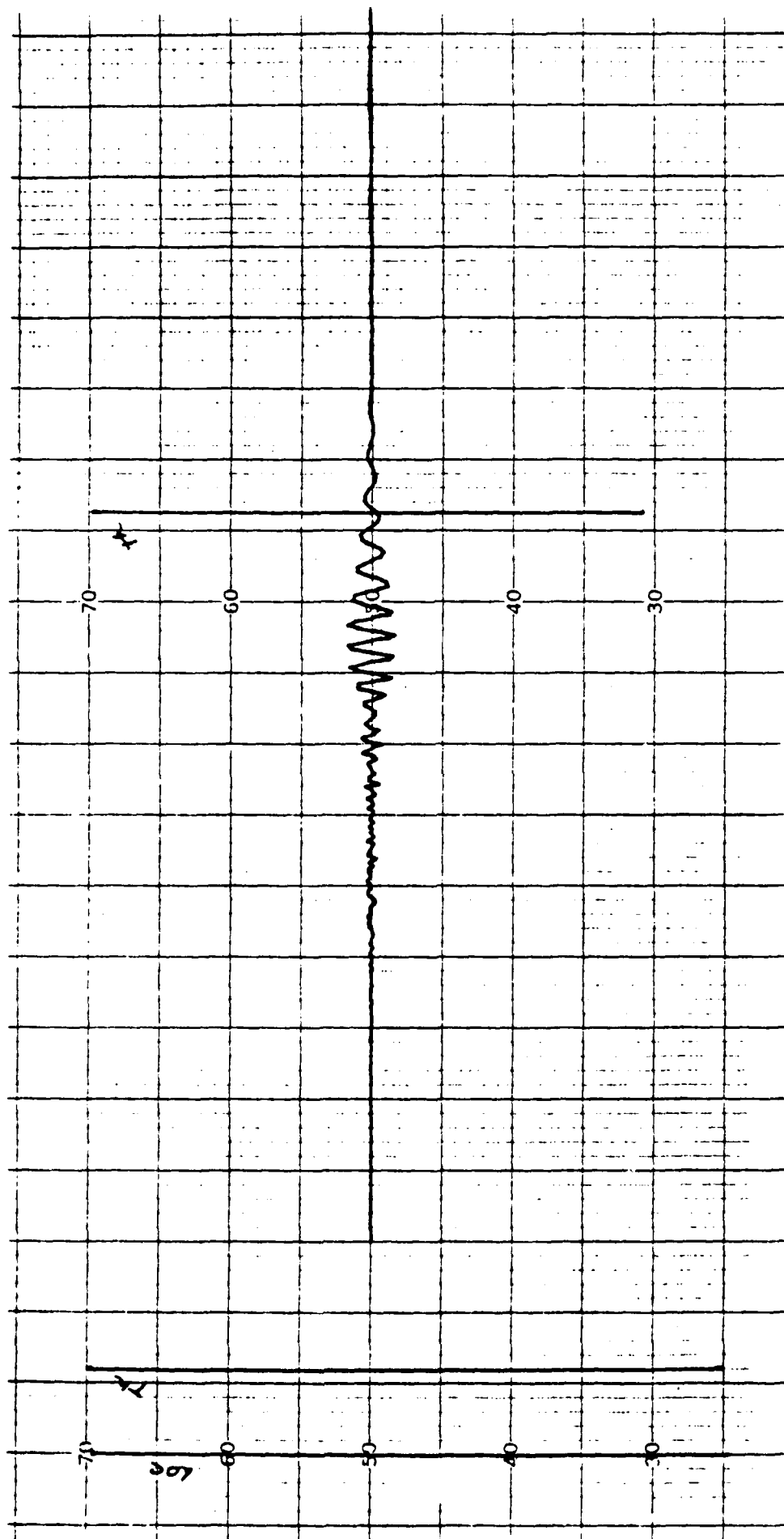


Figure 2-40. Calculated Path Structure Produced by the Wide-aperture, 14-discrete-element Array Designed by R. W. Redlich and having undergone tests at the Ohio University Test Site at Tamiami Airport in Florida. The obstruction is the American Airlines Hangar.

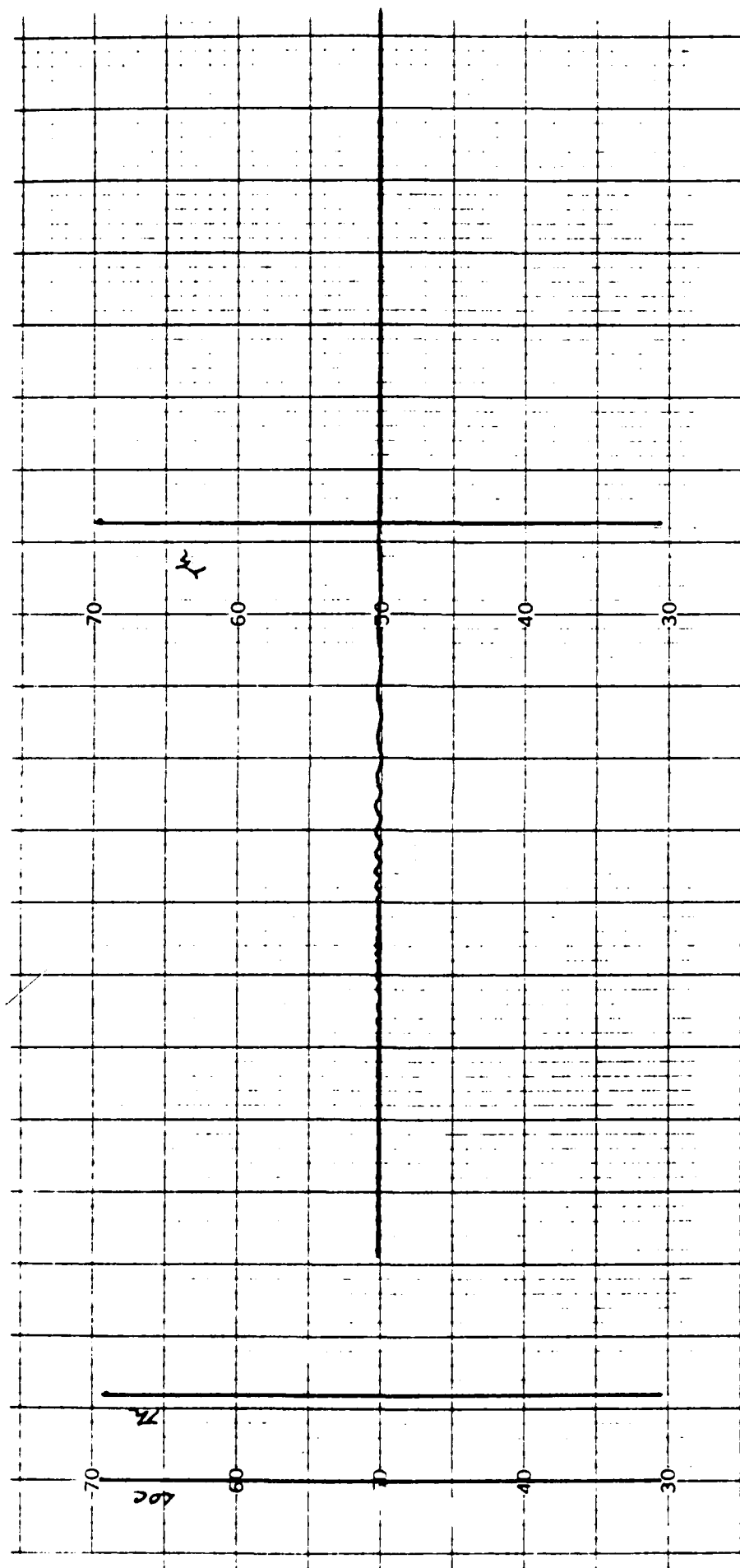


Figure 2-41. Calculated Path Structure Produced by the Wide-Aperture Array. The SBO Pattern used was measured. The obstruction is the tank farm.

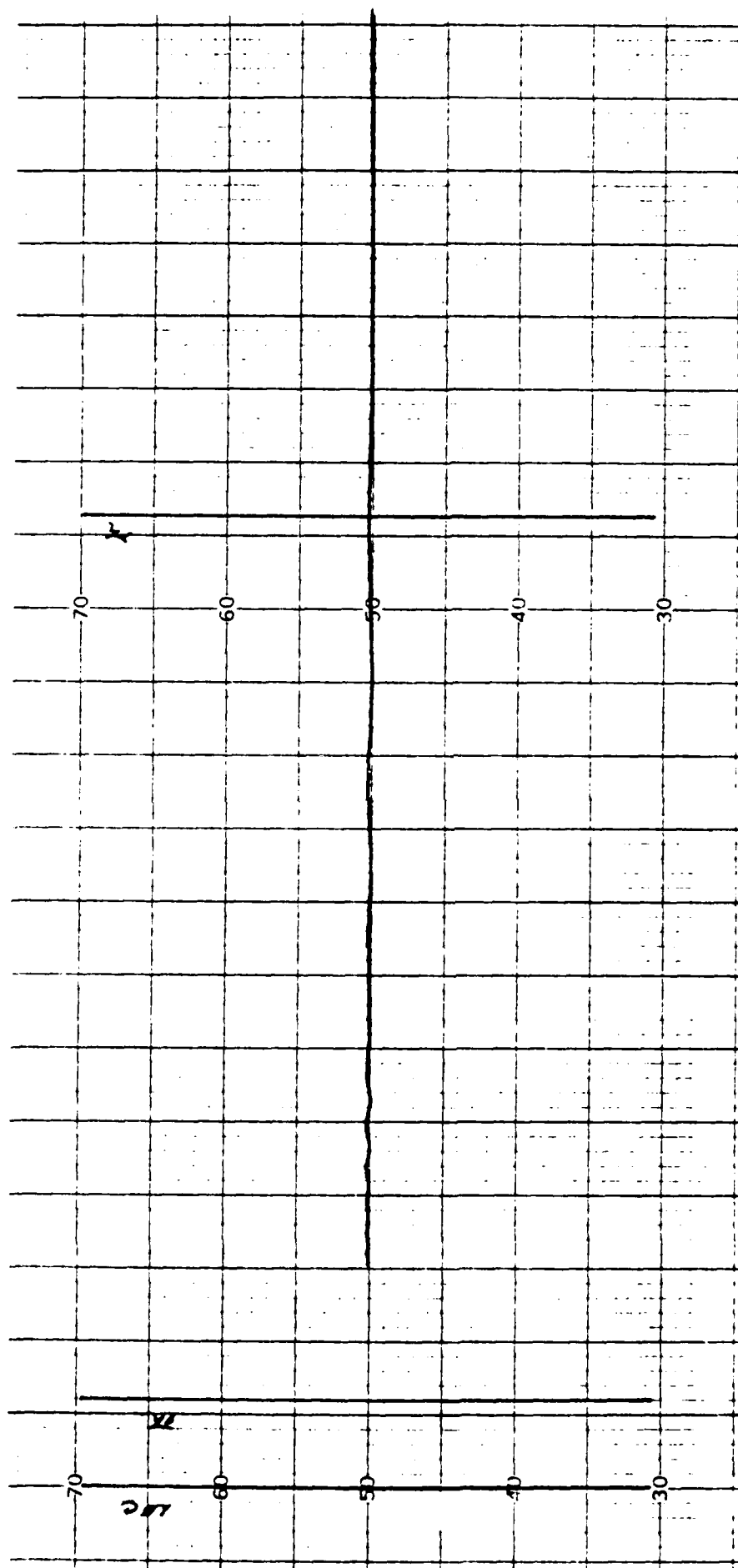


Figure 2-42. Calculated Path Structure Produced by the Wide-Aperture Array. The SBO pattern used was derived from measurements made at Tamiami. The obstruction is the reflecting surface in the United Airlines Maintenance Complex.

CONCLUSIONS.

This section being written only 10 days after this evaluation was begun necessarily must contain only tentative conclusions. Certain desirable pieces of information which are being furnished from the FAA field offices have been delayed due to both weather and mechanical problems. Nevertheless, some important items can be stated as a result of this evaluation.

1. Given current FAA flight inspection tolerances, removal of the system from Category-III status was justified. Repeatability of data clearly indicates that tolerance limits are exceeded in fact.

2. The problem is structure roughness. The character of the roughness indicates that one, at most two, reflectors are contributing significantly to the out-of-tolerance condition.

3. The structure roughness on the 28R localizer is completely different in character than the roughness exhibited on the 28L localizer. The explanation is that a less directional antenna array is being used and the location is nearer the multi-building terminal area complex. This evidence points to the reflectors of concern being north of runway 28R.

4. Analyses from available data support reflections as coming from two sources, viz, a wall in the United Airlines maintenance complex and from storage tanks abeam taxiway Delta approximately 5000 feet from the array.

5. Calculations confirm that the geometries associated with both the United Airlines hangar and the tank farm are consistent with that needed to produce the observed course perturbations.

6. Manipulation and modification of the localizer array for experimental purposes are undesirable because of the need to maintain Category-I service as a minimum with the system. The result is to place increased emphasis on analysis and synthesis using the mathematical model.

7. Arrays with discrete elements lend themselves to manipulation for tailoring purposes better than a wide aperture formed by a parabola.

8. Asymmetrical SBO patterns are evident from the flight recording with larger quantities of energy existing on the north side in the area of the United Airlines hangar. The asymmetry suggests anomalous operation of the antenna system possibly in the feed antennas. This is a prime concern for causing pattern derogation.

9. Increasing the aperture of the parabola is a practical possibility. Calculations are necessary to determine the optimum length for the extension.

10. Calculations performed indicate that the most effective solution to the structure problem on 28R is the application of the wide-aperture, 14-element array.

AD-A140 797

ENGINEERING AND TECHNICAL SERVICES TO IMPROVE
RELIABILITY AND MAINTAINABILITY (U) OHIO UNIV ATHENS
AVIONICS ENGINEERING CENTER J D LONGWORTH ET AL

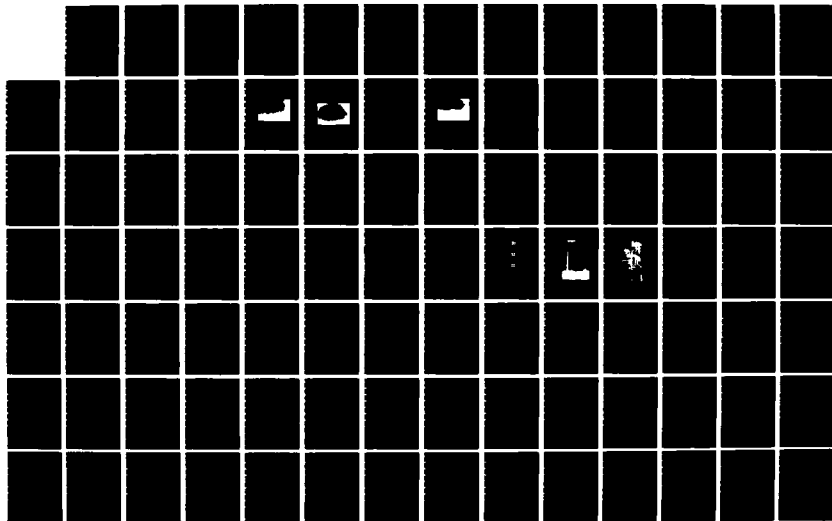
2/4

UNCLASSIFIED

JAN 83 OU/REC/EER-62-1 DOT/FAR/PM-84/7

F/G 17/7

NL





MICROCOPY RESOLUTION TEST CHART
NATIONAL BUREAU OF STANDARDS-1963-A

11. Use of discrete elements provides a noteworthy capability, viz, a capability to tailor the SBO pattern to place nulls or minima on specific azimuth angles where reflecting objects exist.

RECOMMENDATIONS.

The following recommendations are derived from the evaluation work performed and are consistent with the conclusions listed above.

1. Corrective action should be implemented proceeding from the simplest to the more complicated and expensive.

2. The anomalous SBO pattern indicated that significantly more energy is being radiated on the north side of the runway which happens to be the area where some critical reflectors exist. This asymmetrical pattern should be corrected, if possible, by tuning the array feeds.

3. If array feed modification will not produce improved SBO patterns then consistent with calculations for determining optimum parabola length, the screening of the parabola should be extended.

4. Failing improvement by feed and screen modification, a wide-aperture, discrete element array should be tested in place. Calculations for the wide-aperture, 14-element array indicate that substantial improvement can be obtained. This should be verified.

5. Should alternate possibilities be desired, then the standard Cat-III array such as serving runway 24R at Los Angeles can be used, but almost certainly there will be requirements for tailoring to minimize SBO energy that will be incident on critical obstructions.

6. Use of an array of 14 discrete elements could also be considered if it is fed as one portion of a two-frequency system, the other being the clearance array which is now in place. In other words, the present course array, viz, the parabola would be replaced by a set of discrete elements, probably log-periodic dipoles.

A DEMONSTRATION OF TWO SOLUTIONS TO THE CATEGORY-III LOCALIZER PROBLEM ON
RUNWAY 28R AT SAN FRANCISCO INTERNATIONAL AIRPORT.

SUMMARY AND CONCLUSIONS.

Analytical and experimental work has been completed on the localizer serving runway 28R at San Francisco International Airport which clearly reveals that Category-III quality signals can be obtained by either of two means. One is to increase the height of the parabolic screen, which is an integral part of the localizer array, by six feet. This will result in structure roughness being reduced to 60% of tolerance limits. The other approach is to replace the present transmitting antenna system with the recently designed 14-element, wide-aperture array. This will result in a reduction of structure roughness to 70% of tolerance values.

The confidence in the above statements is extremely high because each of these two solutions was examined in place at San Francisco. In the case involving the screen extension, a check on structure improvement was also made by FAA flight inspection, and their data indicated a reduction to 40% or tolerance limits. All data appears consistent and repeatable, especially when one considers that 20% of tolerance equates to measurement of one microampere of course deviation indicator current.

There are two principal areas producing the problem of meeting Category-III localizer tolerances. One is the United Airlines maintenance complex to the north and northwest of the localizer array. The other is the American Airlines, jumbo-jet hangar on the north side of the runway at approximately the half-way point. The existing parabolic-type antenna system provides the better capability to minimize the effects of the American Airlines hangar and with the increase in height of the parabolic screen from 18 to 24 feet provides good protection from the reflections from the United Airlines facility. The wide-aperture, log-periodic array appears to give almost total protection from the United Airlines complex, but allows slightly greater illumination of the American Airlines facility. Both of these, however, do provide performance sufficient to meet Category-III tolerances comfortably.

Three discrete tests confirmed the United Airlines complex as being the source of the multipath which caused the out-of-tolerance condition. Although the complex is quite large, it consists of many discrete wall surfaces, and it is not intuitively obvious that this type of a multifaceted, reflecting area has a very high probability of producing a significant effect. The probability of obtaining phase coherence of the energies reflecting from the many surfaces is very small. The conclusion is clear, however, that even with multifaceted surfaces located behind a screen such as the parabolic type at San Francisco, sufficient energy can be reflected in a coherent manner to produce course scalloping that exceeds Category-III limits which are, of course, very tight at 5 microamperes in Zones 3 and 4.

Clear from this work also is the fact that wide-aperture arrays can be tremendously effective in reducing magnitudes of path perturbations caused by reflections from large objects near the runway area. Category-III performance would not be available if wide-aperture arrays were not available. Both the 178-foot aperture of the parabola and the 128-foot aperture of the log-periodic array tested are appropriately called wide-aperture types.

INTRODUCTION AND STATEMENT OF THE PROBLEM.

The U. S. Flight Inspection Manual, OA P 8200.1, in section 217.5 gives the tolerance for localizer course structure in Zones 3 and 4. The values measured repeatedly by FAA flight check were 6 to 8 microamperes and thus presented unacceptable conditions, especially if averaging techniques were not applied.

This report is a sequel to Technical Memorandum B-6 dated December 1982 which presented the results of analyses of FAA flight records and predictions of multipath effects using the mathematical models resident on the IBM 370-44 computer at Ohio University.

Following the analytical work, an Ohio University team travelled to San Francisco in January 1983 to make additional measurements with its own flight and tracking equipment. Several questions which were quite important had not been resolved. One of these questions was whether the course, sideband-only radiation pattern, was asymmetrical and anomalous on the north side. If it were, then there would be hope that normalizing the array would produce improvement. Another need for measurements was to confirm some of the analytical results, such as predictions as to the location and character of the path perturbations produced by individual reflecting objects. For example, the course transmitter was shut off and measurements made with clearance signal that was known to illuminate strongly the American Airlines hangar.

Data obtained from the FAA from measurements made in late December gave inclusive results concerning the United Airlines complex as the source of the reflected energy. A log-periodic antenna element had been used to radiate energy towards the United Airlines complex but no significant change was noted in the magnitude of the course perturbations. Also, extending the parabolic screen by 80 feet horizontally to the north had not produced noticeable changes. At the beginning of the Ohio University work at San Francisco, there had been no data obtained that indicated conclusively that the United Airlines complex was the problem.

The objective of this work has been to identify not only what was causing the out-of-tolerance condition of the localizer course but also to provide recommendations in which great confidence could be placed for correcting their problem. One obvious method for obtaining confidence is to implement the recommended change and make real-world measurements.

Because there has been considerable emphasis by the FAA that a solution be obtained and it be obtained in as short a time as possible, an approach involving the recently designed 14-element, wide-aperture localizer array was also begun by Ohio University. This involved a request to the FAA that 14 log-periodic antennas (LPD) be made available for use at San Francisco. Also, it necessitated removing some of the hardware from the Ohio University test site at the Tamiami Airport, Florida and moving it to San Francisco. Distribution networks, in particular, were needed.

A dual approach to finding a solution to the problem evolved. First, there was a search for the cause of the problem with the hope that once it was found the method for solving it would be apparent, and second, the set-up of the new localizer array was begun. The data from this latter would have some far-reaching significance since the only tests scheduled for the wide-aperture array were to be the near-ideal Tamiami site. The question as to how well the array would serve in solving an actual siting problem would not be resolved. With field tests at San Francisco, an important set of data is now on hand to answer that question.

APPROACHES.

The approaches that were used in the process of obtaining a solution to the San Francisco localizer problem can be broken down as follows.

1. The operation of the existing array was examined. This involved measurements of performance in terms of path structure and sideband-only radiation patterns produced by the course array. Also, energy distributions along the parabolic reflecting screen were determined in an attempt to identify possible anomalies.

2. Experiments to identify the source of the multipath causing the localizer problem were conducted. These consisted of first energizing a single-antenna element located on the north side of the parabolic antenna and directing the radiation towards the United Airlines maintenance complex. Following this, the height of the parabolic screen was lowered in three increments to assess the effects of the expected increase in illumination. Each increment consisted of eight wires or approximately 12 inches of height. It should be noted that this particular parabolic screen is comprised of approximately 150, horizontal, No. 12 stranded copper conductors.

3. An investigation to identify possible modifications that could be made to the existing array to effect a solution to the problem was performed. Phasing of the feed elements for the parabolic system was checked and modifications made. Phasing of illumination of the offending reflecting surfaces was checked to determine if cancellation could be achieved simply. Finally, extensions to the parabolic screen either horizontally or vertically or both were considered.

4. Implementation of prospective solutions was accomplished. The two practical candidates were raising the height of the reflecting screen and establishment of the 14-element, wide-aperture array.

DATA COLLECTION AND DISCUSSION.

In measurements at San Francisco, the Ohio University micro was used. Also available on this mission was the Ohio University Minilab Mark IIIa. Both were flown in a Beechcraft Model A36. Azimuth references were provided by means of a Warren-Knight Model WK 83 Theodolite. A localizer structure pattern obtained for the as-found condition is shown in figure 2-43. The out-of-tolerance condition is evident and the record is consistent with earlier FAA flight checks.

A. Investigation of Asymmetrical Course SBO Distribution. One early objective of the mission to San Francisco was to determine, with some precision, the amount of asymmetry present in the SBO pattern of the course array. Such an asymmetrical condition was suggested by earlier FAA measurements, but because of the great nonlinearity in the FAA AGC recordings, it had not been possible to determine with confidence the quantitative difference in the amount of SBO radiating in the north, rear quadrant (that containing the United Airlines complex) and that to the south rear quadrant. The reasoning was that if a significant amount of difference existed, clearly it was an anomaly and a modification could be accomplished once the anomaly in the structure or feed was found. Figure 2-44 shows a plot of the data taken from an AGC trace made on a five-mile orbit of the station.

These data show, at most, a 4db difference or asymmetry which gave sufficient encouragement to investigate the array for anomalous phase or amplitude conditions. Measurements using a vector voltmeter were made of currents on the screen. Adjustments in the phase of feed elements were made but no significant improvements were obtained.

B. LPD Auxiliary Radiator Experiments. In spite of the inconclusive results obtained earlier during FAA tests, the decision was made to repeat, in effect, those tests but with emphasis on maintaining the course width at standard values in spite of the fact that some SBO energy had been tapped off to excite the LPD element. The objective was to determine whether the course roughness would change in position, in amplitude, and/or in period.

With approximately 7 milliwatts of SBO, one-half of that available was fed to the LPD antenna which was directed towards the United Airlines complex. The system was normalized by attenuating the CSB and a flight check made of the width to establish it at its original value. Figure 2-45 shows the results in terms of the structure roughness. This record should be compared directly to figure 2-43 showing the original, as-found conditions. The important item to note is that of the three variables of amplitude, spatial period, and location, only the amplitude has changed. The increased amplitude indicates that more energy is being reflected which is what one would expect if an auxiliary radiator of SBO (sideband-only) energy is directed towards the reflector. The fact that the period or location has not changed is strong evidence that the illumination is on the same reflecting surfaces which produced the path perturbations that were observed as the original problem.

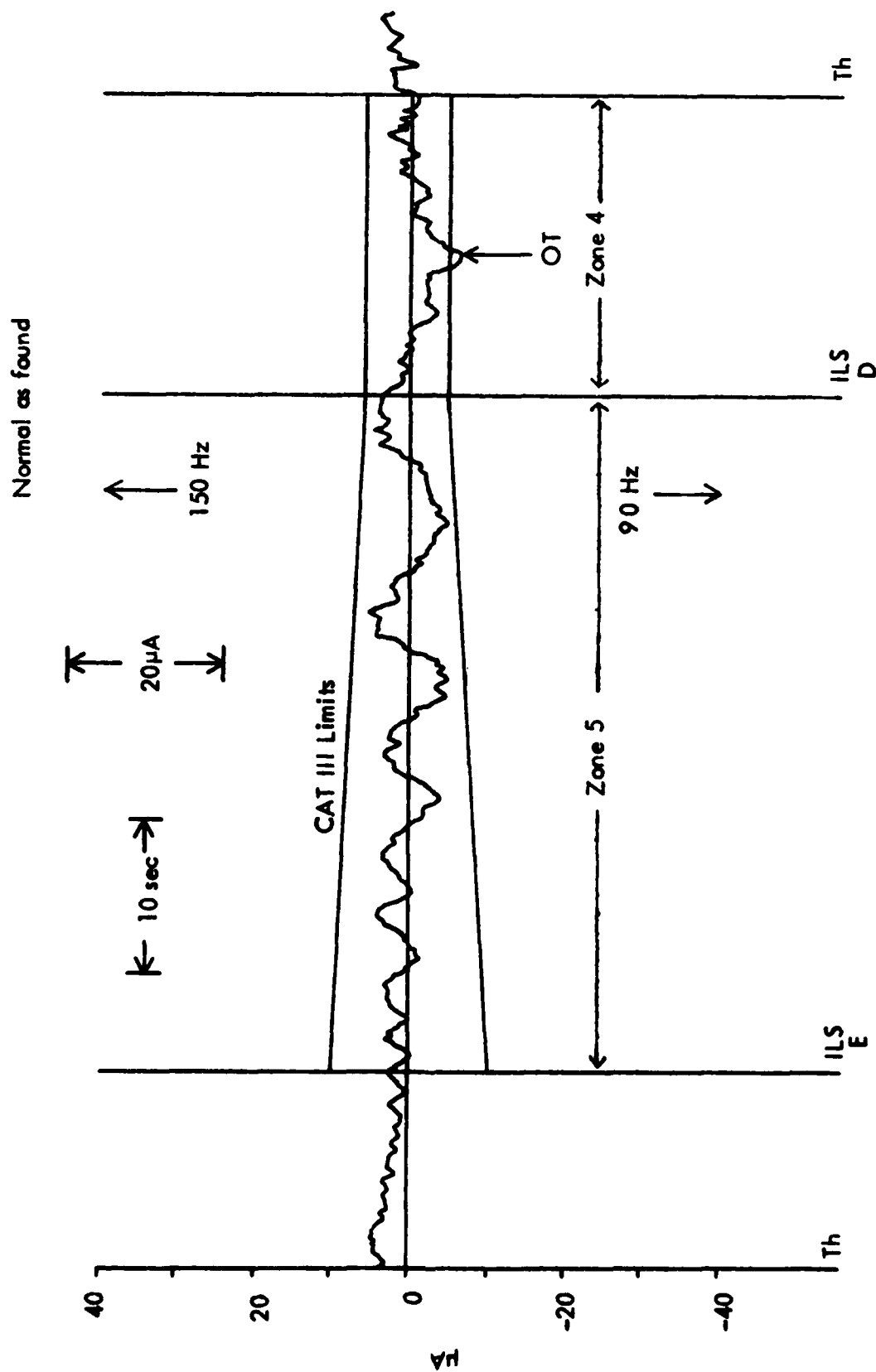


Figure 2-43. Flight Recording Showing the As-found, Out-of-tolerance Structure in ILS Zone 4. The regular scalloping indicating a single source area is evident.

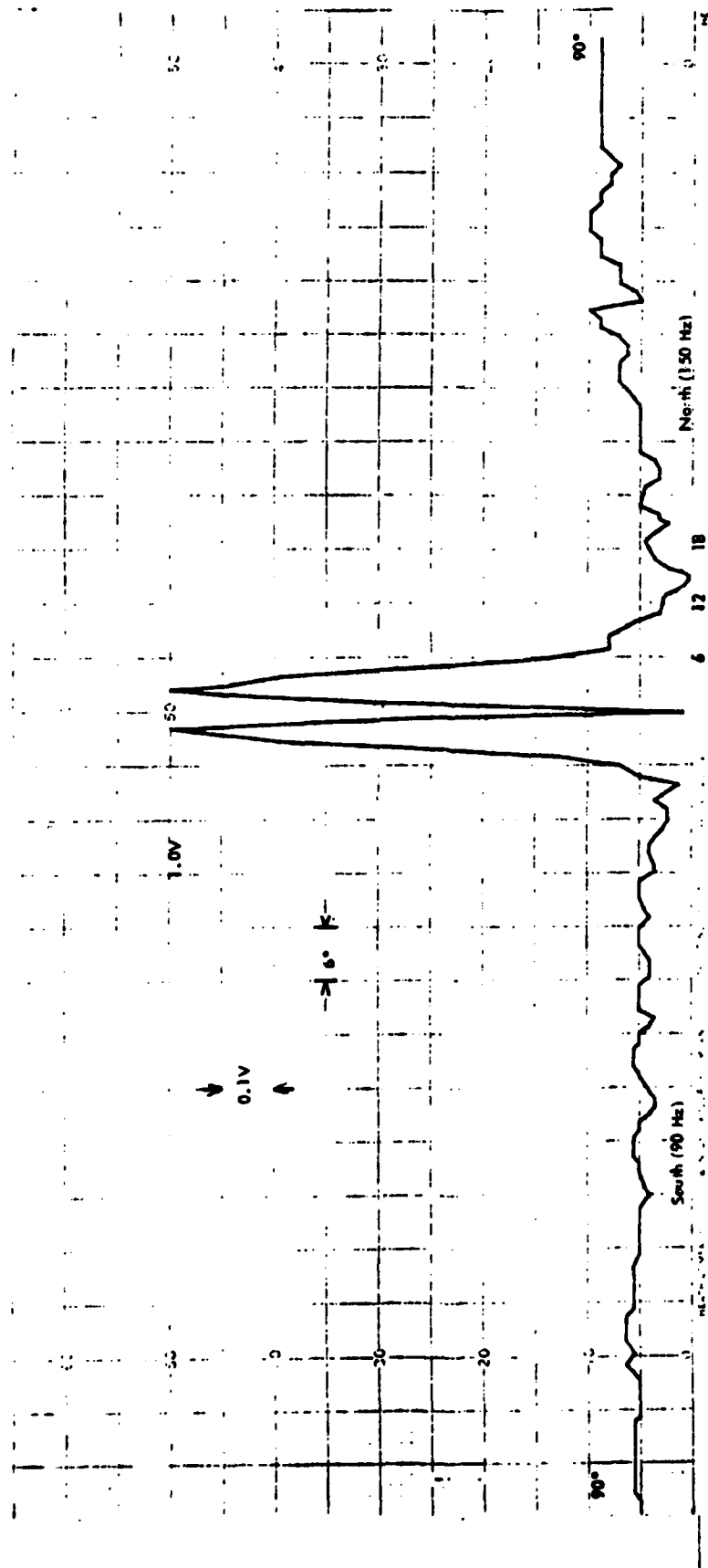


Figure 2-44. Sideband Only Radiation Pattern of the San Francisco Parabolic Localizer.
Ohio University Recording (Digitized and Scaled Linearity).

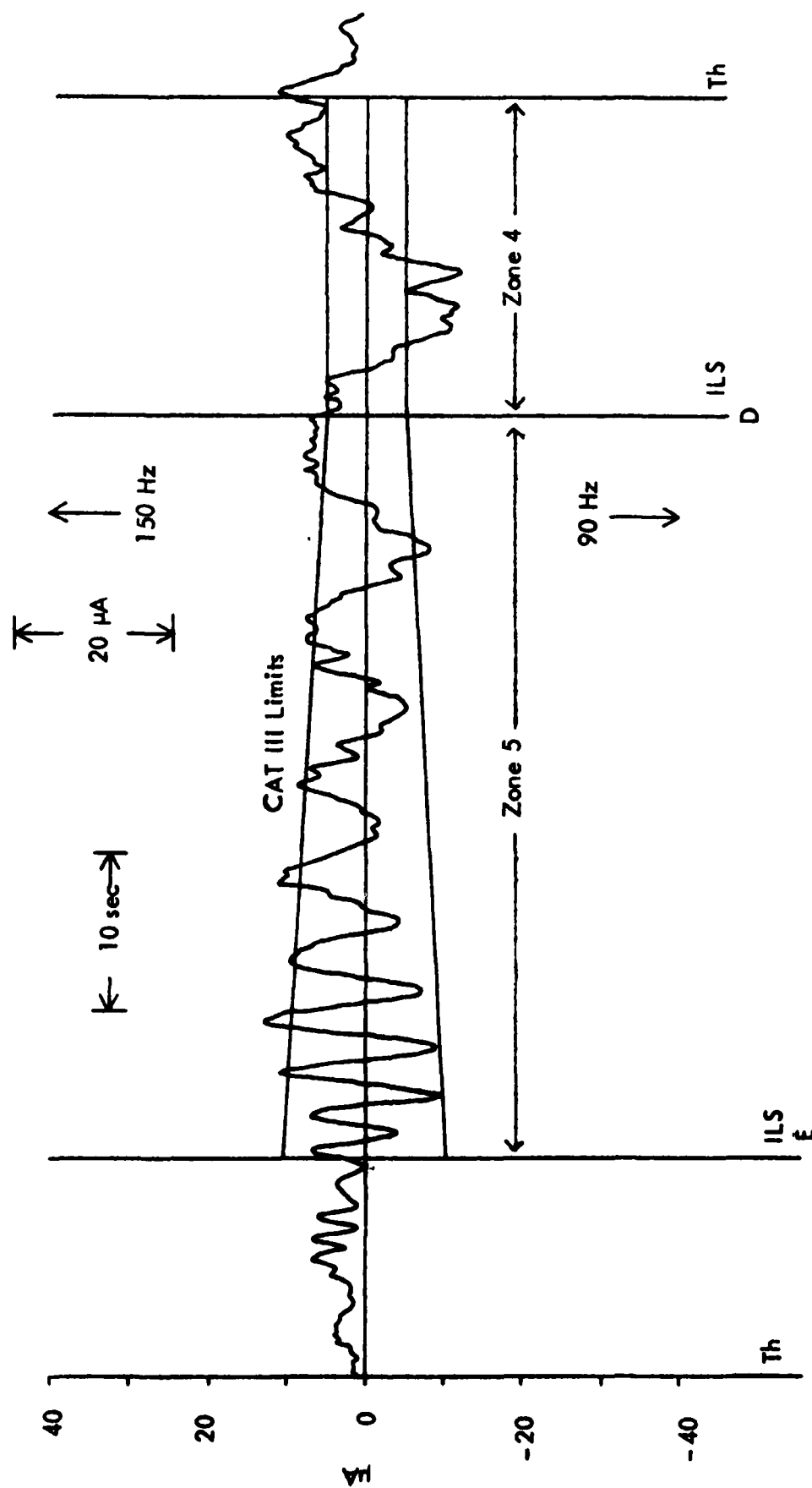


Figure 2-45. Flight Recording of the Structure Produced When Additional Course SBO Energy Is Directed to the United Airlines Maintenance Complex. Note that the location and period of the scalloping remains constant whereas the amplitude of the scallops has increased.

Once identification of the reflecting surfaces had been accomplished, it was desirable to confirm the area and also to obtain information as to possible means of correcting the problem. Phasing of the SBO energy was attempted with little success. One reason for this was the limited time for access to the runway to make ground observations and the generally unsatisfactory nature of the ground observations that were being obtained with a van. Since the phasing was not considered as a viable means of producing an ultimate solution because of attendant monitoring difficulties, efforts in this direction were not continued.

Reference to materials on diffraction of electromagnetic waves gave indications that the problem was likely arising because of localizer signal energy diffracting over the top of the screen into the United Airlines complex. Because it was easier to remove sections of the reflecting surface rather than construct additional, higher screen sections, several parametric measurements were made with the screen lowered in approximately one-foot increments. The screen is composed of horizontally-run #12 wires with approximately $1\frac{1}{2}$ inch spacing between them. For the measurements, the first 8 wires were removed, then 8 more, and finally 7. After each of these had been accomplished, two flight measurements of the structure in Zones 4 and 5 were made. As usual, the repeatabilities from run to run were excellent. Figures 2-46, 2-47 and 2-48 show the results in the form of increasing amplitudes of the scallops in Zones 4 and 5. The average peak-to-peak amplitude went from 6 microamperes with the original height to an average of 13 microamperes with 23 wires removed. This allowed a relationship to be established between the height of the screen and the size of course scallops. From this, it was easy to extrapolate to determine the potential benefits of increasing the height of the screen.

The possibility of obtaining significant improvement in the structure by raising the height of the reflecting screen was reported to the San Francisco Airway Facilities Sector office. The manager responded by delivering a tremendous supporting effort to raise the height of the screen by 6 feet. Because this was done in such an expeditious manner, it was possible to make measurements within 36 hours of the modified antenna. The modification consisted of a section of chicken-wire screen run at the top of the original screen, thus providing for 6 feet of increased height. Figure 2-49 shows the results with the structure now at 60% of Category-III tolerance limits. This is clearly a solution to the problem. Figures 2-50 and 2-51 show the parabolic screen with the additional section of chicken wire temporarily in place at the top. This configuration was measured by FAA flight inspection and found to produce a structure which was 40 to 50% of tolerance limits.

As mentioned earlier, because of the importance of obtaining a prompt solution to the localizer structure problem, work was simultaneously underway on a parallel approach. This involved establishing the 14-element, wide-aperture localizer which has been recently designed and was under evaluation at the Tamiami Airport, Miami, Florida. The array was set up immediately in front of the parabolic antenna system and flight checked to determine if it had any detrimental effects on the commissioned localizer performance.

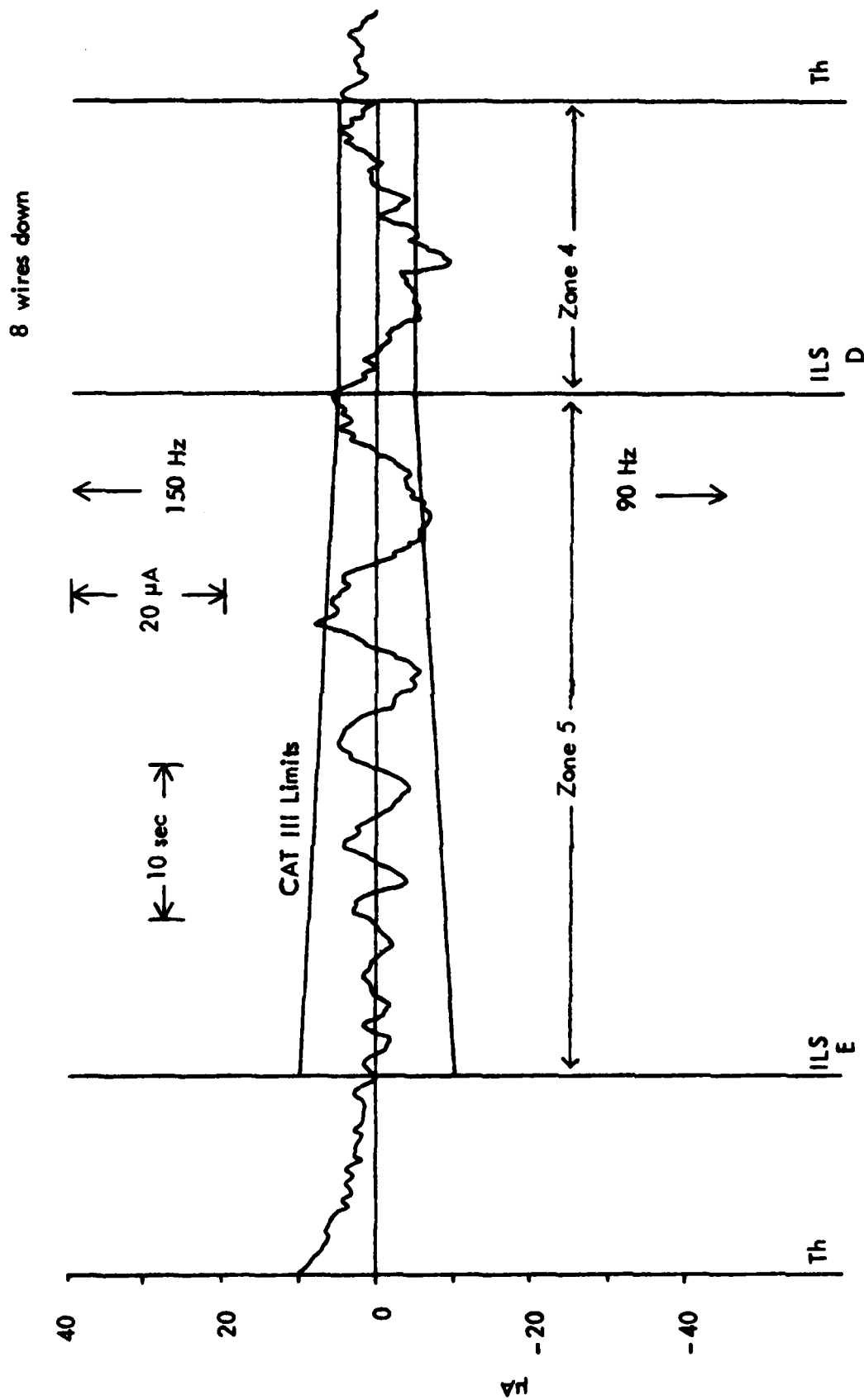


Figure 2-46. Flight Recording of the Course Structure Produced for Normal Conditions Except the Height of the Parabolic Screen Has Been Lowered By 8 Horizontal Wire Elements.

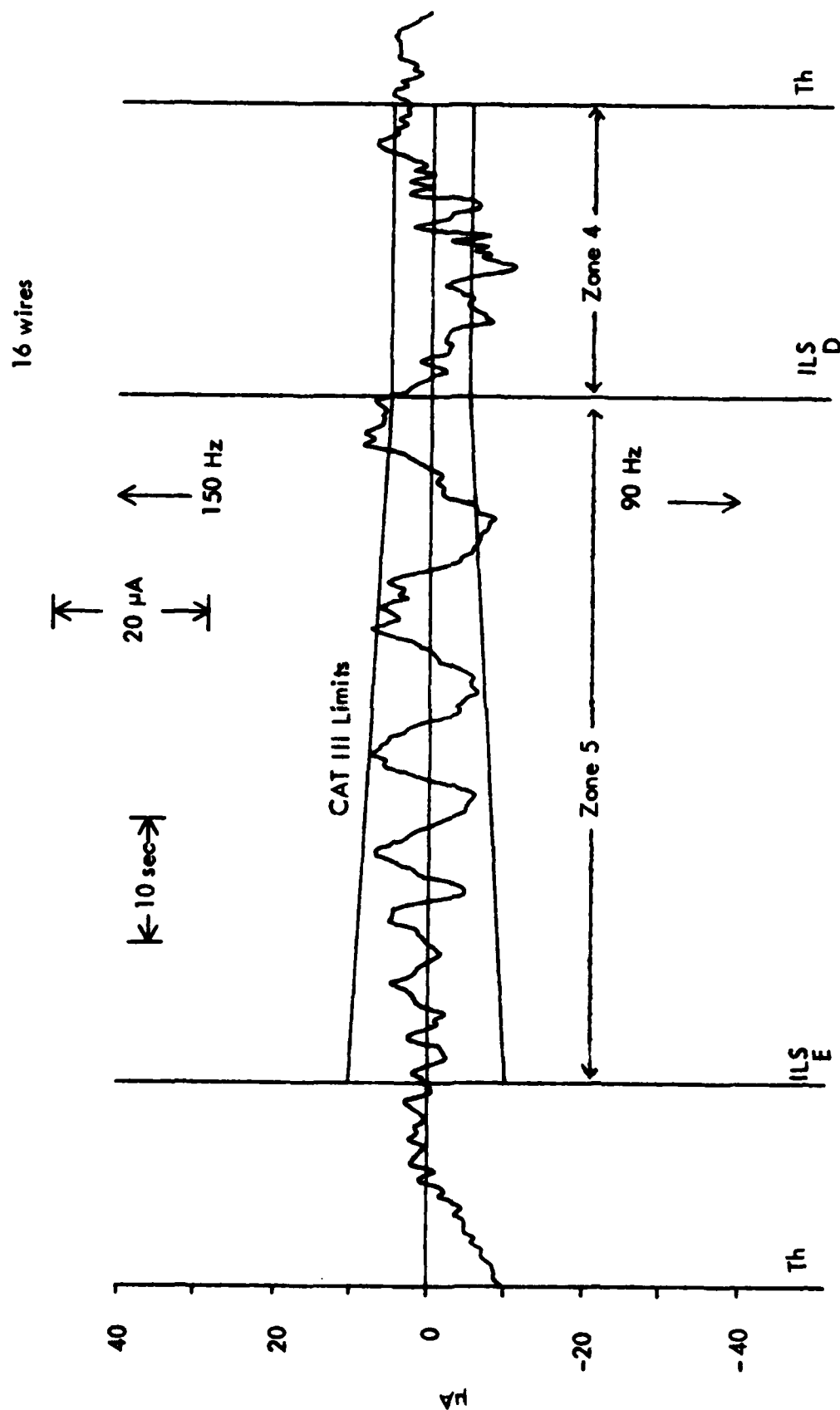


Figure 2-47. Flight Recording With Conditions Similar to Figure 2-46 Except that 16 Wire Elements Have Been Removed Thus Lowering the Height of the Screen Approximately 24 inches.

10-2200

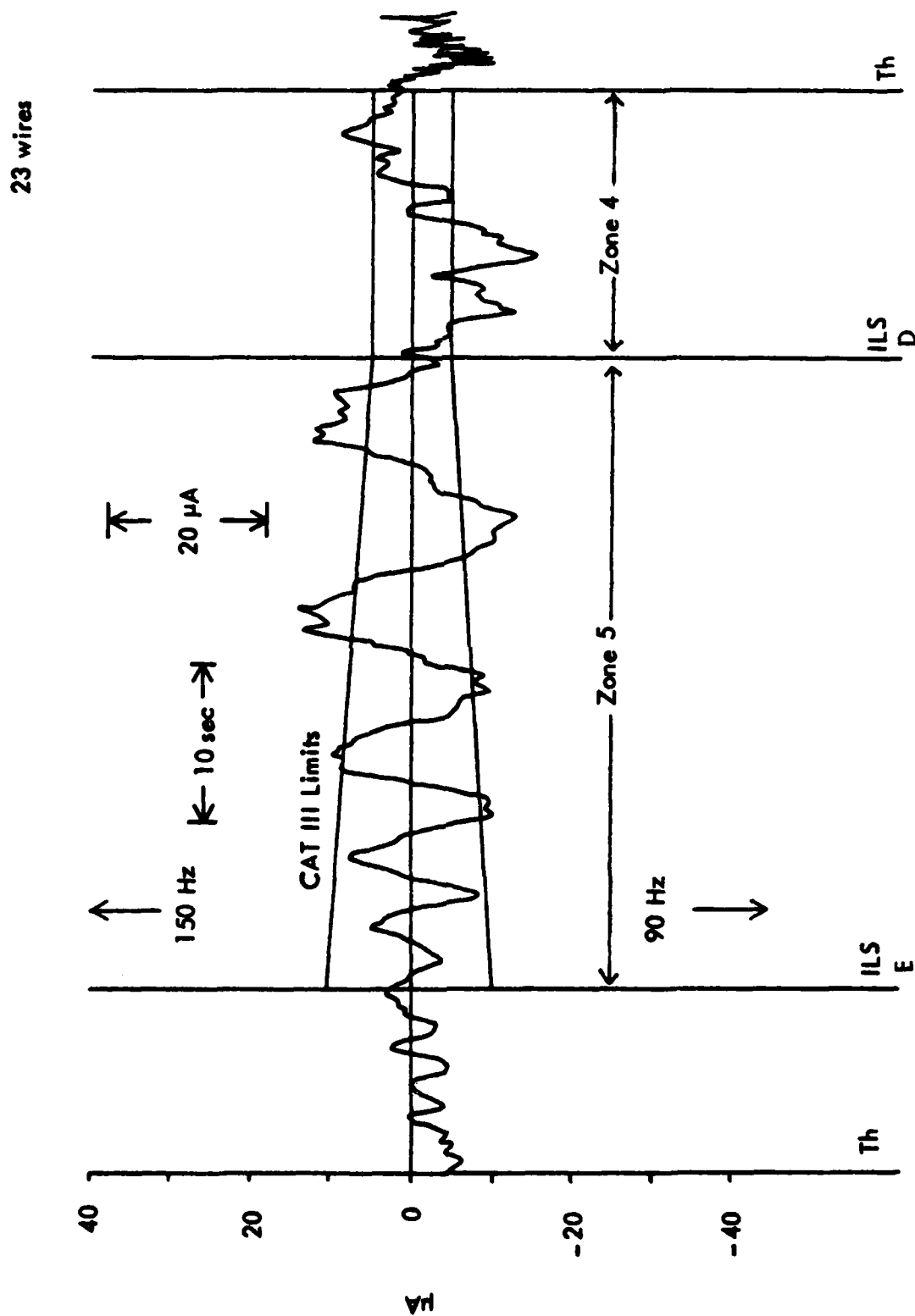


Figure 2-48. Flight Recording With Conditions Similar to Figure 2-46 Except that 23-wire Elements Have Been Removed Thus Lowering the Height of the Reflecting Screen by Approximately 3 Feet.

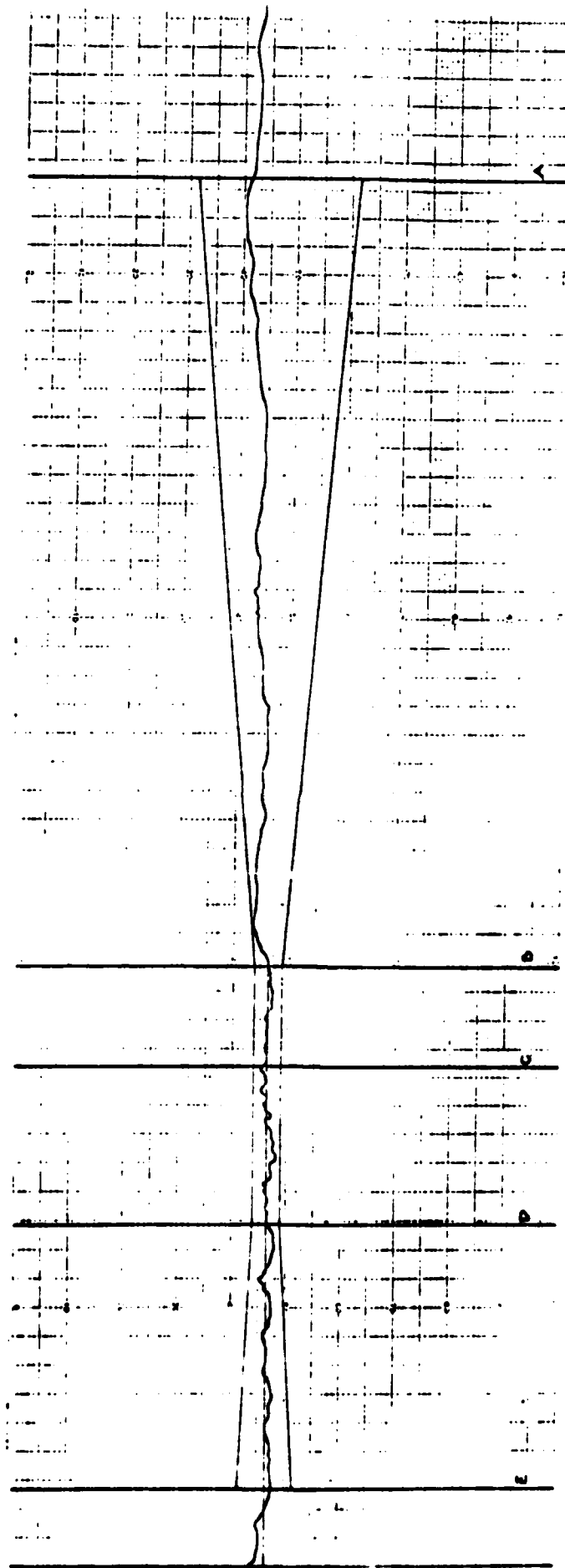


Figure 2-49. Flight Recording Showing the Improvement Obtained in the Structure When the Parabolic Screen is Raised 6 Feet. This clearly indicates that raising the height of the screen is indeed a solution to the localizer structure problem. This record shows that roughness reaches only 60% of Category-III tolerances in ILS Zone 4.



Figure 2-50. Photograph of Parabolic Antenna Array With 6-foot Extension In Place. The extension was produced by introducing a wooden framework on top of the existing metal structure.

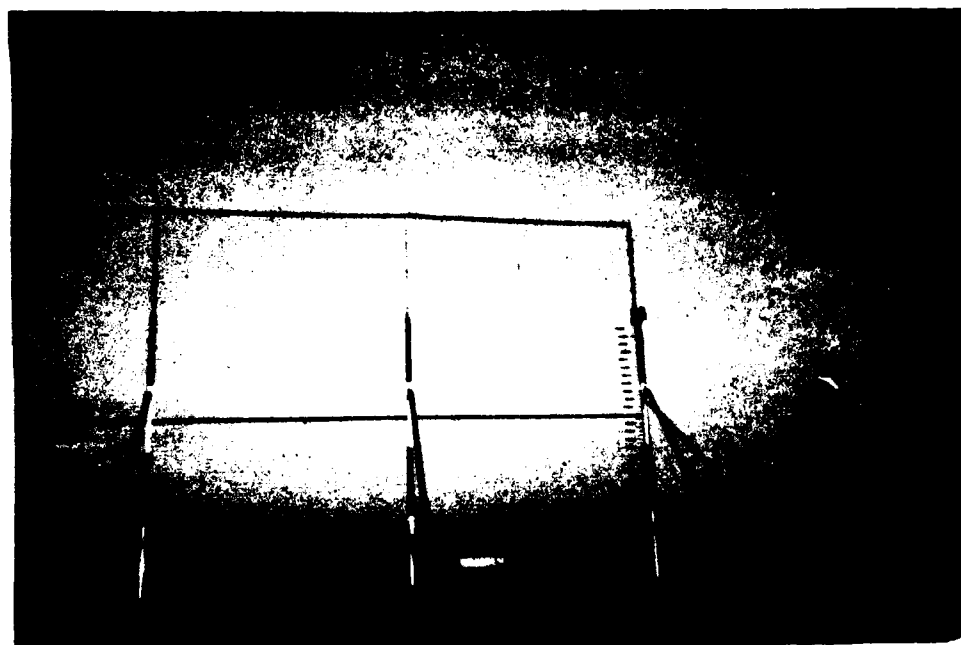


Figure 2-51. Another Photograph of the 6-foot Extension Constructed At the Top of the Existing Parabolic Reflecting Screen. The aircraft is the FAA Saberliner in the process of flight checking the system.

Measurements showed that it had no effect. Care was taken to insure that symmetrical conditions were maintained throughout the existence of the array in that position. Figure 2-52 shows the 14-element array in place.

Measurements made with this array showed complete relief of the reflections from the United Airlines complex; however, effects of SBO reflecting from the American Airlines hangar are apparent but to only 70% of Category-III tolerance limits. Figure 2-53 shows a copy of the flight recording made with the array adjusted for standard width conditions of 3.0 degrees. Clearly this array, too, is a solution to the San Francisco localizer problem on 28R.

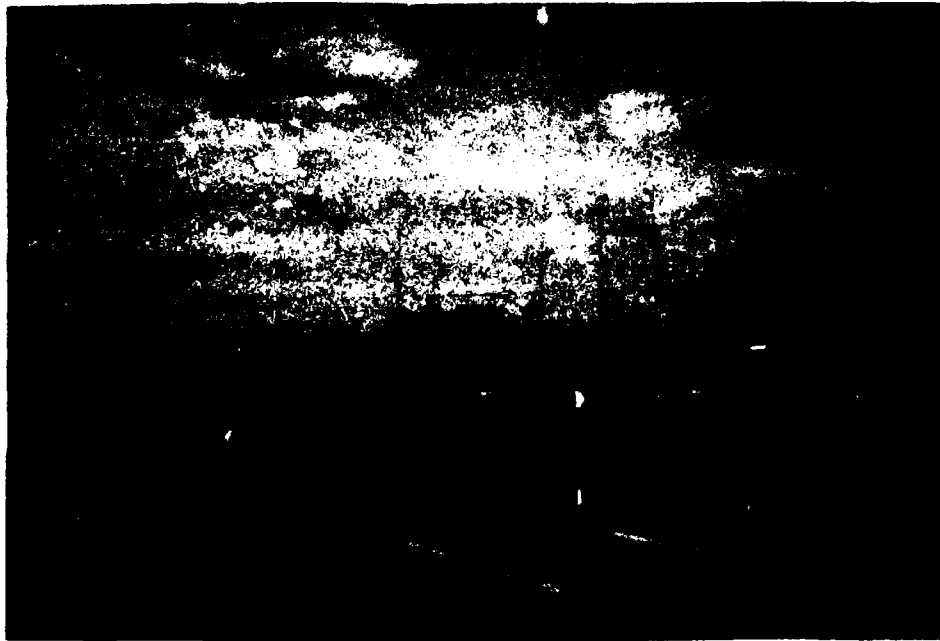


Figure 2-52. Photograph of the 14-element, Log-periodic, Wide-aperture Array in Place in Front of the Existing Parabolic Antenna System. This array produced no detectable effect on the course structure produced by the parabolic array.

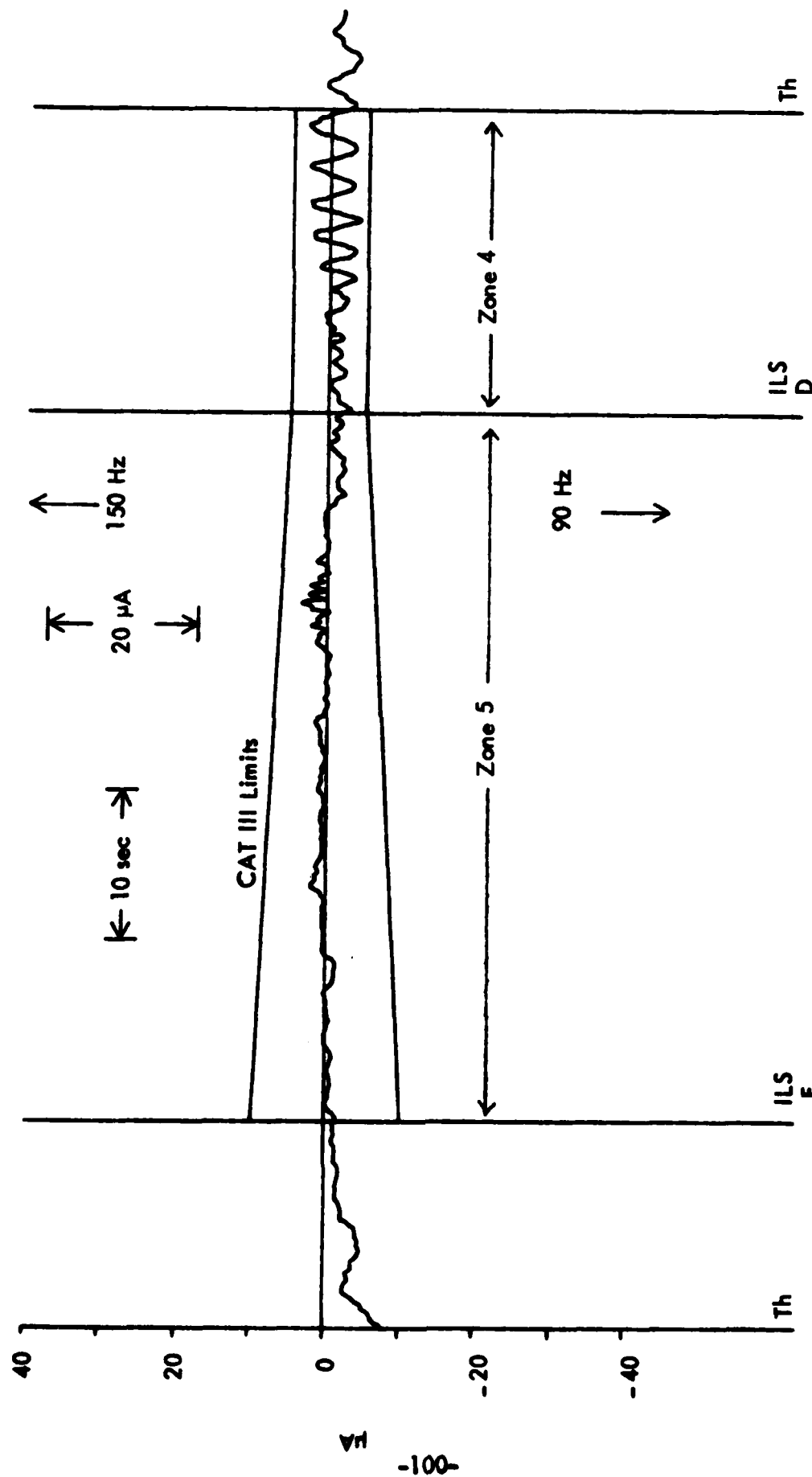


Figure 2-53. Flight Recording of Course Structure Produced With the 14-element, Log-periodic, Wide-aperture Array. The effects of the United Airlines Complex is essentially gone; however, more evident now are the effects in Zone 4 of the American Airlines jumbo-jet hangar. Nevertheless, only 70% of tolerance limits are reached and this, too, becomes a possible solution to the Category-III requirements problem.

RECOMMENDATIONS.

From information obtained from both analytical and experimental phases of the work effort, two very specific recommendations can be made with full confidence that implementation of either will produce an acceptable Category-III course structure especially in the problem areas of ILS Zones 4 and 5.

First, the recommendation is that the parabolic reflecting screen be raised approximately 6 feet making the overall surface nearly 24 feet high. The purpose is to reduce the magnitude of the energy diffracting over the top and onto the United Airlines maintenance complex. This complex has been positively identified as being the problem reflector. Any conducting screen can be used. The degree of conductivity is not critical.

Second, the recommendation is that the parabolic antenna system could be replaced with the newly designed 14-element, log periodic, wide-aperture array to obtain acceptable path structure throughout the entire range of interest for Category III including Zones 4 and 5. This array has low-level back radiation and has sufficient directivity in the forward direction to allow satisfactory operation in spite of the presence of the American Airlines jumbo-jet hangar at a 15-degree azimuth north from the runway centerline.

MODIFICATION TO THE FA-5723 AND FA-8633 CLEARANCE TRANSMITTERS.

CONCLUSIONS.

A newly designed Auxiliary Monitor Dectector Unit for the FA-5723 and the FA-8633 clearance transmitters has been tested at Ohio University, Midway Airport, Chicago, Illinois and Fulton County Airport, Atlanta, Georgia. The design provides a monitoring of the load termination of the above transmitters. Results of the field testing were as follow:

1. The Auxiliary Monitor Dectector provides load termination protection for the clearance transmitter.
2. Installation and testing procedures are adequate to provide required information to field personnel.

SUMMARY.

Modification AF-P 6750.1, Chapter 289, Change 288 dated 5/5/80 was found not to perform as intended on all FA-5723 and FA-8633 clearance transmitters. This is attributed to a variation in the adjustment of the transmitters at the capture-effect glide-slope sites in question. The difficulty in adjusting the original modification after installation was observed at several sites and field modification of the units was attempted. While the field modifications appeared to function at some sites it was found that the possibility of a modulation level reduction existed. To overcome this problem and that of the transmitter-to-transmitter variability, a new circuit has been designed and tested.

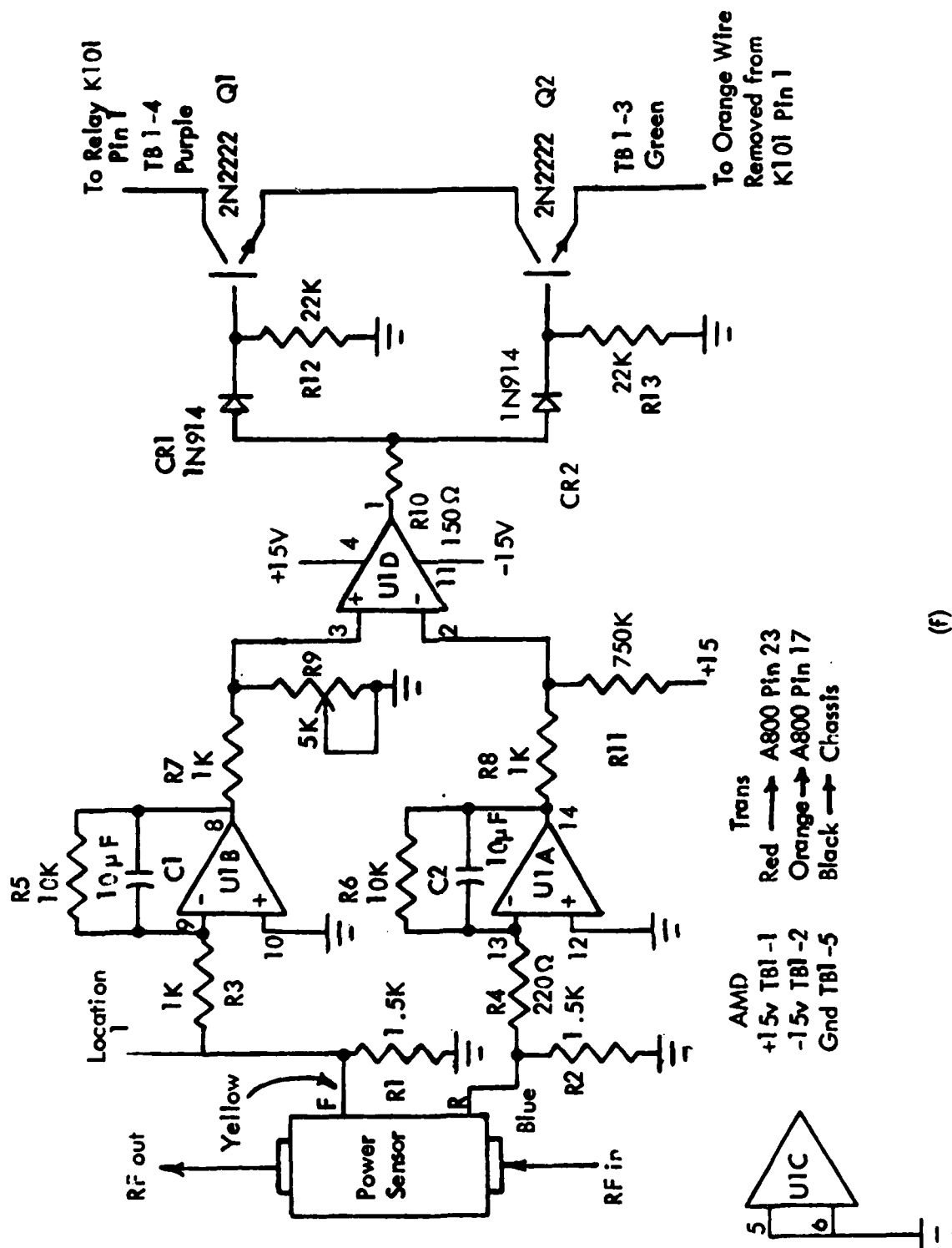


Figure 12-18 Auxiliary Monitor Detector.

(f)

ILS SET-UP PROCEDURES

ILS INVESTIGATION OF GROUND-CHECK PROCEDURES FOR ILS GLIDE SLOPES.

INTRODUCTION AND BACKGROUND.

Aircraft instrument landing systems are designed to provide operational capability to permit the pilot of any appropriately equipped aircraft to approach and land at an airport during conditions of marginal visibility. Safety is clearly essential for ILS operation. The performance record is impressive; these systems have been working for four decades and no accident has been attributed to ILS failure. Thus, the impetus for the work presented here is not safety, but cost.

Currently, the integrity of ILS operation is maintained by costly periodic airborne measurements in addition to some form of near-field monitoring. A lower cost alternative, which is the topic of this paper, substitutes near-field ground measurements for the airborne measurements.

A possible deficiency in ground measurements, as opposed to airborne measurements, is that path variations caused by terrain irregularities beyond the measuring point cannot be sensed. An illustration is shown in figure 3-1. To account for the effects of terrain irregularities using ground measurements, a program is outlined here which employs a terrain-sensitive glide slope model in conjunction with near-field ground measurements to verify that a glide slope system is performing within safety tolerances.

An additional consideration of the ground-based measurements is the sensitivity of the current near-zone monitor to environmental variations. Specifically, conditions can exist, such as snow on the ground plane that cause the near-field monitor to sense an out-of-tolerance situation, although the far-field glide path is within tolerance. Circumstances such as this are clearly not in the best interests of safety, as they deprive the pilot of electronic guidance, often when it is most needed. To reduce the occurrence of unnecessary system outages resulting from the over-sensitivity of the near-field monitor, the measurement procedure presented in this paper can be performed as the monitor approaches an out-of-tolerance condition to determine whether the monitor indication is representative of the far-field signal or is merely influenced by some extraneous factor.

The objective of this work is to investigate the feasibility of ground checking a glide slope facility both as a substitute for flight checking and for routine system maintenance. The means of this investigation will be the use of computer models to study near-zone glide slope signal behavior and to correlate near-field measurements to far-field glide path characteristics. Basically, these measurements will be made by rising a horizontal dipole receiving antenna along a mast at selected locations. Standard equipment such as a Portable ILS Receiver (PIR) will be used to provide CDI as a function of receiver antenna height.

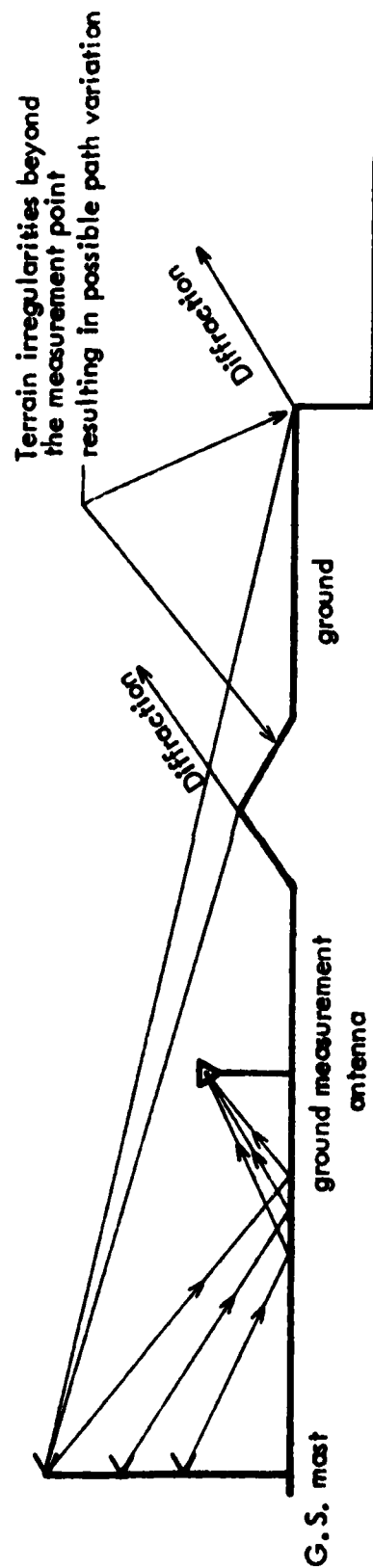


Figure 3-1. Geometry Illustrating a Possible Deficiency in Ground Measurements Caused by Terrain Irregularities Beyond the Measuring Point.

As a result of this effort to define a new monitoring scheme, a computer model (TGCGS) has been developed to predict near-zone electromagnetic signal behavior. This model accounts for the effects of a sloping three-dimensional and finitely conducting reflecting plane in addition to known near-field effects (spherical wave incidence, ground surface roughness).

Although the theory described in this paper is applicable to any image-type glide slope system, only the capture-effect glide slope (CEGS) is addressed specifically. Hence, a discussion of image systems is given, followed by a brief description of the CEGS. Subsequently, the TGCGS model, used to model the near-zone of the CEGS, is presented. Following the model description is a comparison of measured and modeled results.

NEAR-FIELD MODEL (TGCSG) DESCRIPTION.

EXISTING MODELS. Most of the work concerning the modeling of ILS performance emphasized irregular terrain effect on glide path characteristics. The first ILS modeling efforts were made by Ohio University and subsequently developed at the Ohio University Avionics Engineering Center during recent years.

Techniques based upon physical optics and on the half-plane diffraction solutions were the basic approaches used. The most recent model is the Ohio University GTD model which makes use of both the Geometrical Theory of Diffraction (GTD) and the Uniform Theory of Diffraction (UTD). This model can also estimate the effects of three-dimensional terrain irregularities on system performance.

Another model has been designed as a research tool for use in the study of the effects of various faults on the field patterns of an ILS Glide Slope. This later model has been used with near-field data (360-degree phase proximity point), but is limited to horizontal reflecting surface and plane wave propagation.

The TGCGS model, created for the work addressed here, calculates near-field factors. Specifically, spherical wave propagation, a finitely-conducting ground plane, and ground plane slopes (on two axes) are considered by TGCGS in estimating near-field characteristics.

A list of the parameters modeled by TGCGS is given in appendix B, and a detailed analysis of TGCGS is presented in the following chapters.

MODEL APPLICATIONS. Immediate detection of out-of-tolerance glide-slope system performance is the function of the near-field monitor. However, due to system and/or environmental variations, an out-of-tolerance condition may be sensed by the near-field monitor, although the far-field glide slope performance is within tolerance. Such erroneous detection will cause the glide-slope system to be removed from operation, an action that is clearly not in the best interests of safety. To provide information on system performance independent of the near-field monitor, near-zone ground measurements may be performed. Considerations germane to selecting meaningful measurement locations are discussed below. A major consideration in selecting a measurement location is good linearity of CDI versus antenna height for realistic receiving antenna heights. Sensitivity to fault conditions in the system, in addition to environmental variations, is also an important factor in establishing ground-check locations. Finally, a specific approach for clearance signal ground check is presented.

1. Computer-aided Approach to Selecting Ground Measurement Locations. Practical considerations (proximity to the runway and proximity to the glide slope mast) defines the available space for possible ground-check locations. To better define possible ground-check locations, an imagery grid on the region in front of the antenna mast was established, as is shown in figure 3-2.

For convenience, grid intersection points are identified by four or six digit numbers as follows:

4591 is $X = 45.75 \text{ m}$
 $Y = 91.5 \text{ m}$

and 122244 is $X = 122 \text{ m}$ (in front of the antenna mast)
 $Y = 244 \text{ m}$

For each intersection of this grid, TGCGS has been run for receiving antenna height varying from 0.5 m to 20.0 m. Four examples are given in figures 3-3 through 3-6.

The goal of this analytical research is to exhibit theoretically optimal locations in the sense of linear readings between +150 microamps and -150 microamps for reasonable antenna height (maximum obtainable experimental receiving antenna height = 15 m). For example, curve 91183 exhibits reasonable linearity for obtainable antenna heights.

A first set of possible locations showed off from this systematical study. The next step was to apply fault conditions in the CEGS system and to look at how the readings changed at these locations.

2. Fault conditions. As stated in the introduction, it is important to know how changes in the system can affect the performance of the glide slope. To be representative of glide path variations, the ground check locations must be sensitive to provide measurable and interpretable readings.

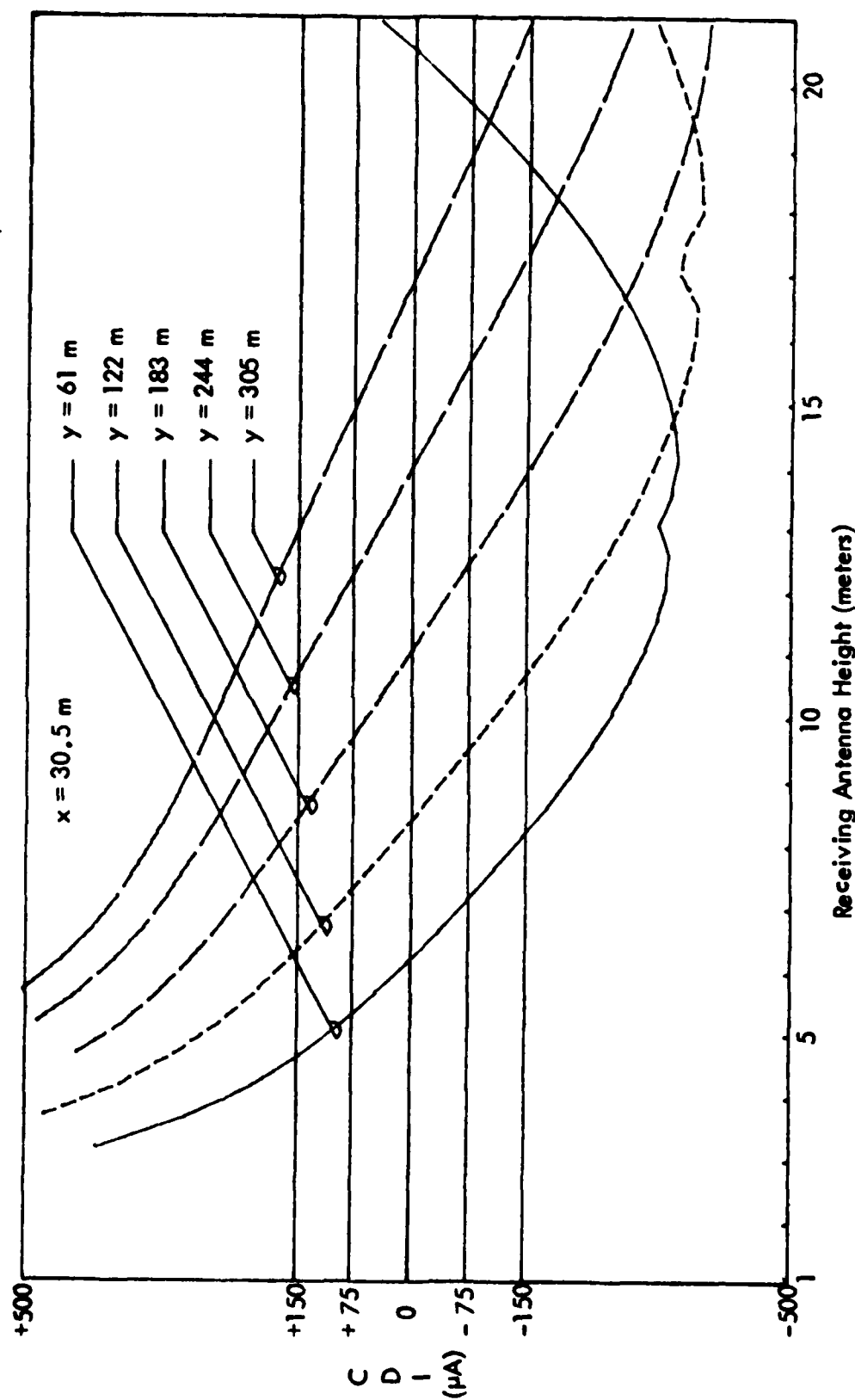


Figure 3-3. CDI vs. Receiving Antenna Height for Grid Line $x = 30.5$ m. Good linearity for obtainable receiving antenna height is seen for curves $y = 61$ m, $y = 122$ m, and $y = 183$ m (modeled).

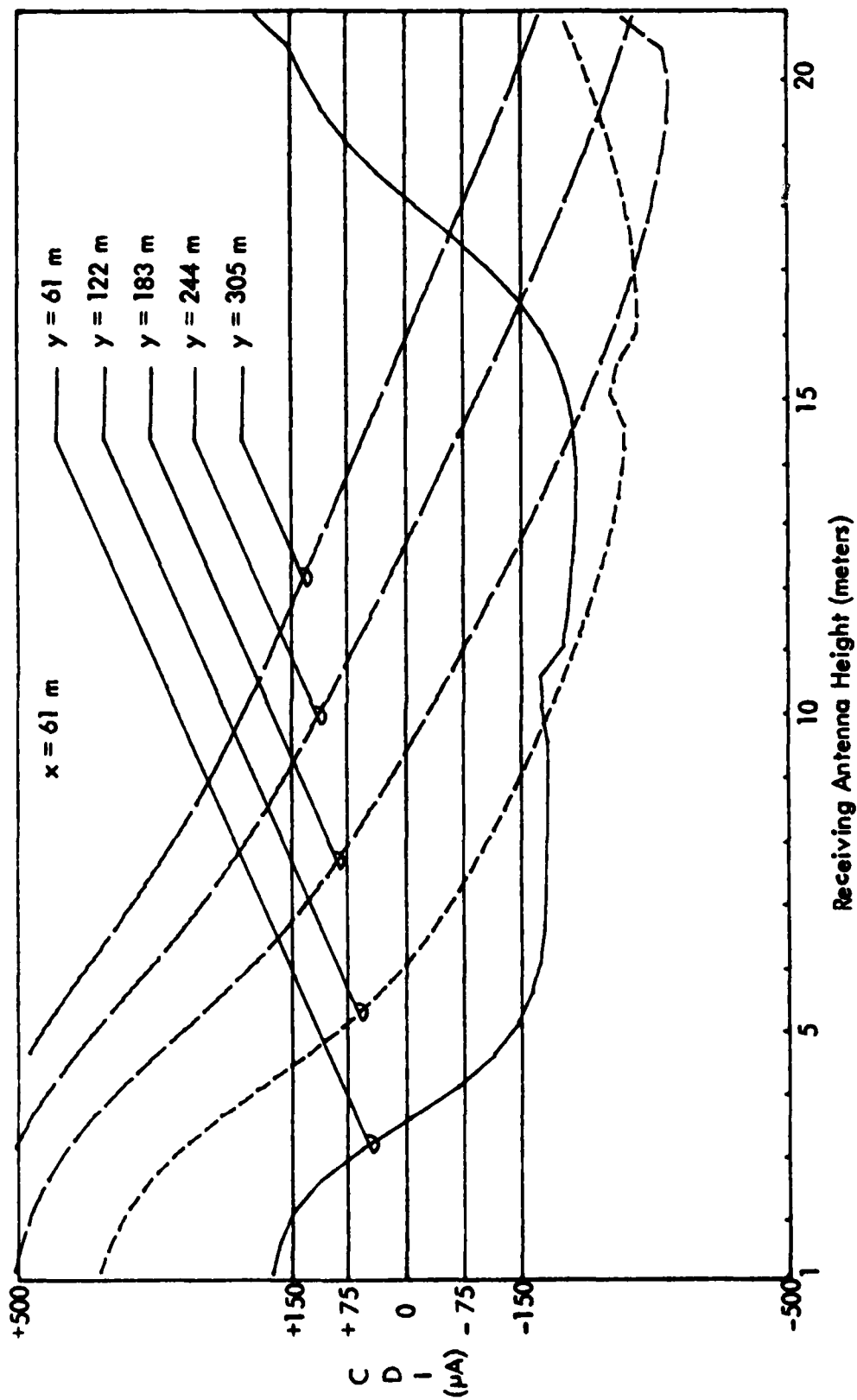


Figure 3-4. CDI vs. Receiving Antenna Height for Grid Line $x = 61$ m. Good linearity for low altitude receiving antenna height is seen for curve $y = 61$ m (modeled).

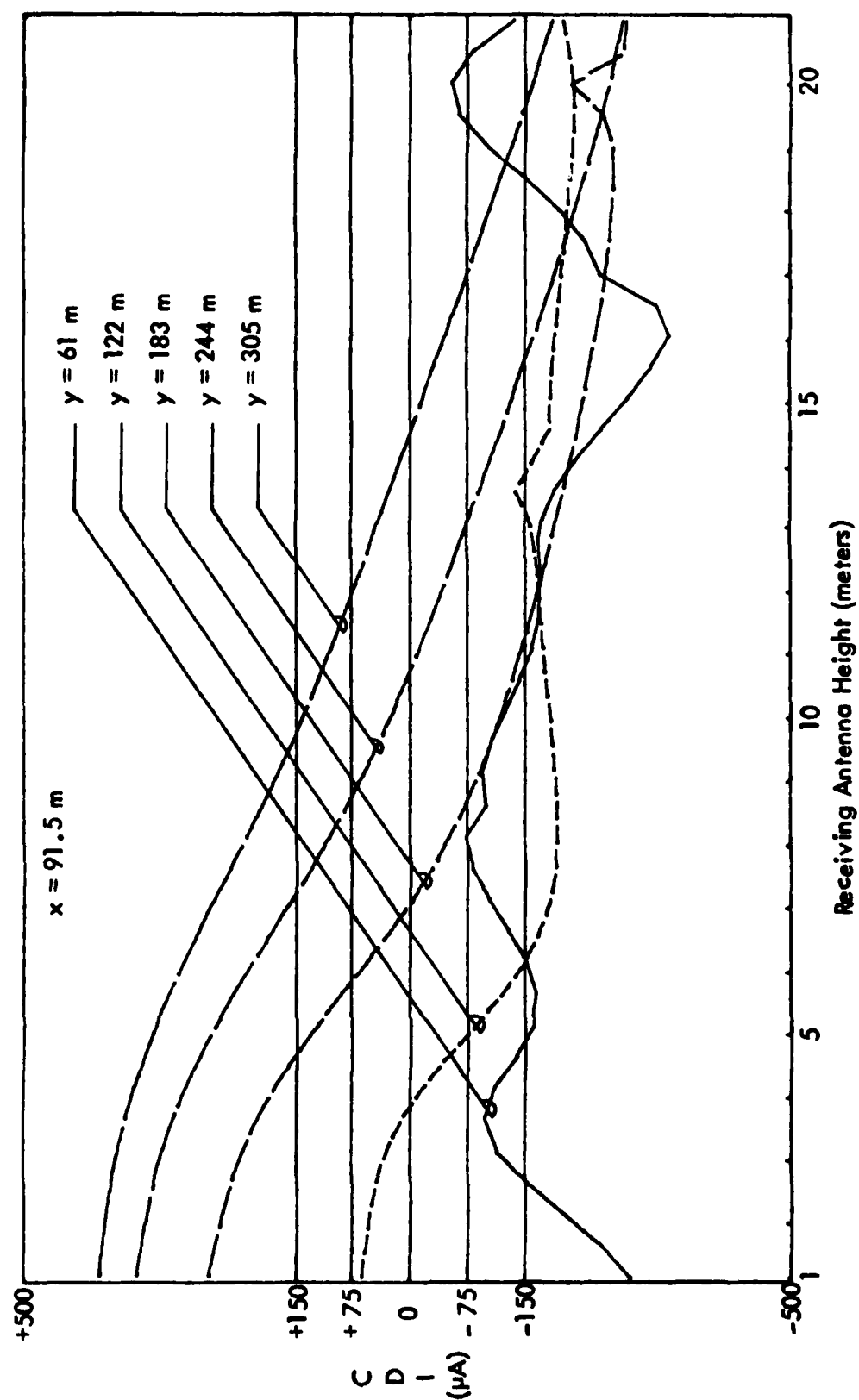


Figure 3-5. CDI vs. Receiving Antenna Height for Grid Line $x = 91.5$ m. Good linearity for obtainable receiving antenna height is seen for curve $y = 183$ m (modeled).

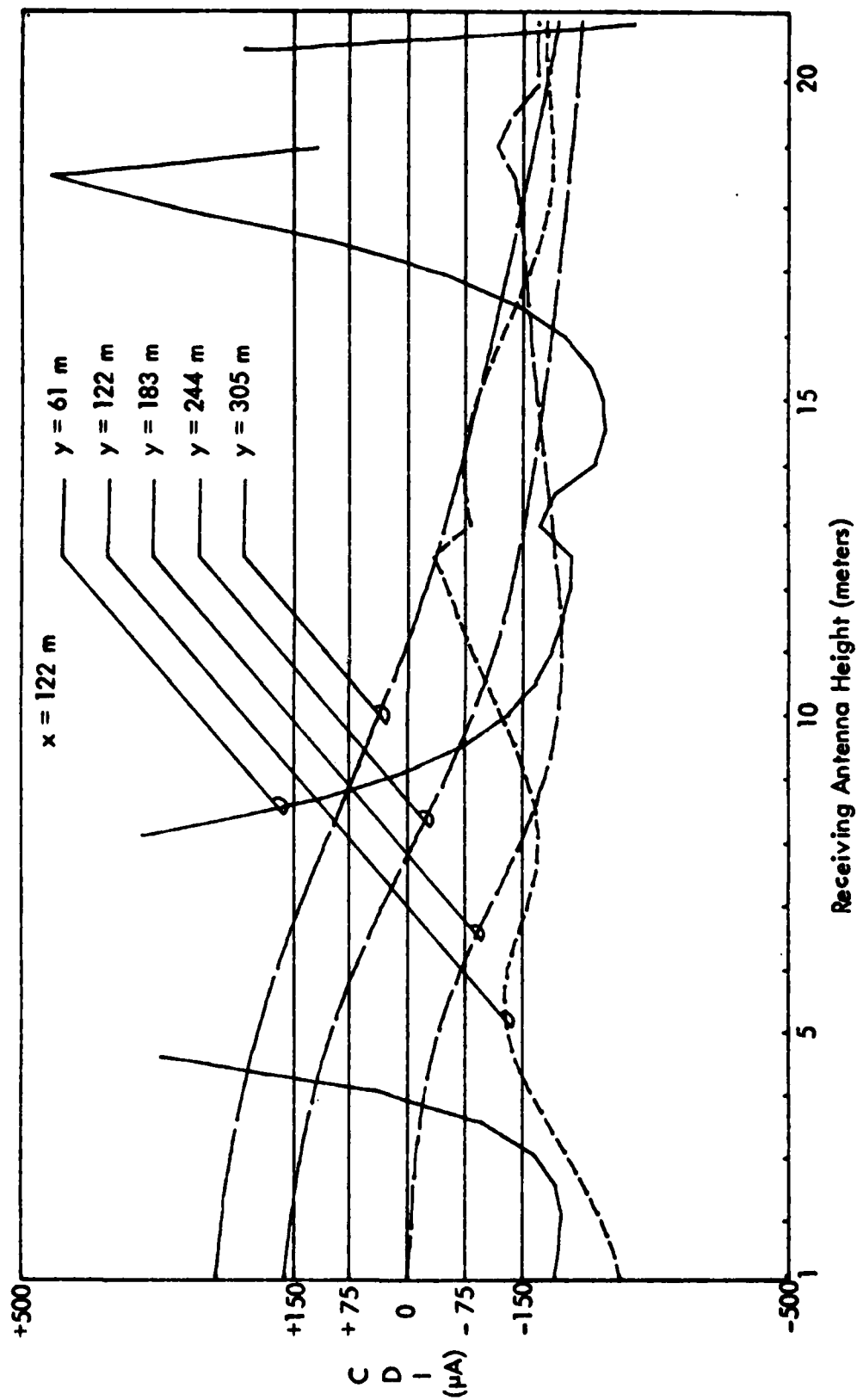


Figure 3-6. CDI vs. Receiving Antenna Height of Grid Line $x = 122$ m (in front of the antenna mast). Good linearity for obtainable receiving antenna height is seen for curve $y = 244$ m (modeled).

Figure 3-7 summarizes the effects of fault conditions on the glide path performance for a flat terrain.

Various fault conditions, representing possible troubles encountered in an operational glide slope, have been inputted in the model. To be able to experimentally reproduce these fault conditions, eleven primary changes have been used:

- * Broad alarm (A-ratio diminished)
- * Narrow alarm (A-ratio increased)
- * +15 degree dephasing in lower antenna
- * -15 degree dephasing in lower antenna
- * +15 degree dephasing in middle antenna
- * -15 degree dephasing in middle antenna
- * +15 degree dephasing in upper antenna
- * -15 degree dephasing in upper antenna
- * -3 dB attenuation in lower antenna
- * -3 dB attenuation in middle antenna
- * -3 dB attenuation in upper antenna

Figures 3-8 through 3-12 depict the theoretical readings for the 122244 point. From these curves, it is seen that if the zero CDI (or DDM) receiving antenna position can be recorded within an average distance of 50 cm around normal system zero CDI (or DDM) location, relevant indications can be interpreted on faults to investigate, if any.

3. Other perturbations. Weather effects like rain or snow may affect the glide slope performance. Therefore, taking advantage of the finite conductivity effect capability of the model, various values for permittivity and conductivity have been inputted.

By comparing figures 3-13 and 3-13a, one can conclude that at the considered observation point (244 m in front of the antenna mast), even though the reflection coefficient can be greatly affected, the resulting DDM stays in a very narrow range. Briefly, conductivity variations do not affect the glide slope performance in a sensitive way.

Snow effect has been considered as an evenly arised ground plane. Figure 3-14 depicts the repercussion of 10, 25 and 50 cm-thick snow layers (evident modification of glide path performance).

4. Ground check location selection. An adequate ground-check location will provide readings showing all the changes of the facility in a measurable and interpretable way.

From the previous analytical study, few locations had showed off because of good linearity in the readings at reasonable antenna heights. For each of these locations, the eleven primary changes have been applied to analyze the response of the system, 244 m in front of the antenna mast. Also, signal strength must be observed from figure 3-12, where signal attenuation versus azimuth angle is illustrated.

Condition	Glide Angle	Course Width	Clearance (Low Angle)
1. Reduction in Middle Antenna Signals	No Change	Widens	Reduces
2. Reduction in Upper Antenna Signals	Decreases	No Change	Reduces
3. Reduction in Clearance Signals	No Change	No Change	Reduces
4. Simult. Reduct. in Mant. & Clear. Sig.	No Change	Widens	Reduces
5. Reduction in Lower Antenna Signals	Increases	Narrows	Increases
6. Reduct. in ess Sigs. (from Primary Xmtr.)	No Change	Widens	No Change
7. De-Phasing Middle Ant. Signals	No Change	Widens	Reduces
8. De-Phasing Upper Ant. Signals	Decreases	No Change	Reduces
9. De-Phasing Lower Ant. Signals	Increases	Narrows	Increases

Figure 3-7. Effect of Faults in CEGS System on Glide Path Performances. These results are for a flat ground plane; irregular terrain may produce different results.

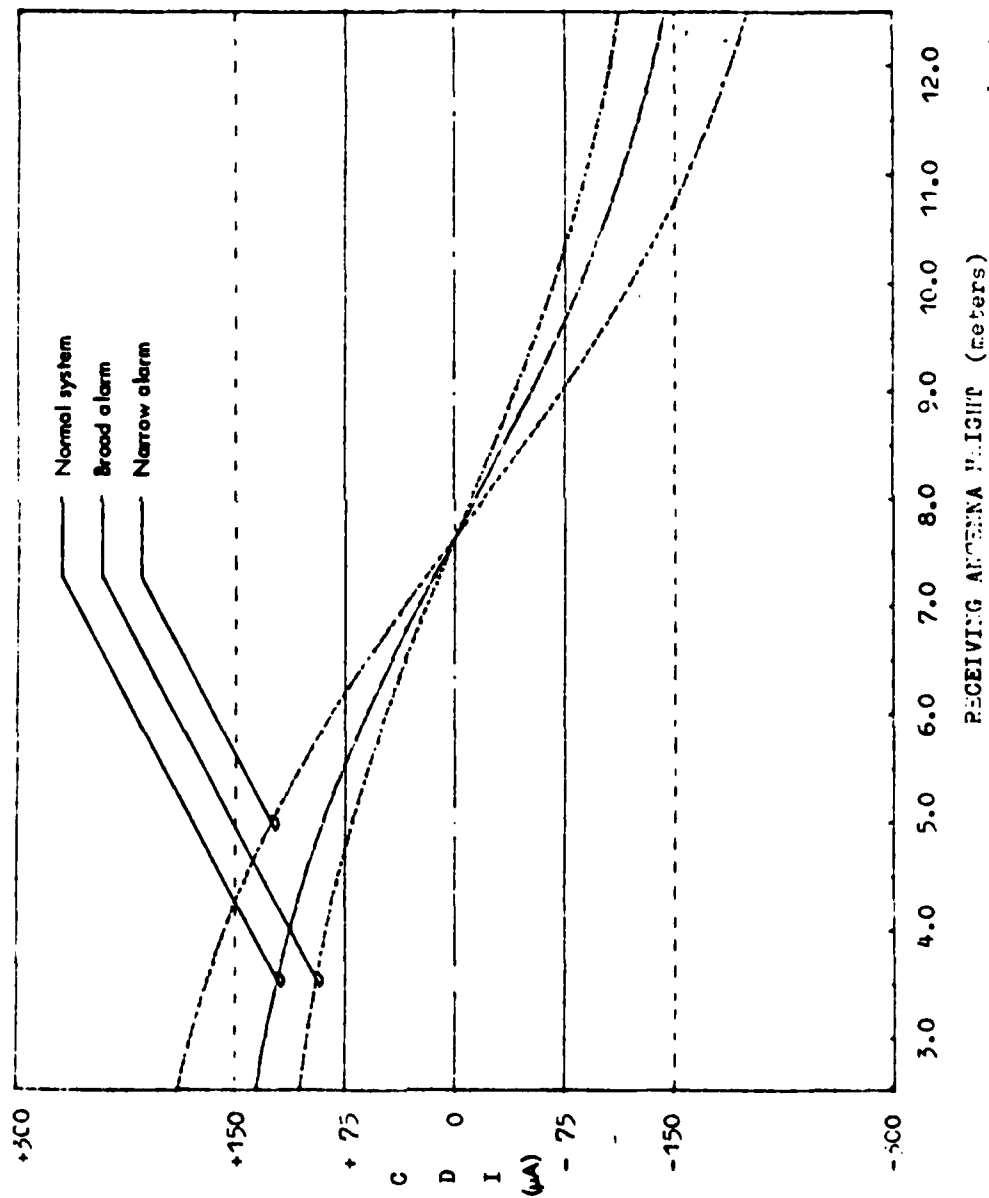


Figure 3-8. Modeled CDI vs. Receiving Antenna Height for Normal System and for Broad and Narrow Alarms.

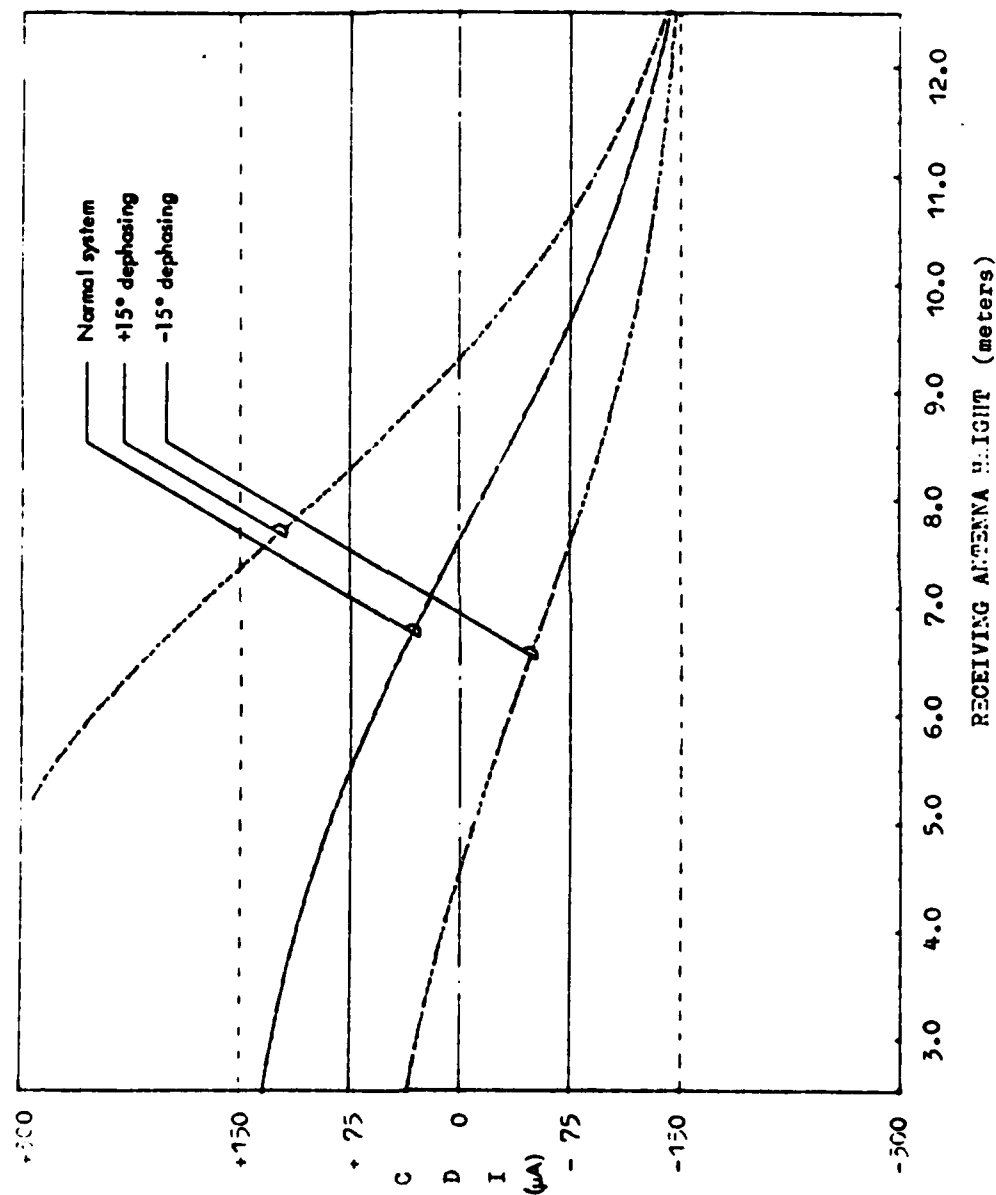


Figure 3-9. Modeled CDI vs. Receiving Antenna Height with $\pm 15^\circ$ Dephasing of the Middle Antenna.

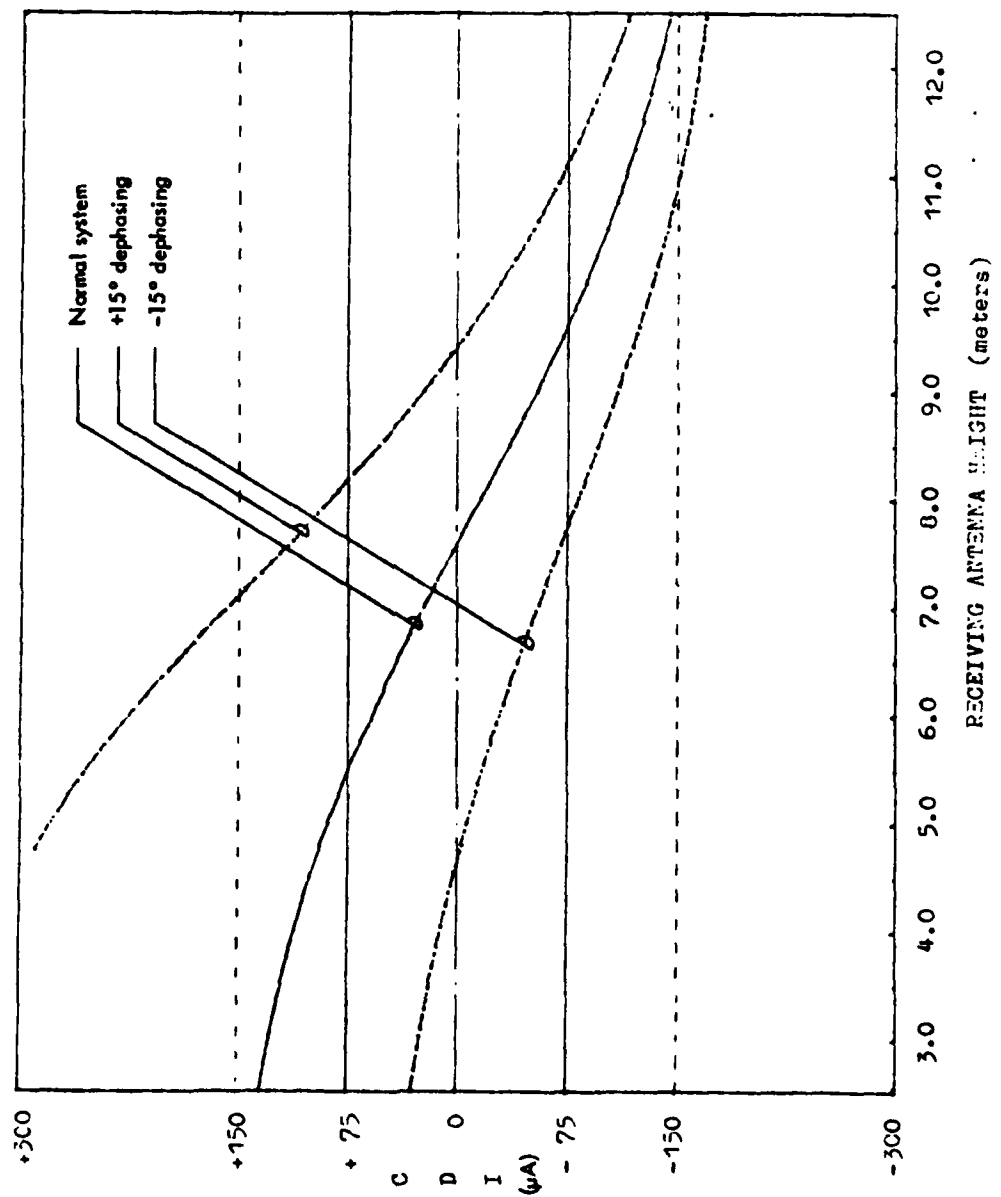


Figure 3-10. Modeled CDI vs. Receiving Antenna Height with $\pm 15^\circ$ Dephasing of the Lower Antenna.

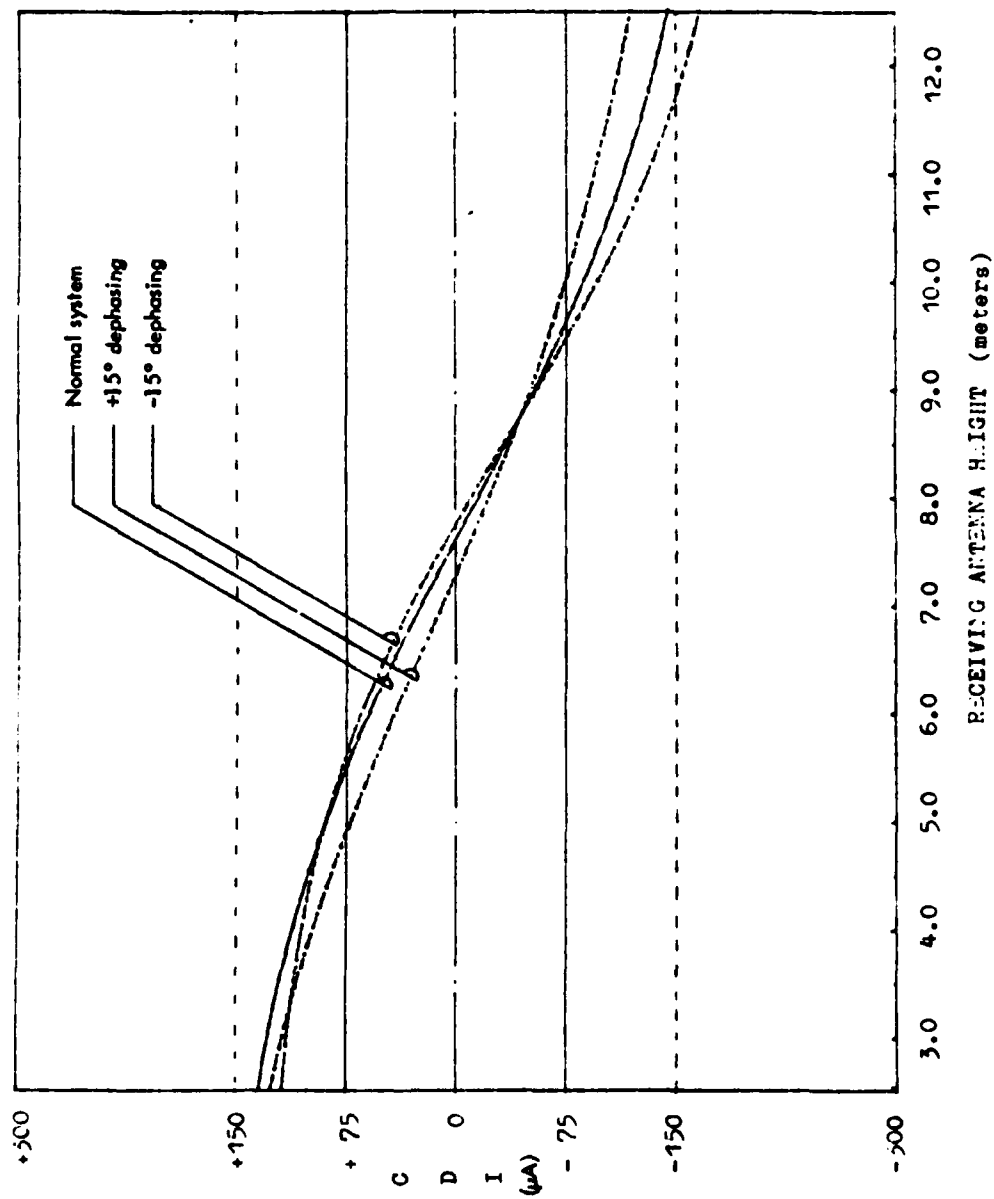


Figure 3-11. Modeled CDI vs. Receiving Antenna Height with $\pm 15^\circ$ Dephasing of the Upper Antenna.

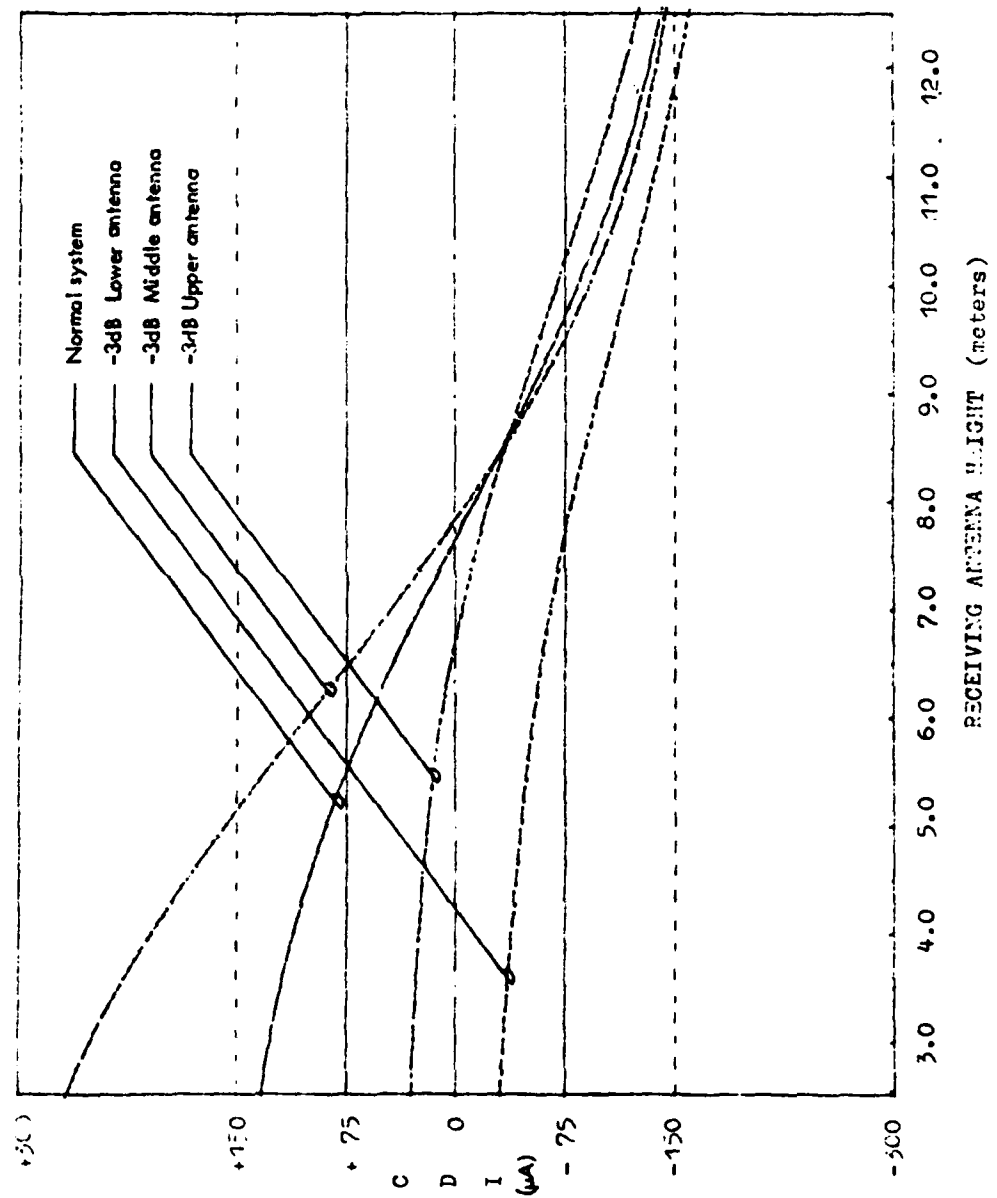


Figure 3-12. Modeled CDI vs. Receiving Antenna Height. Effect of attenuation in antenna currents.

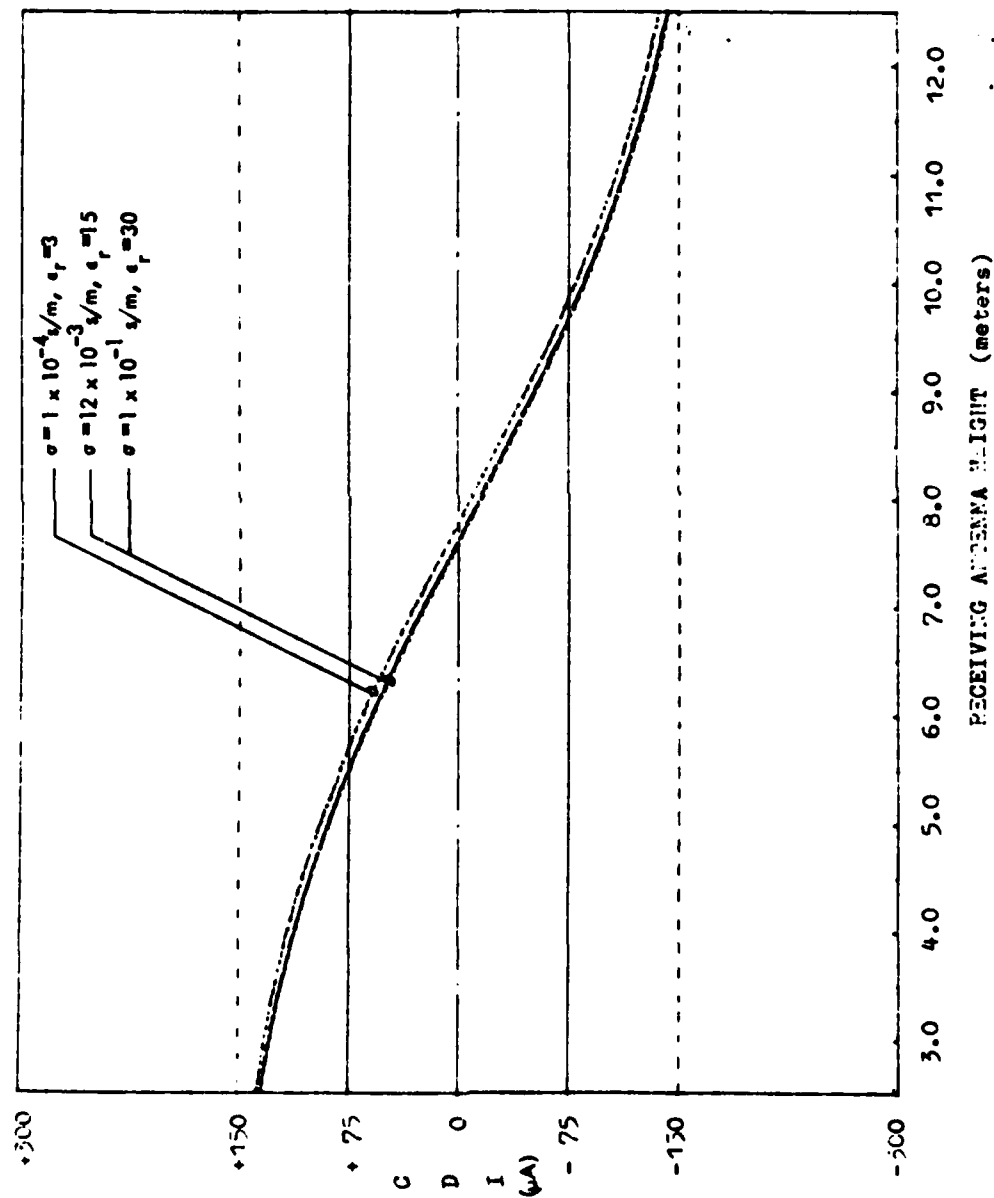


Figure 3-13. Modeled CDI vs. Receiving Antenna Height for Various Reflecting Ground Electric Constants. It appears that modifications in reflecting ground electric constants do not affect the glide path characteristics in a critical way (negligible effect).

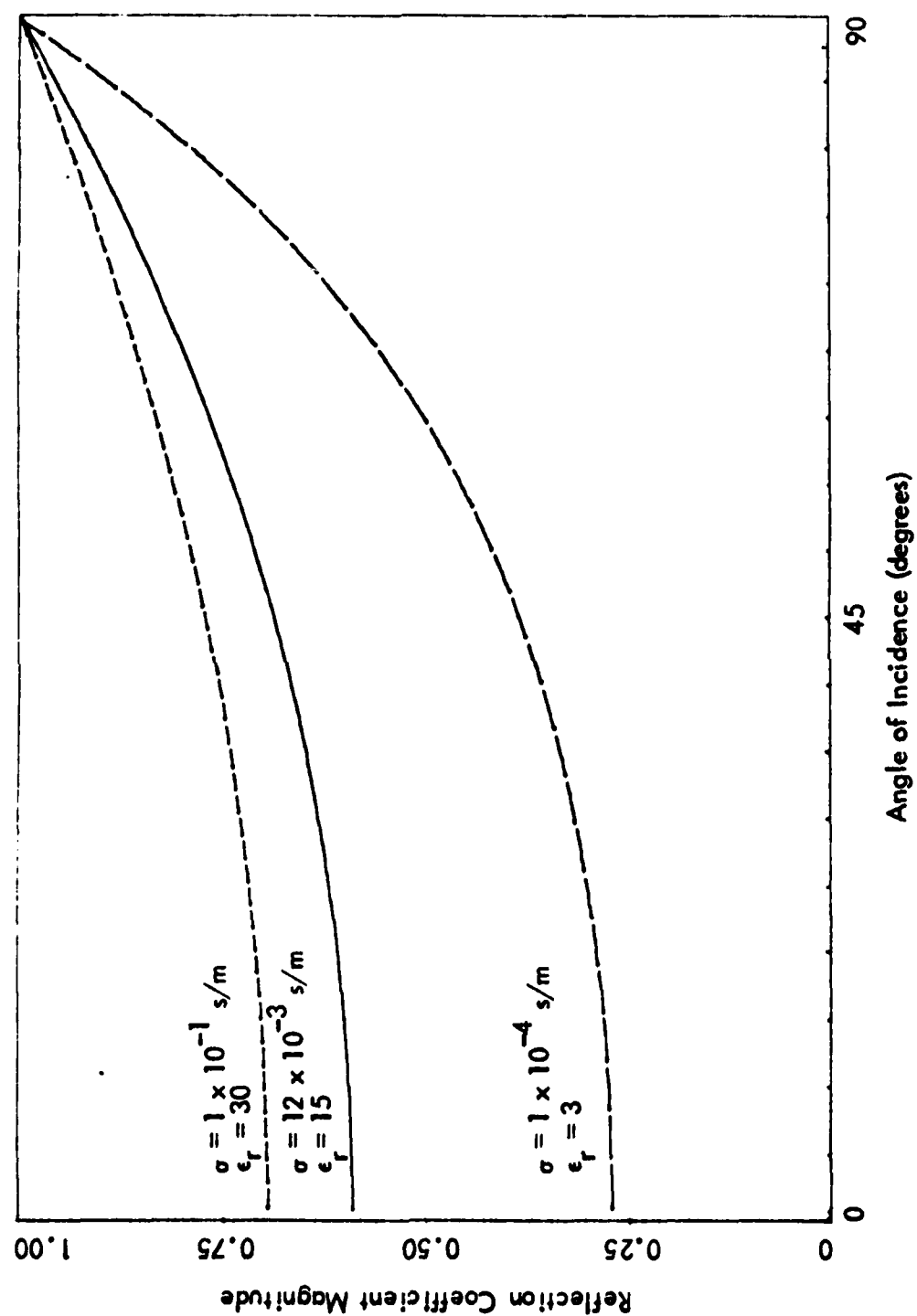


Figure 3-13a. Magnitude of the Horizontally-Polarized Reflection Coefficient vs. Incidence Angle for Various Ground Plane Electrical Constants (modeled).

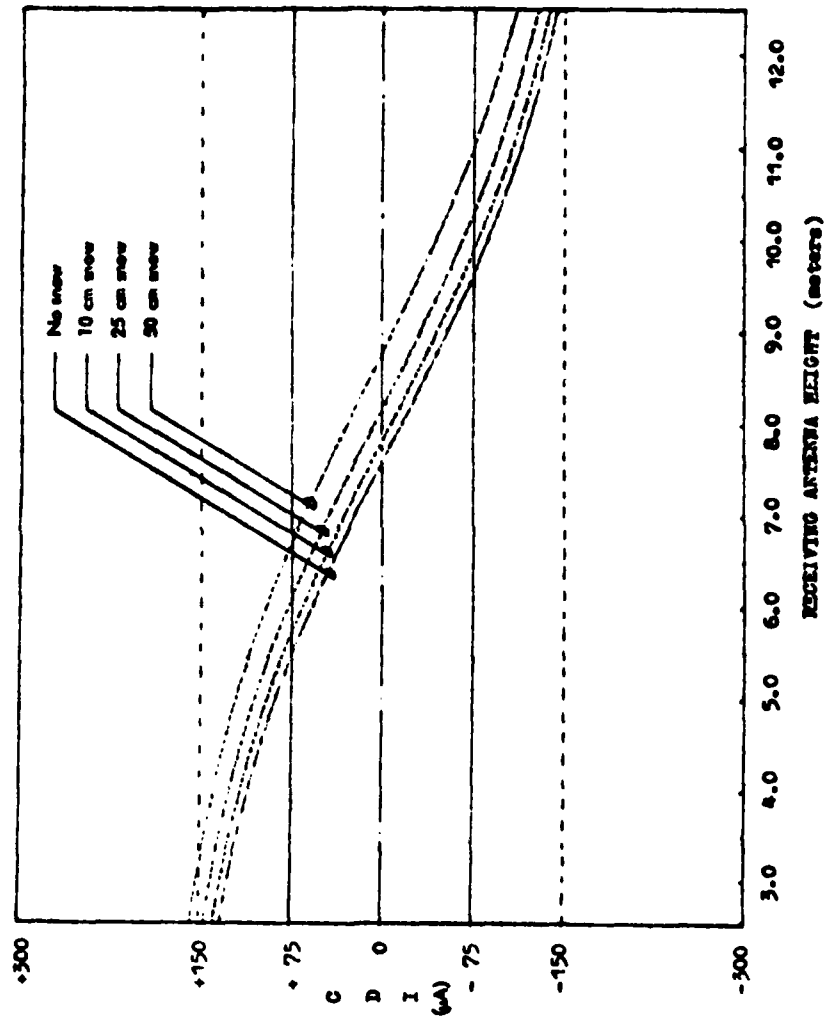


Figure 3-14. Modeled CDI vs. Receiving Antenna Height for Various Snow Depths.
Evident is the change in glide path due to snow thickness.

For instance, locations on the line between 1220 and 0244, being in the relative minimum of the array factor, have been rejected.

From all these considerations, a first set of three optimum locations has been selected :

- . 6161 (on the 45-degree line of figure 3-2)
- . 91183
- . 122244 (in front of the antenna mast)

5. Clearance Signal Checking. To avoid reading alterations due to the capture effect principles at low elevations, the clearance transmitter is turned off during the ground check of the glide path characteristics. Therefore, a specific clearance signal ground check, which consists of signal strength measurements, have been studied.

By recording minima of the clearance signal, one can compare these values with previously-recorded normal clearance signal strength measurements to detect possible anomalies. Figure 3-15 shows how clearance signal minima may change between a normal system configuration and faulty conditions, such as dephasing or attenuation in the upper antenna current.

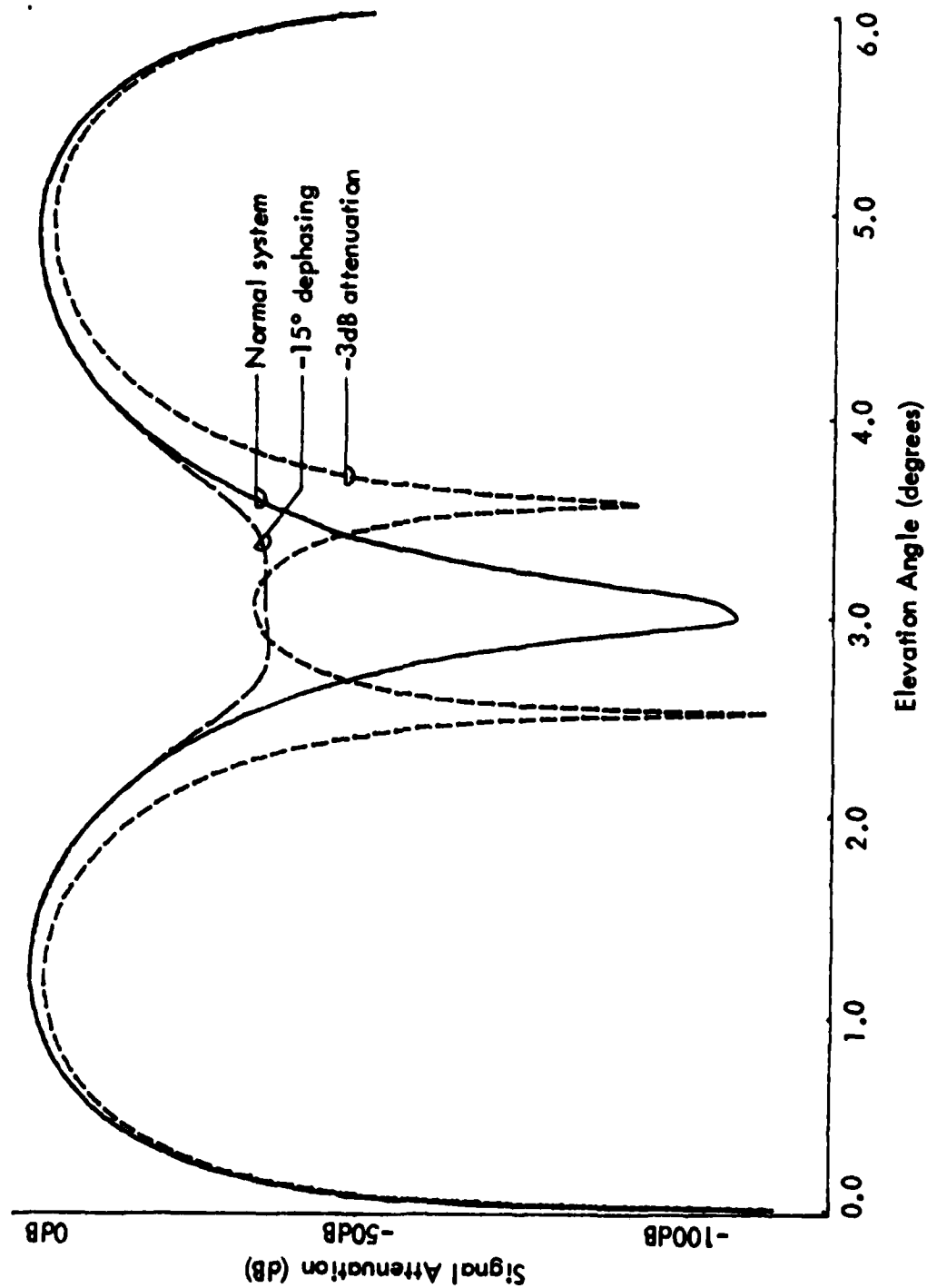


Figure 3-15. Clearance Signal Relative Strength for Normal and Fault Conditions.
Evident is the change of minima for fault conditions (modeled).

DATA (MEASURED AND MODELED).

TAMIAMI AIRPORT. Tamiami Airport (figure 3-16), Miami, Florida, has been chosen as a test site because this airport is essentially flat and met quite well the assumptions of smooth reflecting ground. It is supposed to have a uniform earth complex dielectric constant. Also, no conducting structure nor other obstacle can interfere with the space modulation to affect the glide path performance.

The capture-effect glide slope is in a normal configuration, uses standard equipment and has been successfully tested; flight measurements showed no false course below-path (below 1 degree) while the system was operating as an M-array (i.e., while the clearance transmitter is off); this result indicates that the system is properly phased.

Because the clearance signal can oftentimes mask capture effect problems of the system, the test program specified that the clearance transmitter would be turned off for all measurements collected. Thus, the TGCGS model, designed as a diagnostic prediction tool, cannot handle clearance signal.

The transmitter used was a Wilcox Mark-1C solid-state with 3-element co-linear antennas in corner reflectors Type FA-8976, manufactured by Antenna Products Company. Figure 3-17 shows the transmitter mast.

In-flight measurements were made using the Mark-II Minilab in a Beechcraft Model A-36 Bonanza. A PIR (Portable ILS Receiver) type FA-8766 and the O. U. Microlab were used to collect ground data. Figures 3-18 and 3-19 show the equipment used to collect ground data.

CEGS data concerning the test site of Tamiami airport are given in appendix C.

CEGS DATA. The following section is based on the analysis of three sets of data. A previous study made by Ohio University Avionics Engineering Center at the Tamiami Airport, collected CDI versus antenna height data at a 360-degree phase proximity point of the CGS. A second set of measurements collected data specifically for the study presented here, at locations determined to provide meaningful results. Finally, because of unexpected results appearing in the second data collection effort, a third set of measured data were collected using different equipment and personnel. Measured and modeled data at the 360-degree phase proximity point did agree and are presented in the next chapter. Experimental and theoretical results at another location, thought to be good for CGS ground check, are exposed. Although at that location, measured data were collected by experienced people with reliable equipment and then, do not suffer of any manipulation or reading error, although modeled data at the same locations are consistent with two different models (OUGS3D and TGCGS), experimental and theoretical values do not agree for some unexplained reason.

1. 360-degree phase proximity point data. A series of tests involving the Ohio University's test facility at Tamiami Airport have been

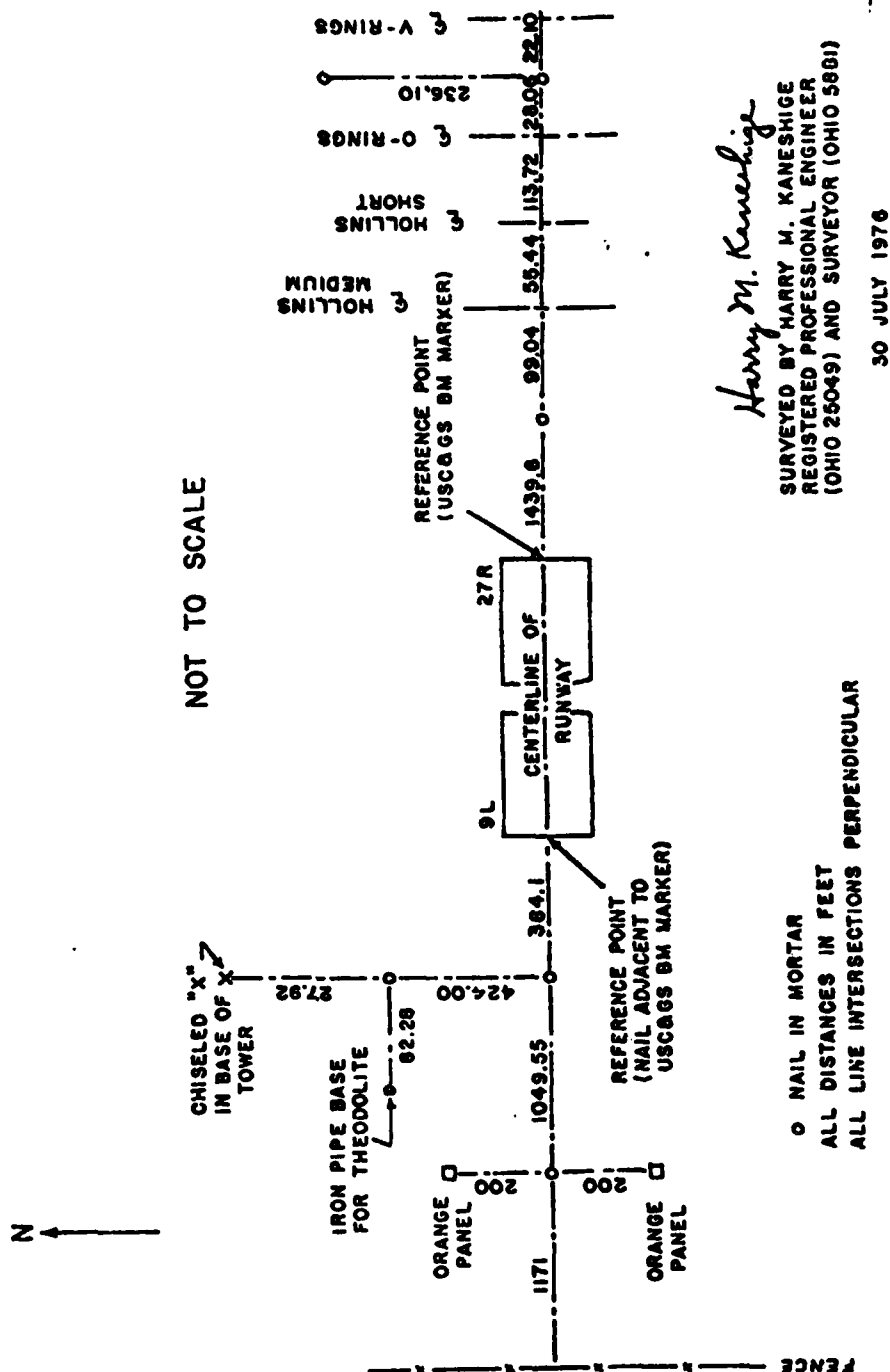


Figure 3-16. Control Points for ILS Site at New Tamiami Airport, Florida.

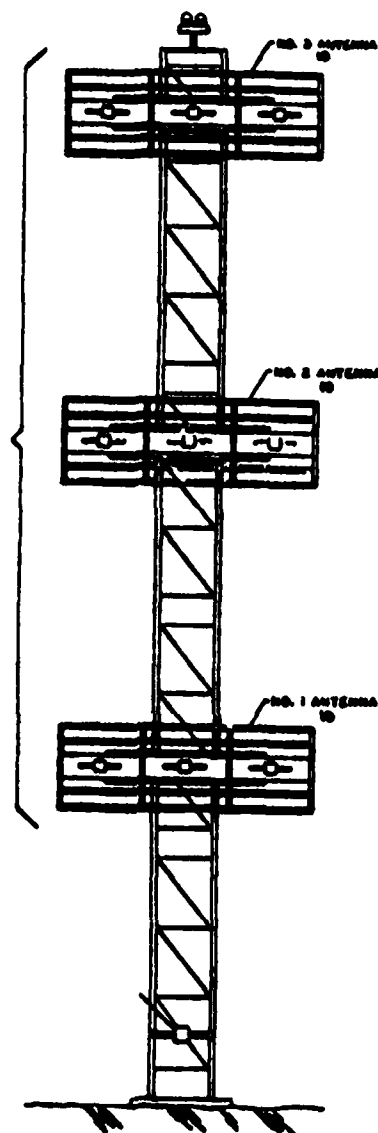


Figure 3-17. CEGS Transmitter Mast Equipped with Three FA8976 Antennas.



Figure 3-18. Ground Measurement Equipment (foreground) and CEGS Array (background).

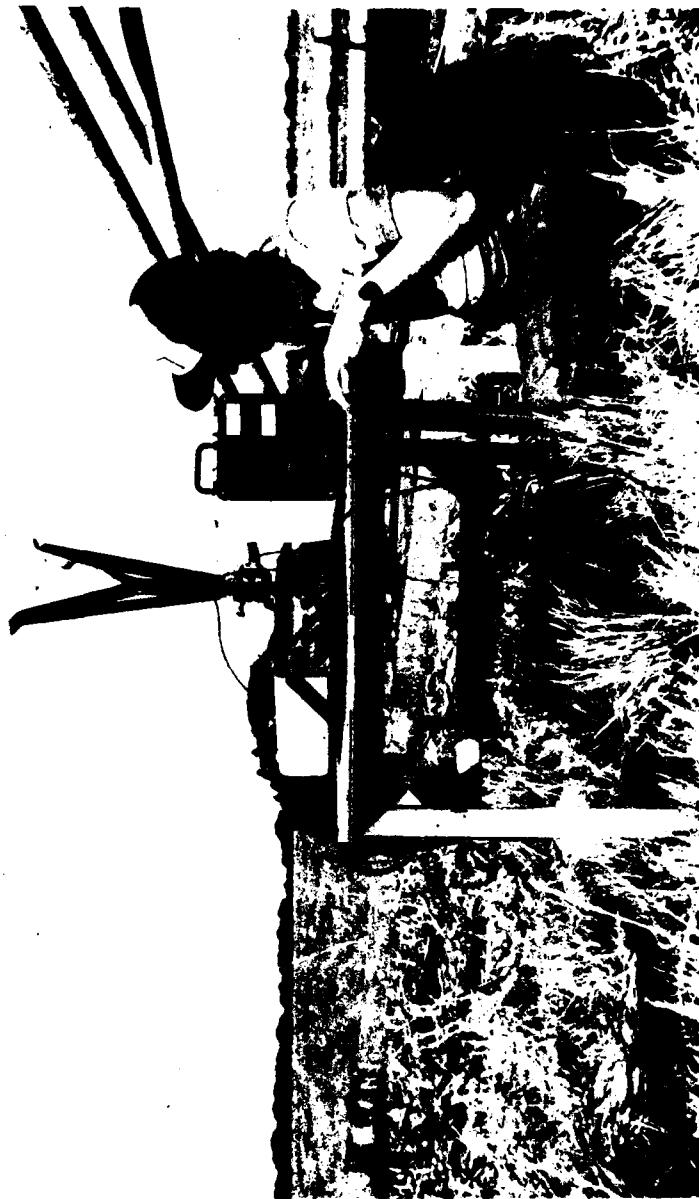


Figure 3-19. Electronic Equipment Used in Collecting Ground Measurements Data; Only the PIR Is Required for the Measurements. The equipment on the left is used solely for calibration.

conducted for extensive fault studies. Perturbations employed include phase delays and advances, changes in modulation indices for main and clearance signals, attenuation in antenna lines, and resetting of power dividers. For selected faults, the near-field monitor, in combination with a PIR, was used to gather measured data at the 360-degree phase proximity point.

The computer model used in calculating the DDM and CDI to be expected in a given set of conditions has been developed with assumptions such as: a flat, smooth, horizontal reflecting plane; a sufficiently uniform earth dielectric constant; and plane wave propagation.

Figure 3-20 shows how close measured data and theoretical values from both models are. This result gives credibility to the TGCGS model.

2. Second data collection. The second data collection has been performed at the locations selected showing good linearity in readings at an obtainable receiving antenna height, from the previous analytical study. Therefore, these locations were theoretically assumed to be adequate points to monitor the glide slope performance. As a confirmation, the OUGS3D computer model gives very similar results, as seen in figure 3-21.

Experimental measurements using a PIR (figures 3-22 and 3-23) provided unexpected results, even well below path, the predominant tone is 90 Hz when 150 Hz is highly anticipated.

By analyzing experimental results, it is seen that a dephasing (-15 degrees) of the middle antenna produces a shift of the readings as expected from the theoretical approach, but the OUGS3D and TGCGS models both predict the predominancy of 150 Hz modulation for receiving antenna height less than 7 meters (normal CEGS) of what does not appear in the experimental readings.

3. Third data collection. Because of these unexpected results, a second data collection effort has been accomplished by another team of the Ohio University Avionics Engineering Center using different equipment (O.U. Micro-Lab). At that time, a complete ground and flight check of the glide slope performance had been performed by experienced people. Thorough airborne analysis of system performance verified proper operation of the glide slope as an M-array (no clearance signals) with acceptable fly-up (150 Hz) well below path (below 1-degree elevation). Subsequent airborne measurements and ground checks were again performed; results of these ground measurements were not significantly different from the first data collection: only 90 Hz modulation predominancy was sensed even at low elevation (figures 3-24 through 3-26). It also has to be noted that narrow and broad alarm conditions cannot be accurately identified from the normal configuration. Thus, these measurements show that, at that point, it is not possible to diagnose a change of the A-ratio in the range narrow-broad alarm, which is a main objective of the ground check.

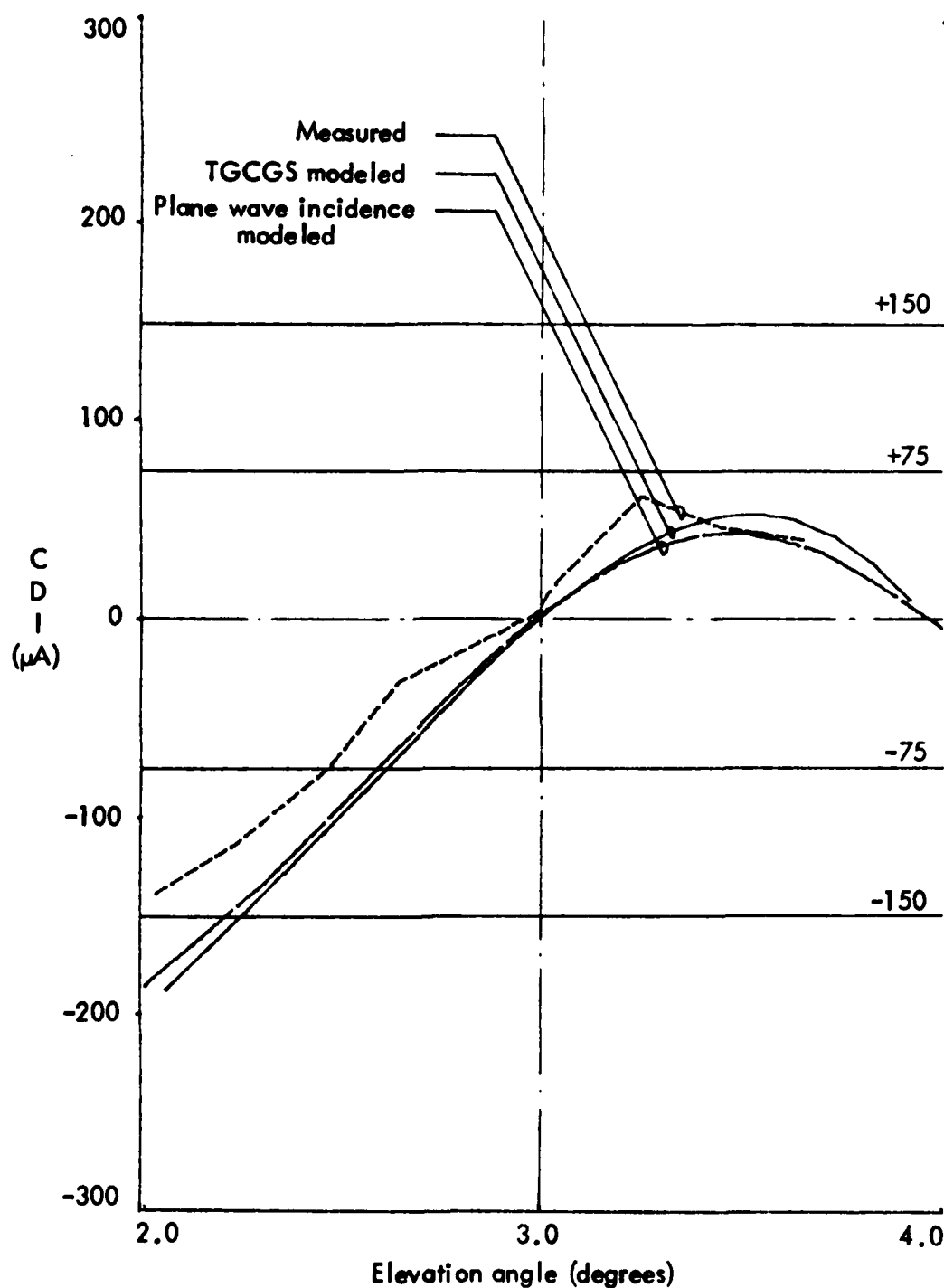


Figure 3-20. Measured and Modeled CDI vs. Elevation Angle for the 360° Phase Proximity Point Located Directly in Front of the Antenna Mast. Similar performance of the two models is evident.

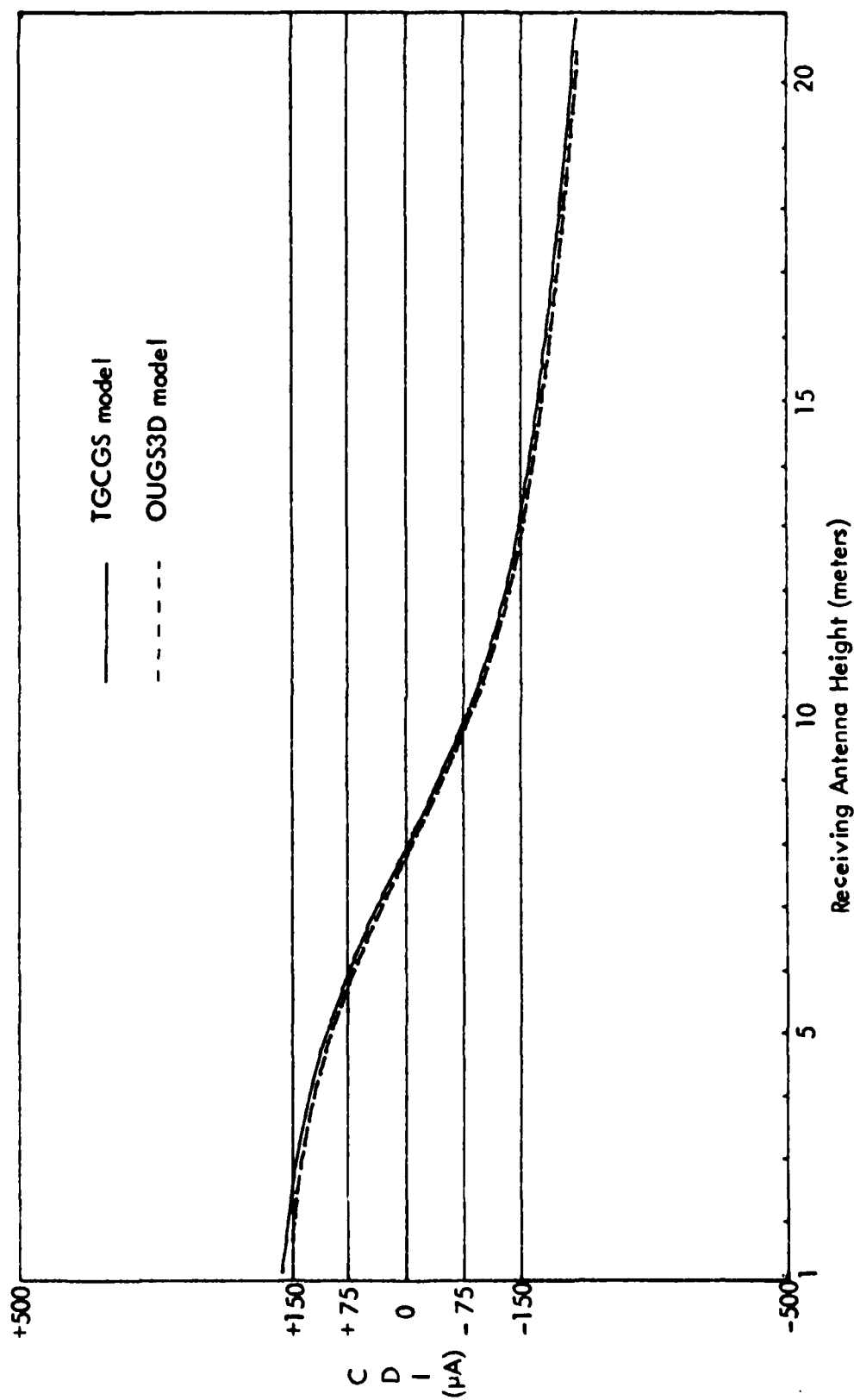


Figure 3-21. Modeled CDI vs. Receiving Antenna Height at the 122244 Ground Check Point for a Normal System. Similar performance of the two models is evident.

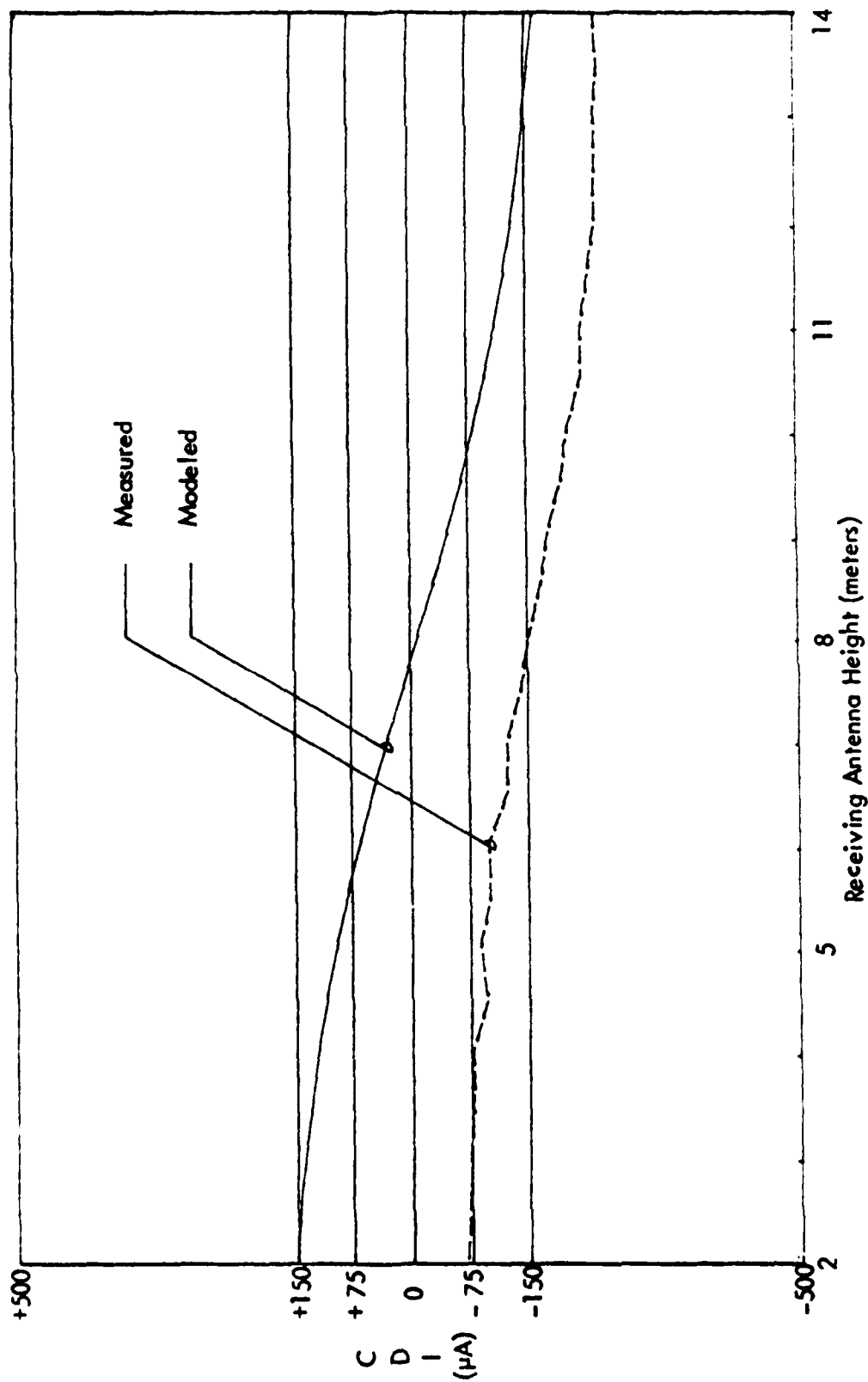


Figure 3-22. Measured and Modeled CDI vs. Receiving Antenna Height (244 m in front of the antenna mast). Normal system (first test).

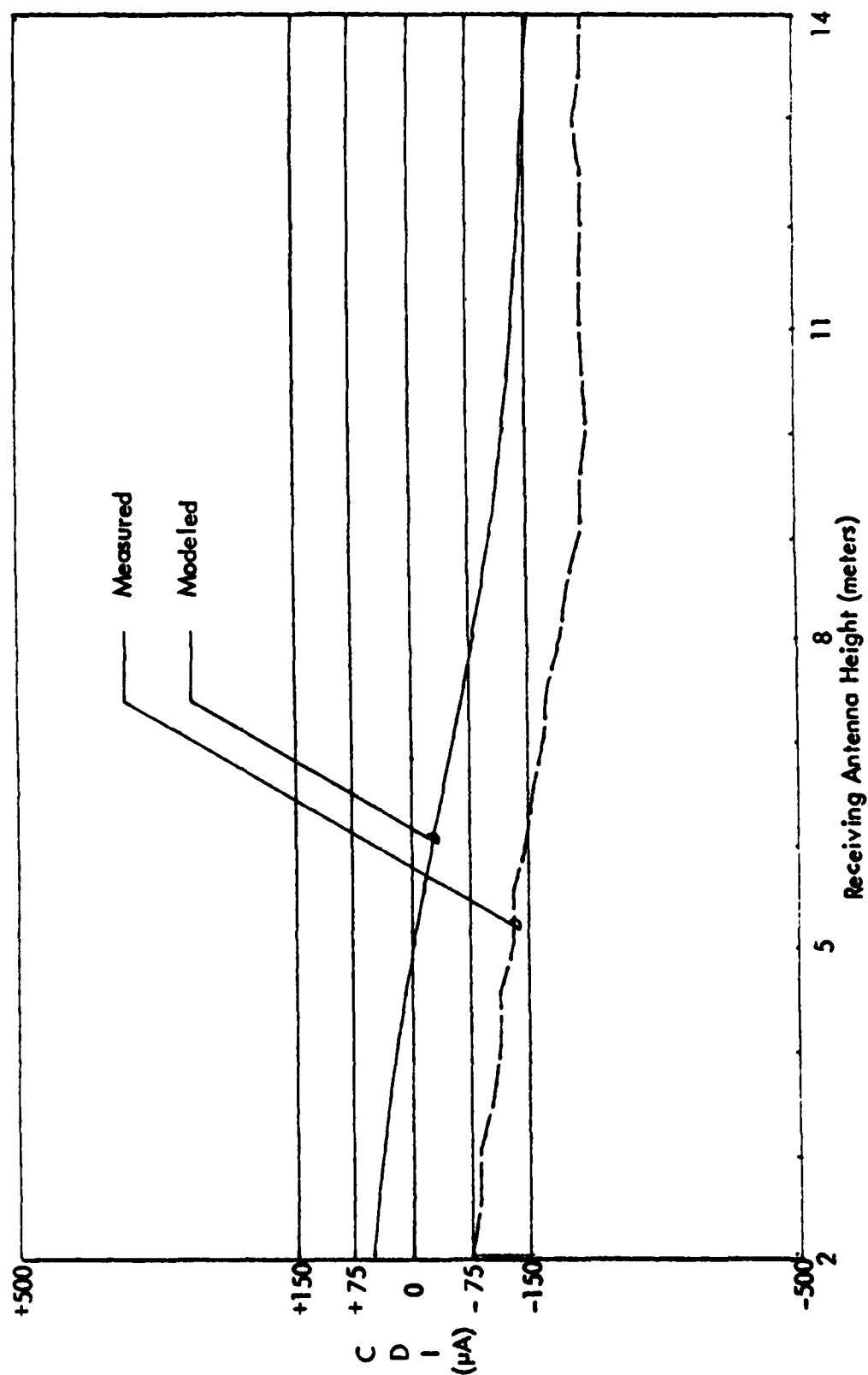


Figure 3-23. Measured and Modeled CDI vs. Receiving Antenna Height (244 m in front of the antenna mast). Dephasing -15° of the middle antenna (first test).

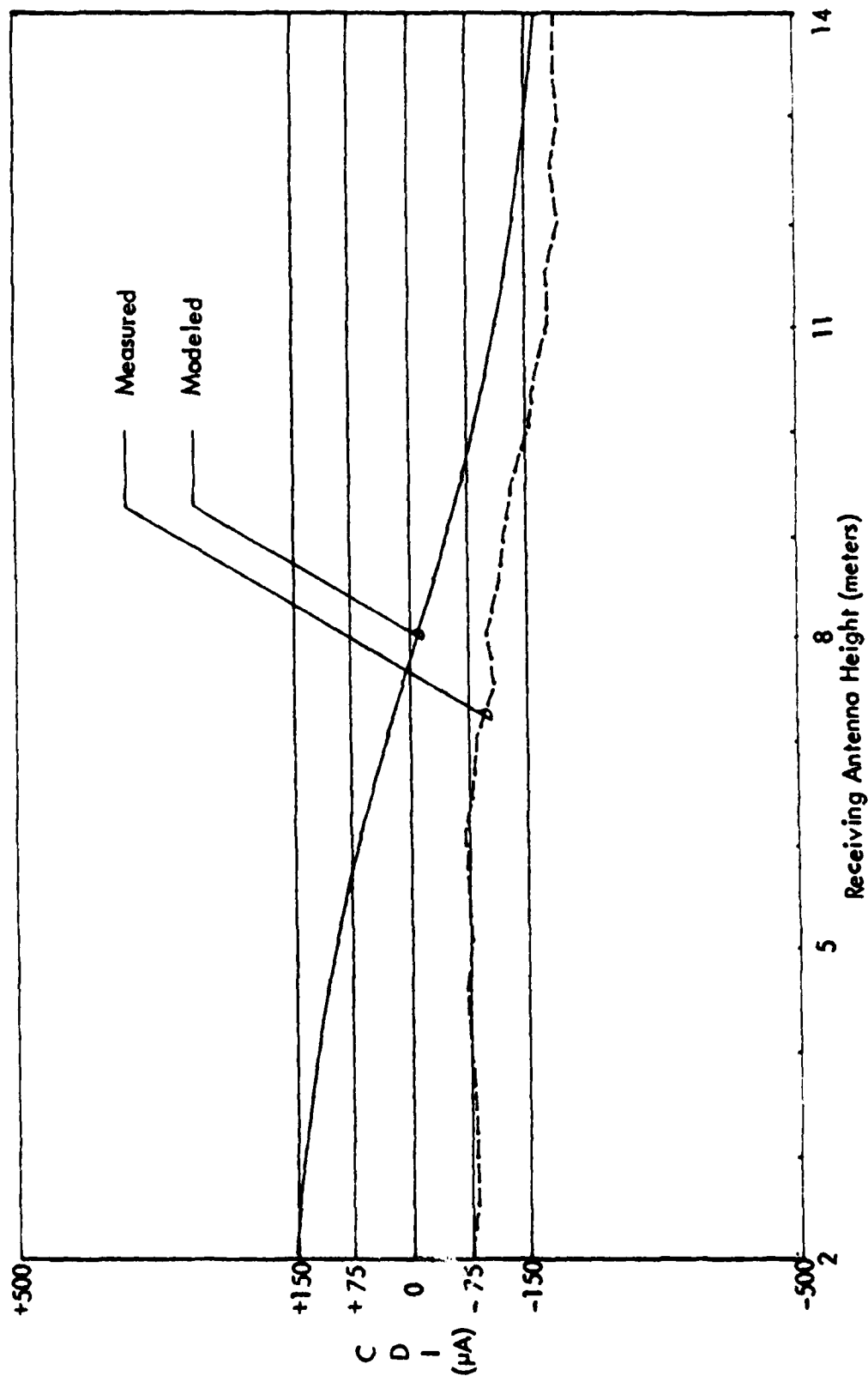


Figure 3-24. Measured and Modeled CDI vs. Receiving Antenna Height (244 m in front of the antenna mast). Normal system (second test).

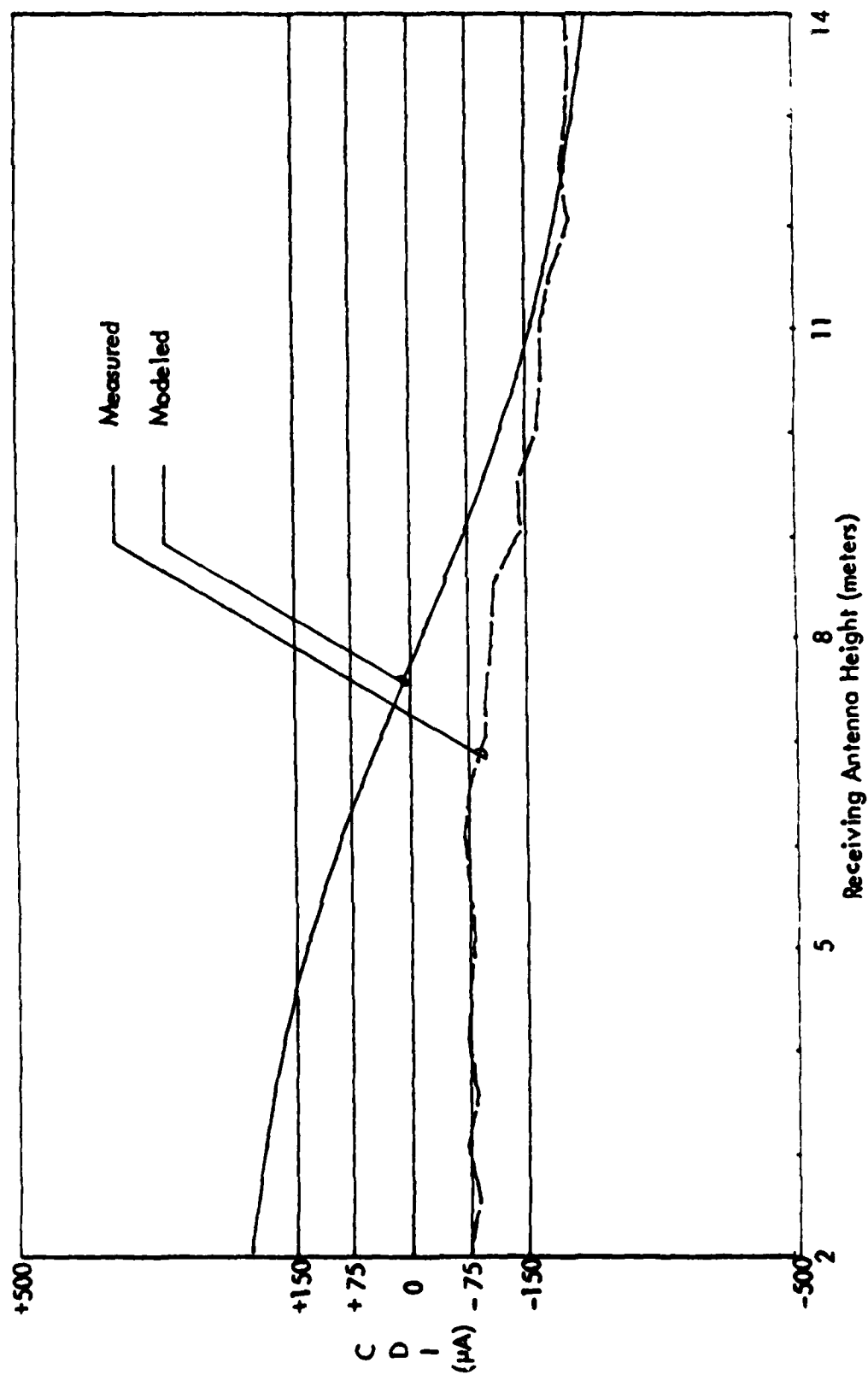


Figure 3-25. Measured and Modeled CDI vs. Receiving Antenna Height (244 m in front of the antenna mast). Narrow alarm (second test).

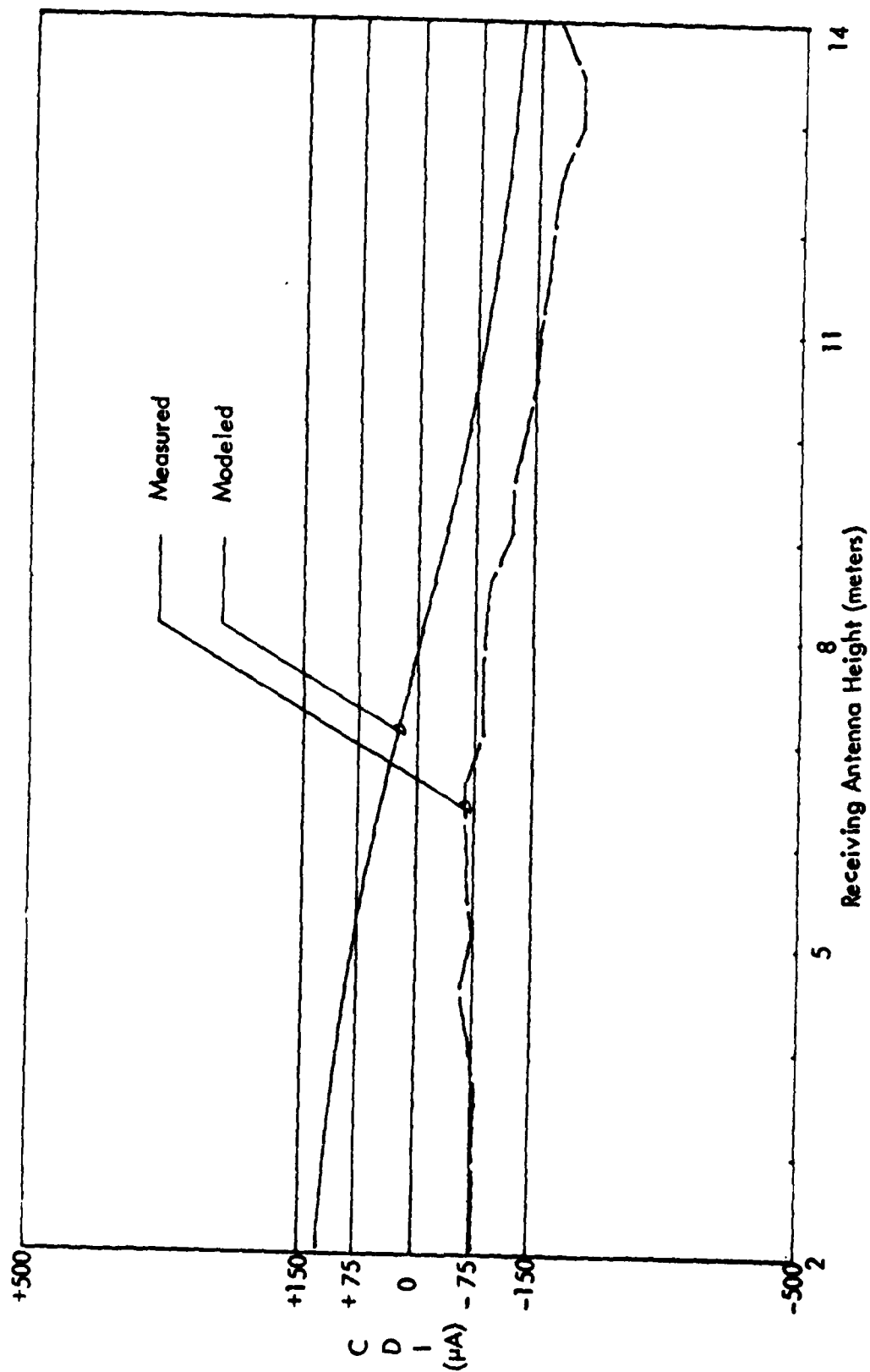


Figure 3-26. Measured and Modeled CDI vs. Receiving Antenna Height (244 m in front of the antenna mast). Broad alarm (second test).

CONCLUSIONS.

The work presented in this report represents the development and the implementation of a near-zone computer model for glide slope performance predictions and its application to investigate the feasibility of capture-effect glide-slope ground checking. Near-field effects (spherical wave incidence) have been combined with non-perfect reflecting ground plane (sloping terrain, finitely conductive reflecting surface, surface roughness) and typical glide slope characteristics (array factor and reflector factor) to establish the TCGGS near-zone computer model. Two ground data-collection efforts, using a capture-effect glide-slope facility, have been performed specifically for this research.

From TCGGS model predictions, it has been shown that:

Spherical wave incidence effect is negligible beyond 10 m away from a FA8976 antenna array source.

Changes in ground electric constants (permittivity and conductivity) do not alter glide path performance in a sensitive way.

From collected ground data analysis compared with TCGGS predictions, it has been shown that:

Even at theoretically optimal ground-check location, ground measurements do not allow any accurate diagnosis of possible faults in the glide-slope performance.

An unexplained phenomena caused experimental results not to match with model predictions even though the credibility of both measured and modeled data is incontestable.

The phenomena mentioned above concerning the experimental results along with time and funding constraints prevented the investigation of the side-band reference 360° ground-check point. It is anticipated that the modeling exercise above can also be applied to the SBR system and a thorough evaluation of the ground-check procedures can be performed once the mismatch in the calculated and measured data is explained.

RECOMMENDATIONS.

For some unexplained reason, experimental results and model predictions presented in this work do not agree, except for the 360-degree phase proximity point data, which were not collected specifically for this research.

Further work on TGCGS validation for ground predictions should start at the 360-degree phase proximity point to analyze why a 90 Hz modulation predominance is present well below path at the 122244 location defined in this paper. Once this phenomena is understood, more suitable CEGS ground-check locations may be discovered to establish the ground checking feasibility and implement its procedure.

The model presented here is designed especially to be used at locations where mutual coupling effects are negligible. Thus, if modeled results are desired for receiving antenna locations closer to the source, further work into mutual coupling effects should be performed to determine appropriate corrections in TGCGS model.

INVESTIGATION OF ILS TRANSMITTER CARRIER OUTPUT MODULATION COMPONENTS.

INTRODUCTION.

Recent advances in ILS technology have permitted the use of the systems for guidance in extremely low visibility conditions. In fact, the introduction of Category III aircraft and ground systems have resulted in the use of the ILS localizer for rollout guidance after landing. These advances point out the requirements for ensuring the integrity of the system; however, it is also important not to specify extremely conservative tolerances so as to make the system unusable when it is needed most. With this in mind, a study to establish recommended allowable audio harmonic content of the 90 Hz and 150 Hz audio navigation tones has been performed.

The investigation consists of preliminary measurements of ILS audio filter response, an ILS receiver model, the validation of the receiver model using experimental tests, and conclusions based upon calculated and measured data. The preliminary measurements were made to verify the audio filter specifications as supplied by various manufacturers and as an input to the receiver model. The receiver computer model is used to calculate the resultant effect on cross pointer current which specific harmonic components might have. The calculations performed using the model were then verified in laboratory tests using a commercial airline receiver and inexpensive general aviation receivers.

THEORETICAL BACKGROUND.

Ideally, the audio frequencies modulating the rf signals are pure sine waves. This is, of course, not always the case and occasionally the waveform does not consist of sine waves. The ILS navigation tones themselves are a good example of this. Figure 3-27 shows the combined 90 Hz and 150 Hz tones summed together in equal amplitude. These two sine waves, of course, can be analyzed separately. This is a requirement in order to determine position based upon the magnitude of the tones.

The analysis of the components or harmonics of a non-ideal sine wave is approached in the same manner. A periodic function $f(t)$ with period T , can be expanded in trigonometric form by a Fourier series:

$$f(t) = a_0 + \sum_{n=1}^{\infty} (a_n \cos n \omega_0 t + b_n \sin n \omega_0 t) \quad (\delta < t < \delta)$$

Where the coefficients a and b are given by

$$a_0 = 1/T \int_{-T/2}^{T/2} f(t) dt$$

$$a_n = 2/T \int_{-T/2}^{T/2} f(t) \cos n \omega_0 t dt$$

$$b_n = 2/T \int_{-T/2}^{T/2} f(t) \sin n \omega_0 t dt$$

By using trigonometric identities, this form may also be represented by

$$f(t) = a_0 + \sum_{n=1}^{\infty} A_n \cos(n \omega_0 t + \phi_n)$$

where

$$A = \sqrt{a_n^2 + b_n^2} \quad \text{and} \quad \phi_n = -\tan^{-1} \frac{b_n}{a_n}$$

From these equations it is evident that the periodic waveform may be separated into its component frequencies $\omega_0, 2\omega_0, \dots, n\omega_0$, etc., with ω being the fundamental frequency and the multiple values being the harmonics. The ratio of these harmonics to the fundamental frequency is the total harmonic distortion:

$$THD = \frac{\sqrt{(\text{harmonics})^2}}{\text{fundamental}}$$

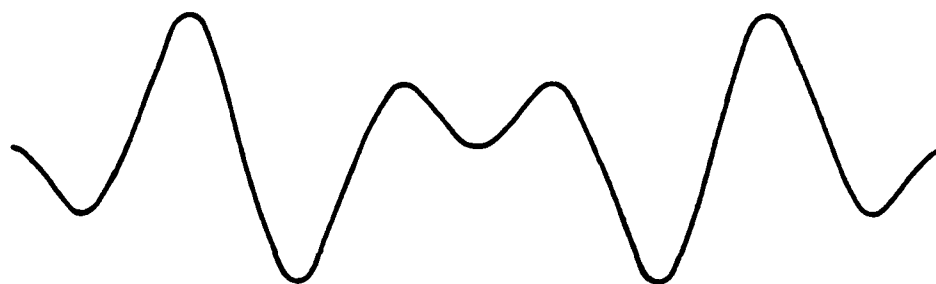


Figure 3-27. Combined 90 Hz and 150 Hz Tones Summed Together in Equal Amplitude.

To study the effects of specific harmonics on the performance of ILS localizer and glide slope receivers, each harmonic frequency is summed in phase with the standard 90 Hz and 150 Hz signals. In this specific case, the main point of interest is the worst case effect on the output ddm caused by the specific harmonic frequency. The maximum amplitude variation for either the 90 Hz or 150 Hz signal is the point at which this will occur. The ddm or difference in the depth of modulation is normally obtained by filtering the complex waveform from the receiver detector in 90 and 150 Hz bandpass filters and then rectifying each signal and applying the rectified signals to a differential amplifier to obtain the difference signal. To obtain the level of the rectified signal from each filter, the average power of the individual frequencies in each filter is calculated across a 1 ohm resistor. In a system in which V varies with time this is:

$$P_{ave} = 1/2 V_m^2 / R \cos \theta$$

where

V_m = magnitude of harmonic voltage

$\cos \theta$ = power factor

The magnitude of the average output power is then the sum of the powers for the individual frequencies.

$$P_{out} = P + P_2 + \dots + P_n$$

Again, the voltage is assumed to be across a 1 ohm resistor and the magnitude of the output voltage is obtained from:

$$V_{out} = 1/2 P_{out}^2 / R$$

The ratio of this voltage level obtained from each filter is then used to calculate the difference in depth of modulation (ddm) output value.

$$ddm = m \left[\frac{V_{90}}{V_{150}} - 1 \right] \text{ for } 90 \text{ Hz} > 150 \text{ Hz}$$

$$\text{and } ddm = m \left[\frac{V_{150}}{V_{90}} - 1 \right] \text{ for } 150 \text{ Hz} > 90 \text{ Hz}$$

where

V_{90} = total output of 90 Hz filter

V_{150} = total output of 150 Hz filter

m = modulation index

These formulae were utilized in a computer program to calculate the change in ddm for the various harmonic frequencies. The program listing and comparisons with measured values are presented in later sections.

PRELIMINARY MEASUREMENTS.

Filter measurements were obtained from bench tests performed on two available ILS receivers. A Rockwell-Collins 51RV-4B receiver, a Narco UGR-3 glide slope receiver, and a Narco NAVIII A localizer receiver were tested to determine the accuracy of published filter specifications. The measured results were then used in the receiver model.

The published specifications for the Collins receiver follow:

Center Frequency:

90 Hz Section: $f(90) = 90.0 \text{ Hz} \pm .25\%$, TA = 25 C
150 Hz Section: $f(150) = 1.6667 f(90) \pm .25\%$, TA 25 C

$$Q = 5.00 \pm 2\%$$

The measured filter response for both the localizer and glide slope sections are shown in figures 3-28 through 3-31. It is noted that the measured filter response correlates very well with that of the published specifications. Also, note that the Collins filters are implemented with active components.

The Narco glide slope receiver filter specifications are:

Center Frequency:

90 Hz Section: $f(90) = 92.2 \text{ Hz} \pm 3\% \pm 4.8\%$ over temperature

$$Q = 2.95 \pm 1.2\%, \pm 2\% \text{ over temperature}$$

150 Hz Section: $f(150) = 152.76 \text{ Hz} \pm 3\% \pm 4.8\%$ over temperature

$$Q = 3.04 \pm 1.2\%, \pm 2\% \text{ over temperature}$$

The measured filter response of the Narco glide slope receiver passive filters are shown in figures 3-32 and 3-33.

The Narco localizer receiver filter specifications were not available; however, figures 3-34 and 3-35 show the measured response.

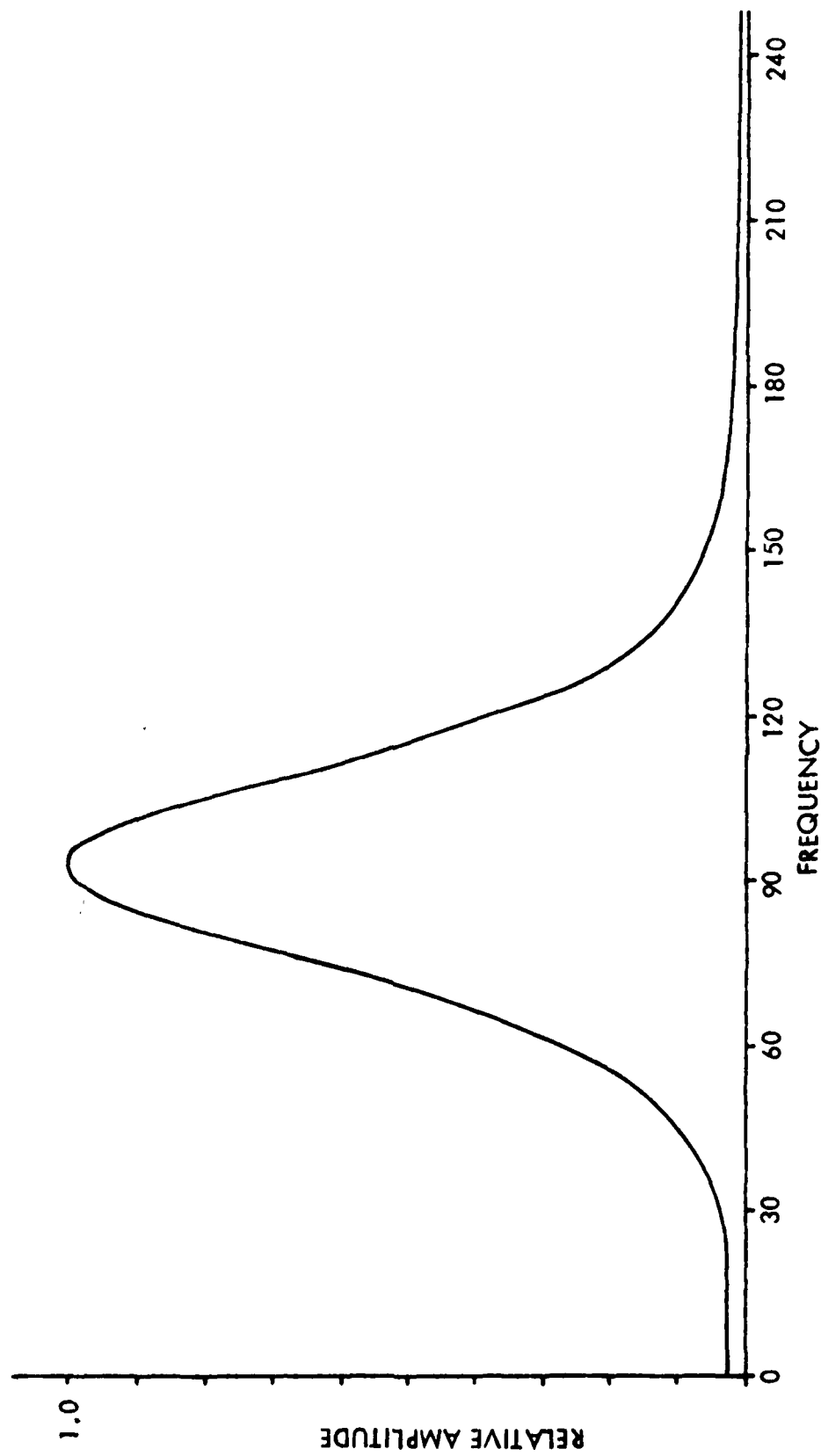


Figure 3-28. Measured Collins Localizer Receiver, 90 Hz Filter Response,
Measured $Q \approx 3$.

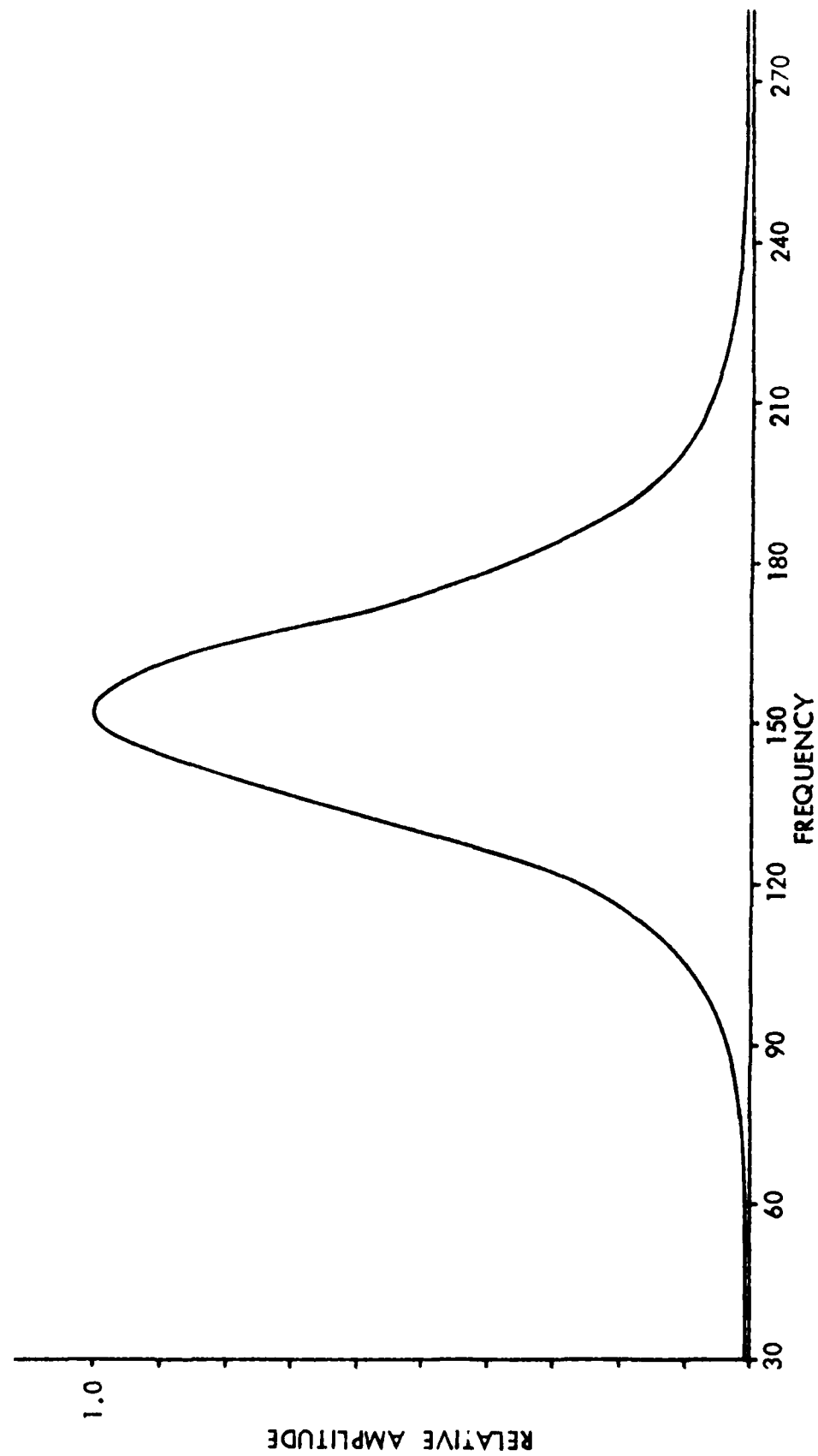


Figure 3-29. Measured Collins Localizer Receiver, 150 Hz Filter Response, Measured $Q = 4.72$.

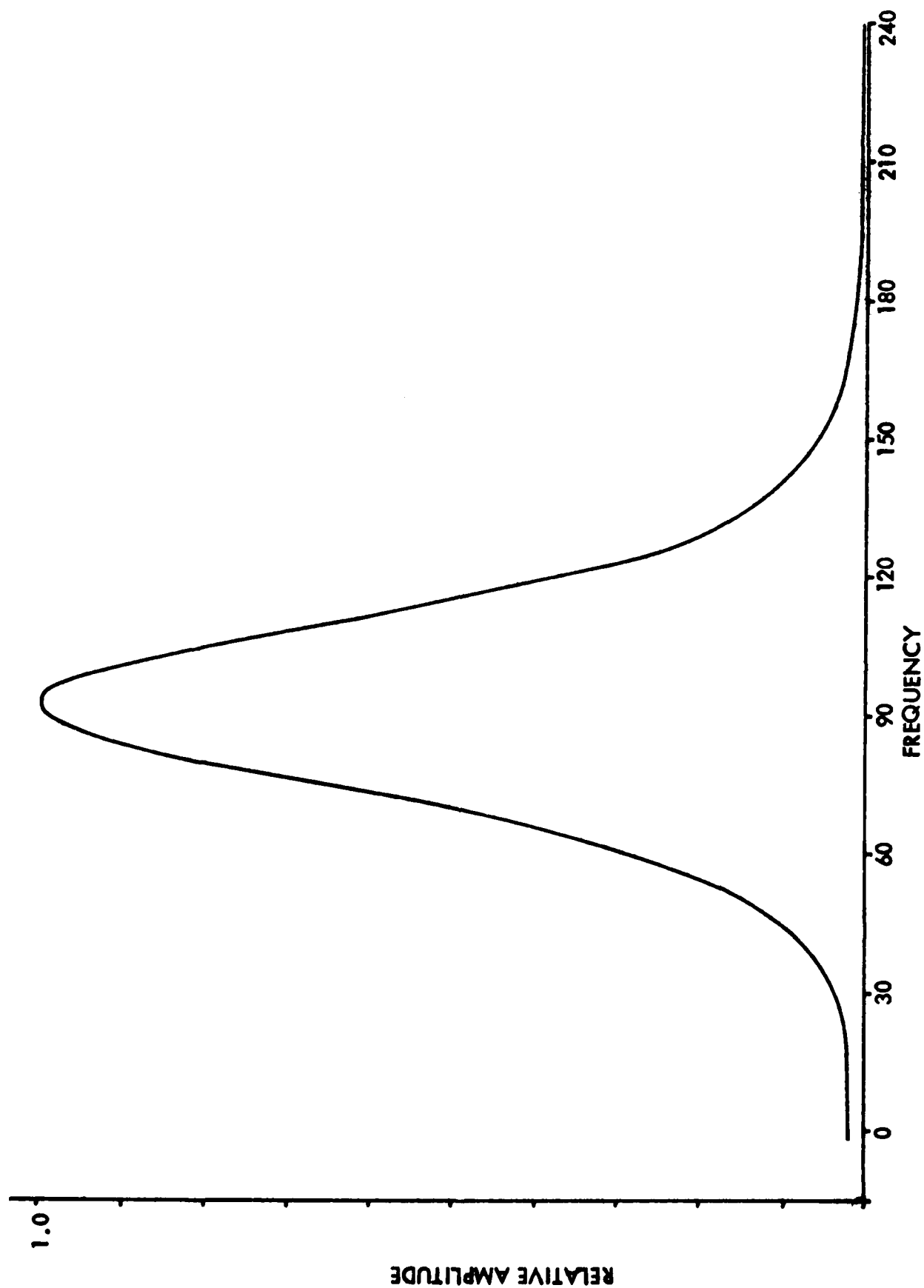


Figure 3-30. Measured Collins Glide Slope Receiver, 90 Hz Filter Response, Measured $Q=2.9$.

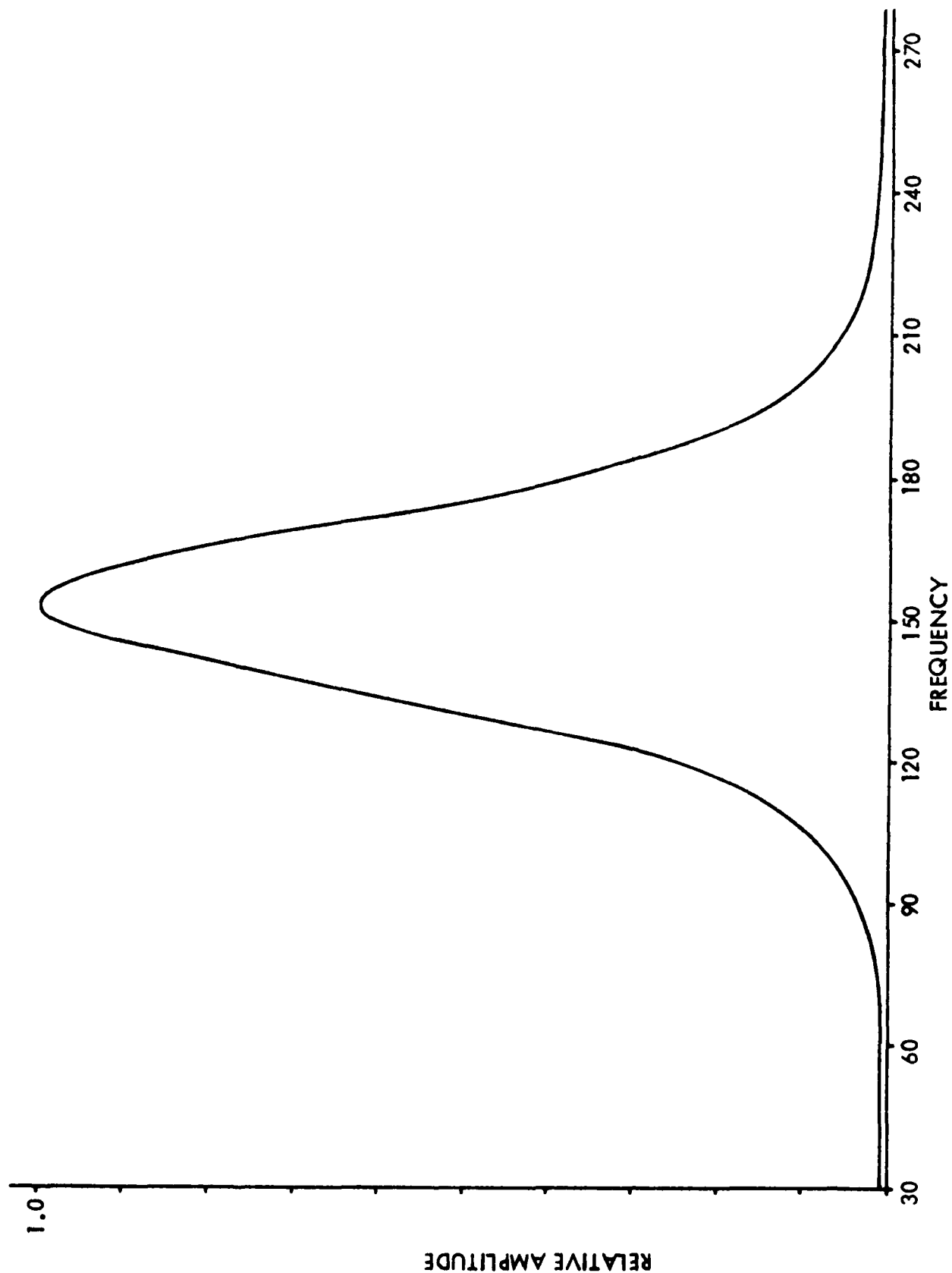


Figure 3-31. Measured Collins Glide Slope Receiver, 150 Hz Filter Response, Measured $Q=5$.

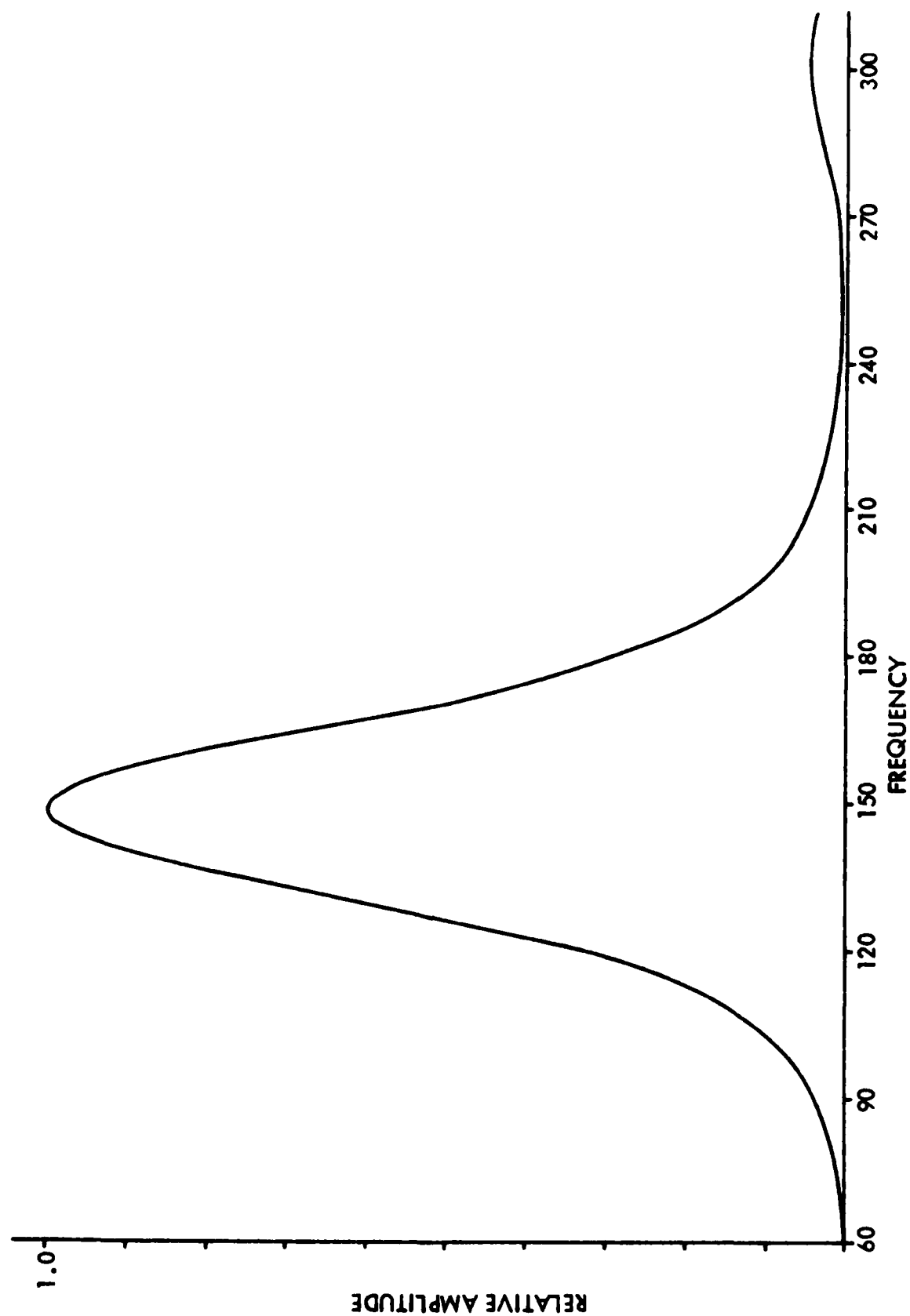


Figure 3-32. Measured Narco Glide Slope Receiver, 150 Hz Filter Response,
Measured $Q=4.8$.

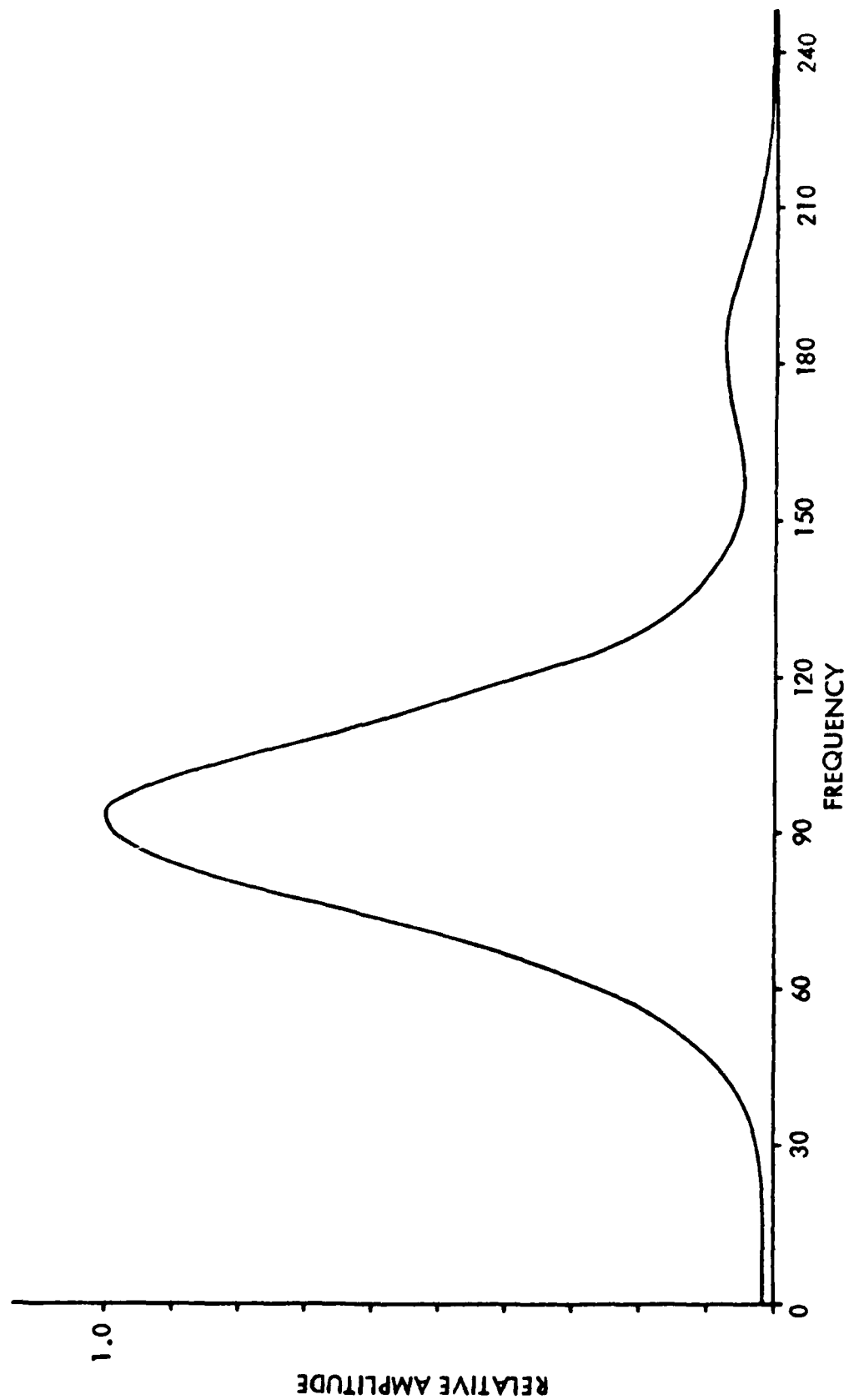


Figure 3-33. Narco Glide Slope Receiver, 90 Hz Response, Measured $Q = 3$.

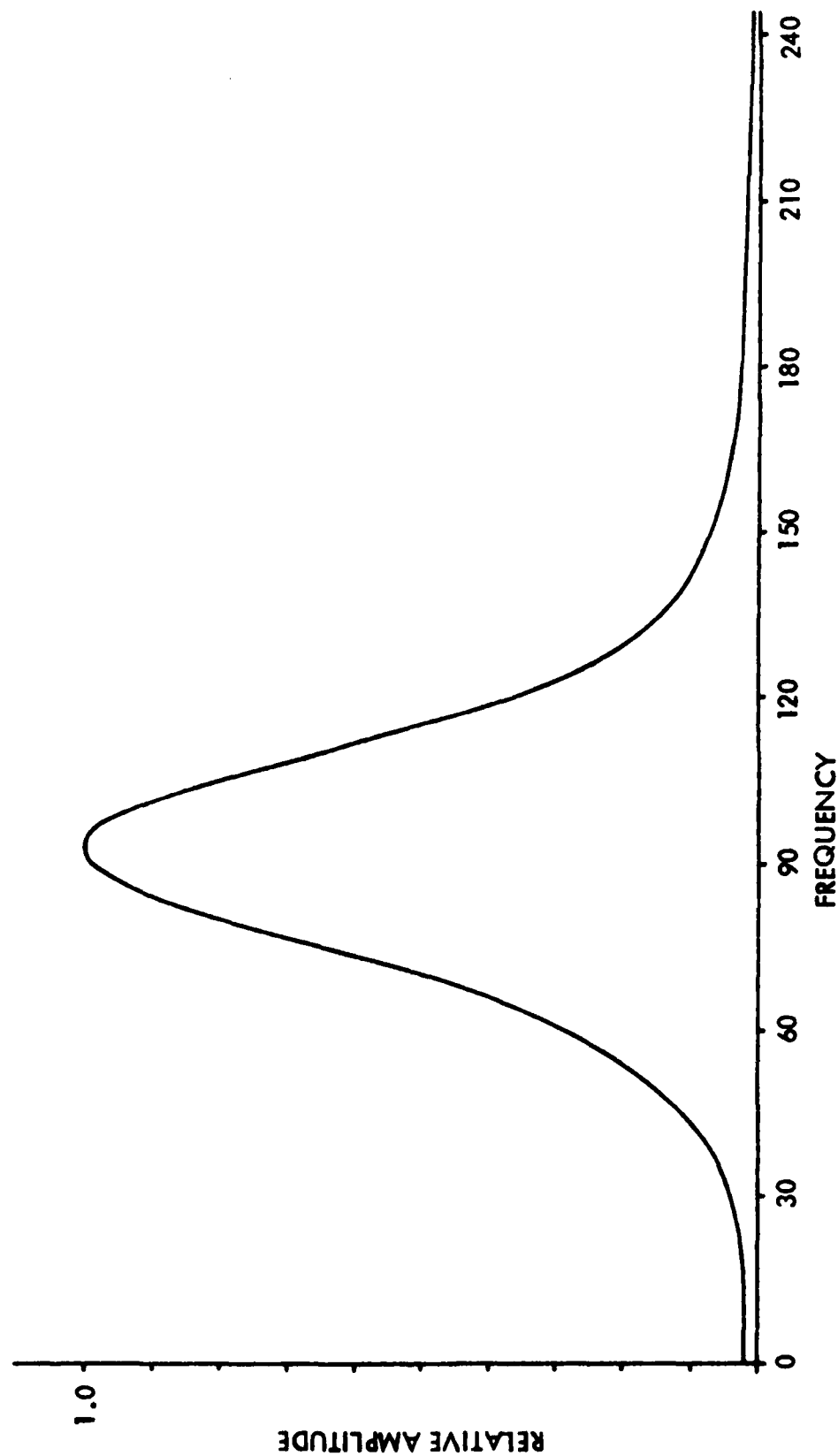


Figure 3-34. Narco Localizer Receiver, 90 Hz Response, Measured $Q = 2.88$.

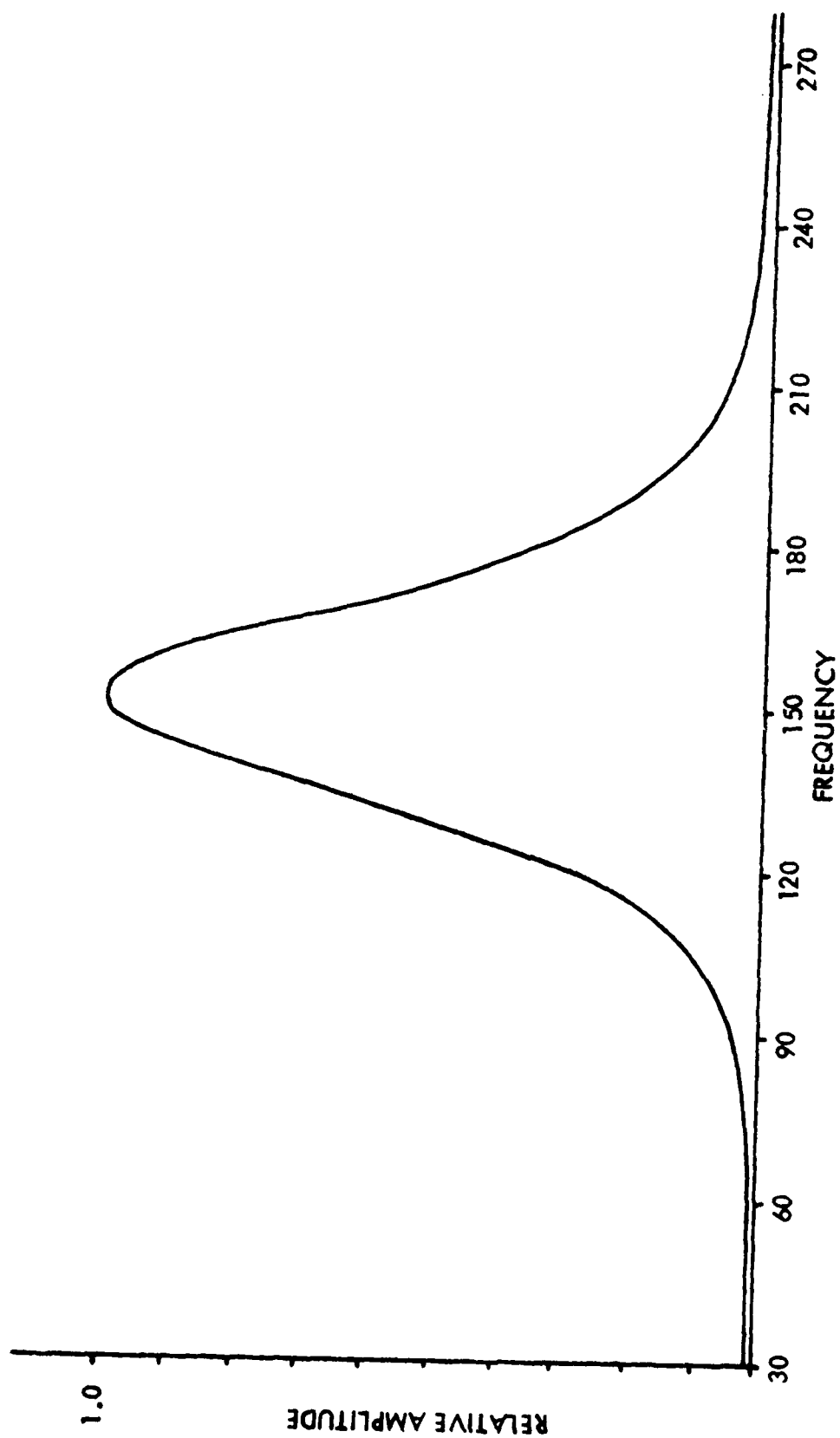


Figure 3-35. Measured Narco Localizer Receiver, 150 Hz Filter Response,
Measured $Q = 4.9$.

ILS RECEIVER MODEL CALCULATIONS.

A Fortran IV computer program was written to perform the calculations presented in the earlier chapter ("Theoretical Background"). The listing for this program is contained in appendix F. The program uses the measured filter response for a specific type of receiver and computes the ddm output for specific levels of harmonics applied to the receiver.

To verify the model, performance calculations of the most severe harmonic were made and then verified by measurements on the individual receivers. Figure 3-36 shows this comparison for the 180 Hz harmonic using the Rockwell Collins 51RV-4B receiver as the filter model. Note that the measured and calculated traces are nearly identical. The test setup used to obtain the measured trace is presented in appendix G.

The program was then used to calculate the variation in the ddm or CDI output caused by the increasing amplitudes of each harmonic. The results of these calculations are tabulated for each individual receiver in tables 3-1 through 3-24 and plots are shown in figures 3-37 through 3-60. From these plots and tables the maximum allowable amplitude of each harmonic frequency can be determined for the on-course signals. Note: the tables present the percentage of the added harmonic frequency and the resultant ddm variation.

Of more interest, recently, is the effect of harmonics higher than current tolerance levels (8%) on a two-frequency localizer in the clearance area. To ascertain this effect, the amplitudes of the 90 Hz and 150 Hz signals are varied to obtain a ddm output of .155 or CDI of 150 microamperes on one side and then the other. The variation in the CDI at these points is then measured. From these results the maximum allowable amplitudes of the individual harmonics can be determined.

Also of importance is the combined effect of specific harmonic levels on the receiver ddm output. This is obtained from the combination of the individual harmonics using the following formula.

$$\text{Total 90 or 150 Hz harmonic content} = \sqrt{\frac{(\text{harmonics})^2}{\text{fundamental}}}$$

To determine this effect, triangular waves (determined to have multiple harmonics) were chosen to obtain the total allowable 90-Hz harmonic content and the total allowable 150-Hz content. The results of this effort are shown in the measured data tables of appendix H.

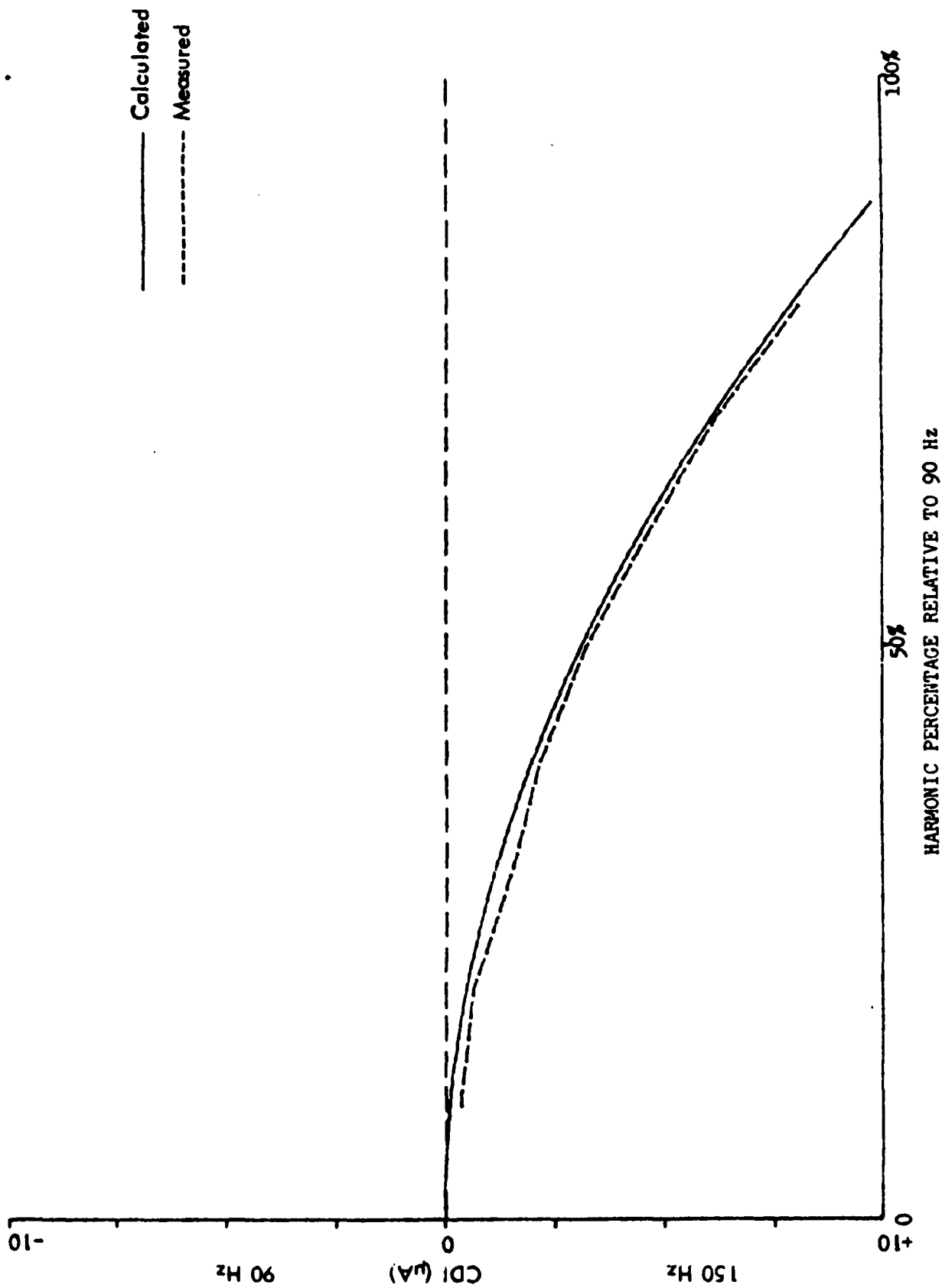


Figure 3-36. Comparison of Measured and Calculated 180 Hz Harmonic Effect on The Collins 51RV4B Receiver CDI.

% Harmonic	DDM	% Harmonic	DDM
1.00000	0.0	51.99998	-0.03747
2.00000	0.0	52.99998	-0.03913
3.00000	-0.00018	53.99997	-0.04061
4.00000	-0.00018	54.99997	-0.04208
5.00000	-0.00037	55.99998	-0.04356
6.00000	-0.00055	56.99998	-0.04502
6.99999	-0.00074	57.99997	-0.04649
8.00000	-0.00092	58.99998	-0.04836
9.00000	-0.00111	59.99997	-0.05002
10.00000	-0.00148	60.99997	-0.05168
11.00000	-0.00166	61.99997	-0.05334
11.99999	-0.00203	62.99997	-0.05519
12.99999	-0.00240	63.99998	-0.05685
13.99999	-0.00277	64.99998	-0.05870
14.99999	-0.00314	65.99998	-0.06054
16.00000	-0.00351	66.99997	-0.06239
16.99998	-0.00406	67.99997	-0.06423
17.99998	-0.00443	68.99997	-0.06608
18.99998	-0.00493	69.99997	-0.06811
19.99998	-0.00554	70.99997	-0.06996
20.99998	-0.00609	71.99998	-0.07199
21.99998	-0.00693	72.99997	-0.07402
22.99998	-0.00738	73.99997	-0.07605
23.99998	-0.00794	74.99997	-0.07809
24.99998	-0.00868	75.99997	-0.08029
25.99998	-0.00941	76.99997	-0.08251
26.99998	-0.01015	77.99997	-0.08454
27.99998	-0.01097	78.99997	-0.08675
28.99998	-0.01163	79.99997	-0.08897
29.99998	-0.01255	80.99997	-0.09100
30.99998	-0.01347	81.99997	-0.09340
31.99998	-0.01421	82.99997	-0.09530
32.99998	-0.01514	83.99997	-0.09801
33.99998	-0.01606	84.99997	-0.10023
34.99998	-0.01698	85.99997	-0.10281
35.99998	-0.01809	86.99997	-0.10521
36.99998	-0.01901	87.99997	-0.10761
37.99998	-0.02012	88.99997	-0.11001
38.99998	-0.02104	89.99997	-0.11241
39.99998	-0.02215	90.99997	-0.11499
40.99998	-0.02344	91.99997	-0.11758
41.99998	-0.02455	92.99997	-0.12016
42.99998	-0.02566	93.99997	-0.12275
43.99998	-0.02695	94.99997	-0.12533
44.99998	-0.02824	95.99997	-0.12792
45.99998	-0.02935	96.99997	-0.13068
46.99998	-0.03083	97.99997	-0.13345
47.99998	-0.03193	98.99997	-0.13604
48.99998	-0.03341	99.99997	-0.13891
49.99998	-0.03470		
50.99998	-0.03618		

Table 3-1. Calculated Response for NARCO Localizer with 30 Hz Harmonic.

% Harmonic	DDM	% Harmonic	DDM
1.00000	-0.00074	51.99998	-1.93250
2.00000	-0.00295	52.99998	-2.00633
3.00000	-0.00664	53.99997	-2.08160
4.00000	-0.01163	54.99997	-2.15813
5.00000	-0.01809	55.99998	-2.23596
6.00000	-0.02603	56.99998	-2.31503
6.99999	-0.03562	57.99998	-2.39547
8.00000	-0.04651	58.99998	-2.47724
9.00000	-0.05870	59.99997	-2.56029
10.00000	-0.07254	60.99997	-2.64454
11.00000	-0.08768	61.99997	-2.73014
11.99999	-0.10447	62.99997	-2.81705
12.99999	-0.12256	63.99998	-2.90515
13.99999	-0.14213	64.99998	-2.99451
14.99999	-0.16299	65.99998	-3.08521
16.00000	-0.18551	66.99997	-3.17712
16.99998	-0.20932	67.99997	-3.27025
17.99998	-0.23460	68.99997	-3.36467
18.99998	-0.26137	69.99997	-3.46018
19.99998	-0.28961	70.99997	-3.55712
20.99998	-0.31914	71.99998	-3.65518
21.99998	-0.35015	72.99997	-3.75447
22.99998	-0.38264	73.99997	-3.85495
23.99998	-0.41660	74.99997	-3.95667
24.99998	-0.45196	75.99997	-4.05963
25.99998	-0.48859	76.99997	-4.16374
26.99998	-0.52680	77.99997	-4.26898
27.99998	-0.56630	78.99997	-4.37547
28.99998	-0.60728	79.99997	-4.48313
29.99998	-0.64973	80.99997	-4.59191
30.99998	-0.69347	81.99997	-4.70188
31.99998	-0.73870	82.99997	-4.81308
32.99998	-0.78540	83.99997	-4.92532
33.99998	-0.83339	84.99997	-5.03873
34.99998	-0.88267	85.99997	-5.15329
35.99998	-0.93343	86.99997	-5.26895
36.99998	-0.98567	87.99997	-5.38581
37.99998	-1.03920	88.99997	-5.50368
38.99998	-1.09420	89.99997	-5.62268
39.99998	-1.15050	90.99997	-5.74280
40.99998	-1.20827	91.99997	-5.86410
41.99998	-1.26716	92.99997	-5.98643
42.99998	-1.32764	93.99997	-6.10980
43.99998	-1.38942	94.99997	-6.23422
44.99998	-1.45272	95.99997	-6.35978
45.99998	-1.51715	96.99997	-6.48640
46.99998	-1.58306	97.99997	-6.61401
47.99998	-1.65028	98.99997	-6.74271
48.99998	-1.71883	99.99997	-6.87238
49.99998	-1.78872		
50.99998	-1.85988		

Table 3-2. Calculated Response for NARCO Localizer with 60 Hz Harmonic.

% Harmonic	DDM	% Harmonic	DDM
1.00000	0.00129	51.99998	3.79814
2.00000	0.00572	52.99998	3.94415
3.00000	0.01274	53.99997	4.09217
4.00000	0.02270	54.99997	4.24428
5.00000	0.03544	55.99998	4.39922
6.00000	0.05113	56.99998	4.55474
6.99999	0.06940	57.99998	4.71404
8.00000	0.09091	58.99998	4.87592
9.00000	0.11491	59.99997	5.04057
10.00000	0.14176	60.99997	5.20780
11.00000	0.17148	61.99997	5.37761
11.99999	0.20415	62.99997	5.55001
12.99999	0.23954	63.99998	5.72499
13.99999	0.27780	64.99998	5.90257
14.99999	0.31996	65.99998	6.08272
16.00000	0.36270	66.99997	6.26545
16.99998	0.40940	67.99997	6.45077
17.99998	0.45906	68.99997	6.63868
18.99998	0.51129	69.99997	6.82935
19.99998	0.56648	70.99997	7.02242
20.99998	0.62463	71.99998	7.21790
21.99998	0.68535	72.99997	7.41595
22.99998	0.74885	73.99997	7.61659
23.99998	0.81530	74.99997	7.81982
24.99998	0.88452	75.99997	8.02544
25.99998	0.95669	76.99997	8.23384
26.99998	1.03126	77.99997	8.44444
27.99999	1.10897	78.99997	8.65764
28.99999	1.18926	79.99997	8.87341
29.99998	1.27251	80.99997	9.09140
30.99998	1.35852	81.99997	9.31216
31.99998	1.44712	82.99997	9.53514
32.99998	1.53868	83.99997	9.76070
33.99998	1.63300	84.99997	9.98866
34.99999	1.72990	85.99997	10.21902
35.99998	1.82976	86.99997	10.45196
36.99998	1.93233	87.99997	10.68712
37.99998	2.03760	88.99997	10.92486
38.99998	2.14558	89.99997	11.16500
39.99998	2.25652	90.99997	11.40736
40.99998	2.36985	91.99997	11.65211
41.99998	2.48632	92.99997	11.89945
42.99998	2.60519	93.99997	12.14901
43.99998	2.72701	94.99997	12.40096
44.99998	2.85142	95.99997	12.65531
45.99998	2.97860	96.99997	12.91188
46.99998	3.10836	97.99997	13.17095
47.99998	3.24108	98.99997	13.43204
48.99998	3.37619	99.99997	13.69581
49.99998	3.51426		
50.99998	3.65472		

Table 3-3. Calculated Response for NARCO Localizer with 180 Hz Harmonic.

% Harmonic	DDM	% Harmonic	DDM
1.00000	0.0	51.99998	0.00628
2.00000	0.0	52.99998	0.00646
3.00000	0.0	53.99997	0.00664
4.00000	0.0	54.99997	0.00683
5.00000	0.0	55.99998	0.00700
6.00000	0.00018	56.99998	0.00738
6.99999	0.0	57.99998	0.00775
8.00000	0.0	58.99998	0.00794
9.00000	0.00018	59.99997	0.00831
10.00000	0.00018	60.99997	0.00849
11.00000	0.00018	61.99997	0.00886
11.99999	0.00037	62.99997	0.00904
12.99999	0.00037	63.99998	0.00941
13.99999	0.00037	64.99998	0.00978
14.99999	0.00055	65.99998	0.00997
16.00000	0.00055	66.99997	0.01015
16.99998	0.00055	67.99997	0.01052
17.99998	0.00074	68.99997	0.01089
18.99998	0.00074	69.99997	0.01126
19.99998	0.00092	70.99997	0.01163
20.99998	0.00092	71.99998	0.01181
21.99998	0.00111	72.99997	0.01218
22.99998	0.00111	73.99997	0.01255
23.99998	0.00129	74.99997	0.01292
24.99998	0.00148	75.99997	0.01329
25.99998	0.00148	76.99997	0.01347
26.99998	0.00166	77.99997	0.01403
27.99998	0.00185	78.99997	0.01440
28.99998	0.00185	79.99997	0.01458
29.99998	0.00203	80.99997	0.01495
30.99998	0.00221	81.99997	0.01532
31.99998	0.00240	82.99997	0.01569
32.99998	0.00240	83.99997	0.01624
33.99998	0.00258	84.99997	0.01661
34.99998	0.00277	85.99997	0.01698
35.99998	0.00295	86.99997	0.01735
36.99998	0.00314	87.99997	0.01772
37.99998	0.00332	88.99997	0.01809
38.99998	0.00351	89.99997	0.01864
39.99998	0.00369	90.99997	0.01901
40.99998	0.00388	91.99997	0.01938
41.99998	0.00406	92.99997	0.01975
42.99998	0.00425	93.99997	0.02012
43.99998	0.00443	94.99997	0.02067
44.99998	0.00461	95.99997	0.02104
45.99998	0.00480	96.99997	0.02160
46.99998	0.00499	97.99997	0.02197
47.99998	0.00535	98.99997	0.02252
48.99998	0.00554	99.99997	0.02289
49.99998	0.00572		
50.99998	0.00591		

Table 3-4. Calculated Response for NARCO Localizer with 240 Hz Harmonic.

% Harmonic	DDM	% Harmonic	DDM
1.00000	0.0	51.99998	0.0
2.00000	0.0	52.99998	0.0
3.00000	0.0	53.99997	-0.00018
4.00000	0.0	54.99997	-0.00018
5.00000	0.0	55.99998	0.0
6.00000	0.0	56.99998	0.0
6.99999	0.0	57.99998	0.0
8.00000	0.0	58.99998	-0.00018
9.00000	0.0	59.99997	-0.00018
10.00000	0.0	60.99997	-0.00018
11.00000	0.0	61.99997	0.0
11.99999	0.0	62.99997	-0.00018
12.99999	0.0	63.99998	0.0
13.99999	0.0	64.99998	0.0
14.99999	0.0	65.99998	-0.00018
16.00000	0.0	66.99997	-0.00018
16.99998	-0.00018	67.99997	-0.00018
17.99998	0.0	68.99997	-0.00018
18.99998	0.0	69.99997	0.0
19.99998	0.0	70.99997	0.0
20.99998	0.0	71.99998	-0.00018
21.99998	-0.00018	72.99997	-0.00018
22.99998	0.0	73.99997	0.0
23.99998	0.0	74.99997	0.0
24.99998	0.0	75.99997	-0.00018
25.99998	-0.00018	76.99997	-0.00018
26.99998	0.0	77.99997	-0.00018
27.99998	0.0	78.99997	0.0
28.99998	0.0	79.99997	-0.00018
29.99998	0.0	80.99997	-0.00018
30.99998	0.0	81.99997	-0.00018
31.99998	0.0	82.99997	-0.00018
32.99998	0.0	83.99997	-0.00018
33.99998	0.0	84.99997	-0.00018
34.99998	0.0	85.99997	-0.00018
35.99998	0.0	86.99997	-0.00018
36.99998	0.0	87.99997	-0.00018
37.99998	-0.00018	88.99997	-0.00018
38.99998	0.0	89.99997	-0.00018
39.99998	0.0	90.99997	-0.00018
40.99998	0.0	91.99997	-0.00018
41.99998	0.0	92.99997	-0.00018
42.99998	0.0	93.99997	-0.00018
43.99998	0.0	94.99997	-0.00018
44.99998	-0.00018	95.99997	-0.00018
45.99998	0.0	96.99997	-0.00018
46.99998	-0.00018	97.99997	-0.00018
47.99998	0.0	98.99997	-0.00018
48.99998	-0.00018	99.99997	-0.00018
49.99998	0.0		
50.99998	0.0		

Table 3-5. Calculated Response for NARCO Localizer with 300 Hz Harmonic.

% Harmonic	DDM	% Harmonic	DDM
1.00000	0.0	51.99998	0.0
2.00000	0.0	52.99998	0.0
3.00000	0.0	53.99997	-0.00018
4.00000	0.0	54.99997	-0.00018
5.00000	0.0	55.99998	0.0
6.00000	0.0	56.99998	0.0
6.99999	0.0	57.99998	0.0
8.00000	0.0	58.99998	-0.00018
9.00000	0.0	59.99997	-0.00018
10.00000	0.0	60.99997	-0.00018
11.00000	0.0	61.99997	0.0
11.99999	0.0	62.99997	-0.00018
12.99999	0.0	63.99998	0.0
13.99999	0.0	64.99998	0.0
14.99999	0.0	65.99998	-0.00018
16.00000	0.0	66.99997	-0.00018
16.99998	-0.00018	67.99997	-0.00018
17.99998	0.0	68.99997	-0.00018
18.99998	0.0	69.99997	0.0
19.99998	0.0	70.99997	0.0
20.99998	0.0	71.99998	-0.00018
21.99998	-0.00018	72.99997	-0.00018
22.99998	0.0	73.99997	0.0
23.99998	0.0	74.99997	0.0
24.99998	0.0	75.99997	-0.00018
25.99998	-0.00018	76.99997	-0.00018
26.99998	0.0	77.99997	-0.00018
27.99998	0.0	78.99997	0.0
28.99998	0.0	79.99997	-0.00018
29.99998	0.0	80.99997	-0.00018
30.99998	0.0	81.99997	-0.00018
31.99998	0.0	82.99997	-0.00018
32.99998	0.0	83.99997	-0.00018
33.99998	0.0	84.99997	-0.00018
34.99998	0.0	85.99997	-0.00018
35.99998	0.0	86.99997	-0.00018
36.99998	0.0	87.99997	-0.00018
37.99998	-0.00018	88.99997	-0.00018
38.99998	0.0	89.99997	-0.00018
39.99998	0.0	90.99997	-0.00018
40.99998	0.0	91.99997	-0.00018
41.99998	0.0	92.99997	-0.00018
42.99998	0.0	93.99997	-0.00018
43.99998	0.0	94.99997	-0.00018
44.99998	-0.00018	95.99997	-0.00018
45.99998	0.0	96.99997	-0.00018
46.99998	-0.00018	97.99997	-0.00018
47.99998	0.0	98.99997	-0.00018
48.99998	-0.00018	99.99997	-0.00018
49.99998	0.0		
50.99998	0.0		

Table 3-6. Calculated Response for NARCO Localizer with 540 Hz Harmonic.

% Harmonic	DDM	% Harmonic	DDM
1.00000	0.0	51.99998	-0.02580
2.00000	0.0	52.99998	-0.02646
3.00000	0.0	53.99997	-0.02779
4.00000	-0.00031	54.99997	-0.02876
5.00000	-0.00031	55.99998	-0.02973
6.00000	-0.00031	56.99998	-0.03070
6.99999	-0.00031	57.99999	-0.03173
8.00000	-0.00066	58.99998	-0.03300
9.00000	-0.00066	59.99997	-0.03433
10.00000	-0.00066	60.99997	-0.03530
11.00000	-0.00097	61.99997	-0.03663
11.99999	-0.00128	62.99997	-0.03760
12.99999	-0.00128	63.99998	-0.03888
13.99999	-0.00194	64.99998	-0.04021
14.99999	-0.00194	65.99998	-0.04118
16.00000	-0.00230	66.99997	-0.04281
16.99998	-0.00261	67.99997	-0.04414
17.99998	-0.00327	68.99997	-0.04542
18.99998	-0.00327	69.99997	-0.04644
19.99998	-0.00358	70.99997	-0.04808
20.99998	-0.00393	71.99998	-0.04935
21.99998	-0.00455	72.99997	-0.05068
22.99998	-0.00490	73.99997	-0.05196
23.99998	-0.00557	74.99997	-0.05359
24.99998	-0.00588	75.99997	-0.05492
25.99998	-0.00618	76.99997	-0.05625
26.99998	-0.00685	77.99997	-0.05788
27.99998	-0.00751	78.99997	-0.05952
28.99998	-0.00917	79.99997	-0.06080
29.99998	-0.00848	80.99997	-0.06243
30.99998	-0.00915	81.99997	-0.06376
31.99998	-0.00945	82.99997	-0.06534
32.99998	-0.01012	83.99997	-0.06703
33.99998	-0.01078	84.99997	-0.06866
34.99998	-0.01144	85.99997	-0.07030
35.99998	-0.01241	86.99997	-0.07193
36.99998	-0.01308	87.99997	-0.07357
37.99998	-0.01374	88.99997	-0.07520
38.99998	-0.01436	89.99997	-0.07684
39.99998	-0.01502	90.99997	-0.07879
40.99998	-0.01599	91.99997	-0.08042
41.99998	-0.01666	92.99997	-0.08205
42.99998	-0.01732	93.99997	-0.08404
43.99998	-0.01829	94.99997	-0.08568
44.99998	-0.01895	95.99997	-0.08762
45.99998	-0.01992	96.99997	-0.08925
46.99998	-0.02090	97.99997	-0.09120
47.99998	-0.02192	98.99997	-0.09319
48.99998	-0.02299	99.99997	-0.09513
49.99998	-0.02355		
50.99998	-0.02452		

Table 3-7. Calculated Response for NARCO Glide Slope with 30 Hz Harmonic.

% Harmonic	DDM	% Harmonic	DDM
1.00000	-0.00163	51.99998	-3.99998
2.00000	-0.00589	52.99998	-4.05872
3.00000	-0.01108	53.99997	-4.21143
4.00000	-0.02355	54.99997	-4.36614
5.00000	-0.03663	55.99998	-4.52435
6.00000	-0.05262	56.99998	-4.68457
6.99999	-0.07193	57.99998	-4.84770
8.00000	-0.09395	58.99998	-5.01343
9.00000	-0.11868	59.99997	-5.18153
10.00000	-0.14647	60.99997	-5.35257
11.00000	-0.17687	61.99997	-5.52653
11.99999	-0.21054	62.99997	-5.70273
12.99999	-0.24717	63.99998	-5.88160
13.99999	-0.28677	64.99998	-6.06276
14.99999	-0.32927	65.99998	-6.24684
16.00000	-0.37439	66.99997	-6.43352
16.99998	-0.42277	67.99997	-6.62250
17.99998	-0.47375	68.99997	-6.81445
18.99998	-0.52771	69.99997	-7.00833
19.99998	-0.58493	70.99997	-7.20518
20.99998	-0.64480	71.99998	-7.40464
21.99998	-0.70723	72.99997	-7.60639
22.99998	-0.77294	73.99997	-7.81075
23.99998	-0.84129	74.99997	-8.01741
24.99998	-0.91292	75.99997	-8.22667
25.99998	-0.98710	76.99997	-8.43823
26.99998	-1.06394	77.99997	-8.65240
27.99998	-1.14405	78.99997	-8.86917
28.99998	-1.22712	79.99997	-9.08825
29.99998	-1.31280	80.99997	-9.30962
30.99998	-1.40139	81.99997	-9.53324
31.99998	-1.49264	82.99997	-9.75951
32.99998	-1.58679	83.99997	-9.98809
33.99998	-1.68392	84.99997	-10.21922
34.99998	-1.78395	85.99997	-10.45239
35.99998	-1.88664	86.99997	-10.68812
36.99998	-1.99224	87.99997	-10.92615
37.99998	-2.10045	88.99997	-11.16647
38.99998	-2.21162	89.99997	-11.40910
39.99998	-2.32576	90.99997	-11.65402
40.99998	-2.44250	91.99997	-11.90119
41.99998	-2.56174	92.99997	-12.15066
42.99998	-2.68446	93.99997	-12.40244
43.99998	-2.80937	94.99997	-12.65650
44.99998	-2.93750	95.99997	-12.91251
45.99998	-3.06799	96.99997	-13.17118
46.99998	-3.20138	97.99997	-13.43174
47.99998	-3.33747	98.99997	-13.69434
48.99998	-3.47650	99.99997	-13.95950
49.99998	-3.61797		
50.99998	-3.76214		

Table 3-8. Calculated Response for NARCO Glide Slope with 60 Hz Harmonic.

% Harmonic	DDM	% Harmonic	DDM
1.00000	0.00193	51.99998	4.43867
2.00000	0.00454	52.99998	4.61003
3.00000	0.01507	53.99997	4.78430
4.00000	0.02652	54.99997	4.96193
5.00000	0.04154	55.99998	5.14264
6.00000	0.05452	56.99998	5.32541
6.99999	0.08108	57.99998	5.51345
8.00000	0.10560	58.99998	5.70376
9.00000	0.13375	59.99997	5.89699
10.00000	0.16512	60.99997	6.09352
11.00000	0.19981	61.99997	6.29328
11.99999	0.23903	62.99997	6.49601
12.99999	0.27926	63.99998	6.70200
13.99999	0.32370	64.99998	6.91096
14.99999	0.37178	65.99998	7.12282
16.00000	0.42277	66.99997	7.33827
16.99998	0.47708	67.99997	7.55637
17.99998	0.53496	68.99997	7.77805
18.99998	0.59606	69.99997	8.00239
19.99998	0.66018	70.99997	8.22994
20.99998	0.72788	71.99998	8.46081
21.99998	0.79879	72.99997	8.69424
22.99998	0.87271	73.99997	8.93130
23.99998	0.95052	74.99997	9.17096
24.99998	1.03094	75.99997	9.41425
25.99998	1.11498	76.99997	9.65979
26.99998	1.20229	77.99997	9.90895
27.99998	1.29288	78.99997	10.16108
28.99998	1.38673	79.99997	10.41612
29.99998	1.48380	80.99997	10.67407
30.99998	1.58419	81.99997	10.93534
31.99998	1.68754	82.99997	11.19953
32.99998	1.79442	83.99997	11.46632
33.99998	1.90462	84.99997	11.73674
34.99998	2.01809	85.99997	12.00976
35.99998	2.13448	86.99997	12.28575
36.99998	2.25449	87.99997	12.56495
37.99998	2.37746	88.99997	12.84681
38.99998	2.50365	89.99997	13.13194
39.99998	2.63311	90.99997	13.41968
40.99998	2.76620	91.99997	13.71038
41.99998	2.90189	92.99997	14.00430
42.99998	3.04122	93.99997	14.30118
43.99998	3.18376	94.99997	14.60103
44.99998	3.32926	95.99997	14.90348
45.99998	3.47834	96.99997	15.20989
46.99998	3.63018	97.99997	15.51722
47.99998	3.78570	98.99997	15.82851
48.99998	3.94397	99.99997	16.14240
49.99998	4.10582		
50.99998	4.27064		

Table 3-9. Calculated Response for NARCO Glide Slope with 180 Hz Harmonic.

% Harmonic	DDM	% Harmonic	DDM
1.00000	0.0	51.99998	0.00066
2.00000	0.0	52.99998	0.00066
3.00000	0.0	53.99997	0.00066
4.00000	0.0	54.99997	0.00066
5.00000	0.0	55.99998	0.00066
6.00000	0.0	56.99998	0.00066
6.99999	0.0	57.99998	0.00066
8.00000	0.0	58.99998	0.00066
9.00000	0.0	59.99997	0.00066
10.00000	0.0	60.99997	0.00066
11.00000	0.0	61.99997	0.00066
11.99999	0.0	62.99997	0.00066
12.99999	0.00036	63.99998	0.00066
13.99999	0.00036	64.99998	0.00066
14.99999	0.00036	65.99998	0.00097
16.00000	0.00036	66.99997	0.00066
16.99998	0.00036	67.99997	0.00097
17.99998	0.0	68.99997	0.00097
18.99998	0.0	69.99997	0.00097
19.99998	0.0	70.99997	0.00097
20.99998	0.00036	71.99998	0.00097
21.99998	0.00036	72.99997	0.00097
22.99998	0.00036	73.99997	0.00097
23.99998	0.00036	74.99997	0.00133
24.99998	0.0	75.99997	0.00097
25.99998	0.0	76.99997	0.00133
26.99998	0.0	77.99997	0.00133
27.99998	0.0	78.99997	0.00133
28.99998	0.00036	79.99997	0.00133
29.99998	0.00036	80.99997	0.00133
30.99998	0.00036	81.99997	0.00133
31.99998	0.00036	82.99997	0.00133
32.99998	0.00036	83.99997	0.00133
33.99998	0.00036	84.99997	0.00133
34.99998	0.00036	85.99997	0.00133
35.99998	0.00036	86.99997	0.00133
36.99998	0.00036	87.99997	0.00163
37.99998	0.00036	88.99997	0.00163
38.99998	0.00036	89.99997	0.00133
39.99998	0.00036	90.99997	0.00163
40.99998	0.00036	91.99997	0.00163
41.99998	0.00036	92.99997	0.00163
42.99998	0.00036	93.99997	0.00163
43.99998	0.00036	94.99997	0.00163
44.99998	0.00066	95.99997	0.00163
45.99998	0.00036	96.99997	0.00163
46.99998	0.00036	97.99997	0.00163
47.99998	0.00066	98.99997	0.00149
48.99998	0.00066	99.99997	0.00149
49.99998	0.00066		
50.99998	0.00066		

Table 3-10. Calculated Response for NARCO Glide Slope with 240 Hz Harmonic.

% Harmonic	DDM	% Harmonic	DDM
1.00000	0.0	51.99999	0.11281
2.00000	0.00036	52.99999	0.11740
3.00000	0.00036	53.99997	0.12104
4.00000	0.00066	54.99997	0.12624
5.00000	0.00097	55.99998	0.13079
6.00000	0.00163	56.99998	0.13569
6.99999	0.00199	57.99998	0.14060
8.00000	0.00261	58.99998	0.14550
9.00000	0.00363	59.99997	0.15041
10.00000	0.00424	60.99997	0.15531
11.00000	0.00526	61.99997	0.16057
11.99999	0.00623	62.99997	0.16579
12.99999	0.00720	63.99998	0.17100
13.99999	0.00817	64.99998	0.17626
14.99999	0.00950	65.99998	0.18183
16.00000	0.01078	66.99997	0.18735
16.99998	0.01211	67.99997	0.19291
17.99998	0.01344	68.99997	0.19879
18.99998	0.01507	69.99997	0.20472
19.99998	0.01671	70.99997	0.21059
20.99998	0.01834	71.99998	0.21647
21.99998	0.02028	72.99997	0.22234
22.99998	0.02222	73.99997	0.22858
23.99998	0.02422	74.99997	0.23476
24.99998	0.02616	75.99997	0.24099
25.99998	0.02815	76.99997	0.24753
26.99998	0.03040	77.99997	0.25407
27.99998	0.03270	78.99997	0.26061
28.99998	0.03530	79.99997	0.26715
29.99998	0.03760	80.99997	0.27369
30.99998	0.04021	81.99997	0.28053
31.99998	0.04286	82.99997	0.28743
32.99998	0.04547	83.99997	0.29463
33.99998	0.04838	84.99997	0.30148
34.99998	0.05104	85.99997	0.30969
35.99998	0.05431	86.99997	0.31589
36.99998	0.05722	87.99997	0.32304
37.99998	0.06049	88.99997	0.33060
38.99998	0.06345	89.99997	0.33775
39.99998	0.06672	90.99997	0.34562
40.99998	0.07030	91.99997	0.35313
41.99998	0.07357	92.99997	0.36100
42.99998	0.07720	93.99997	0.36882
43.99998	0.08077	94.99997	0.37638
44.99998	0.08471	95.99997	0.38455
45.99998	0.08828	96.99997	0.39273
46.99998	0.09222	97.99997	0.40054
47.99998	0.09615	98.99997	0.40908
48.99998	0.10039	99.99997	0.41725
49.99998	0.10433		
50.99998	0.10857		

Table 3-11. Calculated Response for NARCO Glide Slope with 300 Hz Harmonic.

% Harmonic	DDM	% Harmonic	DDM
1.00000	0.0	51.99998	0.0
2.00000	0.0	52.99998	0.0
3.00000	0.0	53.99997	0.0
4.00000	0.0	54.99997	0.0
5.00000	0.0	55.99998	0.0
6.00000	0.0	56.99998	0.0
6.99999	0.0	57.99998	0.0
8.00000	0.0	58.99998	0.0
9.00000	0.0	59.99997	-0.00031
10.00000	0.0	60.99997	0.0
11.00000	0.0	61.99997	0.0
11.99999	0.0	62.99997	0.0
12.99999	0.0	63.99998	0.0
13.99999	0.0	64.99998	0.0
14.99999	0.0	65.99998	0.0
16.00000	0.0	66.99997	0.0
16.99998	0.0	67.99997	0.0
17.99998	0.0	68.99997	0.0
18.99998	0.0	69.99997	-0.00031
19.99998	0.0	70.99997	-0.00031
20.99998	0.0	71.99998	-0.00031
21.99998	0.0	72.99997	-0.00031
22.99998	0.0	73.99997	-0.00031
23.99998	0.0	74.99997	-0.00031
24.99998	0.0	75.99997	-0.00031
25.99998	0.0	76.99997	-0.00031
26.99998	0.0	77.99997	-0.00031
27.99998	0.0	78.99997	-0.00031
28.99998	0.0	79.99997	-0.00031
29.99998	0.0	80.99997	-0.00031
30.99998	0.0	81.99997	-0.00031
31.99998	0.0	82.99997	-0.00031
32.99998	0.0	83.99997	-0.00031
33.99998	0.0	84.99997	-0.00031
34.99998	0.0	85.99997	-0.00031
35.99998	0.0	86.99997	-0.00031
36.99998	0.0	87.99997	-0.00031
37.99998	0.0	88.99997	-0.00031
38.99998	0.0	89.99997	-0.00031
39.99998	0.0	90.99997	-0.00031
40.99998	0.0	91.99997	-0.00031
41.99998	0.0	92.99997	-0.00031
42.99998	0.0	93.99997	-0.00031
43.99998	0.0	94.99997	-0.00031
44.99998	0.0	95.99997	-0.00031
45.99998	0.0	96.99997	-0.00031
46.99998	0.0	97.99997	-0.00031
47.99998	0.0	98.99997	-0.00031
48.99998	-0.00031	99.99997	-0.00031
49.99998	0.0		
50.99998	0.0		

Table 3-12. Calculated Response for NARCO Glide Slope with 540 Hz Harmonic.

% Harmonic	DDM
1.00000	0.0
2.00000	0.0
3.00000	-0.00018
4.00000	-0.00018
5.00000	-0.00018
6.00000	-0.00037
6.99999	-0.00037
8.00000	-0.00074
9.00000	-0.00074
10.00000	-0.00092
11.00000	-0.00111
11.99999	-0.00129
12.99999	-0.00148
13.99999	-0.00166
14.99999	-0.00203
16.00000	-0.00240
16.99998	-0.00258
17.99998	-0.00295
18.99998	-0.00332
19.99998	-0.00351
20.99998	-0.00406
21.99998	-0.00443
22.99998	-0.00480
23.99998	-0.00517
24.99998	-0.00572
25.99998	-0.00609
26.99998	-0.00664
27.99998	-0.00720
28.99998	-0.00775
29.99998	-0.00812
30.99998	-0.00868
31.99998	-0.00923
32.99998	-0.00978
33.99998	-0.01034
34.99998	-0.01107
35.99998	-0.01161
36.99998	-0.01237
37.99998	-0.01292
38.99998	-0.01366
39.99998	-0.01440
40.99998	-0.01514
41.99998	-0.01606
42.99998	-0.01690
43.99998	-0.01754
44.99998	-0.01827
45.99998	-0.01901
46.99998	-0.01993
47.99998	-0.02086
48.99998	-0.02179
49.99998	-0.02252
50.99998	-0.02344

% Harmonic	DDM
51.99998	-0.02436
52.99998	-0.02529
53.99997	-0.02640
54.99997	-0.02732
55.99998	-0.02943
56.99998	-0.02935
57.99998	-0.03027
58.99998	-0.03133
59.99997	-0.03249
60.99997	-0.03359
61.99997	-0.03470
62.99997	-0.03581
63.99998	-0.03692
64.99998	-0.03802
65.99998	-0.03932
66.99997	-0.04061
67.99997	-0.04172
68.99997	-0.04301
69.99997	-0.04412
70.99997	-0.04541
71.99998	-0.04670
72.99997	-0.04799
73.99997	-0.04928
74.99997	-0.05076
75.99997	-0.05205
76.99997	-0.05353
77.99997	-0.05482
78.99997	-0.05630
79.99997	-0.05777
80.99997	-0.05925
81.99997	-0.06073
82.99997	-0.06202
83.99997	-0.06368
84.99997	-0.06516
85.99997	-0.06682
86.99997	-0.06830
87.99997	-0.06977
88.99997	-0.07143
89.99997	-0.07309
90.99997	-0.07457
91.99997	-0.07623
92.99997	-0.07808
93.99997	-0.07955
94.99997	-0.08140
95.99997	-0.08306
96.99997	-0.08472
97.99997	-0.08657
98.99997	-0.08841
99.99997	-0.09008

Table 3-13. Calculated Response for Collins Localizer with 30 Hz Harmonic.

% Harmonic	DDM	% Harmonic	DDM
1.00000	-0.00074	51.99998	-1.82515
2.00000	-0.00277	52.99998	-1.89492
3.00000	-0.00628	53.99997	-1.96548
4.00000	-0.01107	54.99997	-2.03834
5.00000	-0.01717	55.99993	-2.11132
6.00000	-0.02473	56.99998	-2.18674
6.99999	-0.03359	57.99998	-2.26270
8.00000	-0.04393	58.99998	-2.34013
9.00000	-0.05556	59.99997	-2.41876
10.00000	-0.06848	60.99997	-2.49832
11.00000	-0.08269	61.99997	-2.57935
11.99999	-0.09857	62.99997	-2.66149
12.99999	-0.11555	63.99998	-2.74487
13.99999	-0.13401	64.99998	-2.82941
14.99999	-0.15394	65.99998	-2.91520
16.00000	-0.17498	66.99997	-3.00222
16.99998	-0.19750	67.99997	-3.09037
17.99998	-0.22150	68.99997	-3.17965
18.99998	-0.24679	69.99997	-3.27018
19.99998	-0.27318	70.99997	-3.36192
20.99998	-0.30124	71.99998	-3.45473
21.99998	-0.33040	72.99997	-3.54880
22.99998	-0.36123	73.99997	-3.64399
23.99999	-0.39316	74.99997	-3.74026
24.99998	-0.42638	75.99997	-3.83774
25.99998	-0.46109	76.99997	-3.93640
26.99998	-0.49708	77.99997	-4.03611
27.99998	-0.53455	78.99997	-4.13698
28.99998	-0.57313	79.99997	-4.23902
29.99998	-0.61318	80.99997	-4.34210
30.99998	-0.65453	81.99997	-4.44635
31.99998	-0.69717	82.99997	-4.55169
32.99998	-0.74128	83.99997	-4.65810
33.99998	-0.78650	84.99997	-4.76563
34.99998	-0.83320	85.99997	-4.87429
35.99998	-0.88120	86.99997	-4.98394
36.99998	-0.93029	87.99997	-5.09472
37.99998	-0.98105	88.99997	-5.20663
38.99998	-1.03292	89.99997	-5.31953
39.99998	-1.08608	90.99997	-5.43351
40.99998	-1.14053	91.99997	-5.54846
41.99998	-1.19646	92.99997	-5.66457
42.99998	-1.25350	93.99997	-5.78162
43.99998	-1.31182	94.99997	-5.89981
44.99998	-1.37163	95.99997	-6.01896
45.99998	-1.43254	96.99997	-6.13913
46.99999	-1.49475	97.99997	-6.26029
47.99998	-1.55824	98.99997	-6.38250
48.99998	-1.62303	99.99997	-6.50578
49.99998	-1.68911		
50.99998	-1.75643		

Table 3-14. Calculated Response for Collins Localizer with 60 Hz Harmonic.

% Harmonic	DDM
1.00000	0.00129
2.00000	0.00517
3.00000	0.01144
4.00000	0.02044
5.00000	0.03193
6.00000	0.04615
6.99999	0.06276
8.00000	0.08195
9.00000	0.10392
10.00000	0.12828
11.00000	0.15505
11.99999	0.18458
12.99999	0.21651
13.99999	0.25122
14.99999	0.28832
16.00000	0.32800
16.99999	0.37027
17.99998	0.41513
18.99998	0.46256
19.99998	0.51240
20.99998	0.56482
21.99998	0.61983
22.99998	0.67742
23.99998	0.73759
24.99998	0.80016
25.99998	0.86514
26.99998	0.93288
27.99998	1.00302
28.99998	1.07574
29.99998	1.15105
30.99998	1.22876
31.99998	1.30924
32.99998	1.39193
33.99998	1.47721
34.99998	1.56507
35.99998	1.65533
36.99998	1.74818
37.99998	1.84360
38.99998	1.94143
39.99998	2.04166
40.99998	2.14447
41.99998	2.24987
42.99998	2.35748
43.99998	2.46786
44.99998	2.58064
45.99998	2.69563
46.99998	2.81340
47.99998	2.93339
48.99998	3.05594
49.99998	3.18090
50.99998	3.30826

% Harmonic	DDM
51.99999	3.43921
52.99998	3.57055
53.99997	3.70530
54.99997	3.84244
55.99994	3.98199
56.99999	4.12393
57.99998	4.26827
58.99998	4.41520
59.99997	4.56434
60.99997	4.71607
61.99997	4.87001
62.99997	5.02617
63.99998	5.18510
64.99998	5.34621
65.99998	5.50959
66.99997	5.67534
67.99997	5.84368
68.99997	6.01424
69.99997	6.18701
70.99997	6.36217
71.99998	6.53974
72.99997	6.71971
73.99997	6.90189
74.99997	7.08629
75.99997	7.27309
76.99997	7.46210
77.99997	7.65351
78.99997	7.84714
79.99997	8.04316
80.99997	8.24122
81.99997	8.44186
82.99997	8.64453
83.99997	8.84960
84.99997	9.05671
85.99997	9.26621
86.99997	9.47792
87.99997	9.69185
88.99997	9.90900
89.99997	10.12636
90.99997	10.34675
91.99997	10.56954
92.99997	10.79436
93.99997	11.02158
94.99997	11.25083
95.99997	11.48230
96.99997	11.71579
97.99997	11.95150
98.99997	12.18943
99.99997	12.42957

Table 3-15. Calculated Response for Collins Localizer with 180 Hz Harmonic.

% Harmonic	DDM	% Harmonic	DDM
1.00000	0.0	51.99997	0.00521
2.00000	0.0	52.99998	0.00674
3.00000	0.0	53.99997	0.00623
4.00000	0.0	54.99997	0.00664
5.00000	0.0	55.99998	0.00683
6.00000	0.0	56.99998	0.00701
6.99999	0.0	57.99998	0.00738
8.00000	0.00018	58.99998	0.00757
9.00000	0.00018	59.99997	0.00775
10.00000	0.00018	60.99997	0.00812
11.00000	0.00018	61.99997	0.00849
11.99999	0.00018	62.99997	0.00868
12.99999	0.00037	63.99998	0.00886
13.99999	0.00037	64.99998	0.00923
14.99999	0.00055	65.99998	0.00941
16.00000	0.00055	66.99997	0.00978
16.99998	0.00055	67.99997	0.01015
17.99998	0.00074	68.99997	0.01034
18.99998	0.00074	69.99997	0.01071
19.99998	0.00092	70.99997	0.01107
20.99998	0.00092	71.99998	0.01126
21.99998	0.00092	72.99997	0.01163
22.99999	0.00111	73.99997	0.01200
23.99998	0.00111	74.99997	0.01237
24.99998	0.00129	75.99997	0.01255
25.99998	0.00129	76.99997	0.01292
26.99998	0.00148	77.99997	0.01329
27.99998	0.00166	78.99997	0.01366
28.99998	0.00185	79.99997	0.01403
29.99998	0.00185	80.99997	0.01421
30.99998	0.00203	81.99997	0.01452
31.99998	0.00221	82.99997	0.01495
32.99998	0.00240	83.99997	0.01550
33.99998	0.00240	84.99997	0.01569
34.99998	0.00258	85.99997	0.01606
35.99998	0.00277	86.99997	0.01661
36.99998	0.00295	87.99997	0.01698
37.99998	0.00314	88.99997	0.01717
38.99998	0.00332	89.99997	0.01772
39.99998	0.00351	90.99997	0.01809
40.99998	0.00351	91.99997	0.01846
41.99998	0.00388	92.99997	0.01983
42.99998	0.00406	93.99997	0.01938
43.99998	0.00425	94.99997	0.01975
44.99998	0.00443	95.99997	0.02012
45.99998	0.00461	96.99997	0.02049
46.99998	0.00480	97.99997	0.02104
47.99998	0.00498	98.99997	0.02141
48.99998	0.00517	99.99997	0.02197
49.99998	0.00535		
50.99998	0.00572		

Table 3-16. Calculated Response for Collins Localizer with 240 Hz Harmonic.

% Harmonic DDM

1.00000	0.0
2.00000	0.0
3.00000	0.0
4.00000	0.0
5.00000	0.0
6.00000	0.0
6.99999	0.0
8.00000	0.0
9.00000	0.0
10.00000	0.0
11.00000	0.0
11.99999	0.0
12.99999	0.0
13.99999	0.0
14.99999	0.0
16.00000	0.0
16.99998	0.0
17.99998	0.0
18.99998	0.0
19.99998	0.0
20.99998	0.0
21.99998	0.0
22.99998	-0.00018
23.99998	0.0
24.99998	0.0
25.99998	-0.00018
26.99998	0.0
27.99998	0.0
28.99998	-0.00018
29.99998	-0.00018
30.99998	0.0
31.99998	0.0
32.99998	0.0
33.99998	0.0
34.99998	0.0
35.99998	0.0
36.99998	0.0
37.99998	0.0
38.99998	0.0
39.99998	0.0
40.99998	0.0
41.99998	0.0
42.99998	0.0
43.99998	0.0
44.99998	-0.00018
45.99998	0.0
46.99998	0.0
47.99998	0.0
48.99998	-0.00018
49.99998	-0.00018
50.99998	0.0

% Harmonic DDM

51.99998	-0.00018
52.99998	0.0
53.99997	-0.00018
54.99997	-0.00018
55.99998	-0.00018
56.99998	0.0
57.99998	-0.00018
58.99998	0.0
59.99997	-0.00018
60.99997	-0.00018
61.99997	-0.00018
62.99997	-0.00018
63.99998	-0.00018
64.99998	-0.00018
65.99998	-0.00018
66.99997	-0.00018
67.99997	-0.00018
68.99997	-0.00018
69.99997	-0.00018
70.99997	-0.00018
71.99998	-0.00018
72.99997	-0.00018
73.99997	-0.00018
74.99997	-0.00018
75.99997	-0.00018
76.99997	-0.00018
77.99997	-0.00018
78.99997	-0.00018
79.99997	-0.00018
80.99997	-0.00018
81.99997	-0.00018
82.99997	-0.00018
83.99997	-0.00018
84.99997	-0.00018
85.99997	-0.00037
86.99997	-0.00018
87.99997	-0.00018
88.99997	-0.00037
89.99997	-0.00018
90.99997	-0.00037
91.99997	-0.00018
92.99997	-0.00037
93.99997	-0.00018
94.99997	-0.00037
95.99997	-0.00018
96.99997	-0.00037
97.99997	-0.00018
98.99997	-0.00018
99.99997	-0.00037

Table 3-17. Calculated Response for Collins Localizer with 300 Hz Harmonic.

% Harmonic	DDM
1.00000	0.0
2.00000	0.0
3.00000	0.0
4.00000	0.0
5.00000	0.0
6.00000	0.0
6.99999	0.0
8.00000	0.0
9.00000	0.0
10.00000	0.0
11.00000	0.0
11.99999	0.0
12.99999	0.0
13.99999	0.0
14.99999	0.0
16.00000	0.0
16.99998	0.0
17.99998	0.0
18.99998	0.0
19.99998	0.0
20.99998	0.0
21.99998	0.0
22.99998	-0.00018
23.99998	0.0
24.99998	0.0
25.99998	-0.00018
26.99998	0.0
27.99998	0.0
28.99998	-0.00018
29.99998	-0.00018
30.99998	0.0
31.99998	0.0
32.99998	0.0
33.99998	0.0
34.99998	0.0
35.99998	0.0
36.99998	0.0
37.99998	0.0
38.99998	0.0
39.99998	0.0
40.99998	0.0
41.99998	0.0
42.99998	0.0
43.99998	0.0
44.99998	-0.00018
45.99998	0.0
46.99998	0.0
47.99998	0.0
48.99998	-0.00018
49.99998	-0.00018
50.99998	0.0

% Harmonic	DDM
51.99998	-0.00018
52.99998	0.0
53.99997	-0.00018
54.99997	-0.00018
55.99998	-0.00018
56.99998	0.0
57.99998	-0.00018
58.99998	0.0
59.99997	-0.00018
60.99997	-0.00018
61.99997	-0.00018
62.99997	-0.00018
63.99998	-0.00018
64.99998	-0.00018
65.99998	-0.00018
66.99997	-0.00018
67.99997	-0.00018
68.99997	-0.00018
69.99997	-0.00018
70.99997	-0.00018
71.99998	-0.00018
72.99997	-0.00018
73.99997	-0.00018
74.99997	-0.00018
75.99997	-0.00018
76.99997	-0.00018
77.99997	-0.00018
78.99997	-0.00018
79.99997	-0.00018
80.99997	-0.00018
81.99997	-0.00018
82.99997	-0.00018
83.99997	-0.00018
84.99997	-0.00018
85.99997	-0.00037
86.99997	-0.00018
87.99997	-0.00018
88.99997	-0.00037
89.99997	-0.00018
90.99997	-0.00037
91.99997	-0.00018
92.99997	-0.00037
93.99997	-0.00018
94.99997	-0.00037
95.99997	-0.00018
96.99997	-0.00037
97.99997	-0.00018
98.99997	-0.00018
99.99997	-0.00037

Table 3-18. Calculated Response for Collins Localizer with 540 Hz Harmonic.

% Harmonic	DDM	% Harmonic	DDM
1.00000	0.0	51.99999	-0.06114
2.00000	0.0	52.99999	-0.05376
3.00000	0.0	53.99999	-0.06505
4.00000	-0.00033	54.99999	-0.06355
5.00000	-0.00065	55.99999	-0.07075
6.00000	-0.00065	56.99999	-0.07357
6.99999	-0.00099	57.99999	-0.07619
8.00000	-0.00131	58.99999	-0.07930
9.00000	-0.00153	59.99999	-0.08174
10.00000	-0.00229	60.99999	-0.08436
11.00000	-0.00262	61.99999	-0.08698
11.99999	-0.00327	62.99999	-0.08937
12.99999	-0.00360	63.99999	-0.09286
13.99999	-0.00425	64.99999	-0.09580
14.99999	-0.00490	65.99999	-0.09875
16.00000	-0.00556	66.99999	-0.10169
16.99999	-0.00654	67.99999	-0.10496
17.99999	-0.00719	68.99999	-0.10790
18.99999	-0.00785	69.99999	-0.11117
19.99999	-0.00883	70.99999	-0.11411
20.99999	-0.00981	71.99999	-0.11738
21.99999	-0.01079	72.99999	-0.12065
22.99999	-0.01177	73.99999	-0.12425
23.99999	-0.01275	74.99999	-0.12752
24.99999	-0.01406	75.99999	-0.13112
25.99999	-0.01537	76.99999	-0.13439
26.99999	-0.01635	77.99999	-0.13798
27.99999	-0.01766	78.99999	-0.14158
28.99999	-0.01896	79.99999	-0.14518
29.99999	-0.02027	80.99999	-0.14877
30.99999	-0.02158	81.99999	-0.15237
31.99999	-0.02322	82.99999	-0.15629
32.99999	-0.02452	83.99999	-0.15989
33.99999	-0.02616	84.99999	-0.16381
34.99999	-0.02779	85.99999	-0.16774
35.99999	-0.02943	86.99999	-0.17166
36.99999	-0.03106	87.99999	-0.17559
37.99999	-0.03270	88.99999	-0.17951
38.99999	-0.03433	89.99999	-0.18376
39.99999	-0.03629	90.99999	-0.18768
40.99999	-0.03793	91.99999	-0.19193
41.99999	-0.03989	92.99999	-0.19618
42.99999	-0.04185	93.99999	-0.20044
43.99999	-0.04381	94.99999	-0.20469
44.99999	-0.04578	95.99999	-0.20894
45.99999	-0.04807	96.99999	-0.21351
46.99999	-0.05003	97.99999	-0.21776
47.99999	-0.05232	98.99999	-0.22234
48.99999	-0.05429	99.99999	-0.22692
49.99999	-0.05657		
50.99999	-0.05886		

Table 3-19. Calculated Response for Collins Glide Slope with 30 Hz Harmonic.

AD-A140 797

ENGINEERING AND TECHNICAL SERVICES TO IMPROVE
RELIABILITY AND MAINTAINABILITY (U) OHIO UNIV ATHENS
AVIONICS ENGINEERING CENTER J D LONGWORTH ET AL

3/4

UNCLASSIFIED

JAN 83 OU/REC/EER-62-1 DOT/FAA/PH-84/7

F/G 17/7

NL

1



% Harmonic	DDM	% Harmonic	DDM
1.00000	-0.00131	51.99998	-3.36910
2.00000	-0.00490	52.99998	-3.44709
3.00000	-0.01144	53.99997	-3.62914
4.00000	-0.02027	54.99997	-3.76263
5.00000	-0.03139	55.99998	-3.49831
6.00000	-0.04545	56.99998	-4.03641
6.99999	-0.06180	57.99998	-4.17672
8.00000	-0.08076	58.99998	-4.31920
9.00000	-0.10234	59.99997	-4.46414
10.00000	-0.12621	60.99997	-4.61107
11.00000	-0.15270	61.99997	-4.76040
11.99999	-0.18180	62.99997	-4.91193
12.99999	-0.21351	63.99998	-5.06562
13.99999	-0.24752	64.99998	-5.22161
14.99999	-0.28414	65.99998	-5.37991
16.00000	-0.32305	66.99997	-5.54008
16.99998	-0.36458	67.99997	-5.70255
17.99998	-0.40872	68.99997	-5.86724
18.99998	-0.45547	69.99997	-6.03406
19.99998	-0.50452	70.99997	-6.20308
20.99998	-0.55618	71.99998	-6.37415
21.99998	-0.61046	72.99997	-6.54745
22.99998	-0.66703	73.99997	-6.72283
23.99998	-0.72588	74.99997	-6.90025
24.99998	-0.78768	75.99997	-7.07990
25.99998	-0.85144	76.99997	-7.26158
26.99998	-0.91814	77.99997	-7.44528
27.99998	-0.98713	78.99997	-7.63108
28.99998	-1.05841	79.99997	-7.81895
29.99998	-1.13231	80.99997	-8.00884
30.99998	-1.20882	81.99997	-8.20079
31.99998	-1.28762	82.99997	-8.39477
32.99998	-1.36871	83.99997	-8.59073
33.99998	-1.45242	84.99997	-8.78871
34.99998	-1.53874	85.99997	-8.98860
35.99998	-1.62735	86.99997	-9.19054
36.99998	-1.71825	87.99997	-9.39447
37.99998	-1.81144	88.99997	-9.60026
38.99998	-1.90757	89.99997	-9.80812
39.99998	-2.00566	90.99997	-10.01777
40.99998	-2.10637	91.99997	-10.22946
41.99999	-2.20936	92.99997	-10.44304
42.99998	-2.31465	93.99997	-10.65845
43.99998	-2.42222	94.99997	-10.87577
44.99998	-2.53237	95.99997	-11.09492
45.99998	-2.64481	96.99997	-11.31600
46.99998	-2.75970	97.99997	-11.53901
47.99998	-2.87692	98.99997	-11.76363
48.99998	-2.99649	99.99997	-11.99012
49.99998	-3.11835		
50.99998	-3.24260		

Table 3-20. Calculated Response for Collins Glide Slope with 60 Hz Harmonic.

% Harmonic	DDM	% Harmonic	DDM
1.00000	0.00262	51.99999	6.89000
2.00000	0.01046	52.99999	7.15452
3.00000	0.02322	53.99999	7.42427
4.00000	0.04120	54.99999	7.69860
5.00000	0.06441	55.99999	7.97784
6.00000	0.09286	56.99999	8.26231
6.99999	0.12621	57.99999	8.55102
8.00000	0.16479	58.99999	8.84465
9.00000	0.20861	59.99999	9.14285
10.00000	0.25733	60.99999	9.44628
11.00000	0.31128	61.99999	9.75429
11.99999	0.37046	62.99999	10.06688
12.99999	0.43488	63.99999	10.38437
13.99999	0.50419	64.99999	10.70644
14.99999	0.57874	65.99999	11.03308
16.00000	0.65820	66.99999	11.36464
16.99999	0.74321	67.99999	11.70077
17.99999	0.83280	68.99999	12.04147
18.99999	0.92795	69.99999	12.38709
19.99999	1.02800	70.99999	12.73695
20.99999	1.13329	71.99999	13.09139
21.99999	1.24348	72.99999	13.45073
22.99999	1.35990	73.99999	13.81465
23.99999	1.47923	74.99999	14.18315
24.99999	1.60479	75.99999	14.55623
25.99999	1.73558	76.99999	14.93356
26.99999	1.87127	77.99999	15.31579
27.99999	2.01187	78.99999	15.70227
28.99999	2.15770	79.99999	16.09332
29.99999	2.30843	80.99999	16.48897
30.99999	2.46440	81.99999	16.88885
31.99999	2.62527	82.99999	17.29332
32.99999	2.79138	83.99999	17.70236
33.99999	2.96238	84.99999	18.11566
34.99999	3.13830	85.99999	18.53354
35.99999	3.31944	86.99999	18.95566
36.99999	3.50549	87.99999	19.38203
37.99999	3.69644	88.99999	19.81299
38.99999	3.89230	89.99999	20.24818
39.99999	4.09339	90.99999	20.68797
40.99999	4.29938	91.99999	21.13167
41.99999	4.51028	92.99999	21.57996
42.99999	4.72608	93.99999	22.03249
43.99999	4.94679	94.99999	22.48927
44.99999	5.17273	95.99999	22.95030
45.99999	5.40324	96.99999	23.41559
46.99999	5.63867	97.99999	23.88480
47.99999	5.87932	98.99999	24.35858
48.99999	6.12455	99.99999	24.83652
49.99999	6.37469		
50.99999	6.63005		

Table 3-21. Calculated Response for Collins Glide Slope with 180 Hz Harmonic.

% Harmonic	DDM	% Harmonic	DDM
1.00000	0.0	51.99998	0.01014
2.00000	0.0	52.99998	0.01046
3.00000	0.00033	53.99997	0.01079
4.00000	0.00033	54.99997	0.01112
5.00000	0.00033	55.99998	0.01144
6.00000	0.00033	56.99998	0.01177
6.99999	0.00033	57.99998	0.01242
9.00000	0.00033	58.99998	0.01275
9.00000	0.00033	59.99997	0.01341
10.00000	0.00033	60.99997	0.01373
11.00000	0.00065	61.99997	0.01406
11.99999	0.00065	62.99997	0.01471
12.99999	0.00065	63.99998	0.01504
13.99999	0.00065	64.99998	0.01537
14.99999	0.00098	65.99998	0.01602
16.00000	0.00098	66.99997	0.01635
16.99998	0.00131	67.99997	0.01700
17.99998	0.00131	68.99997	0.01733
18.99998	0.00131	69.99997	0.01798
19.99998	0.00163	70.99997	0.01864
20.99998	0.00163	71.99998	0.01896
21.99998	0.00196	72.99997	0.01962
22.99998	0.00196	73.99997	0.01995
23.99998	0.00229	74.99997	0.02060
24.99998	0.00229	75.99997	0.02125
25.99998	0.00262	76.99997	0.02158
26.99998	0.00262	77.99997	0.02223
27.99998	0.00294	78.99997	0.02299
28.99998	0.00327	79.99997	0.02354
29.99998	0.00327	80.99997	0.02387
30.99998	0.00360	81.99997	0.02452
31.99998	0.00392	82.99997	0.02518
32.99998	0.00392	83.99997	0.02583
33.99998	0.00425	84.99997	0.02649
34.99998	0.00458	85.99997	0.02714
35.99998	0.00490	86.99997	0.02779
36.99998	0.00523	87.99997	0.02812
37.99998	0.00523	88.99997	0.02877
38.99999	0.00556	89.99997	0.02975
39.99998	0.00589	90.99997	0.03041
40.99998	0.00621	91.99997	0.03106
41.99998	0.00654	92.99997	0.03139
42.99998	0.00687	93.99997	0.03237
43.99998	0.00719	94.99997	0.03302
44.99998	0.00752	95.99997	0.03368
45.99999	0.00785	96.99997	0.03433
46.99998	0.00817	97.99997	0.03499
47.99998	0.00850	98.99997	0.03564
48.99998	0.00883	99.99997	0.03662
49.99998	0.00916		
50.99998	0.00948		

Table 3-22. Calculated Response for Collins Glide Slope with 240 Hz Harmonic.

% Harmonic	DDM	% Harmonic	DDM
1.00000	0.0	51.99999	0.0
2.00000	0.0	52.99999	0.0
3.00000	0.0	53.99997	0.0
4.00000	0.0	54.99997	0.0
5.00000	0.0	55.99998	0.0
6.00000	0.00033	56.99999	0.0
6.99999	0.0	57.99998	0.0
8.00000	0.0	58.99998	0.0
9.00000	0.00033	59.99997	0.0
10.00000	0.0	60.99997	0.0
11.00000	0.0	61.99997	0.0
11.99999	0.0	62.99997	0.0
12.99999	0.0	63.99998	0.0
13.99999	0.0	64.99998	0.0
14.99999	0.00033	65.99998	0.0
16.00000	0.0	66.99997	0.0
16.99998	0.0	67.99997	0.0
17.99998	0.00033	68.99997	0.0
18.99998	0.00033	69.99997	0.0
19.99998	0.0	70.99997	0.0
20.99998	0.0	71.99998	0.0
21.99998	0.0	72.99997	0.0
22.99998	0.0	73.99997	0.0
23.99998	0.0	74.99997	0.0
24.99998	0.0	75.99997	0.0
25.99998	0.0	76.99997	0.0
26.99998	0.0	77.99997	0.0
27.99998	0.0	78.99997	0.0
28.99998	0.00033	79.99997	0.0
29.99998	0.00033	80.99997	0.0
30.99998	0.0	81.99997	0.0
31.99998	0.0	82.99997	0.0
32.99998	0.00033	83.99997	0.0
33.99998	0.0	84.99997	0.0
34.99998	0.0	85.99997	0.0
35.99998	0.0	86.99997	0.0
36.99998	0.00033	87.99997	0.0
37.99998	0.0	88.99997	0.0
38.99998	0.0	89.99997	0.0
39.99998	0.0	90.99997	0.0
40.99998	0.0	91.99997	0.0
41.99998	0.0	92.99997	0.0
42.99998	0.0	93.99997	0.0
43.99998	0.0	94.99997	0.0
44.99998	0.0	95.99997	0.0
45.99998	0.0	96.99997	0.0
46.99998	0.0	97.99997	0.0
47.99998	0.0	98.99997	0.0
48.99998	0.0	99.99997	0.0
49.99998	0.0		
50.99998	0.0		

Table 3-23. Calculated Response for Collins Glide Slope with 300 Hz Harmonic.

% Harmonic	DDM	% Harmonic	DDM
1.00000	0.0	51.99998	0.0
2.00000	0.0	52.99998	0.0
3.00000	0.0	53.99997	0.0
4.00000	0.0	54.99997	0.0
5.00000	0.0	55.99998	0.0
6.00000	0.00033	56.99998	0.0
6.99999	0.0	57.99998	0.0
8.00000	0.0	58.99999	0.0
9.00000	0.00013	59.99997	0.0
10.00000	0.0	60.99997	0.0
11.00000	0.0	61.99997	0.0
11.99999	0.0	62.99997	0.0
12.99999	0.0	63.99998	0.0
13.99999	0.0	64.99998	0.0
14.99999	0.00013	65.99998	0.0
16.00000	0.0	66.99997	0.0
16.99998	0.0	67.99997	0.0
17.99998	0.00033	68.99997	0.0
18.99998	0.00033	69.99997	0.0
19.99998	0.0	70.99997	0.0
20.99998	0.0	71.99998	0.0
21.99998	0.0	72.99997	0.0
22.99998	0.0	73.99997	0.0
23.99998	0.0	74.99997	0.0
24.99998	0.0	75.99997	0.0
25.99998	0.0	76.99997	0.0
26.99998	0.0	77.99997	0.0
27.99998	0.0	78.99997	0.0
28.99998	0.00033	79.99997	0.0
29.99998	0.00033	80.99997	0.0
30.99998	0.0	81.99997	0.0
31.99998	0.0	82.99997	0.0
32.99998	0.00033	83.99997	0.0
33.99998	0.0	84.99997	0.0
34.99998	0.0	85.99997	0.0
35.99998	0.0	86.99997	0.0
36.99998	0.00033	87.99997	0.0
37.99998	0.0	88.99997	0.0
38.99998	0.0	89.99997	0.0
39.99998	0.0	90.99997	0.0
40.99998	0.0	91.99997	0.0
41.99998	0.0	92.99997	0.0
42.99998	0.0	93.99997	0.0
43.99998	0.0	94.99997	0.0
44.99998	0.0	95.99997	0.0
45.99998	0.0	96.99997	0.0
46.99998	0.0	97.99997	0.0
47.99998	0.0	98.99997	0.0
48.99998	0.0	99.99997	0.0
49.99998	0.0		
50.99998	0.0		

Table 3-24. Calculated Response for Collins Glide Slope with 540 Hz Harmonic.

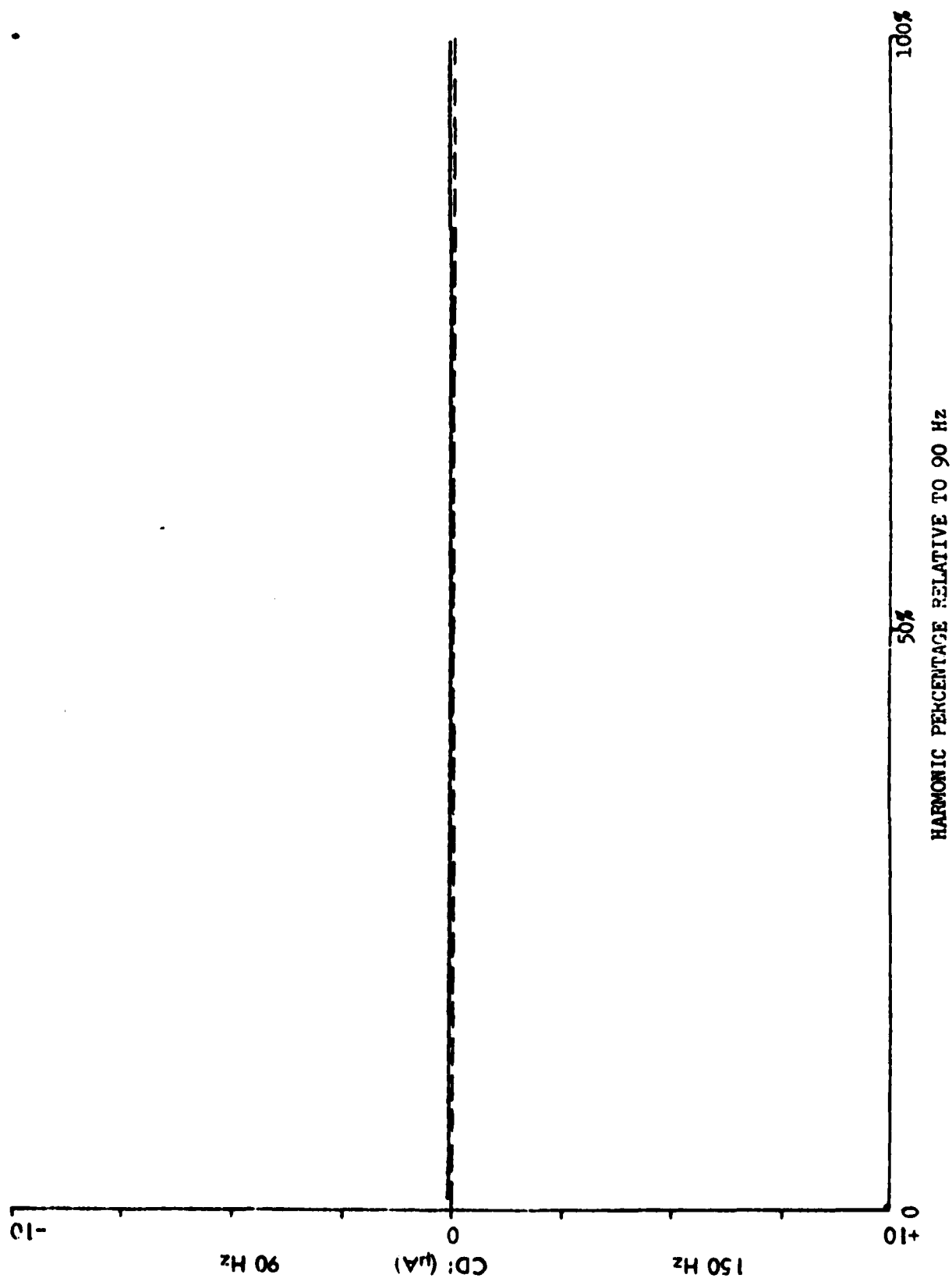


Figure 3-37. Calculated Response for NARCO Localizer with 30 Hz Harmonic.

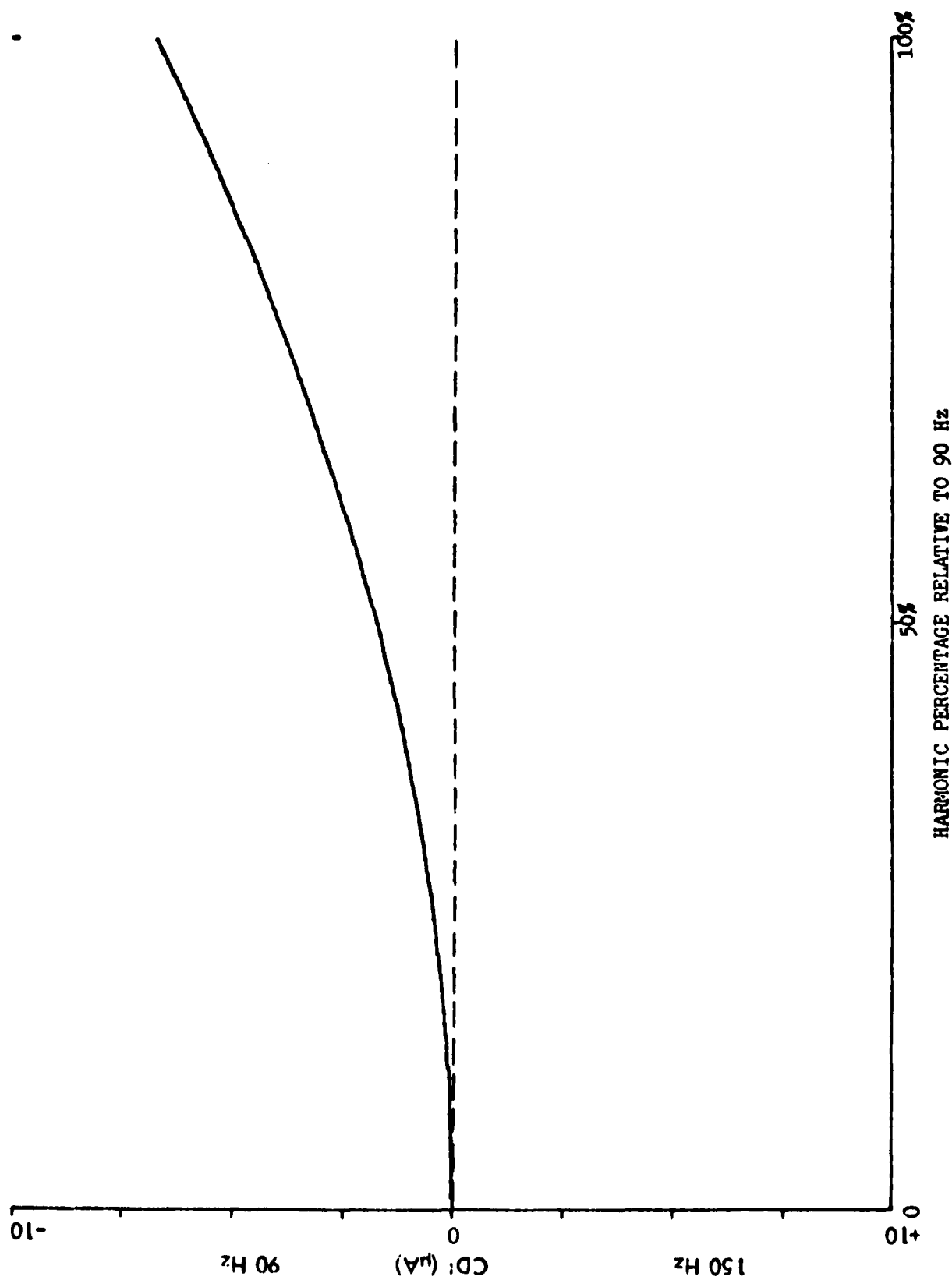


Figure 3-38. Calculated Response for NARCO Localizer with 60 Hz Harmonic.

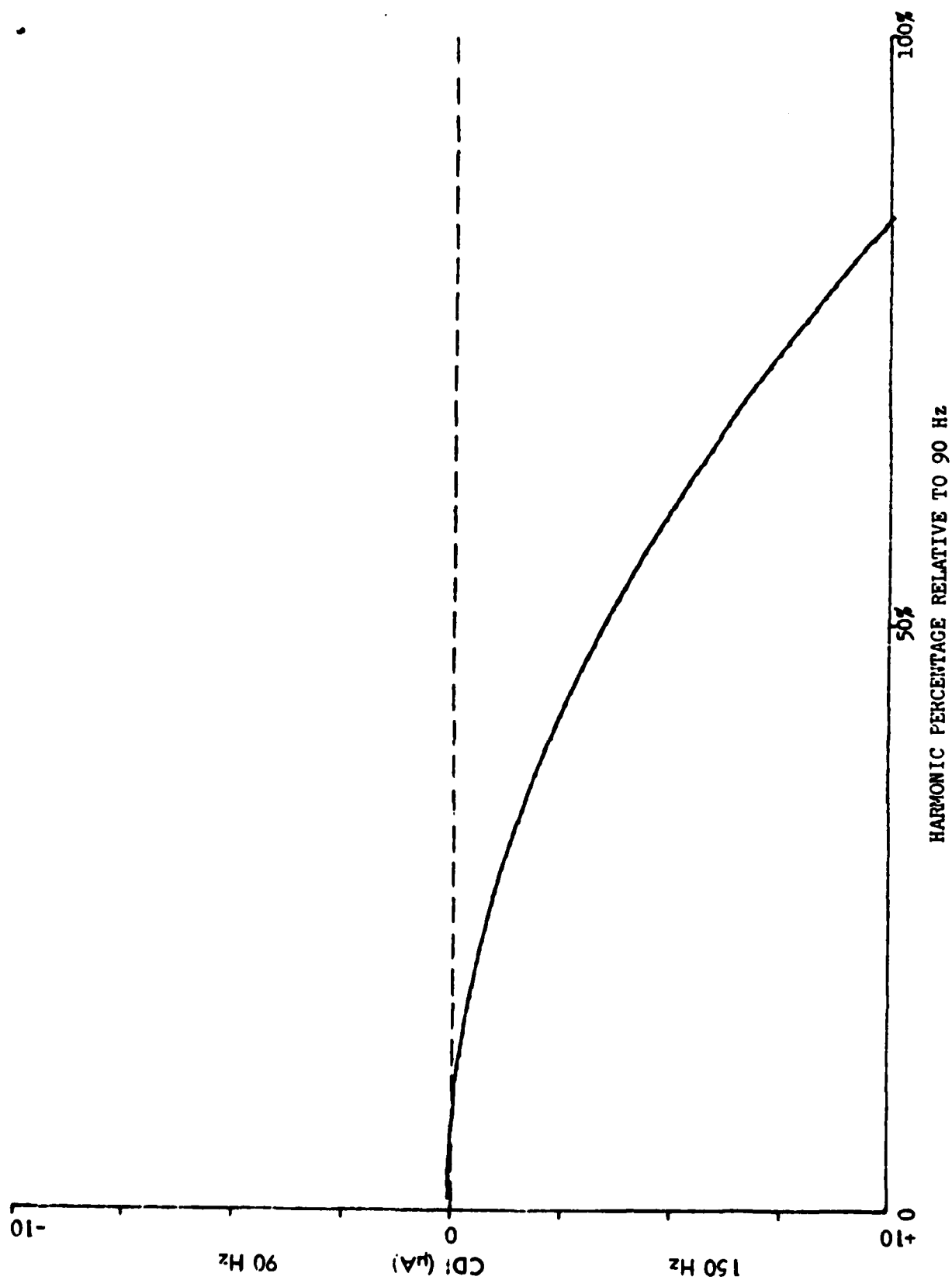


Figure 3-39. Calculated Response for NARCO Localizer with 180 Hz Harmonic.

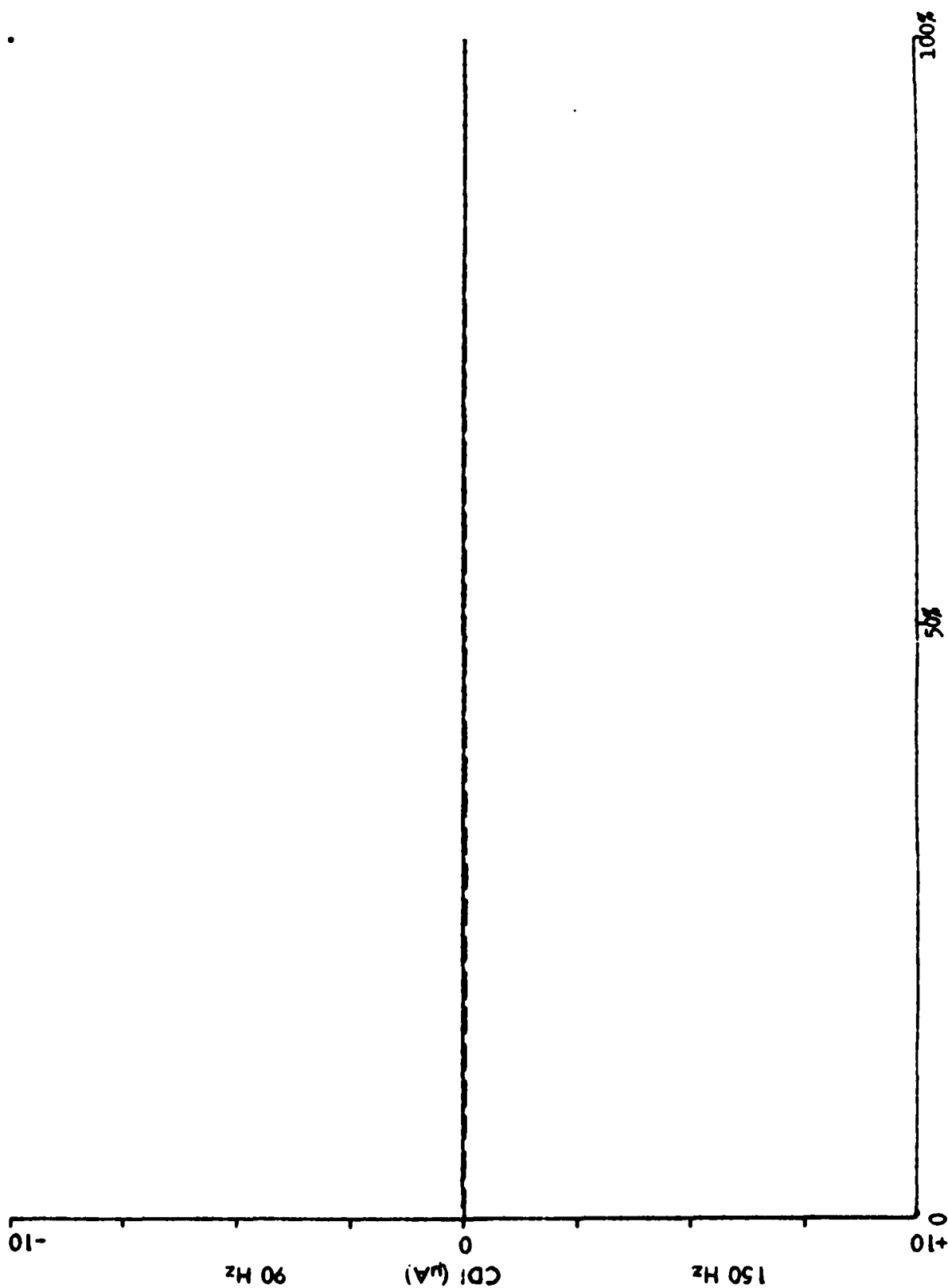


Figure 3-40. Calculated Response for NARCO Localizer with 240 Hz Harmonic.

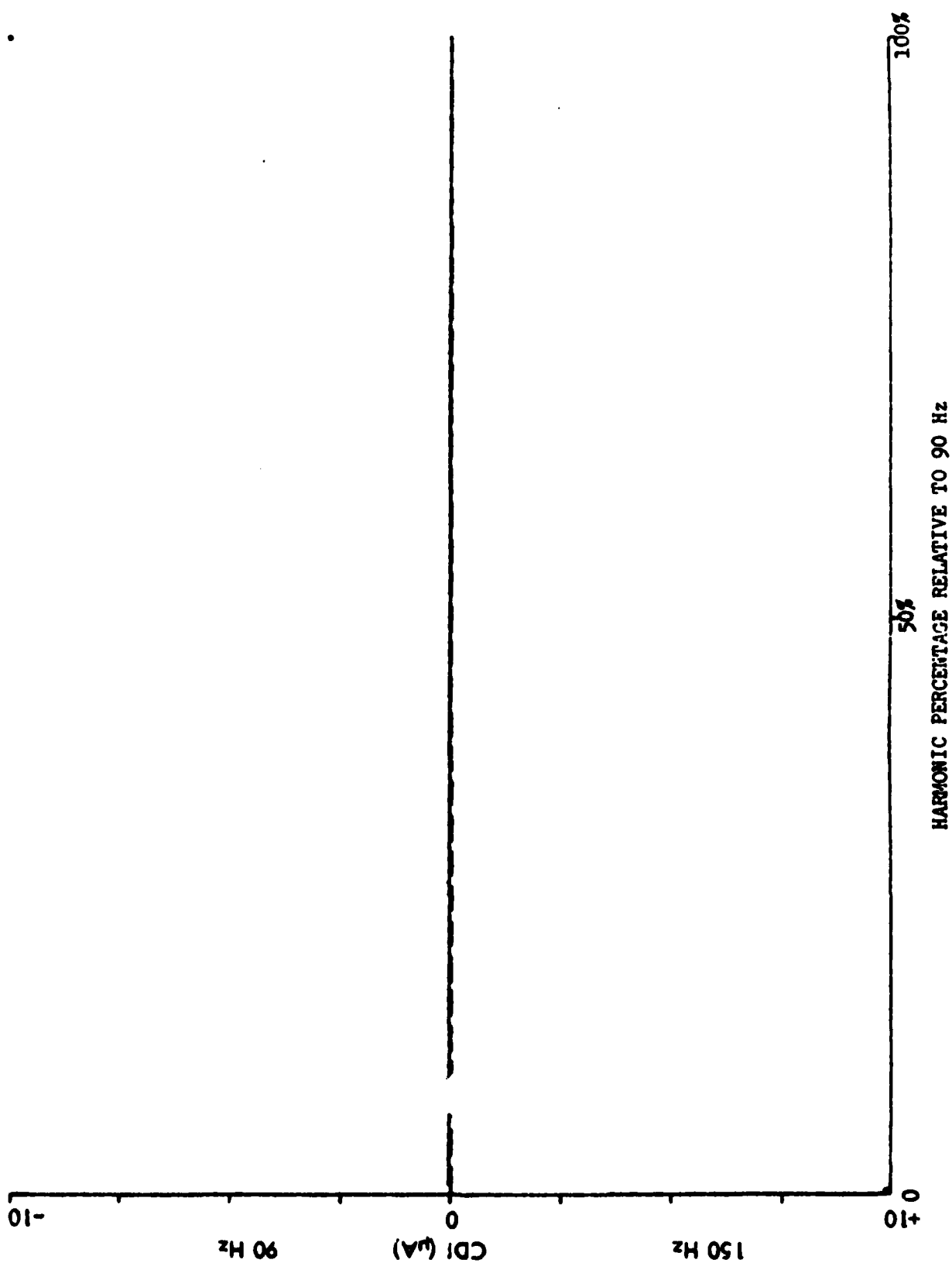


Figure 3-41. Calculated Response for NARCO Localizer with 300 Hz Harmonic.

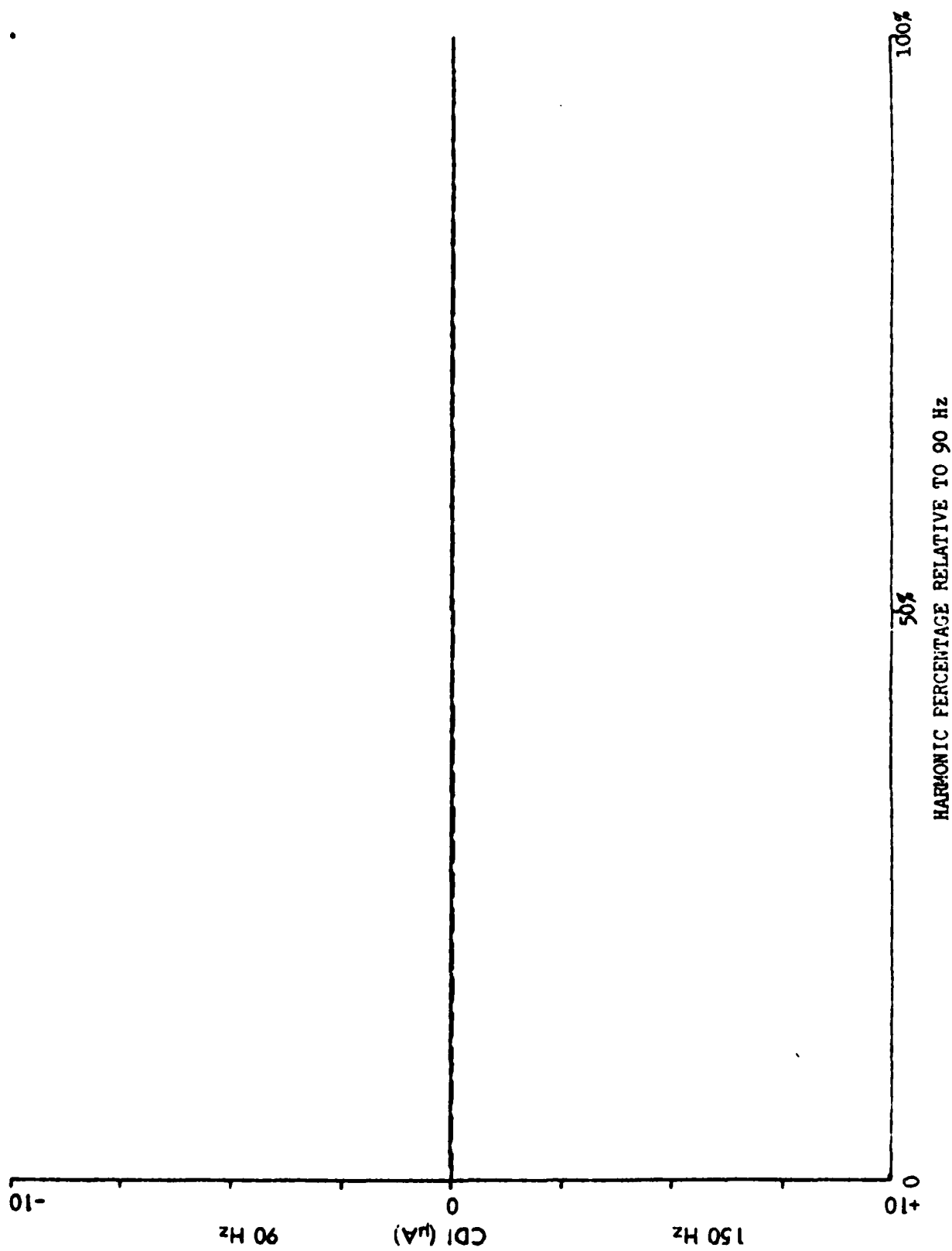


Figure 3-42. Calculated Response for NARCO Localizer with 540 Hz Harmonic.

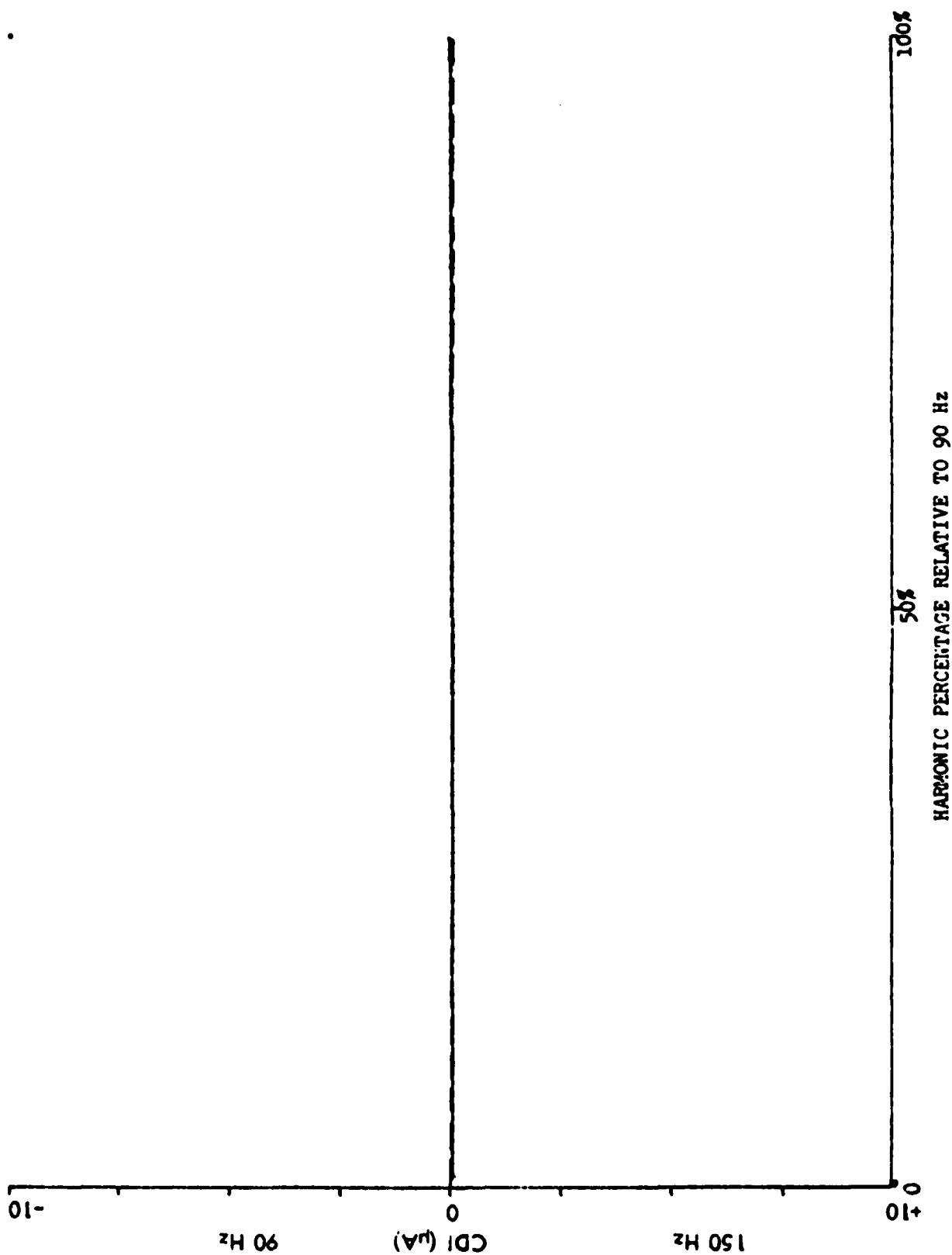


Figure 3-43. Calculated Response for NARCO Glide Slope with 30 Hz Harmonic.

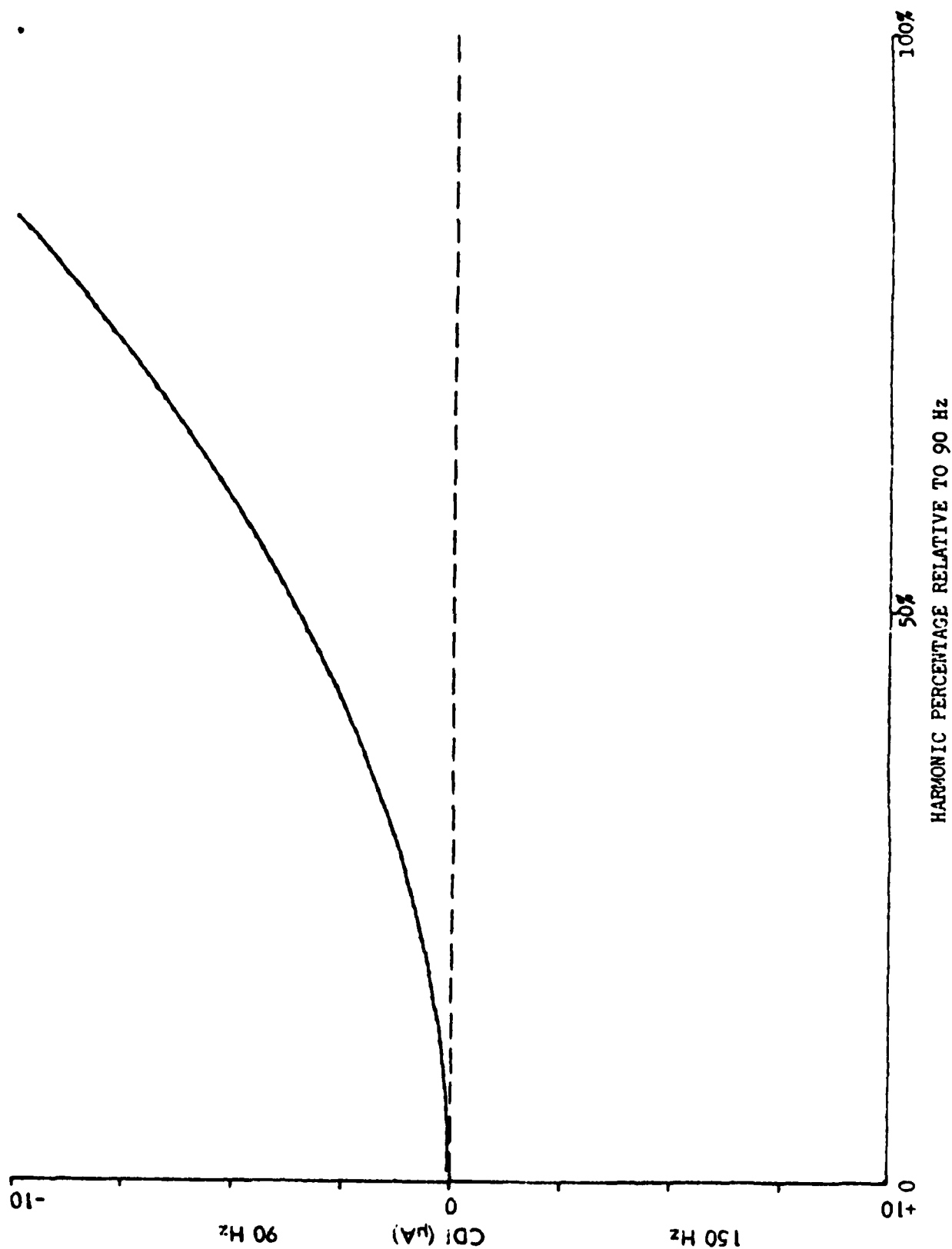


Figure 3-44. Calculated Response for NARCO Glide Slope with 60 Hz Harmonic.

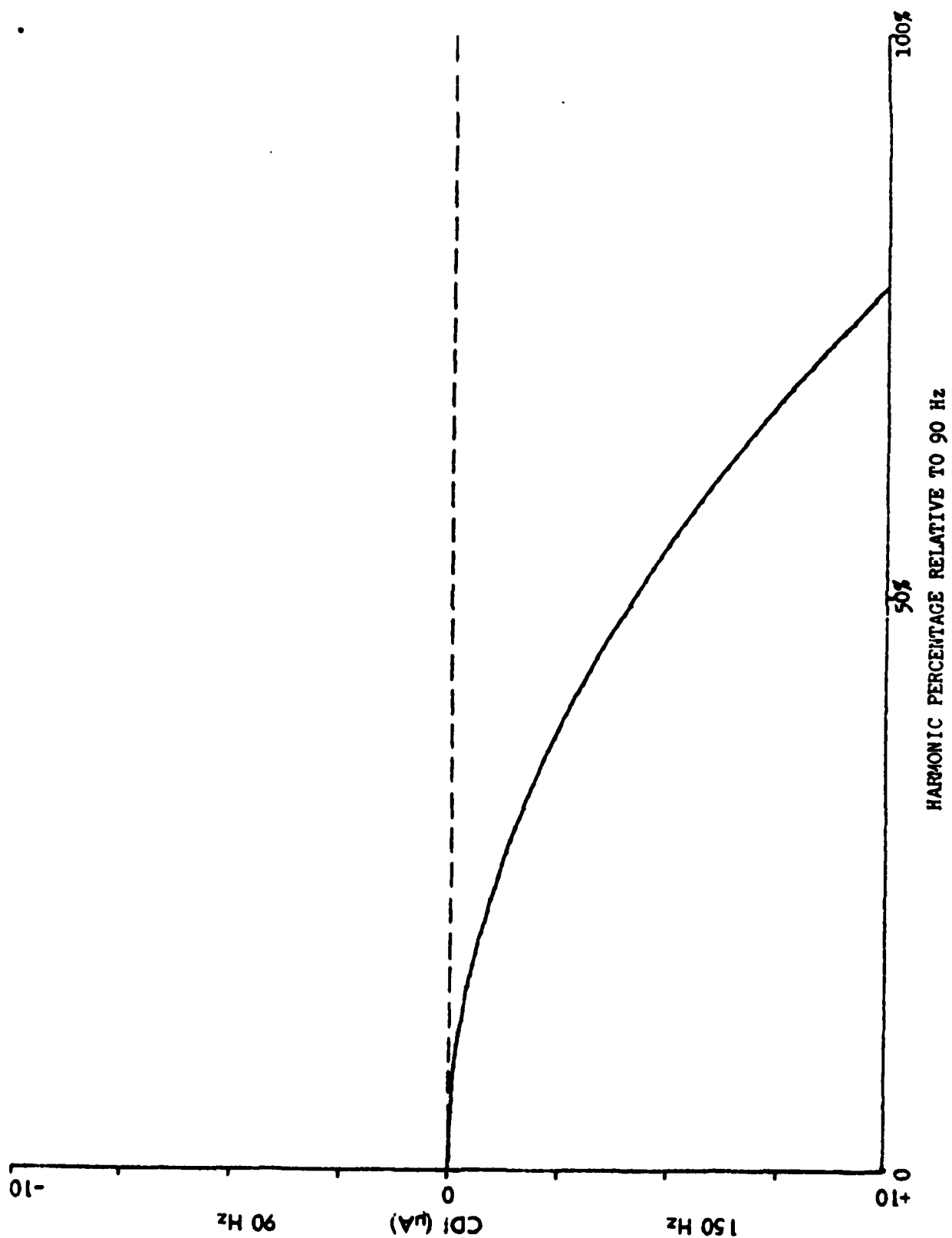


Figure 3-45. Calculated Response for NARCO Glide Slope with 180 Hz Harmonic.

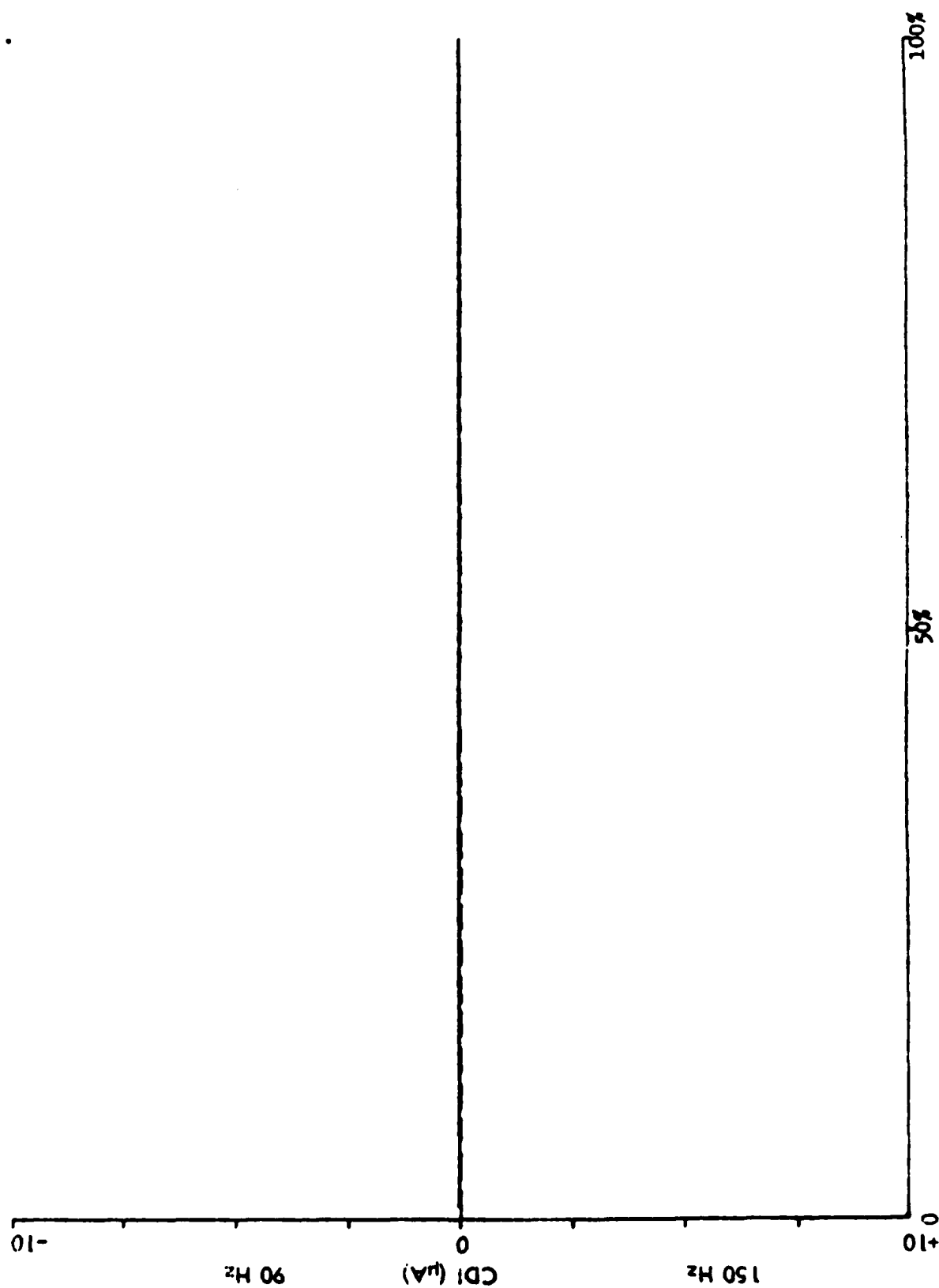


Figure 3-46. Calculated Response for NARCO Glide Slope with 240 Hz Harmonic.

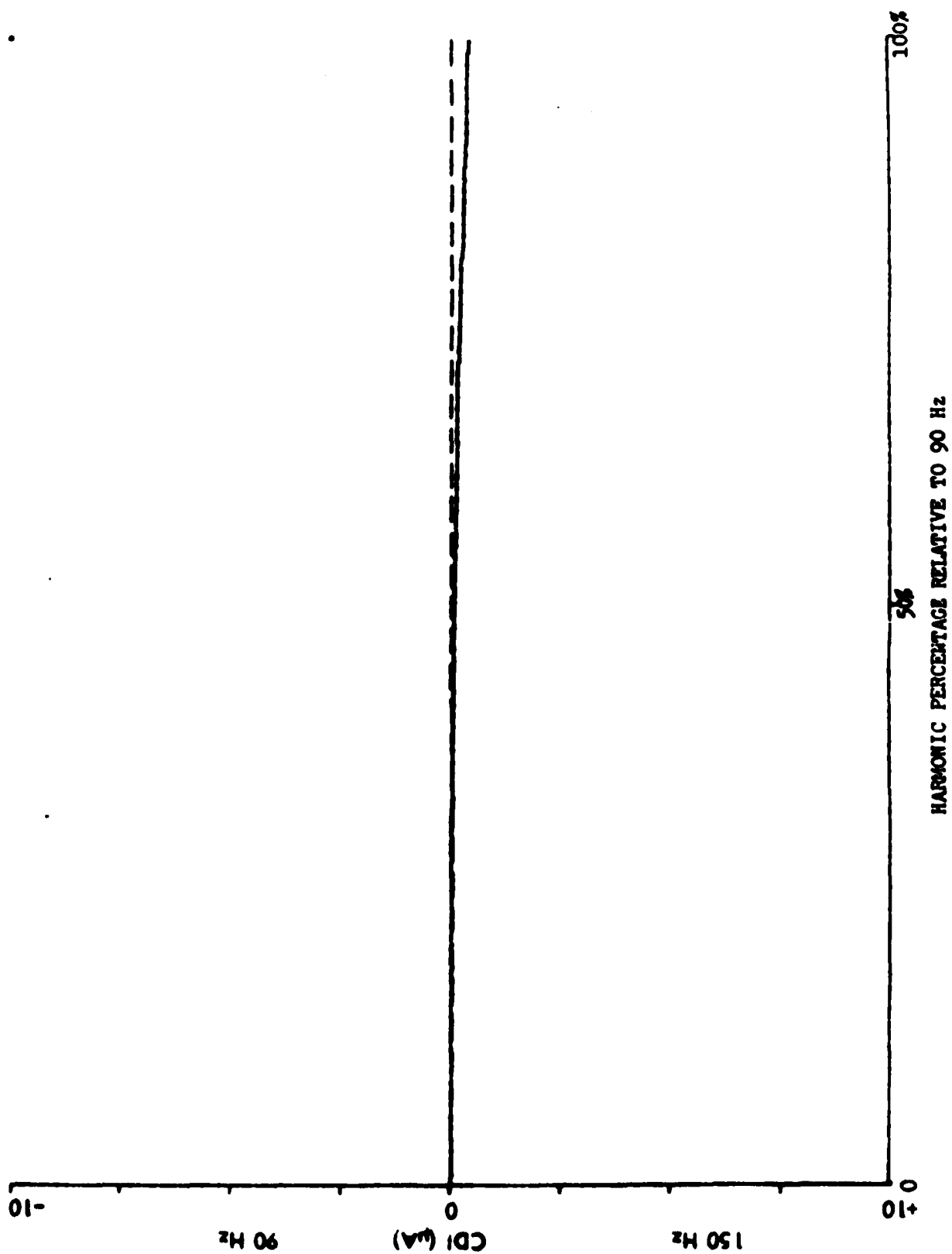


Figure 3-47. Calculated Response for NARCO Glide Slope with 300 Hz Harmonic.

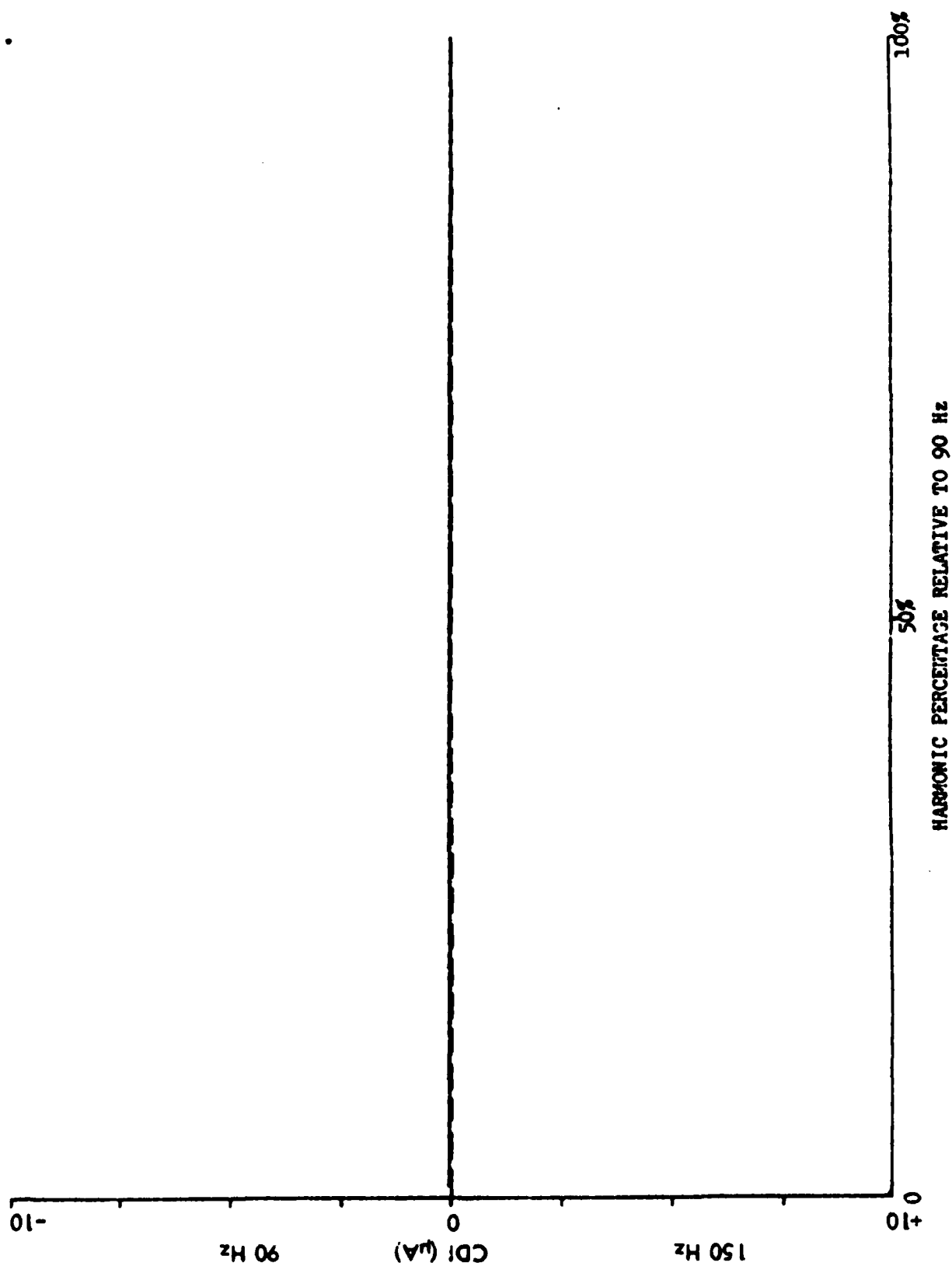


Figure 3-48. Calculated Response for NARCO Glide Slope with 540 Hz Harmonic.

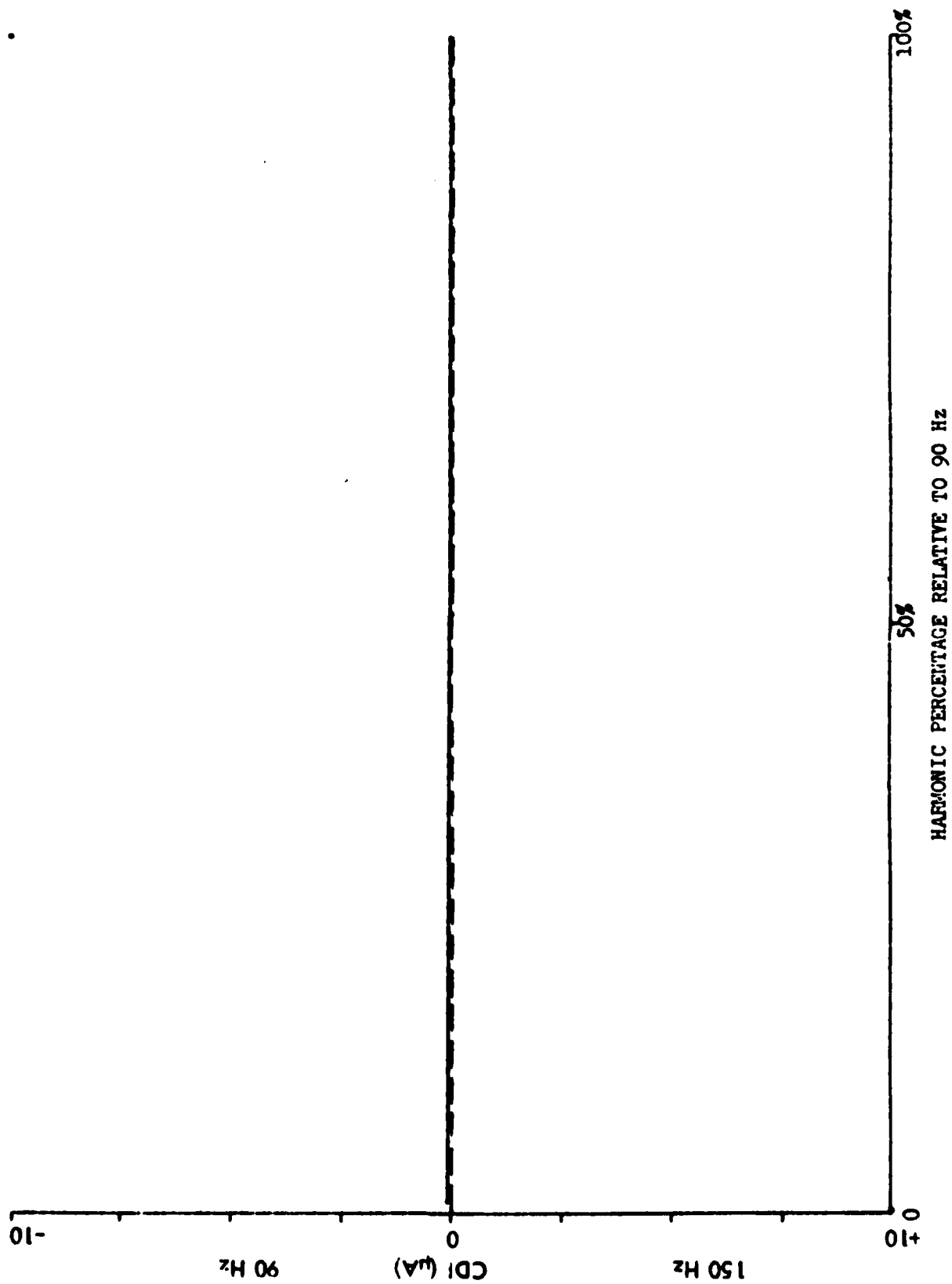


Figure 3-49. Calculated Response for Collins Localizer with 30 Hz Harmonic.

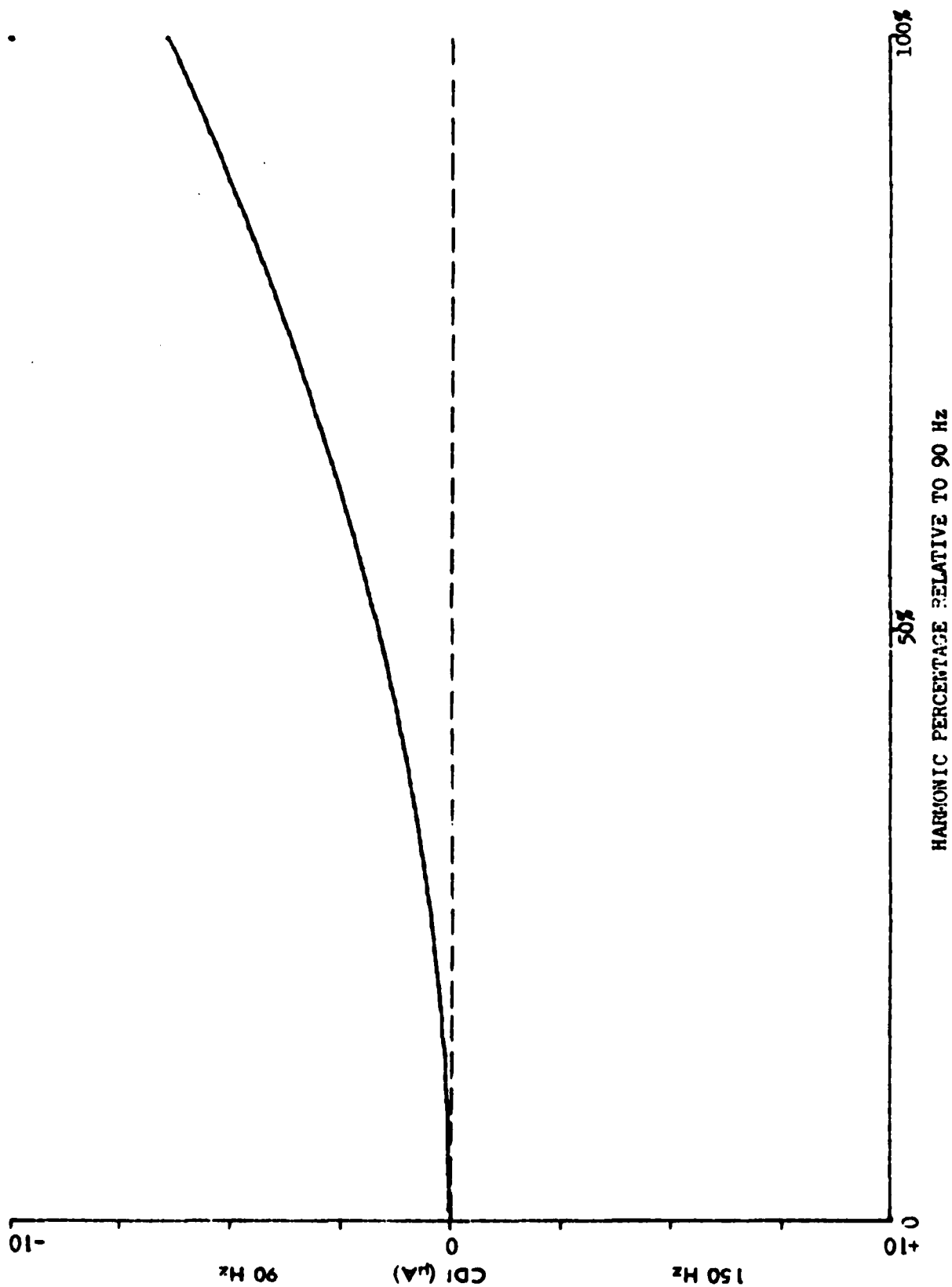


Figure 3-50. Calculated Response for Collins Localizer with 60 Hz Harmonic.

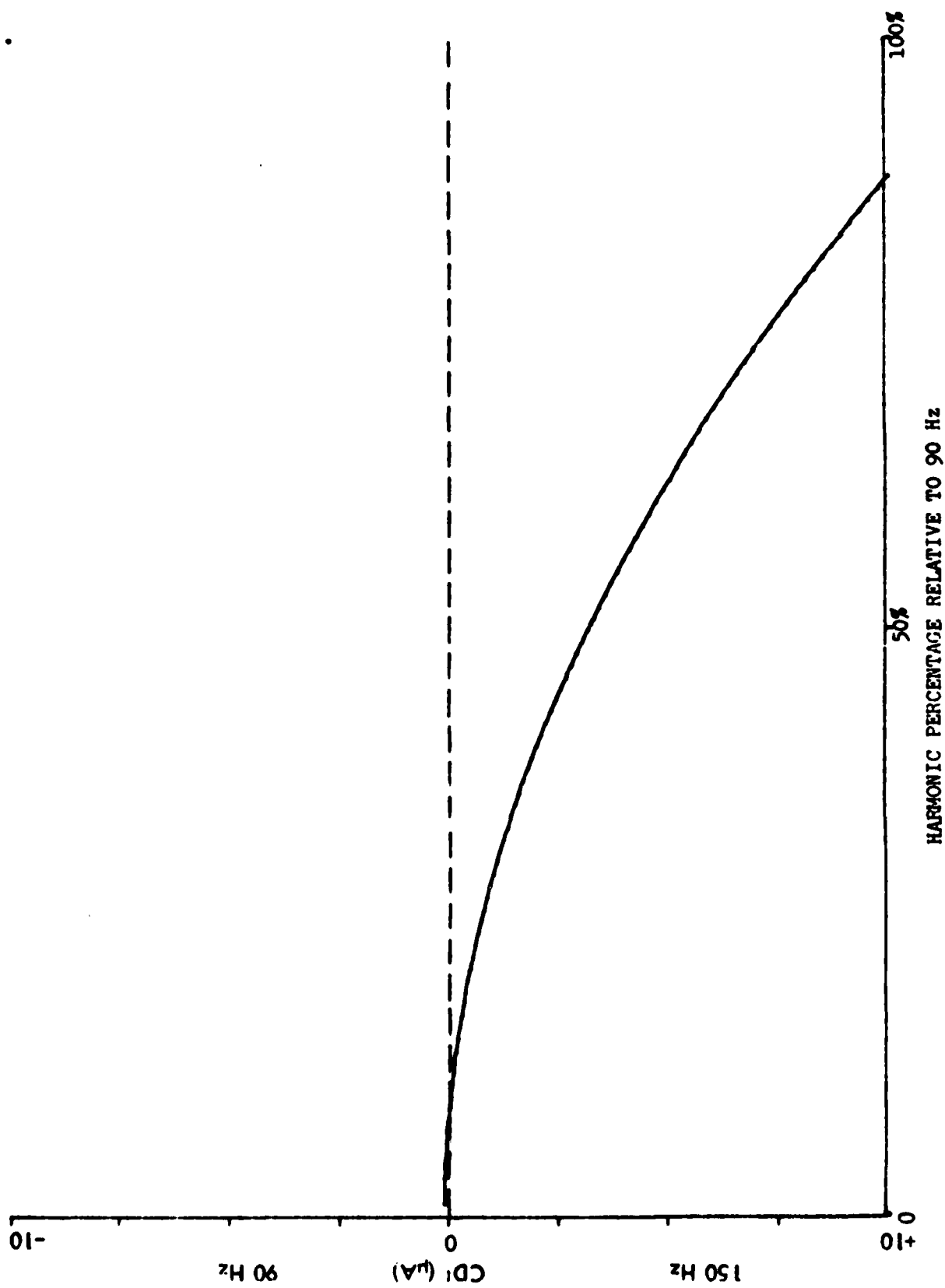


Figure 3-51. Calculated Response for Collins Localizer with 180 Hz Harmonic.

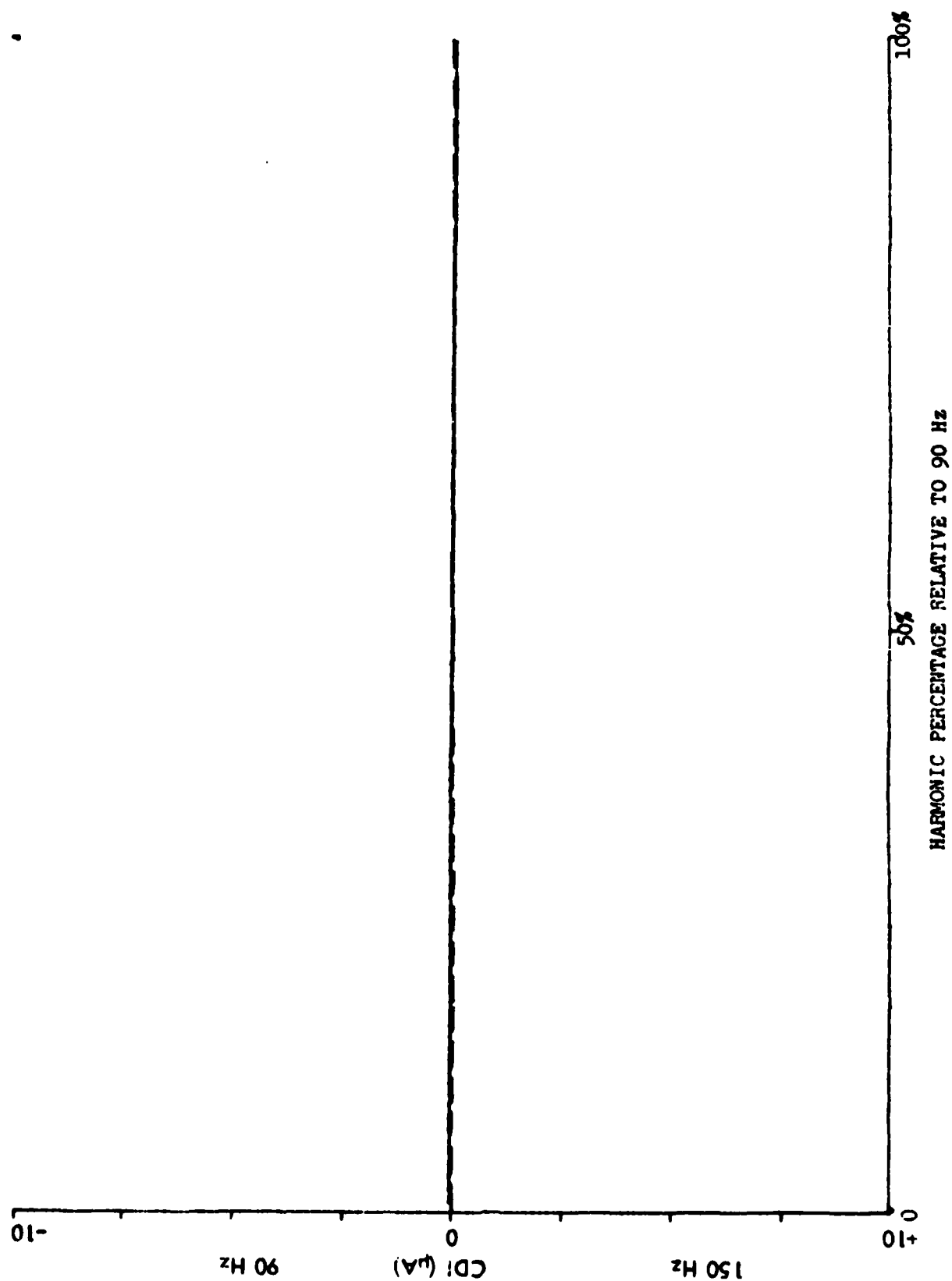


Figure 3-52. Calculated Response for Collins Localizer with 240 Hz Harmonic.

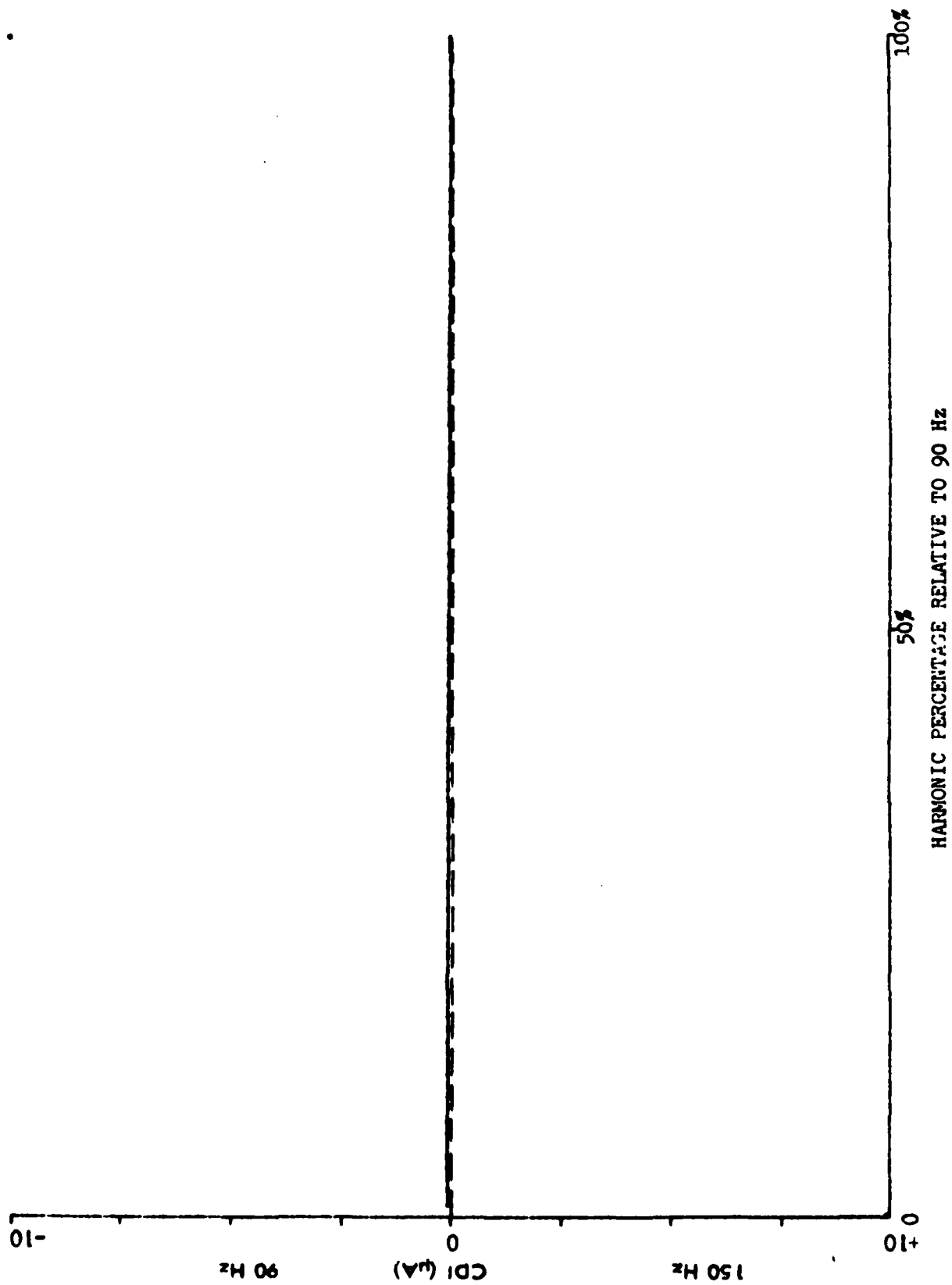


Figure 3-53. Calculated Response for Collins Localizer with 300 Hz Harmonic.

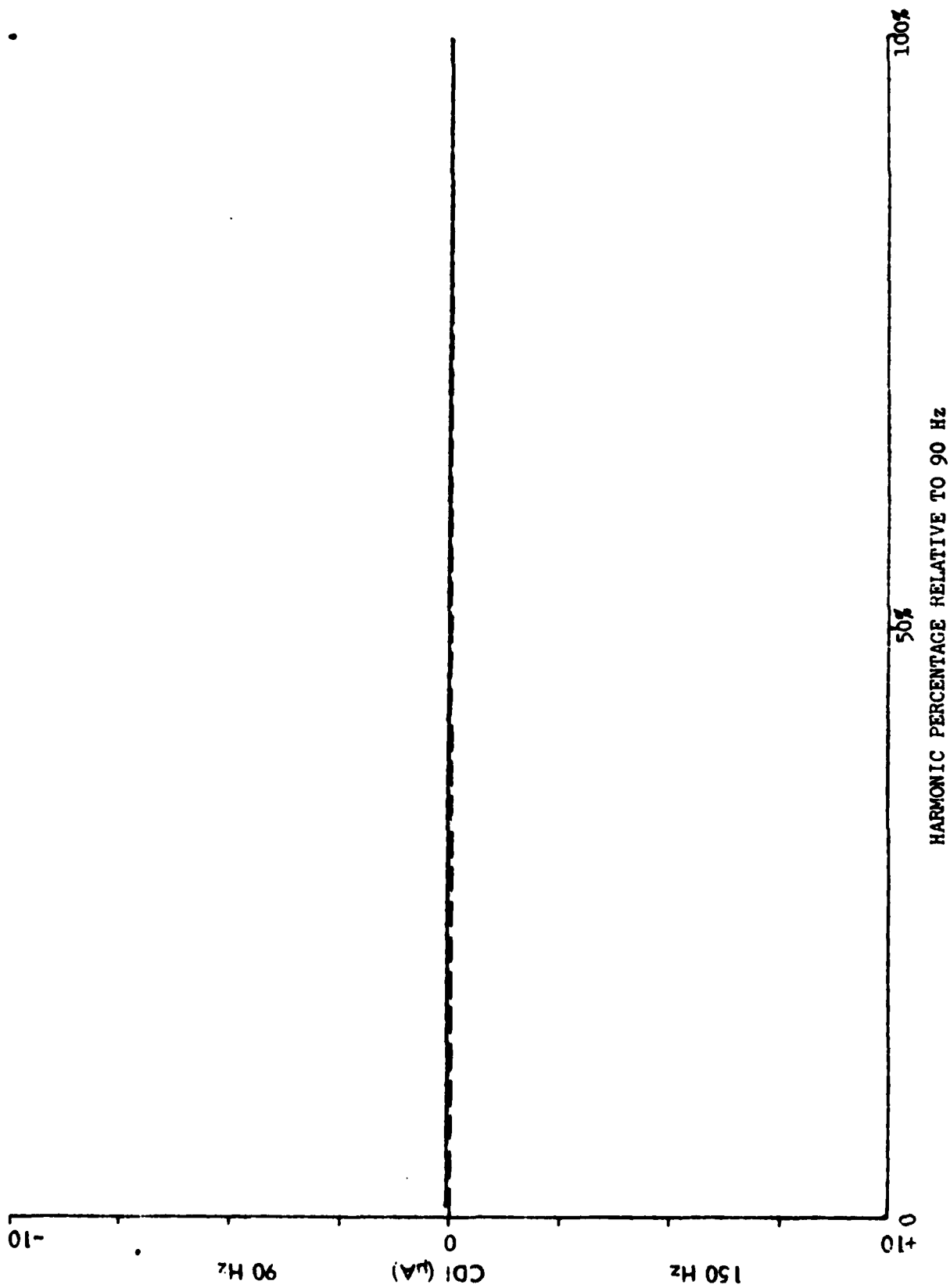


Figure 3-54. Calculated Response for Collins Localizer with 540 Hz Harmonic.

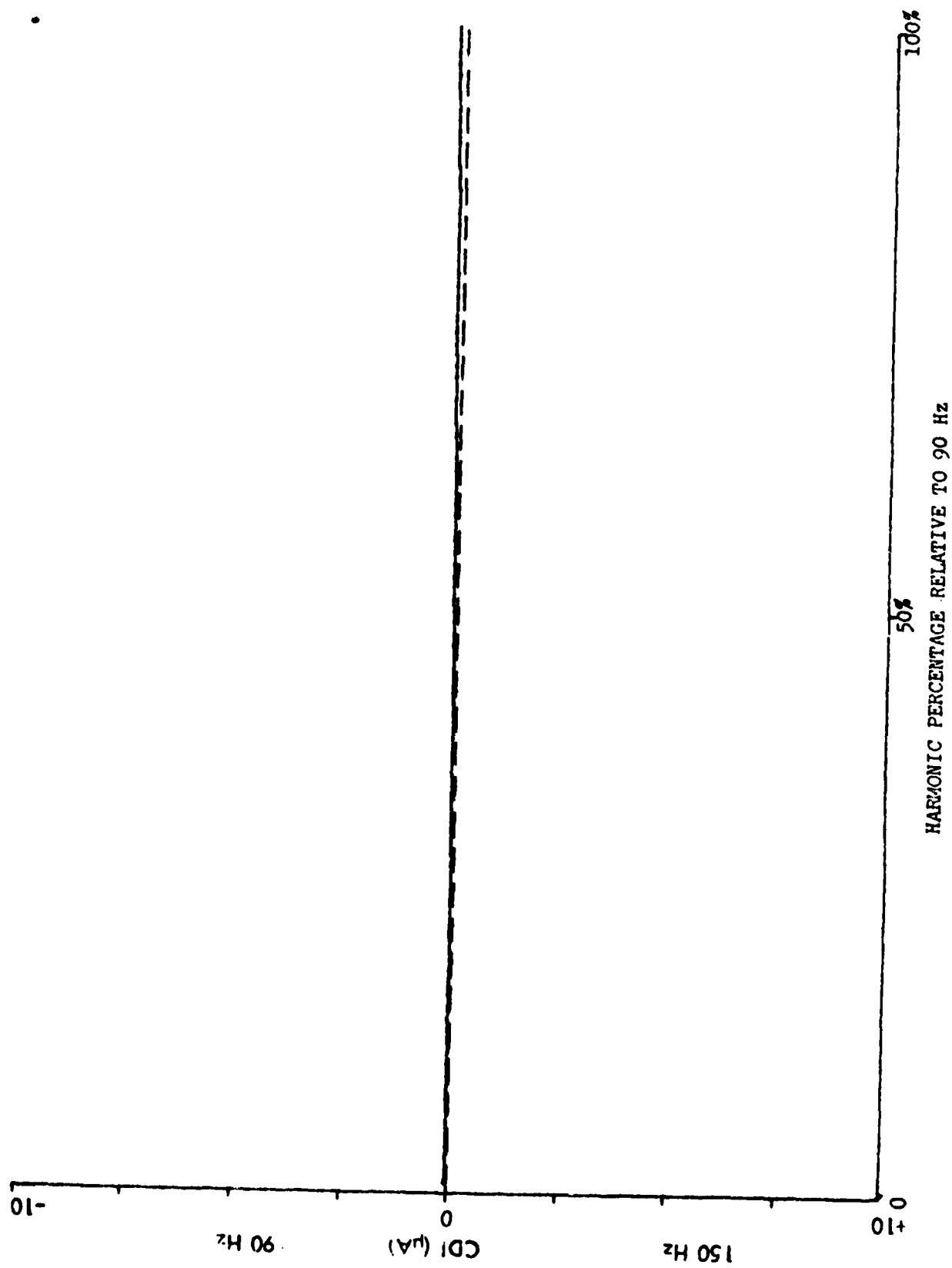


Figure 3-55. Calculated Response for Collins Glide Slope with 30 Hz Harmonic.

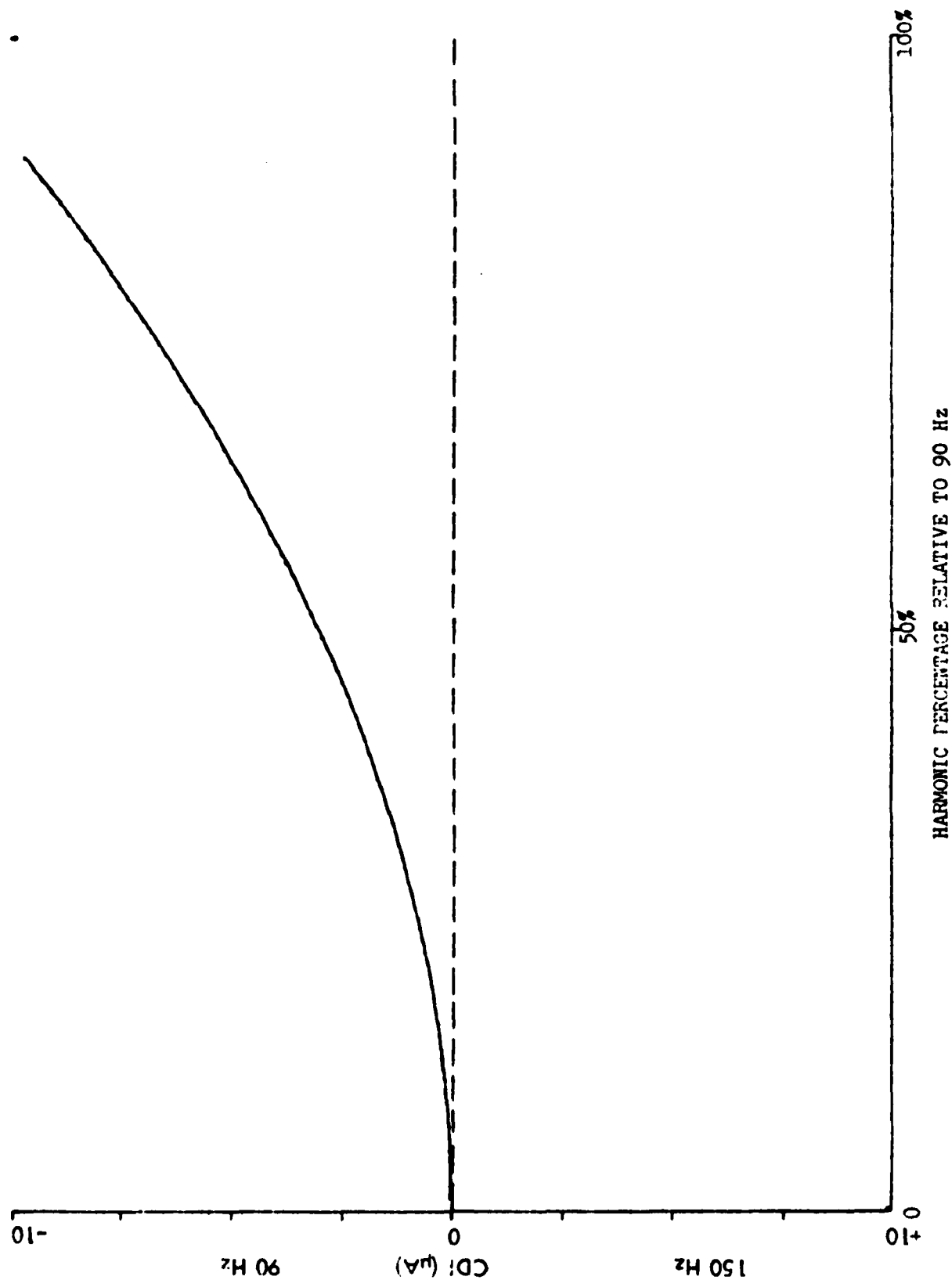


Figure 3-56. Calculated Response for Collins Glide Slope with 60 Hz Harmonic.

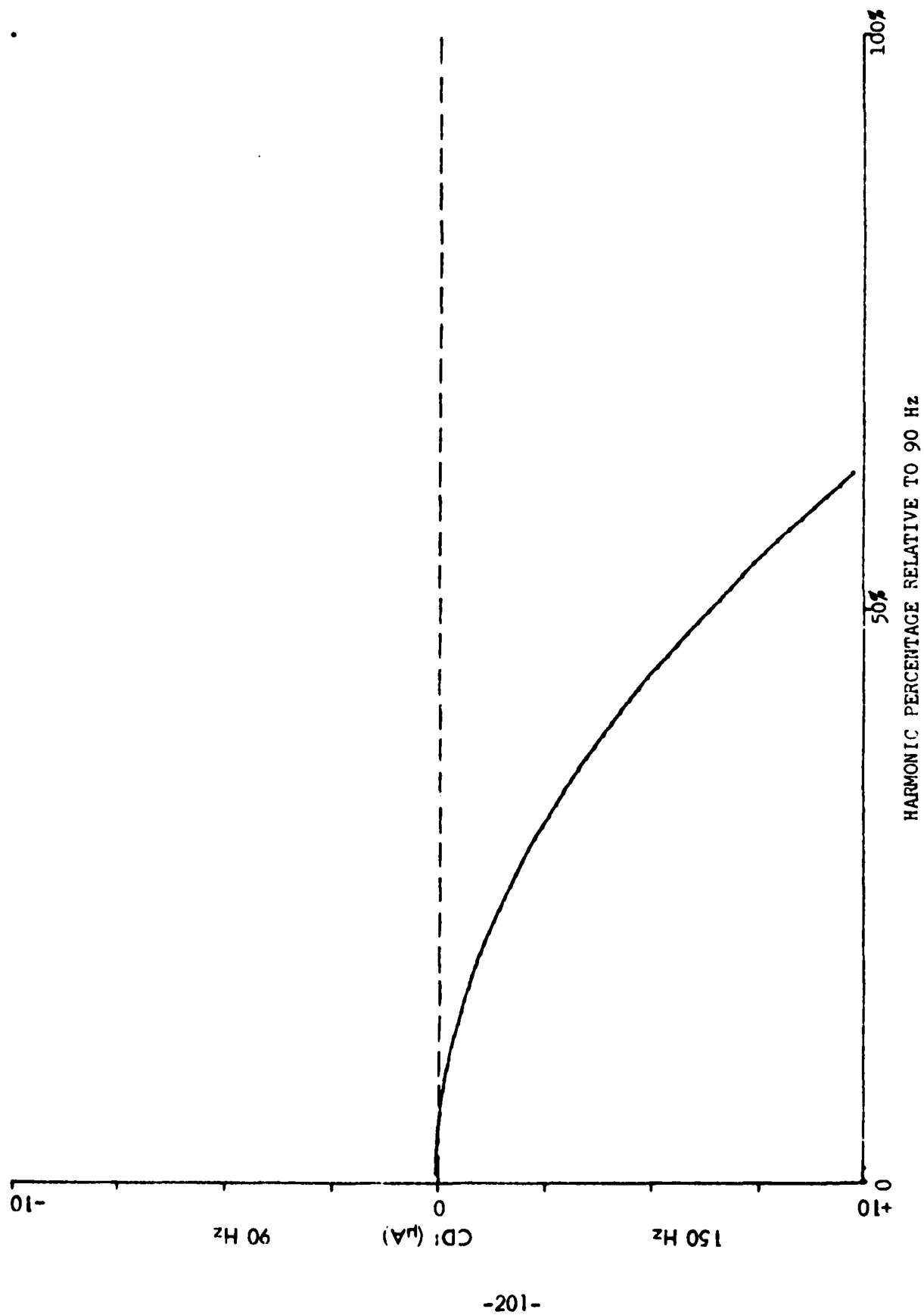


Figure 3-57. Calculated Response for Collins Glide Slope with 180 Hz Harmonic.

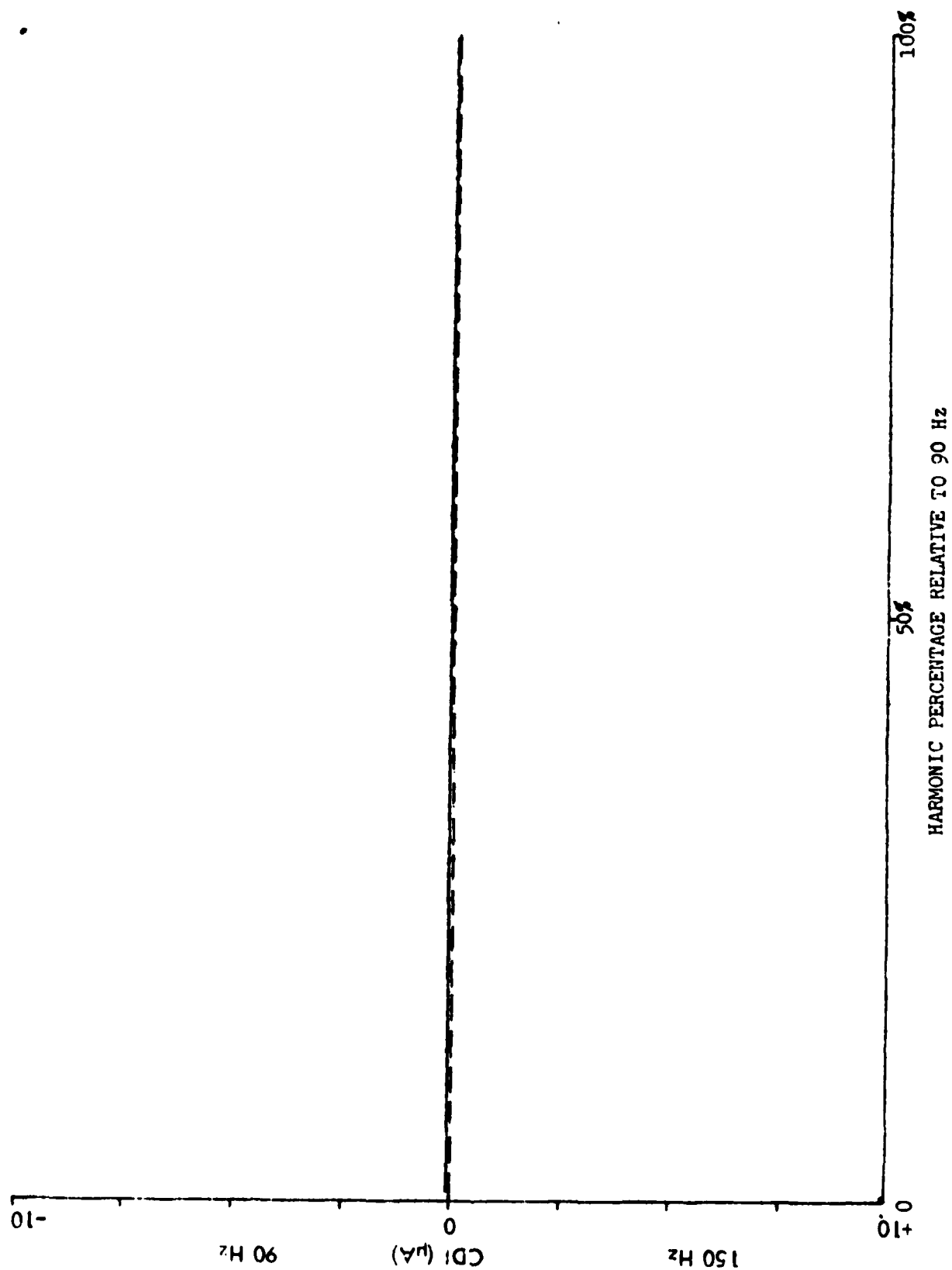


Figure 3-58. Calculated Response for Collins Glide Slope with 240 Hz Harmonic.

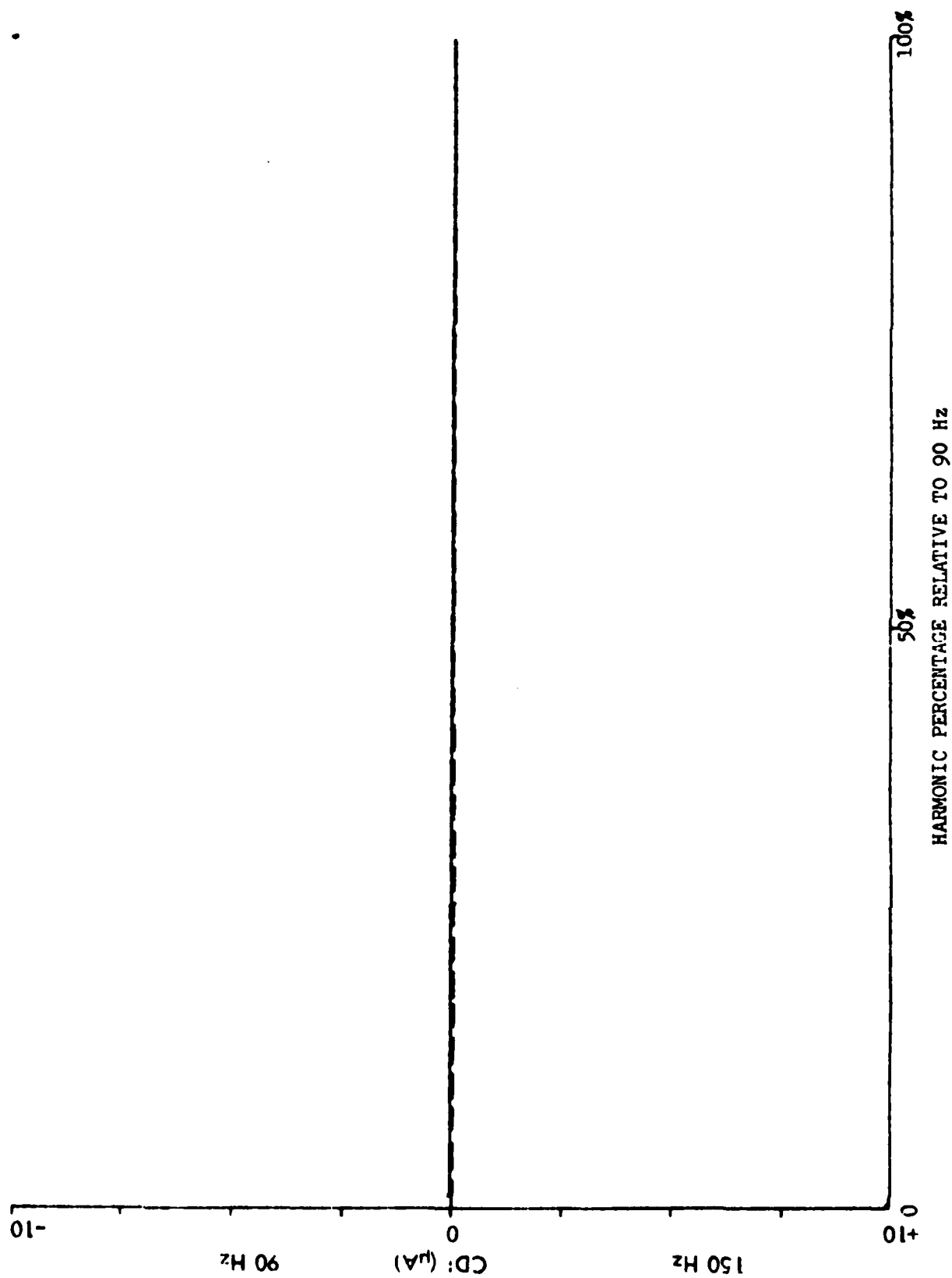


Figure 3-59. Calculated Response for Collins Glide Slope with 300 Hz Harmonic.

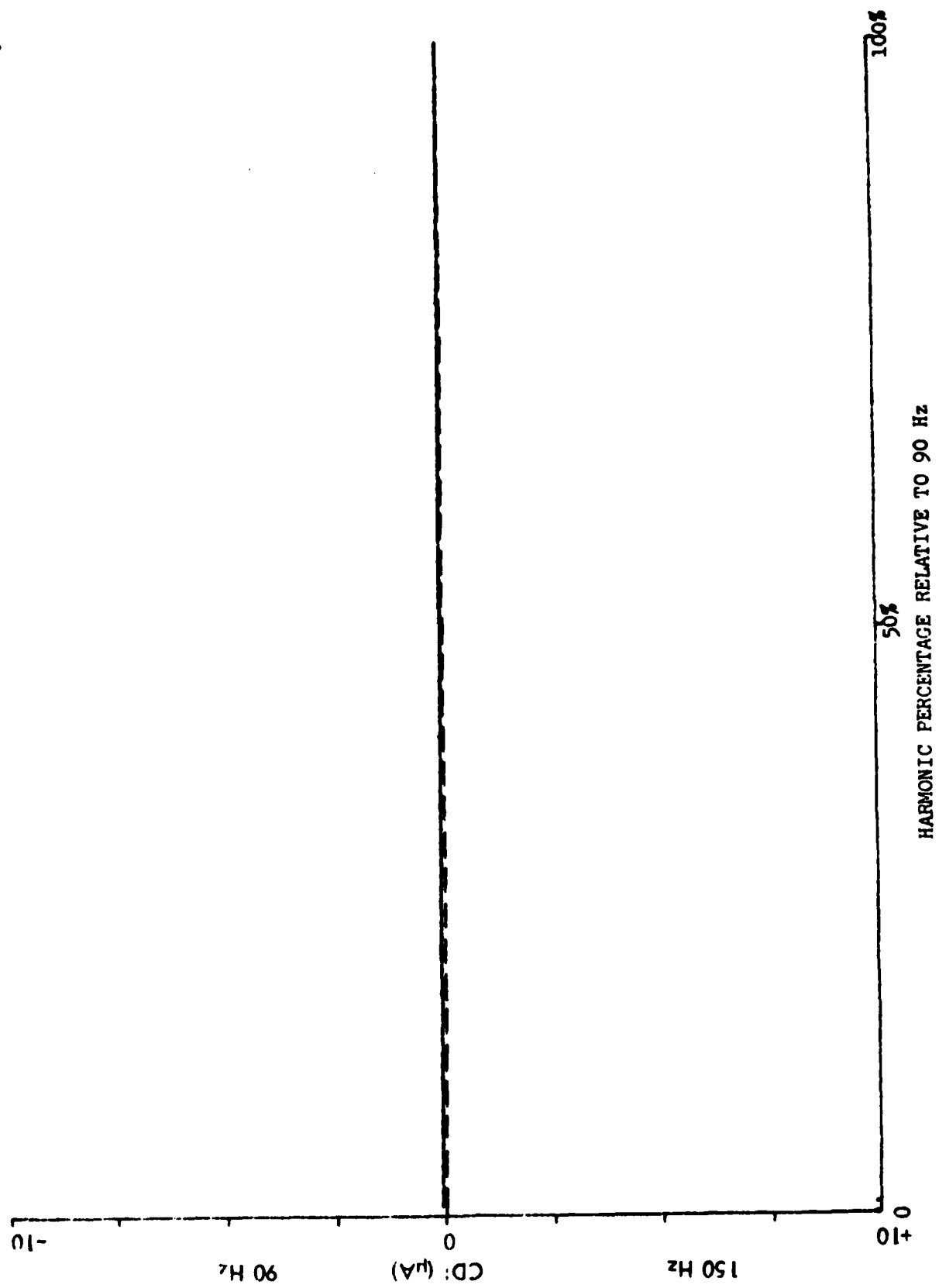


Figure 3-60. Calculated Response for Collins Glide Slope with 540 Hz Harmonic.

CONCLUSIONS AND RECOMMENDATIONS.

Using the validated receiver model program developed in this study, the maximum allowable individual harmonics and total harmonic content of the 90 Hz and 150 Hz signals can be computed. This program allows for any range of filter specifications.

The data obtained from bench measurements and calculated data using the least stringent airborne receiver show that:

1. When the amplitude of harmonic frequency is approximately 25% of the amplitude of the navigation tones (90 Hz or 150 Hz) measured at the input of 90/150 Hz filters, it would allow the CDI current reading to be within tolerance limits.
2. The maximum total 90-Hz harmonic content equals 11.74% and 150-Hz harmonic content equals 11.35% in the case of a glide slope, and maximum total 90-Hz harmonic content equals 11.70% and 150-Hz harmonic content equals 11.03% in the case of a localizer.

No degradation in clearance area ddm should occur with less than a 15% harmonic level using the Narco localizer receiver as a model.

INVESTIGATORS AND ACKNOWLEDGEMENTS

This final report is the consolidation of work performed and reported by the staff at the Avionics Engineering Center, Department of Electrical and Computer Engineering, College of Engineering and Technology, Ohio University, Athens, Ohio. Contributions are from all levels - from undergraduate student interns to faculty and staff. A number of FAA personnel in the field, at headquarters, and at Regional Offices have also contributed in a variety of ways.

The following is a list of principal contributors and others who served to bring this work to a successful completion:

Dr. Richard H. McFarland has served as project director. He has also served as pilot for data collection and principal data analyst on all tasks. He authored the material on "Evaluation of Waveguide Glide Slope Performance Runway 23, Buffalo, New York"; "Investigation of the Problem of Excess Roughness in the CAT III Localizer Course Structure for Runway 24R at Los Angeles International Airport"; "Investigation of Anomalous Performance of the International Falls Null Reference Glide Slope" (co-authored); "An Evaluation of Localizer Performance and Causes of Derogation at San Francisco International Airport" (co-authored); and "A Demonstration of Two Solutions to the CAT III Localizer Problem on Runway 28R at San Francisco International Airport".

Mr. Joe D. Longworth has served as project engineer and as technical editor for this final report. He has served as principal engineer for much of the experimental work. He authored the "Modification to the FA-5723 and FA-8633 Clearance Transmitters"; "Investigation of ILS Transmitter Carrier Output Modulation Components" (co-authored); "An Evaluation of Localizer Performance and Causes of Derogation at San Francisco International Airport" (co-authored).

Mr. M. Jamil co-authored the "Investigation of ILS Transmitter Carrier Output Modulation Components."

Mr. Walter Phipps served as data collection specialist for all airborne work. He also was responsible for calibrations and references for the measurement equipment. He co-authored the "Investigation of Anomalous Performance of the International Falls Null Reference Glide Slope."

Mr. Thierry d'Estaintot authored the "ILS Investigation of Ground-check Procedures for ILS Glide Slopes."

Dr. Robert W. Lilley has coordinated the efforts involving the Ohio University IBM 370 computer. This has resulted in improved program operation and enhanced graphics capabilities.

Report production was furnished by Mes. Shirley Mellema, Joyce Longworth and Ann Breese. Mr. Samson Wong provided drafting support.

FAA personnel in Headquarters, Central, and Southern and Eastern Regions, have been most helpful and supportive in the conduct of this work. For this, the staff is extremely grateful.

BIBLIOGRAPHY

1. Installation and Test of the Compensated Waveguide Antenna at Buffalo, New York, Runway 23, Glide Slope Site, FAA Report FAA-RD 76-9, by Staff, Westinghouse Defense and Electronics Systems Center, Baltimore, Maryland, February 1976.
2. Engineering and Technical Services to Improve Reliability and Maintainability of the Instrument Landing System (ILS) Components, Final Report FAA-R-6750.3 AAF-420, prepared for FAA, Avionics Engineering Center, Ohio University, Athens, Ohio, December 1980.
3. Petersen, Kent, Preliminary Obstruction Evaluation, Airway Facilities Service, FAA, Los Angeles.
4. Baker, Roger, Dossier, Western Pacific Region, FAA, January 1982.
5. Moore, Donald, private communication, December 8, 1981.
6. U. S. Flight Inspection Manual OAP8200.1 Section 217.
7. Historical Data - Regional File of FAA Flight Check Data, July 8, 1971 - December 7, 1979.
8. Topo Charts CE-D-6603, June 1, 1970.
9. In-Service Improvements and Modernization of All Components of the Instrument Landing Systems, Volume II-Sections XI and XII, EER 35-1, prepared for Federal Aviation Administration, Washington, D.C. 20590, July 1978, pp. 11-634 through 11-640.

APPENDICES

APPENDIX A. ADDITIONAL FIGURES FOR LOS ANGELES, CA., RUNWAY 24R
INVESTIGATION.

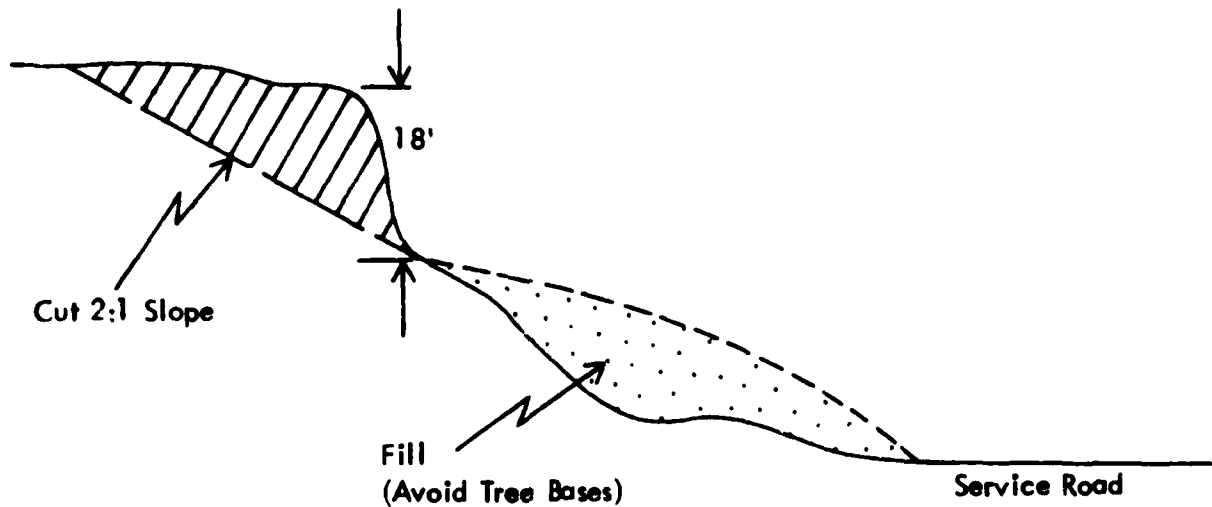


Figure A-1. Recommended Cut and Fill Operation On Embankment Centered 6400 Feet From the Array, 650 Feet North of the Runway to Give Acceptable Category III Localizer Performance. Original earth contour taken from Petersen.

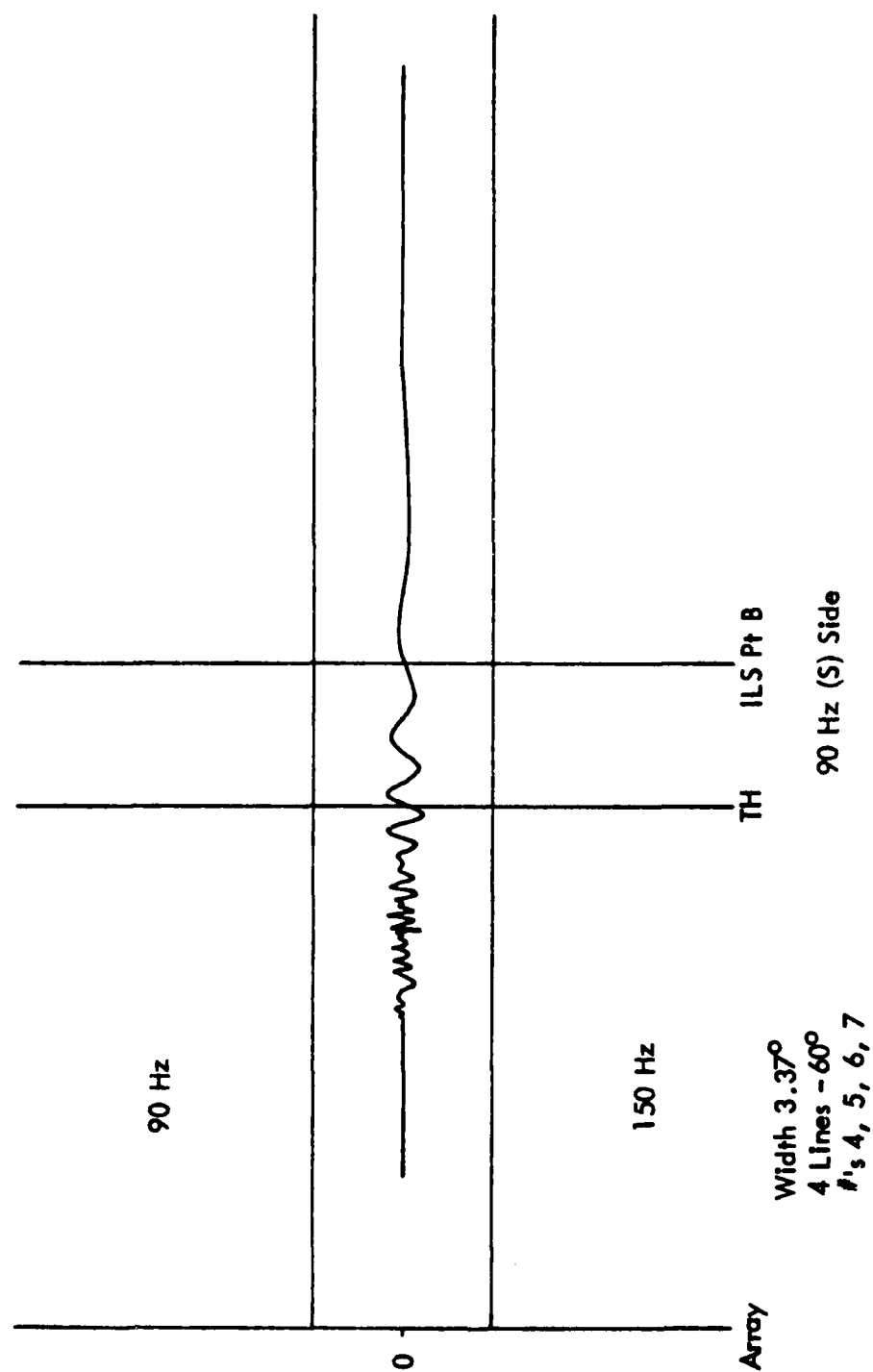


Figure A-2. Calculated Localizer Course Structure Resulting from 60-Degree Phase Delays inserted in Antenna Feeds #4, #5, #6, and #7 on the 90 Hz Side. The reflector is a wall 400 feet long, 40 feet high displaced 608 feet from the runway centerline.

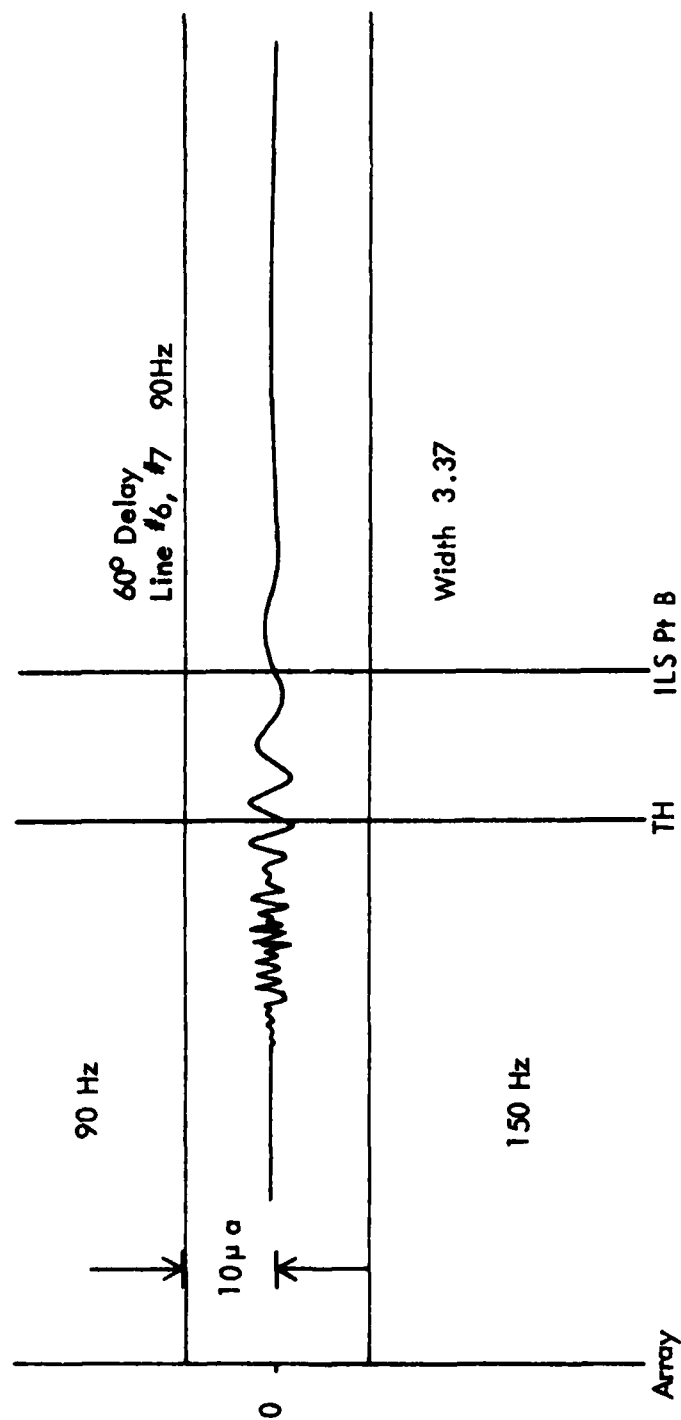
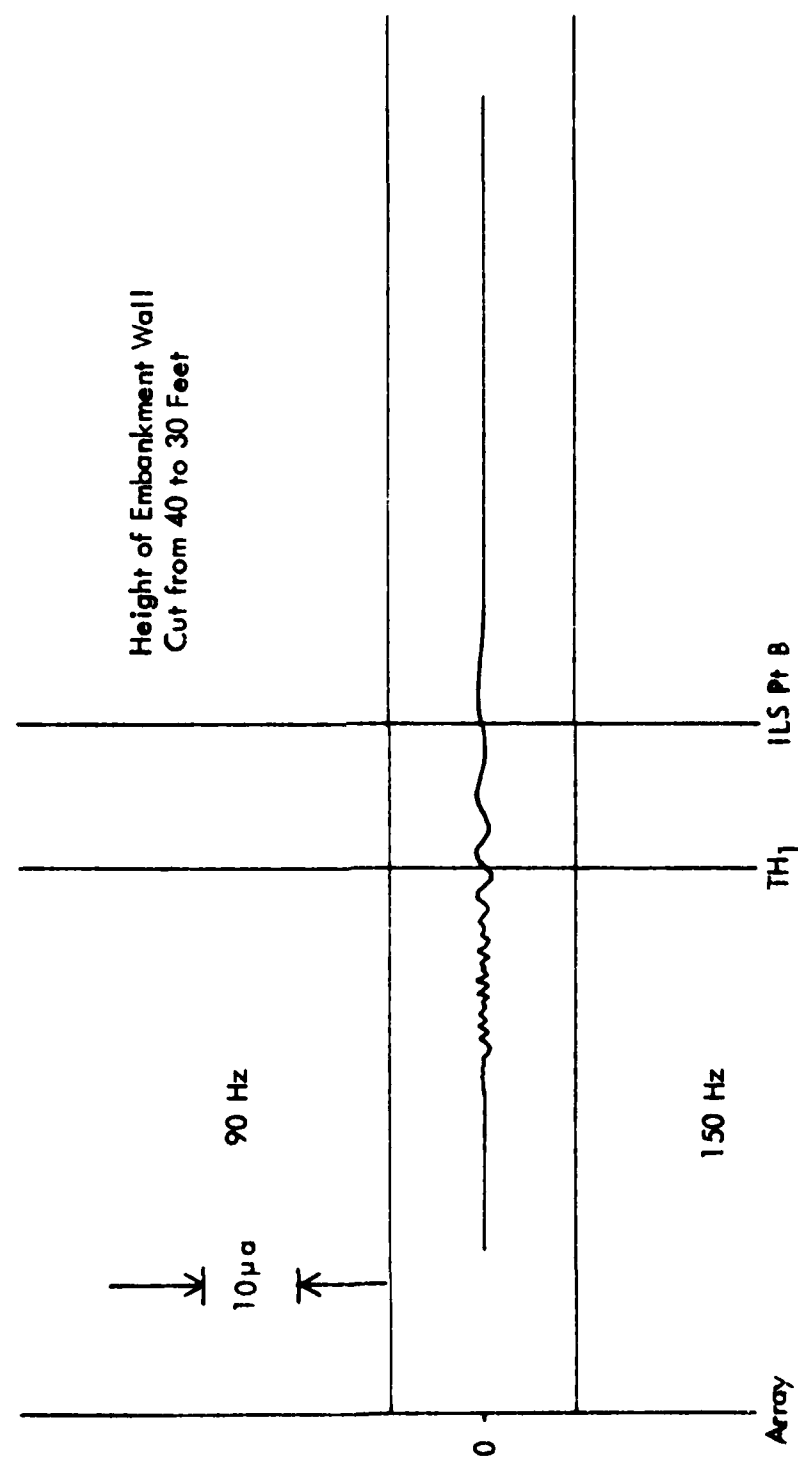


Figure A-3. Calculated Course Structure for 60-Degree Phase Delay placed in Lines #6 and #7 of the 90 Hz Side. Course width is set for 3.37°. The 40-foot high wall is in place as in Figure 2-17.



APPENDIX B: MODEL ANALYSIS.

1. Inputs-Outputs. Because the readings provided by the ground measurement equipment are respectively DDM and CDI for the PIR and the OU Microlab used for ground measurements, DDM and CDI as functions of receiving antenna height are the outputs of TGCGS.

To obtain model estimates of CDI, inputs to the model are the ground characteristics (geometry, electric constants and surface roughness) and the location and currents of the glide slope antennas.

2. Sloping reflecting plane. The geometry of the ground is assumed to be a single plane, and is assumed to extend sufficiently far in front of the antenna mast to cover the reflecting zone. To account for a sloping ground plane, five degrees of freedom, described by X_1 , Y_1 , Z_1 , ALPHA and BETA, can be treated by TGCGS for a three-dimensional modeling of the ground.

To define the reflecting plane geometry, three points, M1, M2 and M3, are necessary. The values of (x,y,z) coordinates are given in the reference system shown in figure B-1.

The subroutine TNFTE computes angles alpha and beta, used later in subroutine TANTCO.

TANTCO computes the image antenna location according of the reflecting plane geometry. Output TGCGS file 6C gives these locations in the reference system.

3. Finite conductivity. Because typical ground planes are not perfect conductors, the electric field is not totally reflected and some phase shift is introduced upon reflection. Consequently, a reflection coefficient is introduced as (figure B-2):

$$\Gamma = \frac{\frac{\eta}{\cos\theta_t} - \frac{\eta_0}{\cos\theta_o}}{\frac{\eta}{\cos\theta_t} + \frac{\eta_0}{\cos\theta_o}} \quad \text{with} \quad \eta = \frac{\mu_0}{(\epsilon_r \epsilon_0)^2 + \left(\frac{\sigma}{\omega}\right)^2} \quad \epsilon_r \epsilon_0 + j \frac{\sigma}{\omega}$$

$$\text{where } \eta_0 = \text{free space impedance} = \frac{\mu_0}{\epsilon_0}$$

$$\mu_0 = \text{free space permeability, } \epsilon_0 = \text{free space permittivity}$$

$$\epsilon_r = \text{reflecting medium relative permittivity}$$

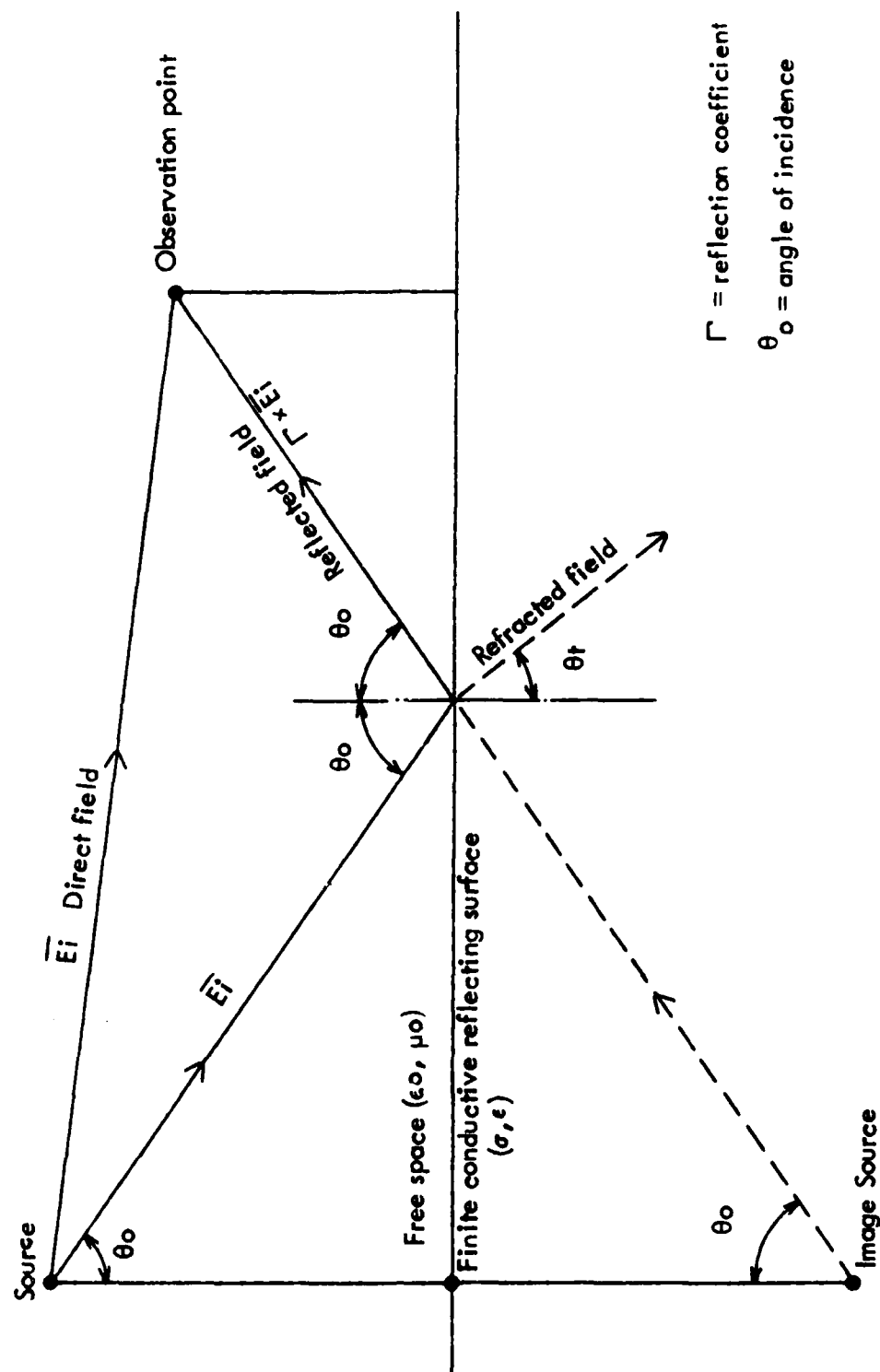


Figure B-2. Image Theory for Reflected Field.

σ = reflecting medium conductivity

θ_0 = angle of incidence

$$\theta_t = \text{Arcsin } \frac{\theta_0}{\epsilon_r}$$

$$\omega = 2\pi \cdot f_c$$

f_c = frequency

Subroutine TINCAN computes the incidence angle theta, which is used in subroutine TREFL to determine the reflection coefficient. This reflection coefficient is a complex number that determines the calculated reflected field in phase and magnitude. Figure B-3 shows the modeled values of reflection coefficient as a function of incidence for different ground characteristics.

4. Spherical wave propagation effect. For cases where a planar reflecting surface is sufficiently far from a radiation source, plane wave reflection can be assumed. However, when the source and reflecting plane are in close proximity, spherical wave incidence must be analyzed to determine the reflected field.

Brekhovskikh suggests that spherical wave incidence on a planar reflecting surface can be analyzed by representing the spherical wave as an infinite series of plane waves. Because the reflection coefficients for plane waves are known, the contribution of a reflected spherical wave can be computed by summing the contribution of each of the plane wave's components of the spherical wave (figure B-4).

Chamberlin presents this analysis applied to very high frequency wave propagation and gives the following results.

The reflected field for a spherical wave on a plane boundary is shown to be:

$$E_r = E_i \cdot (\Gamma + K)$$

E_i = complex incident field

E_r = complex reflected field

Γ = plane wave reflection coefficient

K = lateral waves correction term

where $K = A \cdot B \cdot \frac{1}{Rr}$

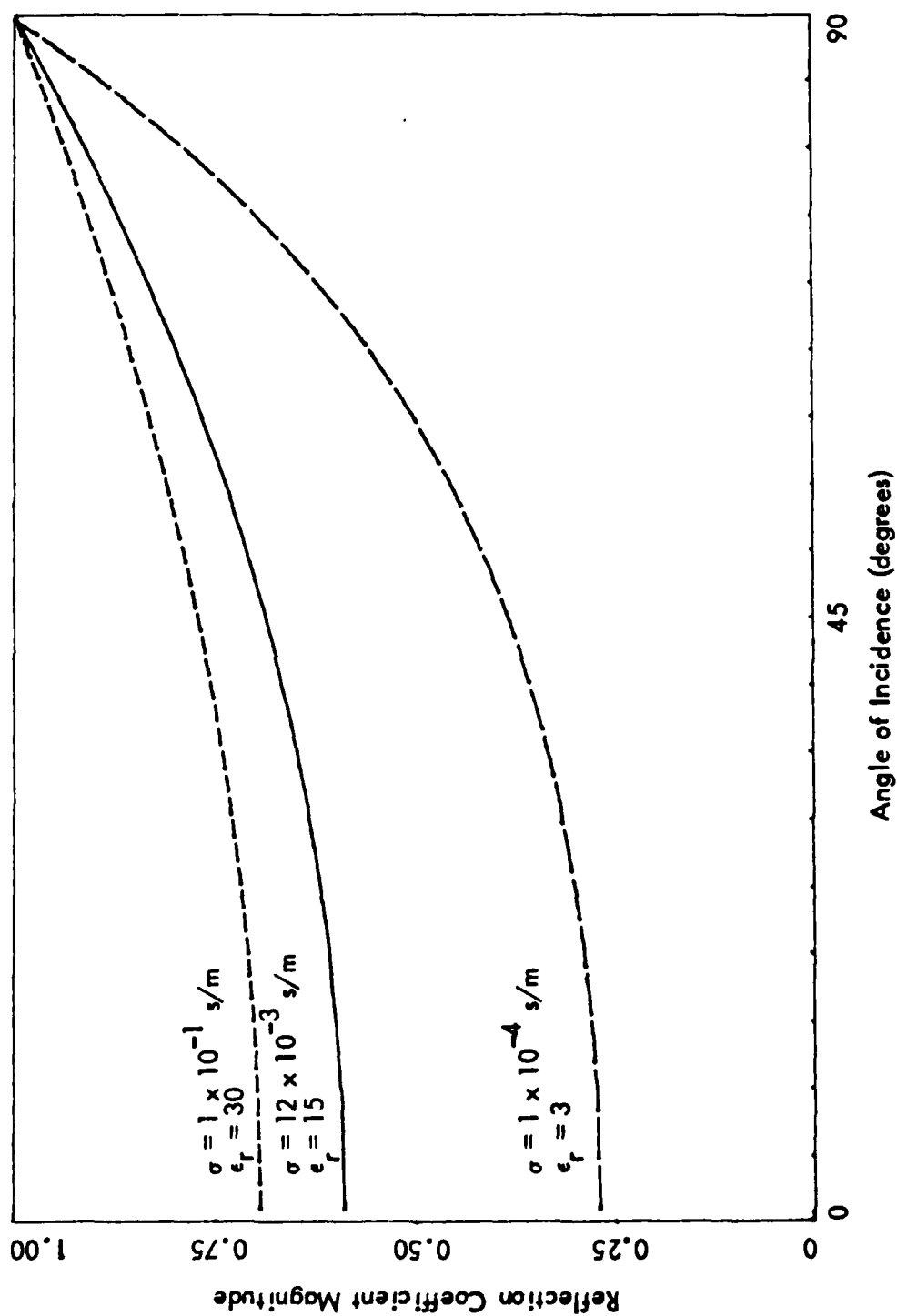


Figure B-3. Magnitude of the Horizontally-Polarized Reflection Coefficient vs. Incidence Angle for Various Ground Plane Electrical Constants (modeled).

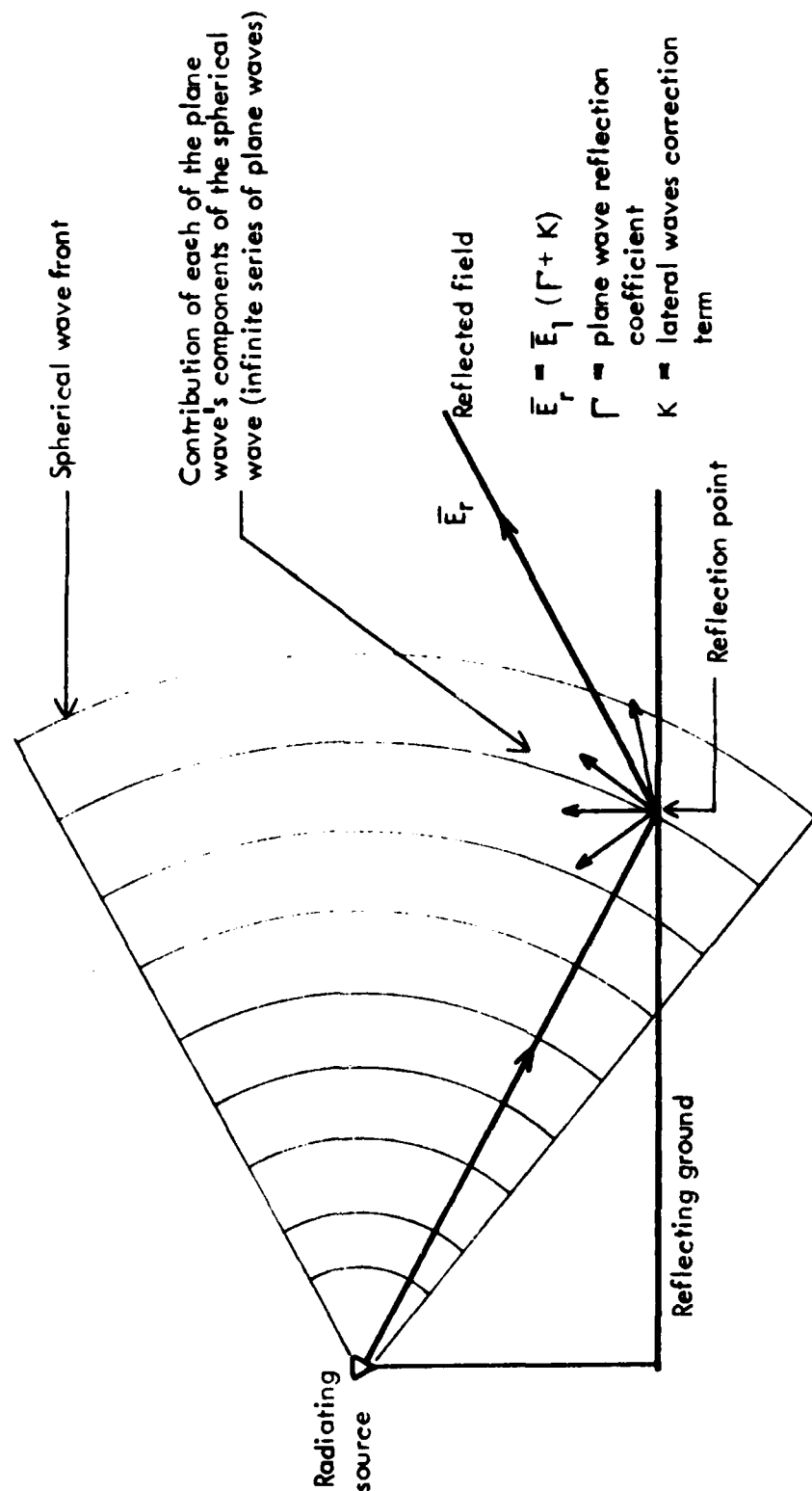


Figure B-4. Geometry Illustrating How to Reduce Spherical Wave Incidence into Infinite Series of Plane Wave Reflections.

$$A = \frac{\epsilon_r \cdot (1 - \epsilon_r)}{q_o \cdot (\epsilon_r \gamma_o + q_o)^3}$$

$$B = 2\epsilon_r \cdot (1 - \epsilon_r) + 3\epsilon_r \gamma_o^2 + q_o \gamma_o \cdot (2\epsilon_r - 1 - \gamma_o^2) - \epsilon_r \gamma_o^4$$

and

$$q_o = \epsilon_r - (\sin \theta_o)^2$$

$$\gamma_o = \cos \theta_o$$

r = distance source-observation point

$$\beta = \frac{2\pi}{\lambda}, \lambda = \text{wavelength}$$

As seen the equation, the first order approximation is merely the incident wave multiplied by the plane wave reflection coefficient. The second order term, N , is referred to as a correction term which describes the lateral wave. The second-order contribution attenuates relatively quickly compared to the plane wave reflected field with the distance source-observation point.

Figure B-5 gives the magnitude of the reflection coefficient with and without spherical wave incidence effect, and the magnitude of the spherical wave incidence effect as calculated by subroutine TREFL and TRSFL. It should be noted that this effect is insignificant for distances from the source greater than 10 meters (for an incidence angle of 80 degrees). Further analysis shows this distance is typical for all incidence angles of interest.

5. Array factor. In many installations, the antenna used in the glide slope facility is not a simple single-element antenna, but rather consists of three independent dipole elements backed by a corner reflector (e.g., the Antenna Products Company FA-8976, depicted in figure B-6).

The advantages of using multi-element antenna as opposed to single-element is that greater directivity can be achieved in the horizontal radiation pattern with the multi-element type.

If I_1, I_2, I_3 are the complex currents of the three dipoles, separated electrically by 240 degrees, the array factor is given by (figure B-7):

$$AF(\theta) = (I_2 + I_1 \cdot e^{j\beta d \sin \theta} + I_3 \cdot e^{-j\beta d \sin \theta}) \cdot EP(\theta)$$

and the element pattern for a half-wave dipole is:

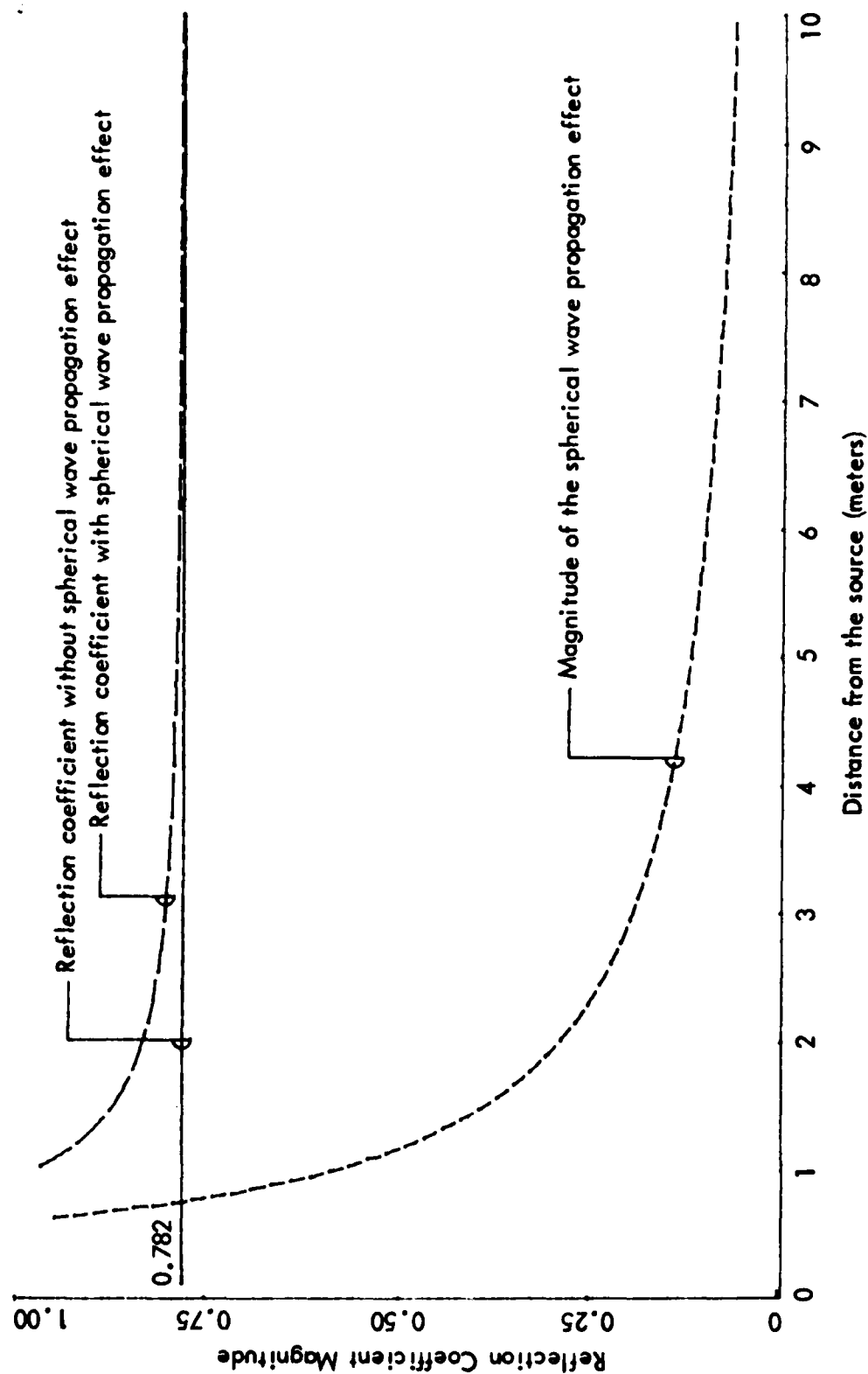


Figure B-5. Spherical Wave Propagation Effect on Reflection Coefficient (angle of incidence = 80° , $\sigma = 1 \times 10^{-4}$ s/m, $\epsilon_r = 3$). As seen, the effect of spherical wave reflection as opposed to plane wave reflection becomes negligible beyond 10 meters (modeled).

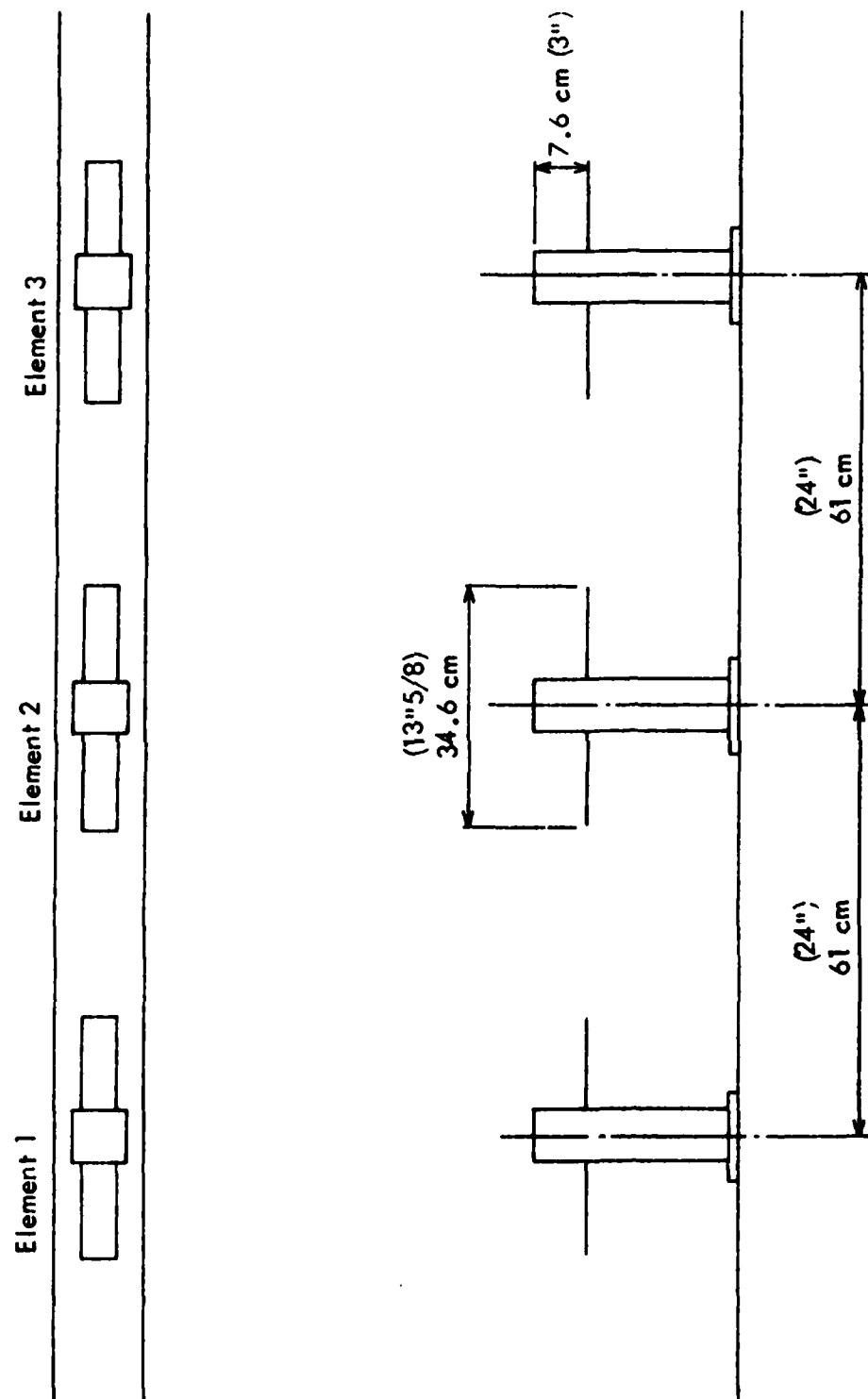


Figure B-6. Antenna Products Company FA8976.

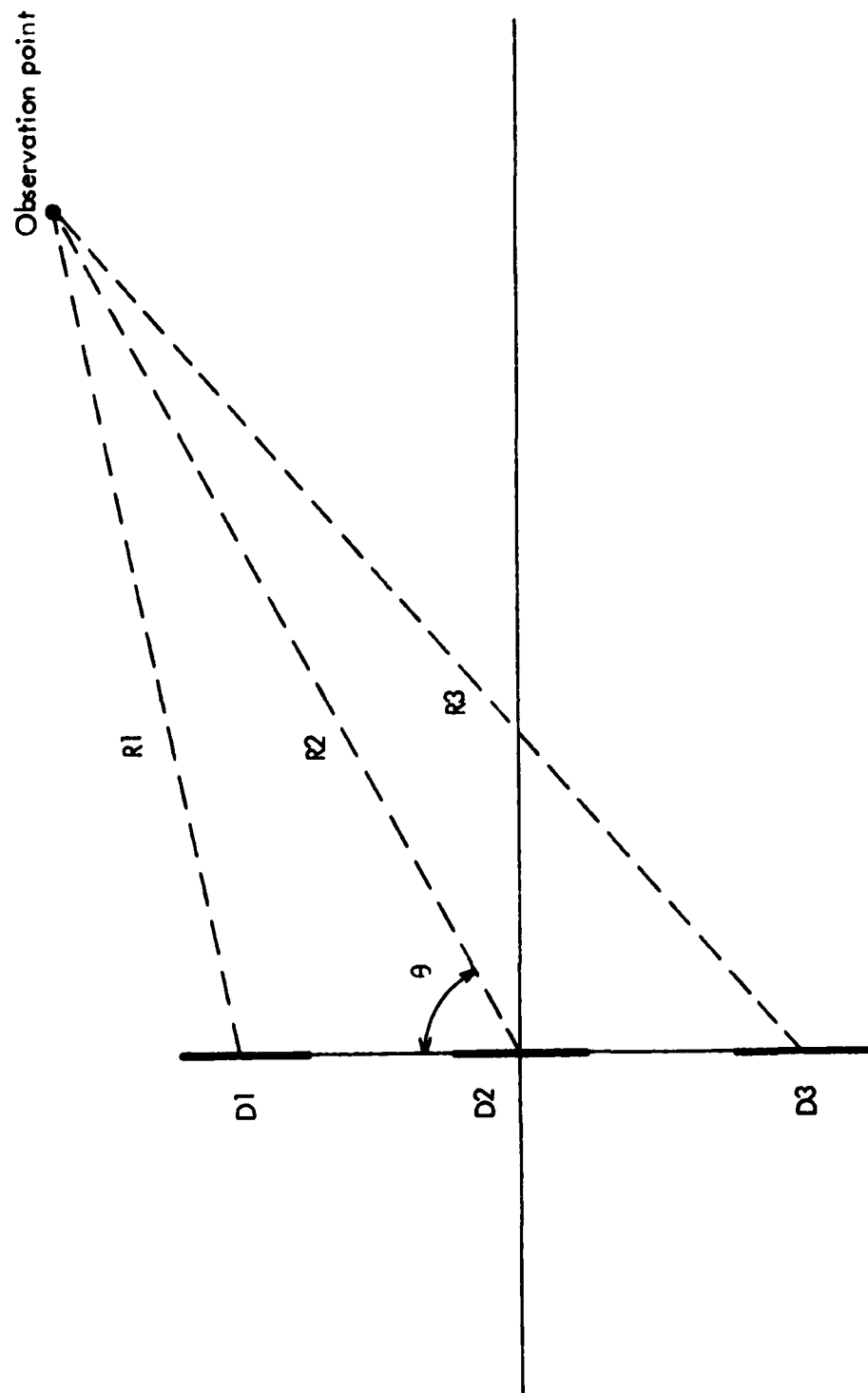


Figure B-7. Three-Element Colinear Antenna Array.

$$EP(\theta) = \frac{\cos(\pi/2 \cdot \cos\theta)}{\sin\theta}$$

The subroutine TAF compute the array factor combined with the element pattern of each antenna.

The magnitude and phase of the current in each of the three dipole elements are the required input data. When single element antennas are used, the computer code will default to an array factor of unity.

Figure B-8 depicts the modeled amplitude of such a multi-element antenna for a normal system and for when the outer element is attenuated 3dB with no change in phase.

6. Reflector factor. Like the three dipoles disposed as an array give azimuth directivity, the 90-degree metallic structure backing the dipoles acts as a corner reflector to provide vertical directivity.

Using image theory, as shown in figure B-9, the reflector factor is represented by RF.

Figure B-10 shows the value of the reflector factor function of the elevation angle as modeled by subroutine TRF.

7. Ground plane surface roughness. In the near-zone, for low altitude receiving antenna height, ground plane surface roughness has a certain effect on the reflected field because of a non-grazing angle of incidence.

The roughness coefficient is given by RUFN.

Subroutine TRUFN calculates RUFN, which is used in subroutine TCEF when the reflection coefficient is computed.

Figure B-11 shows the modeled magnitude of the roughness coefficient versus angle of incidence for various roughness parameters.

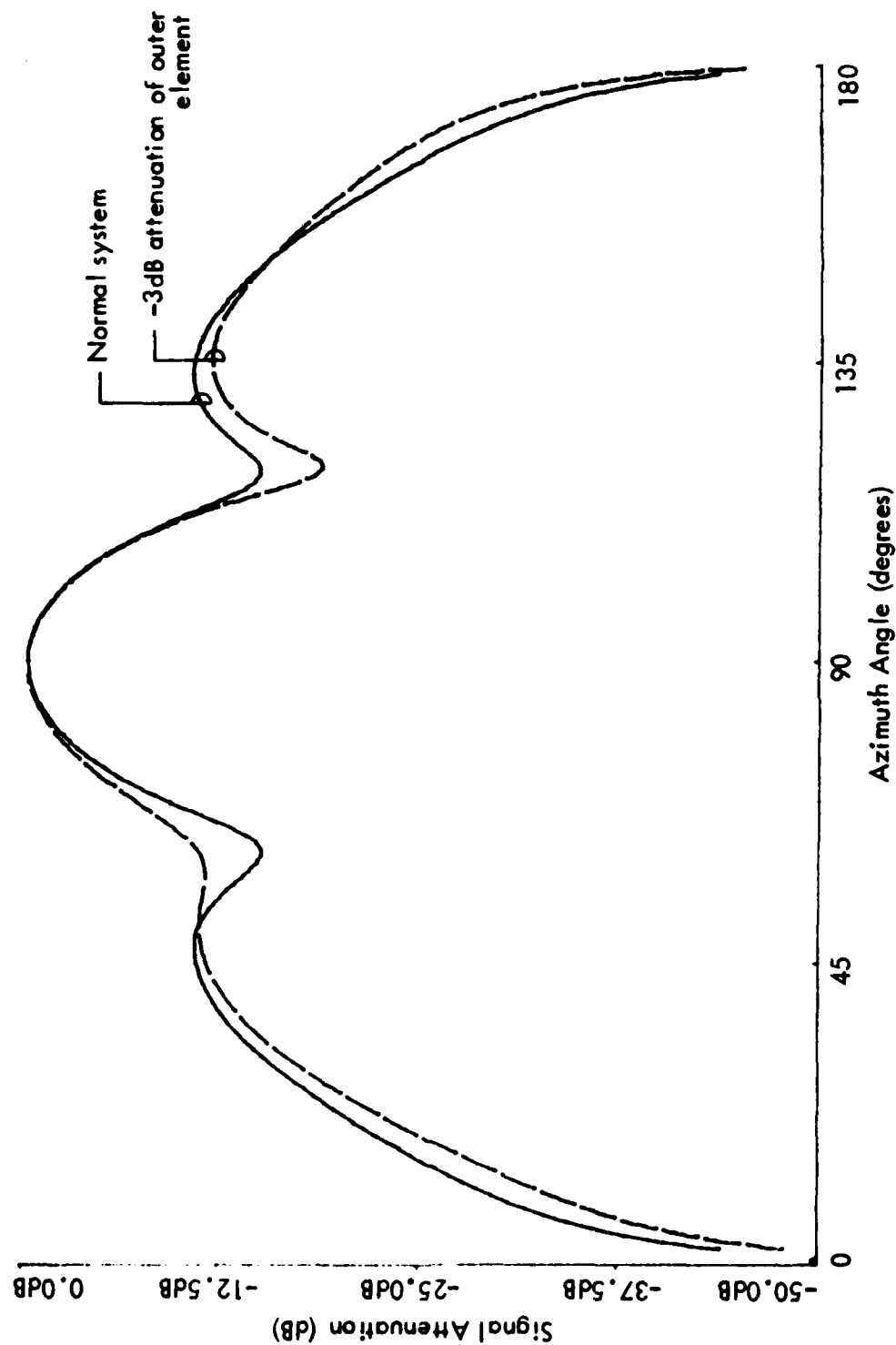


Figure B-8. Modeled Array Factor vs. Azimuth Angle for Normal and Faulty System. For normal system, two relative minima are observed at angles of about 30° and 120° (relative maxima of attenuation). Relative minima are modified under faulty conditions.

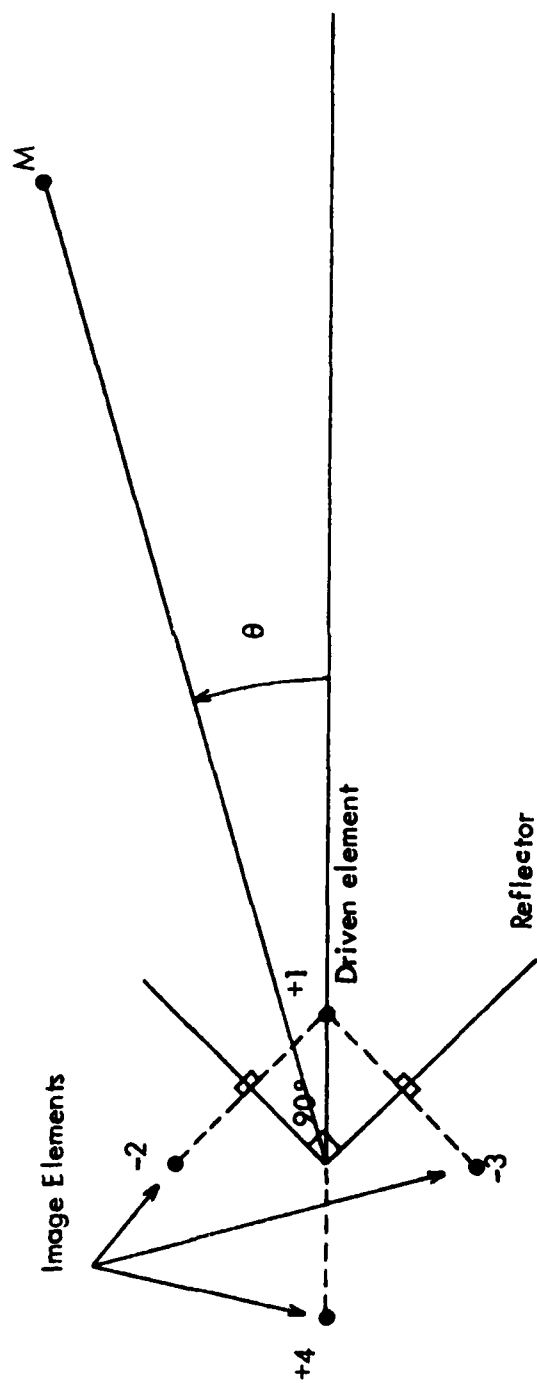


Figure B-9. Image Theory Applied to Corner Reflector.

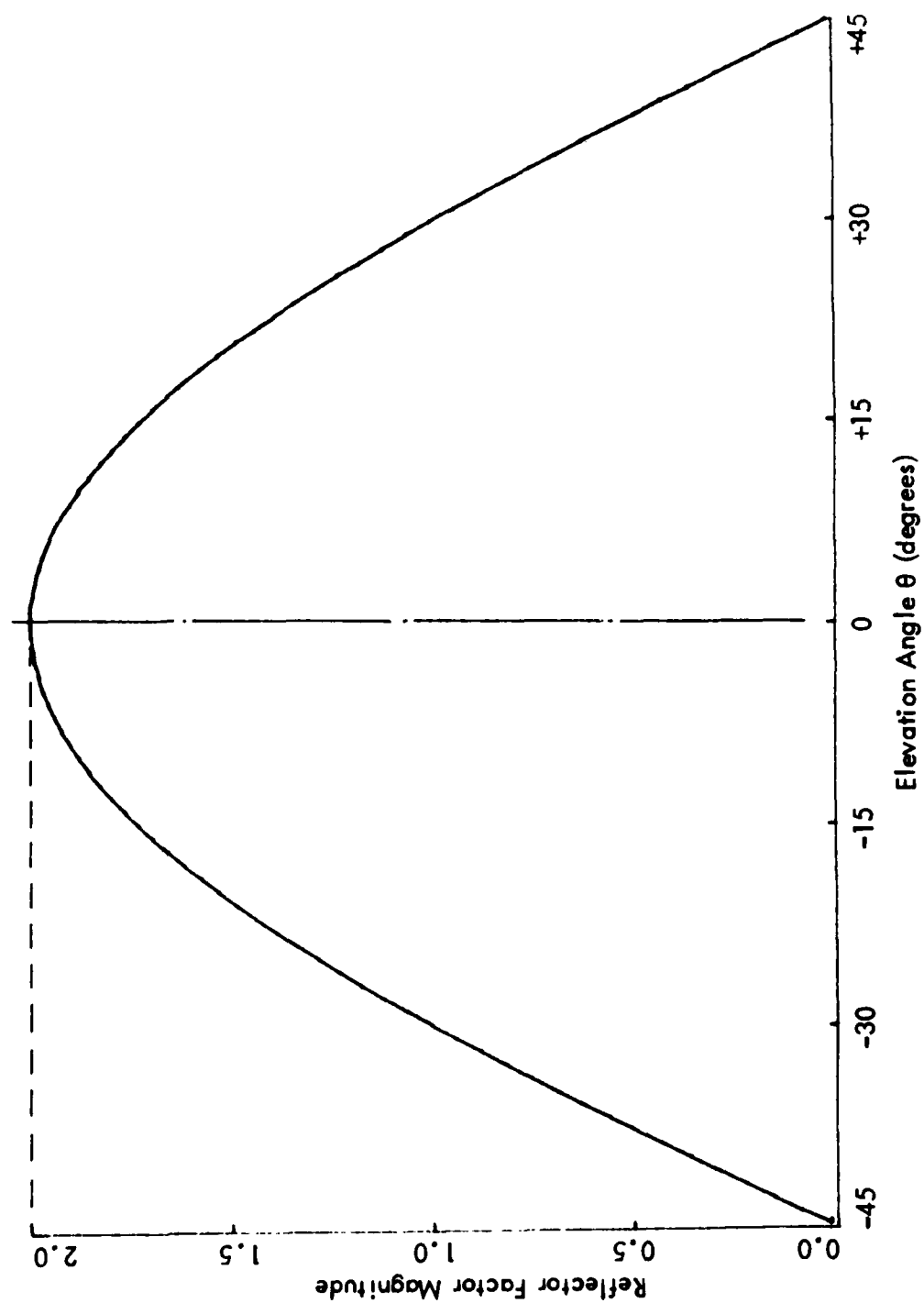


Figure B-10. Modeled Reflector Factor Magnitude vs. Elevation Angle

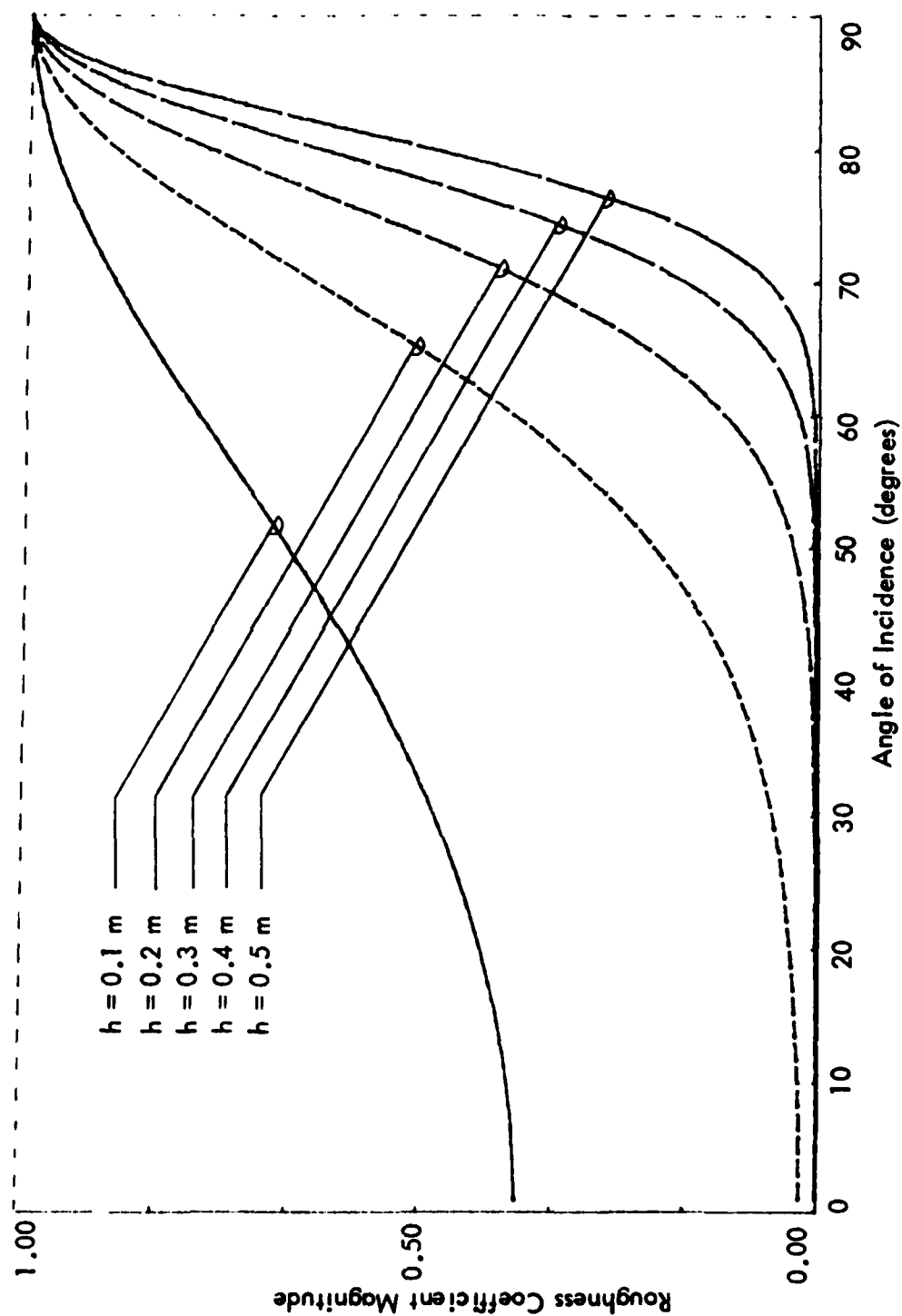


Figure B-11. Modeled Magnitude of the Roughness Coefficient vs. Angle of Incidence for Various Roughness Parameters (roughness parameter = h).

APPENDIX C: PARAMETERS MODELED BY TGCGS.

Inputs:

Ground plane information:

- Geometry (3 points)
- Conductivity, permittivity

Antenna information:

- Frequency
- Location (offset)
- Carrier current and phase
- Sideband current and phase
- Modulation levels

Locations of simulated receiver:

- Straight line
- Circular path

Model limitation:

One reflecting plane

Model computation characteristics:

Non-horizontal reflecting plane

Finite conductivity

Array factor

Reflector factor

Ground plane surface roughness

Spherical wave propagation effect

Outputs:

Electric field for carrier and sideband
signal

UDM and CDI function of observation point
locations

APPENDIX D: GENERAL DATA FOR TAMiami AIRPORT CEGS.

Antenna Tower : located 137.83 m (451.92 ft) from the runway
centerline

Upper Antenna : height = 12.93 m (42.39 ft)
: offset = 31.97 cm (12.4 in) toward runway

Middle Antenna: height = 8.62 m (28.26 ft)
: offset = 0.00 cm

Lower Antenna : height = 4.31 m (14.13 ft)
: offset = 19.05 cm (7.5 in) away from runway

Transmitter Wilcox Mark 1C solid-state with 3-element colinear
antennas in corner reflectors type FA8976 manufactured by Antenna
Products Company:

- Operating frequency = 331.1 MHz
- Main Course signal = 331.1 MHz + 4 kHz
- Clearance signal = 331.1 MHz - 4 kHz
- Carrier power = 2.9 W
- Sideband power = 37.5 mWatt
- Clearance power = 0.29 Watt

Other relevant data are given in TGENDAT file (Appendix E).

APPENDIX E. PROGRAM LISTINGS.

```

*****
C          MODIFIED DECEMBER 16, 1982
C
C          WRITTEN BY THIERRY LANGLOIS D'ESTAINOT
C          TCGS = THIERRY GROUND CHECKING OF GLIDE SLOPE
C
C          THIS IS THE MAIN FORTRAN PROGRAM TO COMPUTE
C          NEAR-FIELD CDI .
C          INPUTS ARE GIVEN IN FILE TGENDAT TCGS
C *****
C          WRITE(6,110) NOT
110 FORMAT(10X, '***** GROUND CHECK TEST NO.= ',12, ' *****
>**** ',//)
C
C          WRITE TERRAIN DATA
C
C          WRITE(6,112)
C          WRITE(6,111) XD1,YD1,ZD1
C          WRITE(6,114) XD2,YD1,ZD2
C          WRITE(6,113) XD1,YD3,ZD3
112 FORMAT(6X, '***',2X, 'TERRAIN DATA : ',//)
111 FORMAT(10X, 'XD1=',F8.2,2X, 'YD1=',F8.2,2X, 'ZD1=',F8.2)
114 FORMAT(10X, 'XD2=',F8.2,2X, 'YD2=',F8.2,2X, 'ZD2=',F8.2)
113 FORMAT(10X, 'XD3=',F8.2,2X, 'YD3=',F8.2,2X, 'ZD3=',F8.2,/)
C          WRITE(6,1100) EPSI0,MU,EPSI,SIGMA
1100 FORMAT(10X, 'EPSI0=',D9.3,2X, 'MU=',D9.3,2X, 'EPSI=',
>D9.3,2X, 'SIGMA=',D9.3)
C
C          WRITE ANTENNA DATA
C
C          WRITE(6,115)
115 FORMAT(/,6X, '***',2X, 'ANTENNA DATA : ',//)
C          WRITE(6,116) FRQY,MO,P,NANT
116 FORMAT(10X, 'FREQUENCY=',D8.3,1X, 'HZ',5X, 'MO=',F5.2,5
>X, 'P=',F8.3,3X, 'ANT. NUMBER=',12)
C
C          WRITE PATTERN CUT CHOICE
C
C          GO TO (133,134),NCUT
133 WRITE(6,121) NO
121 FORMAT(/,6X, '***',2X, 'LINEAR CUT FROM M1 TO M2 ;',13,1X, 'POINTS OF
> OBSERVATION')
C          WRITE(6,122) X1,X2
122 FORMAT(10X, 'X1=',F8.2,10X, 'X2=',F8.2)
C          WRITE(6,123) Y1,Y2
123 FORMAT(10X, 'Y1=',F8.2,10X, 'Y2=',F8.2)
C          WRITE(6,124) Z1,Z2
124 FORMAT(10X, 'Z1=',F8.2,10X, 'Z2=',F8.2)
C          GOTO 90
134 WRITE(6,125) RO
125 FORMAT(/,6X, '***',2X, 'HALF-CIRCULAR CUT WITH CENTER AT ANTENNA MAST
> LOCATION AND RADIUS ',F6.2)
C
C          TO COMPUTE NON FLAT TERRAIN EFFECT
C
C          90 CALL TNFE
C
C          APPROXIMATION ON BETA
C
C          WRITE(6,120)
120 FORMAT(/,6X, '***',2X, 'COMPUTED TERRAIN AND PHYSICAL DATA : ',//)
C          KA=2.00*PI*FRQY/SOL
C          WRITE(6,158) ALPHA,BETA,KA
158 FORMAT(10X, 'ALPHA=',F10.7,5X, 'BETA=',F10.7,5X, 'KA='
>,F10.3)
C
C          DETERMINATION OF ANTENNA COORDINATES IN NON FLAT TERRAIN SYSTEM
C

```



```

      DO 200 I=1,NANT
      CALL TANTCO(I)
200 CONTINUE
C
C      NO IS THE NUMBER OF OBSERVATING POINTS.
C      TWO TYPE OF PATTERN CUT: - LINEAR CUT BETWEEN (X1,Y1,Z1)
C                                  AND (X2,Y2,Z2)
C
C                                  - HALF-CIRCULAR CUT AROUND
C                                  THE ANTENNA MAST, RADIUS RO.
C
      DO 220 K=1,NO
      CALL TPATCT(K)
C
C      TO CALCULATE PHI(I) AND THETA(I) IN TRANSFORMED COORDINATE SYSTEM
C
      DO 210 L=1,NANTZ
      CALL TPHTHR(L)
C
C      TO COMPUTE ELECTRIC FIELDS FOR EACH ANTENNA
C
      CALL TCEF(L)
      CESST=CESST+CESS(L)
      CECST=CECST+CECS(L)
      WRITE(6,160) L,XA(L),YA(L),ZA(L),PHI(L),RHO(L),THETA(L),R(L),RS(L)
      >,KAPPA(L)
210 CONTINUE
160 FORMAT(2X,11,2X,10(F8.3,2X))
C
C      TO COMPUTE DDM AND CDI
C
      CALL TDDCDI
C
C      TO COMPUTE THE ELEVATION ANGLE OF
C      THE OBSERVATION POINT WITH RESPECT
C      TO THE BASE OF THE ANTENNA
C
      ELEVAN=DATAN(ZO/YO)/PI180
      WRITE(10,998) ELEVAN,CDI
998 FORMAT(5X,2F15.7)
      WRITE(8,999) XO,YO,ZO,ELEVAN,DDM,CDI
999 FORMAT(5X,3(F6.2,2X),4(F14.6))
      CESST=(0.,0.)
      CECST=(0.,0.)
220 CONTINUE
      WRITE(8,997)
997 FORMAT('')
      STOP
      END

```

```

C ***** TGCGS DATA GENERAL *****
C
C
C *****
C BLOCKDATA FILE WRITTEN TO EXPLAIN AND INPUT ALL NECESSARY
C DATA OF TGCGS .
C *****
C DIMENSION T(6)
C REAL *8
C >UA(6),REFUM5,REFUM6,REPH4,REPH5,REPH6,REFUM4,VA(6),NA(6),RF(6),
C >PI,PI180,AF(6),EFC,LAMBDA,
C >XCOEF(6),YCOEF(6),ZCOEF(6),DDM,CDI,MO,P,DUM4,
C >DUM1,DUM2,DUM3,XAR(200),YAR(200),
C >HNDF(6),MAG
C REAL *8 AT,PT,AP,PP

C *****
C NUMBER OF THE TEST = NOT
C *****
C NOT=44
C COMMON /A/PI,PI180,NOT
C COMMON/AA/AT,PT,AP,PP
C COMMON/TERDAT/ XD1,XD2,XD3,YD1,YD3,ZD1,ZD2,ZD3
C REAL *8 XD1,XD2,XD3,YD1,YD2,YD3,ZD1,ZD2,ZD3
C COMMON/AB/ALPHA,BETA,KA
C REAL *8 ALPHA,BETA,KA
C COMMON/ANPDAT/NANT,NANT2,XA(6),YA(6),ZA(6)
C REAL *8 XA,YA,ZA
C COMMON/PATCT/X1,Y1,Z1,X2,Y2,Z2,RO,NCUT
C REAL *8 X1,Y1,Z1,X2,Y2,Z2,RO
C COMMON/OBSPTS/XO,YO,ZO,THO(6),NO
C REAL *8 XO,YO,ZO,THO
C COMMON/PHTHR/PHI(6),THETA(6),R(6),RHO(6)
C REAL *8 PHI,THETA,R,RHO
C COMMON/DASCOMP/MSDI(3,3),PSDI(3,3),A
C REAL *8 MSDI,PSDI,A
C COMMON/DACOMP/MCDI(3,3),PCDI(3,3)
C REAL *8 MCDI,PCDI
C COMMON/TOTCEF/CESST,CECST
C COMPLEX*16 CESST,CECST,CREFL,CREFM,CRSFL
C COMMON/FREQSL/FREQY,SOL
C REAL *8 FREQY,SOL
C COMMON/TINIT/MO,P
C REAL *8 MO,P
C COMMON/INCAN/KAPPA(6),RS(6)
C REAL *8 KAPPA,RS
C COMMON/EPSIMU/EPSI,SIGMA,MU,EPSIO
C REAL *8 EPSI,SIGMA,MU,EPSIO
C COMMON/DCCDI/DDM,CDI
C REAL *8 DDM,CDI

C COMPLEX*16 CISS(6),CICS(6),CESS(6),CECS(6),COEF(6),
C >CESSX(6),CESSY(6),CESSZ(6),CECSX(6),CECSY(6),CECSZ(6),
C >CDUM1,CDUM2,CE(6),CET,CSFI,CSF

C PI=4.00*DATAN(1.00)
C PI180=PI/180.
C *****
C XD1 ARE THE COORDINATES OF THE REFLECTING PLANE (NON HORIZONTAL)
C IN FRONT OF THE GS ANTENNA MAST. THESE COORDINATES SERVE TO COM-
C PUTE THE EM FIELDS USING IMAGE THEORY.
C *****

C XD1=0.
C YD1=0.
C ZD1=0.
C XD2=0.
C ZD2=0.

```

```

YD3=1590.,.305
ZD3=0.,.25.,.305
C*****
C   XA,YA,ZA ARE THE COORDINATES OF THE ANTENNAS
C   NANT = NUMBER OF ANTENNAS
C*****
NANT=3
NANT2=NANT*2
XA(1)=452.67.,.305
YA(1)=0.
ZA(1)=14.13.,.305
XA(2)=451.92.,.305
YA(2)=0.
ZA(2)=28.26.,.305
IF (NANT,LE,2) GOTO 500
XA(3)=450.93.,.305
YA(3)=0.
ZA(3)=42.39.,.305
500 CONTINUE
REAL*8 RUM1(6),RUM2(6),RUM3(6),RUM4(6),ELEVAN
C*****
C   MSD1,PSD1,MCD1,PCD1 ARE THE MAGNITUDES AND PHASES
C   OF ALL THE ANTENNA ELEMENTS.
C   THE FIRST INDEX REFERS TO THE FURTHEST ELEMENT FROM
C   THE RUNWAY AS 1,
C   2 IS THE MIDDLE ELEMENT,
C   3 IS THE CLOSEST ELEMENT TO THE RUNWAY.
C   THE SECOND INDEX REFERS TO THE ANTENNA NUMBER :
C   1 IS THE LOWER ANTENNA
C   2 IS THE MIDDLE ANTENNA
C   3 IS THE UPPER ANTENNA .
C
C   S REFERS TO SIDEBAND ONLY,
C   C REFERS TO CARRIER AND SIDEBAND .
C
C   A = A-RATIO
C*****
C   A=.234262D0
C   A=.300
C   A=.41897D0
C   B=.7079D0
C   C=3.0
C   D=15.
C   D=-15.
MSD1(1,1)=0.500
MSD1(2,1)=0.500
MSD1(3,1)=0.500
MSD1(1,2)=1.000
MSD1(2,2)=1.000
MSD1(3,2)=1.000
MSD1(1,3)=0.500
MSD1(2,3)=0.500
MSD1(3,3)=0.500
MCD1(1,1)=1.00
MCD1(2,1)=1.000
MCD1(3,1)=1.000
MCD1(1,2)=0.500
MCD1(2,2)=0.500
MCD1(3,2)=0.500
MCD1(1,3)=0.00
MCD1(2,3)=0.00
MCD1(3,3)=0.00
PSD1(1,1)=180.+38.
PSD1(2,1)=180.
PSD1(3,1)=180.+38.
PSD1(1,2)=38.00

```

```

PSDI(2,2)=0.00
PSDI(3,2)=38.00
PSDI(1,3)=180.+38.
PSDI(2,3)=180.
PSDI(3,3)=180.+38.

PCDI(1,1)=38.00
PCDI(2,1)=0.00
PCDI(3,1)=38.00
PCDI(1,2)=180.+38.
PCDI(2,2)=180.
PCDI(3,2)=180.+38.
PCDI(1,3)=0.00
PCDI(2,3)=0.00
PCDI(3,3)=0.00
C*****
C   GENERAL INITIALIZATIONS
C   FREQUENCY = FRQY
C   SPEED OF LIGHT = SOL
C   PERMEABILITE = MU
C   MODULATION COEFFICIENT = MO
C   CDI COEFFICIENT = P
C   CONDUCTIVITY = SIGMA
C   FREE SPACE PERMITTIVITY = EPSIO
C   RELATIVE PERMITTIVITY = EPSI
C*****
C   FRQY=3.3008
C   SOL=2.997925008
C   MO=0.4
C   P=857.1428571
C   MU=4.0-7*PI
C   SIGMA=12.0-3
C   SIGMA=1.0-1
C   SIGMA=1.0-4
C   EPSIO=1.00/(MU*(SOL**2.))
C   EPSI=15.00
C   EPSI=30.00
C   EPSI=3.00
C   WRITE(9,31) A,C,D,SIGMA,EPSI
31 FORMAT(1X,'A=',F7.4,2X,'ATTEN.(DB)=' ,F7.2,2X,'DEPHAS.(DEG.)=' ,F7.2
>,2X,'SIGMA=' ,D9.3,2X,'EPSI=' ,D9.3,/)
C   WRITE(9,32)
32 FORMAT(7X,'X0',6X,'Y0',7X,'Z0',10X,'ELEVAN',9X,'ODM',10X,'CDI',
>/)
C*****
C   TWO TYPES OF PATTERN CUTS :
C   NCUT = 1 --> LINEAR CUT FROM M1 (X1,Y1,Z1)
C   TO M2 (X2,Y2,Z2)
C   NCUT = 2 --> HALF-CIRCULAR CUT
C   CENTER AT SECOND ANTENNA LOCATION (NO OFFSET)
C   RADIUS = RO
C*****
C   X1=451.92*.305
C   Y1=244.
C   Z1=1.
C   X2=451.92*.305
C   Y2=244.
C   Z2=15.
C   NO=57
C   NCUT=1
C   RO=75.

```

```

SUBROUTINE TCEF(L)
COMMON/A/PI,PI180,NOT
REAL*8 PI,PI180
COMMON/ANPDAT/NANT,NANT2,XA(6),YA(6),ZA(6)
COMMON/INCAN/KAPPA(6),RS(6)
REAL*8 KAPPA,RS
COMMON/PHTHR/PHI(6),THETA(6),R(6),RHO(6)
REAL*8 PHI,THETA,R,RHO
COMMON/AB/ALPHA,BETA,KA
REAL*8 ALPHA,BETA,KA
COMMON/TOTCEF/CESST,CECST
COMPLEX*16 CESST,CECST
COMMON/FRQYSL/FRQY,SOL
REAL*8 FRQY,SOL
COMMON/HRUFN/H
REAL*8 H
COMPLEX*16 CISS(6),CICS(6),CESS(6),CECS(6),COEF(6),CSAF(6),CCAF(6)
>,CREFL,CRSFL,CREFM,CRUFN
REAL*8 GAMMA(6),RF(6)
C*****
C      PURPOSE : TO COMPUTE COMPLEX VECTOR ELECTRIC FIELD
C                FOR EACH ANTENNA
C
C      NEEDS : A , ANPDAT , INCA , PHTHR , TOTCEF , FRQYSL AND HRUFN
C*****
      GAMMA(L)=-KA*R(L)
C
C      REFLECTOR FACTOR
C
      CALL TRF(PHI(L),RF(L))
      COEF(L)=RF(L)*1.00/R(L)*CDEXP(DCMPLX(0.00,GAMMA(L)))
      IF (L.LE.NANT) GOTO 410
      M=L-NANT
C
C      PLANE WAVE INCIDENCE REFLECTION COEFFICIENT
C
      CALL TREFL(KAPPA(M),CREFL)
C
C      SPHERICAL WAVE INCIDENCE EFFECT
C
      CALL TRSFL(KAPPA(M),R(L),CRSFL)
C
C      ROUGHNESS FACTOR
C
      CALL TRUFN(H,KAPPA(M),CRUFN)
      CREFM=(CREFL-CRSFL)*CRUFN
      CSAF(L)=CSAF(M)*CREFM
      CCAF(L)=CCAF(M)*CREFM
      GOTO 411
C
C      ARRAY FACTOR
C
410 CALL TAF(L,THETA(L),CSAF(L),CCAF(L))
C
C      ANGLE OF INCIDENCE
C
      CALL TINCAN(L)
411 CESS(L)=COEF(L)*CSAF(L)
      CECS(L)=COEF(L)*CCAF(L)
C
      CESST=CESST+CESS(L)
      CECST=CECST+CECS(L)
C
      RETURN
      END

```

```

SUBROUTINE TAF(L,TETA,CSF,CCF)
COMMON/A/PI,PI180,NOT
REAL*8 PI,PI180
COMMON/PHTHR/PHI(6),THETA(6),R(6),RHO(6)
REAL*8 PHI,THETA,R,RHO
COMMON/DASCMP/MSDI(3,3),PSDI(3,3),A
REAL*8 MSDI,PSDI,A
COMMON/DACOMP/MCDI(3,3),PCDI(3,3)
REAL*8 MCDI,PCDI
COMPLEX*16 CS1,CS2,CS3,CC1,CC2,CC3,CS11,CS13,CSAF(6),CCAF(6),CSF,C
>CF,CT1,CT3,CTT
REAL*8 PSI1,PSI3,DC,TETA
C*****
C      PURPOSE : TO COMPUTE THE ARRAY FACTOR FOR THE THREE ELEMENT
C              ANTENNA .
C
C      NEEDS A , PHTHR , DASCMP AND DACOMP
C*****

CS1=MSDI(1,L)*DCMPLX(DCOS(PSDI(1,L)*PI180),DSIN(PSDI(1,L)*PI180))
CS2=MSDI(2,L)*DCMPLX(DCOS(PSDI(2,L)*PI180),DSIN(PSDI(2,L)*PI180))
CS3=MSDI(3,L)*DCMPLX(DCOS(PSDI(3,L)*PI180),DSIN(PSDI(3,L)*PI180))
CC1=MCDI(1,L)*DCMPLX(DCOS(PCDI(1,L)*PI180),DSIN(PCDI(1,L)*PI180))
CC2=MCDI(2,L)*DCMPLX(DCOS(PCDI(2,L)*PI180),DSIN(PCDI(2,L)*PI180))
CC3=MCDI(3,L)*DCMPLX(DCOS(PCDI(3,L)*PI180),DSIN(PCDI(3,L)*PI180))
PSI1=(4.00*PI/3.00)*DCOS(TETA)
PSI3=-PSI1

CS11=CDEXP(DCMPLX(0.00,PSI1))
CS13=CDEXP(DCMPLX(0.00,PSI3))

DC=DCOS((PI/2.00)*DCOS(TETA))/DSIN(TETA)

CSF=(CS2+CS1*CS11+CS3*CS13)*DC*A
CCF=(CC2+CC1*CS11+CC3*CS13)*DC
CSAF(L)=CSF
CCAF(L)=CCF
RETURN
END

```

```

SUBROUTINE TANTCO(I)
COMMON/ANPDAT/NANT,NANT2,XA(6),YA(6),ZA(6)
REAL*8 XA,YA,ZA
COMMON/AB/ALPHA,BETA,KA
REAL*8 ALPHA,BETA,KA
COMMON/TERDAT/ XD1,XD2,XD3,YD1,YD3,ZD1,ZD2,ZD3
REAL*8 XD1,XD2,XD3,YD1,YD2,YD3,ZD1,ZD2,ZD3
REAL*8 UA(6),VA(6),NA(6)
C*****
C      PURPOSE : TO COMPUTE IMAGE ANTENNA COORDINATES
C                IN NON-FLAT TERRAIN SYSTEM.
C      NEEDS AB , ANPDAT AND TERDAT
C      OUTPUT : K=I+NANT , XA(K),YA(K),ZA(K) .
C*****
      UA(1)=(XA(1)-XD1)*DCOS(ALPHA)+(ZA(1)-ZD1)*DSIN(ALPHA)
      VA(1)=-(XA(1)-XD1)*DSIN(ALPHA)*DSIN(BETA)+(YA(1)-YD1)*DCOS(BETA)+(
>ZA(1)-ZD1)*DCOS(ALPHA)*DSIN(BETA)
      NA(1)=-(XA(1)-XD1)*DSIN(ALPHA)*DCOS(BETA)-(YA(1)-YD1)*DSIN(BETA)+(
>ZA(1)-ZD1)*DCOS(ALPHA)*DCOS(BETA)
C
C      CHANGE NA(1) TO -NA(1) FOR DETERMINATION OF IMAGE LOCATION
C
      K=I+NANT
      XA(K)=UA(1)*DCOS(ALPHA)-VA(1)*DSIN(ALPHA)*DSIN(BETA)+NA(1)*DSIN(
>ALPHA)*DCOS(BETA)+XD1
      YA(K)=VA(1)*DCOS(BETA)+NA(1)*DSIN(BETA)+YD1
      ZA(K)=UA(1)*DSIN(ALPHA)+VA(1)*DCOS(ALPHA)*DSIN(BETA)-NA(1)*DCOS(
>ALPHA)*DCOS(BETA)+ZD1
      RETURN
      END

```

```

SUBROUTINE TDDCDI
COMMON/TOTCEF/CESST,CECST
COMPLEX*16 CESST,CECST
COMMON/TINIT/MO,P
REAL*8 MO,P
COMMON/DDCDI/DUM,CDI
REAL*8 DDM,CDI
C*****
C      PURPOSE : TO COMPUTE DDM AND CDI
C
C      NEEDS TOTCEF AND TINIT
C*****

DDM=0.
CDI=0.
DDM=2.*MO*DREAL(CESST/CECST)
CDI=P*DDM
WRITE(6,167) CESST,CECST,DDM,CDI
167 FORMAT(10X,'CESST=',2D12.6,2X,'CECST=',2D12.6,2X,'DDM=',F10.5,2X,'
>CDI=',F15.5)
RETURN
END

```



```

SUBROUTINE TINCAN(I)
COMMON/A/PI,P1180
REAL*8 P1,P1180
COMMON/ANPDAT/NANT,NANT2,XA(6),YA(6),ZA(6)
REAL*8 XA,YA,ZA
COMMON/OBSPTS/XO,YO,ZO,THO(6),NO
REAL*8 XO,YO,ZO,THO
COMMON/INCAN/KAPPA(6),RS(6)
REAL*8 KAPPA,RS
C*****
C      PURPOSE : TO COMPUTE THE INCIDENCE ANGLE OF THE EM WAVES
C                ON THE REFLECTING PLANE.
C
C      NEEDS A , ANPDAT AND INCAN .
C*****
      RS(I)=DSQRT((DABS(XO-XA(I)))**2.+(DABS(YO-YA(I)))**2.)
C      KAPPA(I)=PI/2.-DATAN(ZA(I)/(RS(I)*(1.+(1./ZO))))
      KAPPA(I)=DATAN(RS(I)/(ZO-ZA(I+NANT)))

      IF(I.GT.NANT) GOTO 420
C      WRITE(10,159) RS(I),KAPPA(I)
159  FORMAT(10X,'RS=',F10.5,4X,'KAPPA=',F10.5)
420  CONTINUE
      RETURN
      END

```

```

SUBROUTINE TNFTE
COMMON/TERDAT/ XD1,XD2,XD3,YD1,YD3,ZD1,ZD2,ZD3
REAL*8 XD1,XD2,XD3,YD1,YD2,YD3,ZD1,ZD2,ZD3
COMMON/AB/ALPHA,BETA,KA
REAL*8 ALPHA,BETA,KA
C*****
C      PURPOSE : TO COMPUTE ALPHA AND BETA DUE TO NON-FLAT
C              TERRAIN.
C      NEEDS AB AND TERDAT
C      OUTPUT : ALPHA AND BETA IN RADIANS
C*****
C      APPROXIMATION ON BETA VALID FOR SMALL ANGLES ONLY.
C
      IF ((XD2-XD1) .EQ. 0.) GOTO 91
      ALPHA=DATAN((ZD2-ZD1)/(XD2-XD1))
      GOTO 92
91 ALPHA=0.0
92 IF ((YD3-YD1) .EQ. 0.) GOTO 93
      BETA=DATAN((ZD3-ZD1)/(YD3-YD1))
      GOTO 94
93 BETA=0.0
94 RETURN
      END

```

```

SUBROUTINE TPATCT(K)
COMMON/A/PI,P1180
REAL*8 P1,P1180
COMMON/PATCT/X1,Y1,Z1,X2,Y2,Z2,RO,NCUT
REAL*8 X1,Y1,Z1,X2,Y2,Z2,RO
COMMON/OBSPTS/XO,YO,ZO,THO(6),NO
REAL*8 XO,YO,ZO,THO
COMMON/ANPDAT/NANT,NANT2,XA(6),YA(6),ZA(6)
REAL*8 XA,YA,ZA
C*****
C      PURPOSE : TO COMPUTE OBSERVATION POINT LOCATIONS
C      MOBS=(XO,YO,ZO)
C      ELEVAN = ARCTG(ZO/YO)
C
C      NEEDS : PATCT , OBSPTS AND ANPDAT
C
C      SELECTION OF THE TYPE OF PATTERN CUT: 1 FOR LINEAR
C                                              2 FOR CIRCULAR
C*****
C      GO TO (131,132),NCUT
C
C      LINEAR CUT
C
131 DELX=(X2-X1)/(NO-1.)
    DELY=(Y2-Y1)/(NO-1.)
    DELZ=(Z2-Z1)/(NO-1.)
    XO=X1+DELX*(K-1)
    YO=Y1+DELY*(K-1)
    ZO=Z1+DELZ*(K-1)
    GOTO 80
C
C      HALF-CIRCULAR CUT WITH CENTER AT MAST XY-PLANE LOCATION.
C      HALF-CIRCLE RADIUS GIVEN BY RO
C      CONSTANT ALTITUDE Z=ZO
C
132 THO(K)=PI*(K-1)/(NO-1)
    XO=RO*DCOS(THO(K))+XA(2)
    YO=RO*DSIN(THO(K))+YA(2)
    ZO=Z1
    GOTO 80
80 WRITE(6,199) K,XO,YO,ZO
199 FORMAT(/,2X,'>>',2X,'OBSERVATION POINT ',13,5X,'XO=',F10.5,5X,'YO
>=',F10.5,5X,'ZO=',F10.5,/)
    WRITE(6,162)
162 FORMAT(/,2X,'L',5X,'XA',8X,'YA',8X,'ZA',8X,'PHI',7X,'RHO',6X,'THET
>A',7X,'R',9X,'RS',7X,'KAPPA')
    RETURN
END

```

```

SUBROUTINE TPHTHR(L)
COMMON/A/PI,P1180,NOT
REAL*8 P1,P1180
COMMON/ANPDAT/NANT,NANT2,XA(6),YA(6),ZA(6)
REAL*8 XA,YA,ZA
COMMON/OBSPTS/XO,YO,ZO,THO(6),NO
REAL*8 XO,YO,ZO,THO
REAL*8 DUM1,DUM2,DUM3,RHO
COMMON/PHTHR/PHI(6),THETA(6),R(6),RHO(6)
REAL*8 PHI,THETA,R,RHO
C*****
C      PURPOSE : TO COMPUTE PHI(L), THETA(L) AND R(L)
C              FOR EACH ANTENNA .
C
C      NEEDS A , ANPDAT , OBSPTS AND PHTHR
C*****
      DUM1=XO-XA(L)
      DUM2=YO-YA(L)
      DUM3=ZO-ZA(L)
      RHO(L)=DSQRT(DABS(DUM2)**2.+DABS(DUM3)**2.)
      PHI(L)=DATAN(DUM3/DUM2)
      THETA(L)=PI/2.-DATAN(DUM1/RHO(L))
C
C      DISTANCE ANTENNA CENTER-OBSERVATION POINT R(L)
C
      R(L)=DSQRT(DABS(DUM1)**2.+DABS(DUM2)**2.+DABS(DUM3)**2.)
C      WRITE(9,320) R(L),RHO(L)
320  FORMAT(10X,2(F10.3,5X))
      RETURN
      END

```

```

SUBROUTINE TREFL(TETA1,CREFL)
COMMON/A/PI,PI180,NOT
REAL*8 PI,PI180
COMMON/FREQSL/FREQ,SOL
REAL*8 FREQ,SOL
COMMON/EPSIMU/EPSI,SIGMA,MU,EPSIO
REAL*8 EPSI,SIGMA,MU,EPSIO
REAL*8 TETA1,ETA0,COST,COSI,REFUM1,REFUM2,REFUM3,TRUM2,OMEGA
COMPLEX*16 CETA,CREFL,CTRUM1,CRFUM1
C*****
C      PURPOSE : TO COMPUTE THE COMPLEX REFLECTION COEFFICIENT
C      ASSUMING VALUES FOR CONDUCTIVITY AND PERMITTIVITY .
C      NEEDS A , FREQSL AND EPSIMU
C*****
      ETA0=MU*SOL
      OMEGA=2.00*PI*FREQ
      REFUM1=(EPSI*EPSIO)**2.+(SIGMA/OMEGA)**2.
      REFUM1=DSQRT(MU/REFUM1)
      CRFUM1=CDSQRT(DCMPLX(EPSI*EPSIO,SIGMA/OMEGA))
      CETA=REFUM1*CRFUM1
      REFUM2=DSIN(TETA1)/DSQRT(EPSI)
      REFUM3=DARSIN(REFUM2)
      COST=DCOS(REFUM3)
      CTRUM1=CETA/COST
      TRUM2=ETA0/DCOS(TETA1)
      CREFL=(CTRUM1-TRUM2)/(CTRUM1+TRUM2)
      RETURN
      END

```

```

SUBROUTINE TRF (PHI,RF)
COMMON/A/PI,PI180
REAL *8 PI,PI180
REAL *8 PHI,RF
C *****
C      PURPOSE : TO COMPUTE THE REFLECTOR FACTOR
C
C      NEEDS A
C
C      OUTPUT : RF
C *****
      RF=2.00*DABS(DCOS(PI/2.00*DCOS(PHI))-DCOS(PI/2.00*DSIN(PHI)))
      RETURN
      END

```

```

SUBROUTINE TRSFL(TETA1,R,CRSFL)
COMMON/A/PI,PI180,NOT
REAL*8 PI,PI180
COMMON/FRQYSL/FRQY,SOL
REAL*8 FRQY,SOL
COMMON/EPSIMU/EPSI,SIGMA,MU,EPSIO
REAL*8 EPSI,SIGMA,MU,EPSIO
REAL*8 GAMO,Q0,ANN1,ANN2,ANN3,ANN4,ANN5,SN,SNN,BET,TETA1
COMPLEX*16 CRSFL
C*****
C      PURPOSE : TO COMPUTE THE EFFECT OF SPHERICAL PROPAGATION
C                ON THE PLANE WAVE PROPAGATION REFLECTION FACTOR.
C
C      NEEDS A , FRQSL AND EPSIMU
C*****
      GAMO=DCOS(TETA1)
      Q0=DSQRT(EPSI-(DSIN(TETA1))**2.)
      ANN1=EPSI*(1.00-EPSI)/((Q0**3.)*(EPSI*GAMO+Q0)**3.)
      ANN2=2.00*EPSI*(EPSI-1.00)
      ANN3=3.00*EPSI*(GAMO**2.)
      ANN4=Q0*GAMO*(2.00*EPSI+1.00-(GAMO**2.))
      ANN5=EPSI*(GAMO**4.)

      SN=ANN1*(ANN2+ANN3+ANN4-ANN5)

      BET=2.00*PI*FRQY/SOL

      SNN=SN/(BET*R)

      CRSFL=DCMPLX(0.00,SNN)
      RETURN
      END

```

```

SUBROUTINE TRUFN(H,CHI,CRUFN)
COMMON/A/PI,P1180
REAL*8 P1,P1180
COMMON/FRQYSL/FRQY,SOL
REAL*8 FRQY,SOL
REAL*8 RUFN,DPHI,CHI,H
COMPLEX*16 CRUFN

```

```

C*****
C      PURPOSE : TO ACCOUNT FOR GROUND ROUGHNESS
C
C      NEEDS A , FRQYSL AND INCAN
C*****
      DPHI=FRQY*.00*PI*H*DCOS(CHI)/SOL
      RUFN=DSQRT(DEXP(-(DPHI**2.00)))
      CRUFN=DCMPLX(RUFN,0.000)
      RETURN
      END

```



```
FUNCTION PHASE(D)  
COMMON/A/PI,P1180,NOT  
REAL*8 PI,P1180  
REAL*8 D
```

```
C*****  
C      TO TRANSFORM AN ANGLE FROM DEGREES TO RADIANS  
C*****  
      PHASE=DATAN(D)/P1180  
      RETURN  
      END
```

```

FUNCTION CPLX(MA,PA)
COMMON/A/PI,PI180,NOT
REAL *8 PI,PI180
REAL *8 MA,PA
COMPLEX*16 CPLX

```

```

C *****
C      PURPOSE : TO CONVERT AN EXPONENTIALLY EXPRESSED
C                COMPLEX NUMBER IN ITS TRIGONOMETRIC FORM .
C
C
C      NEEDS A
C *****
C      CPLX=MA*DCMPLX(DCOS(PA*PI180),DSIN(PA*PI180))
      RETURN
      END

```

APPENDIX F. HARMONICS ANALYZER PROGRAM LISTING.

```

C   THIS PROGRAM WRITTEN BY M.JAMIL 4/9/82.
C   THE PURPOSE OF THIS PROGRAM IS TO CALCULATE THE
C   CHANGE IN THE NORMAL DDM READING DUE TO INTERFERENCE
C   AT A SINGLE HARMONIC FREQUENCY.
C   SIGNAL IS INPUTED NEXT.
C   THE PROGRAM THEN CALCULATES THE DDM DUE TO
C   INTERFERENCE.
C   ASSUMPTION: CARRIER AMPLITUDE ONE VOLT.
REAL M
C   DDM(X) IS A FUNCTION STATEMENT TO CONVERT VOLTAGE RATION TO DDM
   DDM(X)=M*(X-1.)
C   CDI(Y) IS A FUNCTION STATEMENT TO CONVERT DDM TO CDI(UA)
   CDI(Y)=Y*(150./COECEF)
   DIMENSION PG(100,2),TEM(100),DIFF(100),FREQ(100,2),AM(100),CDI(10
10)
   START = 30.0
   NP = 18
   AMAX = 0.0
   BMAX = 0.0
   DO 1 J = 1,2
   DO 1 I = 1,NP
   READ (1, 100) A,FREQ(I,J)
   IF (A.GT.AMAX.AND.J.EQ.1) AMAX = A
   IF (A.GT.BMAX.AND.J.EQ.2) BMAX = A
   PG (I,J) = A
1   CONTINUE
C   LO90 AND LO150 ARE THE ADDRESSES IN PG CONTAINING THE FILTER RESPONSE
C   FOR 90 AND 150 HZ., RESPECTIVELY
   LO90=IFIX((90./START)+.5)
   LO150=IFIX((150./START)+.5)
C   S90 AND S150 ARE THE OUTPUTS OF THE 90 AND 150 HZ. FILTERS
C   WHEN THEY ARE BOTH FED WITH 1 VOLT OF 90 AND 150 HZ.
   S90=SQRT((PG(LO90,1)**2/2)+(PG(LO150,1)**2/2))
   S150=SQRT((PG(LO90,2)**2/2)+(PG(LO150,2)**2/2))
   FACTOR=S90/S150
   FACTOR=S150/S90
   WRITE (6, 205) FACTOR
205  FORMAT (1X,' RATIO BETWEEN BOTH FILTERS=', F10.4)
100  FORMAT (F10.3, F10.3)
   M=0.2
   WRITE(6,1000)
1000  FORMAT(' SELECT PROPER MODULATION PERCENTAGE 1=LOC 2=GS')
   READ(5,1001)N
1001  FORMAT(I1)
   IF(N.EQ.1) GO TO 1002
   M=0.4
1002  DDMOFF=DDM(FACTOR)
   COECEF=.175
   IF(N.EQ.1) COECEF=.155
   CDIOFF=CDI(DDMOFF)
C   COMPUTE FILTER RESPONSE TO PLUS OR MINUS 150 UA INPUT SIGNAL
C   CAL1 IS THE RESPONSE (DDM) TO PLUS 150 UA INPUT SIGNAL
   CAL1=DDM(FACTOR*2.26)
   CALUA1=CDI(CAL1)-CDIOFF
   CAL2=DDM(FACTOR/2.26)
   CALUA2=CDI(CAL2)-CDIOFF
   WRITE(6,501) DDMOFF,CDIOFF
501  FORMAT(1X,'OFFSET DUE TO FILTER IMBALANCE: ',F7.5,'(DDM)',3X,F7.2
,,'(UA)')
   GAIN1=ABS(CALUA1)/149.61
   GAIN2=ABS(CALUA2)/149.61
   AVGAIN=(GAIN1+GAIN2)/2.
C   SSYM IS PORTION OF TOTAL GAIN CONTAINED BETWEEN 0 AND 150 UA
C   SYNC IS PORTION OF TOTAL GAIN CONTAINED BETWEEN 0 AND MINUS 150 UA
   SSYM=GAIN1/(2.*AVGAIN)
   SYNC=1.-SSYM
   PRINT 505,AVGAIN,SSYM,SYNC
505  FORMAT(1X,'AMPLIFIER GAIN',F7.4,' SYMMETRY ',F6.4,'/',F6.4)
   WRITE(6,502)
502  FORMAT(1X,'ENTER 1 FOR ON COURSE 2 FOR WIDTH')
   X=1.0
   READ(5,1001) LW

```

```

      IF(LW.EQ.2)X=2.07
900  WRITE(6,503)
503  FORMAT(1X,'FREQUENCY OF INTERFERING SIGNAL')
      READ(5,100) FREQI
      IN=IFIX(FREQI/START+.5)
C   SB190 AND SB1150 REPRESENT THE CONTRIBUTION OF THE INTERFERING
C   SIGNAL AFTER THE 90 AND 150 HZ. FILTERS, RESPECTIVELY
      DO 600 J=1,100
        AM(J)=J*.01
        SB190=AM(J)*PG(IN,1)
        SB1150=AM(J)*PG(IN,2)
C   THE TOTAL OUTPUT OF EACH FILTER (TOT90 AND TOT150) IS THE CONTRIBU-
C   TION OF THE INTERFERENCE SIGNAL AND THE GUIDANCE SIGNAL(ASSUMED TO BE
C   ONE VOLT FOR BOTH 90 AND 150 HZ. AT THE INPUT TO THE FILTER)
        TOT90=SQRT((SB190**2/2)+(PG(LO90,1)*X)**2/2)+(PG(LO150,1)/X)**2/
        12))
        TOT150=SQRT((SB1150**2/2)+(PG(LO90,2)*X)**2/2)+(PG(LO150,2)/X)**
        12/2))
C   RATIO1 IS THE 90/150 VOLTAGE RATIO WITH INTERFERENCE
        RATIO1=TOT90/TOT150
        RATIO1=TOT150/TOT90
C   DDM1 IS THE RESULTANT DDM WITH THE FILTER BIAS TAKEN OUT
        DDM1=DDM(RATIO1)-DDMOFF
C   CDI1 IS THE CDI AMITH INTERFERING SIGNAL WITH BIAS TAKEN OUT
        CDI1(J)=CDI(DDM1)
        AM(J)=AM(J)*100.
        WRITE(9,504)AM(J),CDI1(J)
        CDI1(J)=CDI1(J)*(-1)
504  FORMAT(1X,2F10.2)
600  CONTINUE
      CALL VTMOPL(AM,CDI1,0.0,-10.,100.,10.,J,0,0,0)
      STOP
      END
      SUBROUTINE VTMOPL(X,Y,XMIN,YMIN,XMAX,YMAX,N,ITYPE,NPBS,ISYM)
C   TYPES OF PLOTS POSSIBLE WITH THIS SUBROUTINE ARE AS FOLLOWS:
C   ITYPE=0: LINE PLOT- NO SMOOTHING
C   ITYPE=1: LINE PLOT- SMOOTHING
C   ITYPE=2: SYMBOL PLOT- NO CONNECTING LINE
C   ITYPE=3: SYMBOL PLOT- LINE CONNECTING DATA POINTS
C   ITYPE=4: SYMBOL PLOT- SMOOTHED LINE CONNECTS DATA POINTS
C   ITYPE=5: SMOOTHED DASHED LINES
C   INPBS INDICATES THE NUMBER OF POINTS BETWEEN SYMBOLS
C   ISYM IS THE INTEGER EQUIVALENT OF THE SYMBOL TO BE USED
C   IN THE PLOT. IT MUST BE WITHIN THE RANGE OF 0-13, INCLUSIVE.
C   FOR DASHED LINES ISYM IS THE TYPE OF DASH LINEFROM 1 TO 4
C   FOR ITYPE=0 AND ISYM.NE.0 DASHED LINES ALSO PRODUCED
      IX=1
      IY=1
      DIMENSION X(3750),Y(3750),XPLT(3750),YPLT(3750),BUF(5000)
      CALL PLOTS(BUF,20000,11)
      I=0
      XFACT=15.
      YFACT=10.
      IF(IX.EQ.2) GOTO 40
C   IX.NE.2
      IF(IY.GE.3) GOTO 50
C   PATTERN A CDI PLOT .
      XFACT=8.2
      YFACT=6.12
      GOTO 50
C   IX.EQ.2 THEN PLOT & ANGLE
40  IF(IY.GE.3) GOTO 41
C   CDI & ANGLE , PATTERN B
      XFACT=6.28
      YFACT=7.91
      GOTO 50
C   AMPLITUDE & ANGLE PLOT .
41  XFACT=8.2
      YFACT=5.0
50  CONTINUE
      XYRATO=(XFACT/15.)/(YFACT/10.)
      JDASH=0

```

```

4     J=1
5     CONTINUE
      I=I+1
      IF(I.GT.N) GO TO 20
      IF((X(I).LT.XMIN).OR.(X(I).GT.XMAX)) GO TO 20
      IF((Y(I).LT.YMIN).OR.(Y(I).GT.YMAX)) GO TO 20
      XPLT(J)=(X(I)-XMIN)*15./(XMAX-XMIN)
      YPLT(J)=(Y(I)-YMIN)*10./(YMAX-YMIN)
      J=J+1
      GO TO 5
20    CONTINUE
      IF(I.GT.N.AND.J.LE.2) GO TO 7
      IF(J.LE.2) GO TO 4
      NPTS=J-1
      XPLT(NPTS+1)=0.
      YPLT(NPTS+1)=0.
      XPLT(NPTS+2)=1.
      YPLT(NPTS+2)=1.
      KTYP=0
      IF(ITYPE.EQ.1) NPTS=-NPTS
      IF(ITYPE.EQ.2) KTYP=-NPBS
      IF(ITYPE.EQ.3) KTYP=NPBS
      IF(ITYPE.EQ.4) KTYP=NPBS
      IF(ITYPE.EQ.4) NPTS=-NPTS
      IF(ITYPE.EQ.5) NPTS=-NPTS
      IF(ITYPE.EQ.5) JDASH=ISYM
      IF(ITYPE.EQ.0) JDASH=ISYM
      CALL FDASH(JDASH,0.,0.,XYRATO)
      CALL FSymb(.23)
      CALL FLINE(XPLT,YPLT,NPTS,1,KTYP,ISYM)
      IF(I.GT.N) GO TO 7
      GO TO 4
7     CONTINUE
      CALL PLOT(0.,0.,-3)
      RETURN
      END

```

APPENDIX G. TESTS.

The bench testing was done at Clippinger Laboratories, Ohio University. Figure G-1 shows the setup to obtain 90 Hz and 150 Hz filter response data. Figure G-2 shows the setup for obtaining the change in CDI current readings due to the change in amplitude of the subharmonics. Figure G-3 shows the setup for total harmonics distortion measurements. Figure G-4 shows the circuit of the summing amplifier. Figures G-5 and G-6 show the general view of bench test area.

A. List of Equipment.

Test equipment used in this investigation:

IFR-401 NAV Signal Generator - Used to generate the standard localizer and glide slope signals.

HP 3581A Wave Analyzer - Used to measure the individual harmonic voltages and to obtain 90 Hz and 150 Hz filter responses when used in conjunction with a chart recorder.

Heath Chart Recorder - Used to obtain hard copies of 90 Hz and 150 Hz filter responses.

Wavetek 3000 Signal Generator - Used to generate the carrier frequency (108.1 MHz or 334.7 MHz)

Fluke 8120A Digital Multimeter - This meter used as a Cross-Pointer Deflection Indicator (CDI).

Seattle Tech. 100 Precision ILS Calibrator - Used to generate 90 Hz, 150 Hz or a 90/150 Hz composite audio signals. This unit used in conjunction with Wavetek 3000 Signal Generator.

HP 3312A Function Generator - Used to generate 30, 60, 180, 240, 270, 300 and 540 Hz sine wave signal and 90 Hz or 150 Hz triangular wave signal. This unit used in conjunction with Wavetek 3000 Signal Generator.

Fluke 1953A Frequency Counter - Used for low frequency measurements.

HP Power Supply - The DC power supply for Collins Nav Receiver. It was held at a constant 27.5 volts.

OU Power Supply - The ± 15 VDC power supply for summing amplifier.

B. Standard Test Conditions.

Environmental Conditions - The room temperature kept at $72^{\circ}\text{F} \pm 4^{\circ}$.

Warm up - The receivers were not subjected to any tests before at least 20 minutes warm-up. Signal generators were allowed 1 hour warm-up.

Spurious Responses - All output signals were monitored during each test.

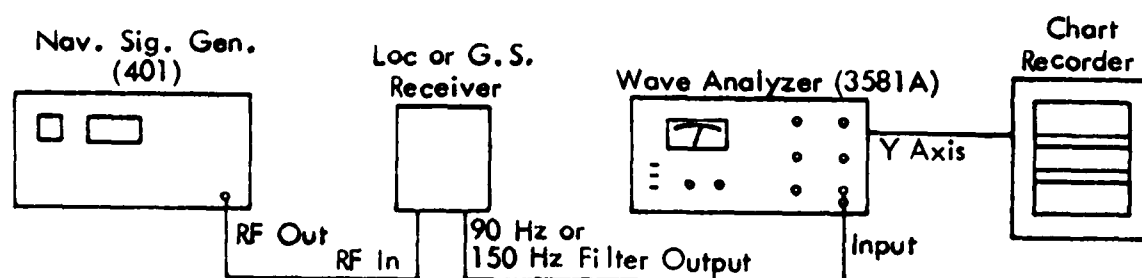


Figure G-1. Set Up to Obtain 90 Hz or 150 Hz Filter Response Data.

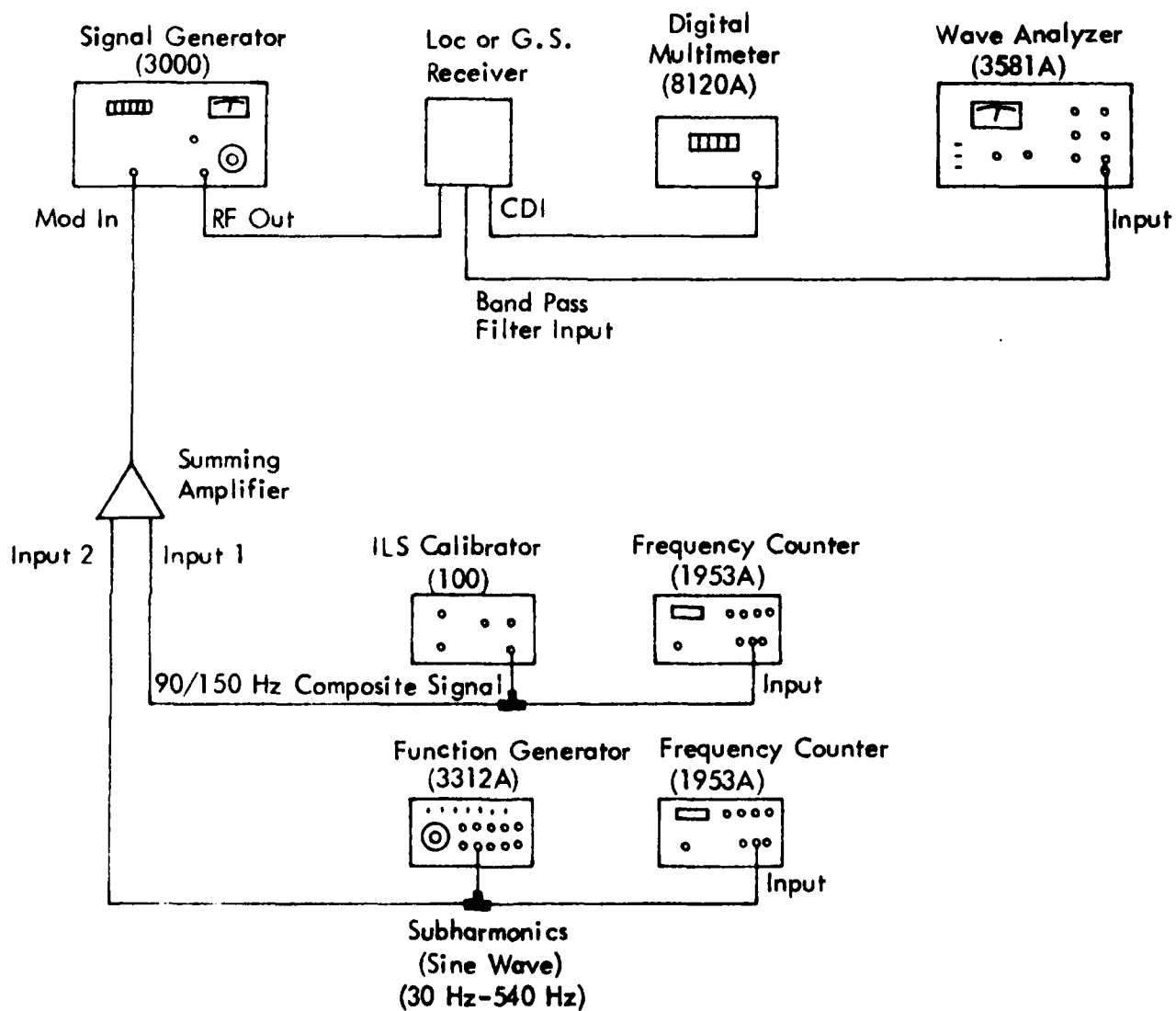


Figure G-2. Set Up for Obtaining the Change in CDI Current Readings Due To the Change in Amplitude of Subharmonics.

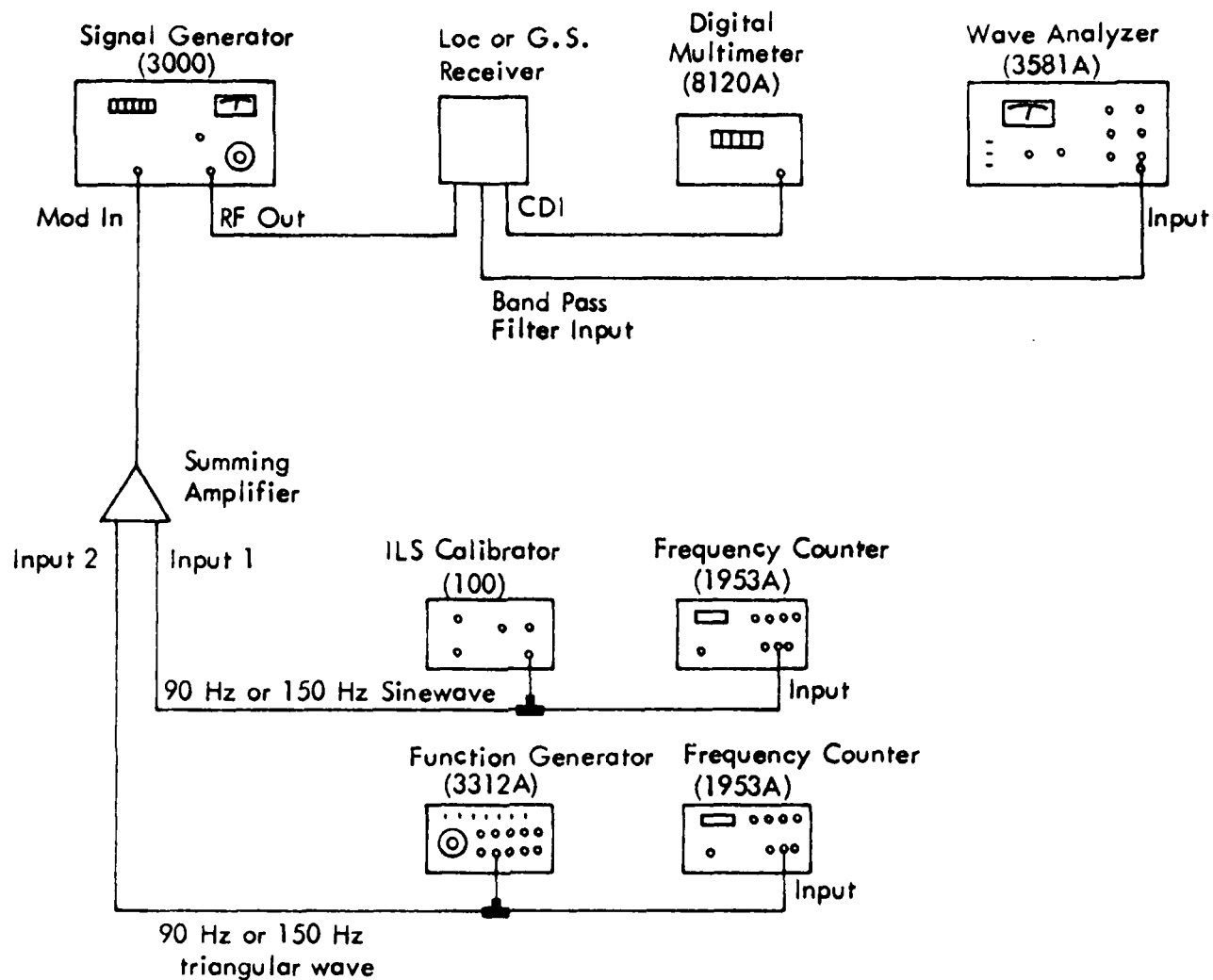
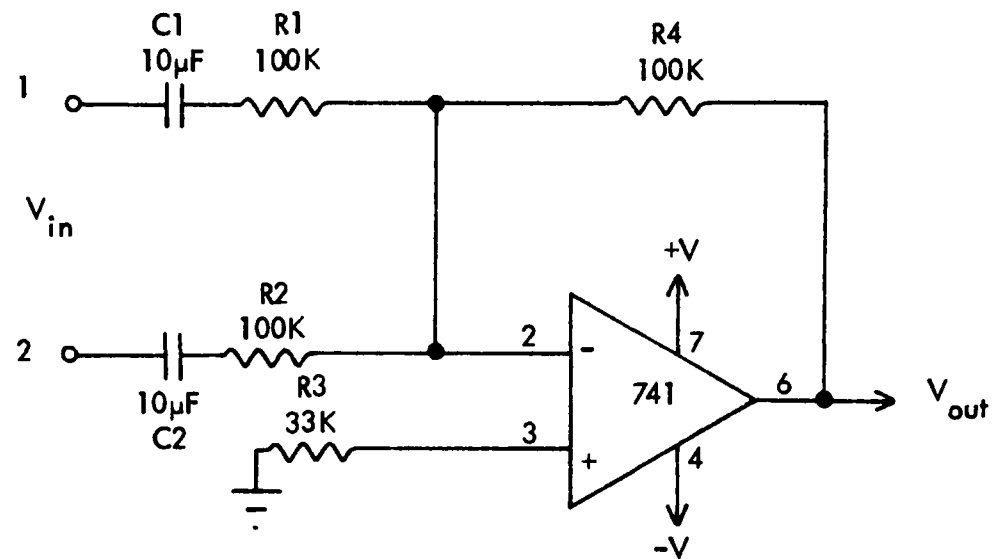


Figure G-3. Set Up for Total Harmonic Distortion Measurements.



$$V_{out} = -(V_{in1} + V_{in2})$$

$$V = \pm 15\text{VDC}$$

Note: V_{out} cannot exceed $\pm V$.

Figure G-4. Summing Amplifier.



Figure G-5. General View of Bench Test Area.

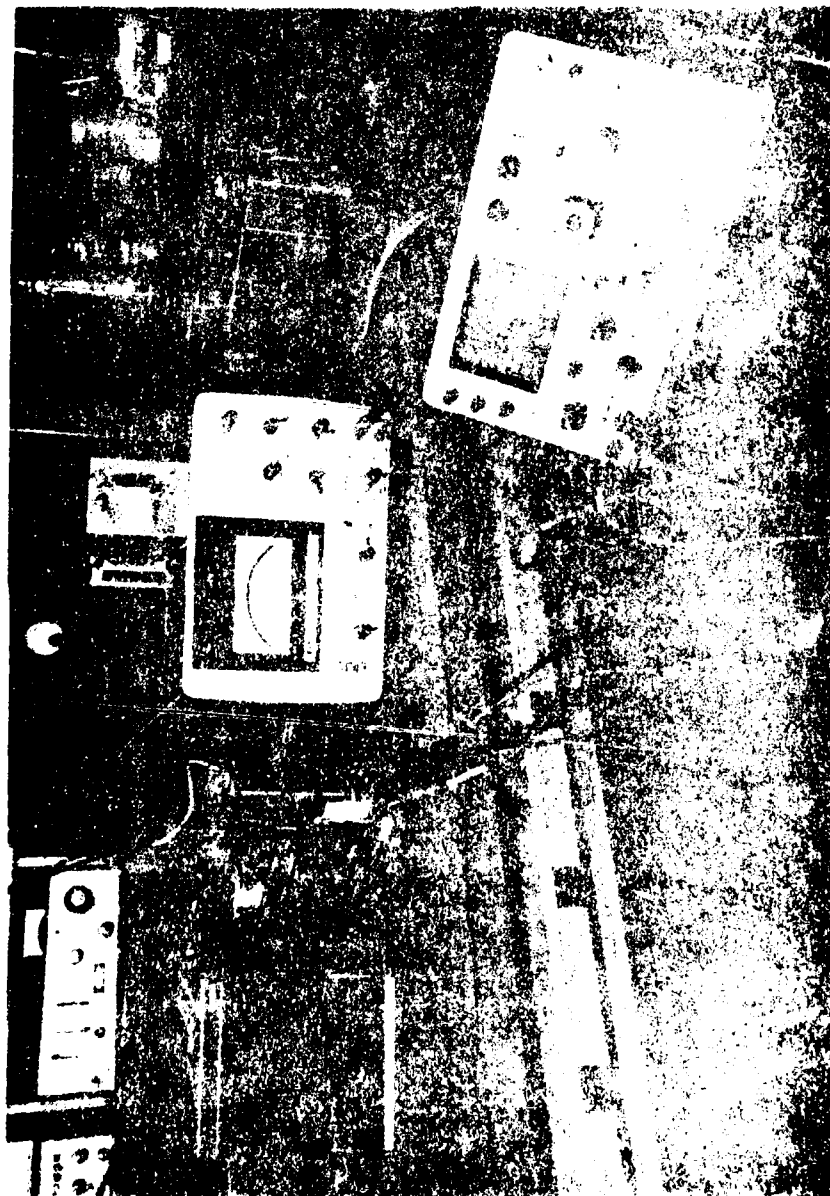


Figure G-6. General View of Bench Test Area.

APPENDIX H: EXPERIMENTAL RESULTS.

The following is a tabulated results section. The final results matrix was obtained from bench tests.

The Collins localizer/glide slope receiver, Narco localizer receiver, and Narco glide slope receiver were used to obtain the bench data. Tables H-1, H-2, H-3, and H-4 show the change in CDI current readings due to individual harmonics obtained from the Collins localizer receiver, Collins glide slope receiver, Narco glide slope receiver, and Narco localizer receiver, respectively. Tables H-5, H-6, H-7, and H-8 summarize the harmonic voltages obtained to compute the total harmonic distortion using Collins localizer receiver, Collins glide slope receiver, Narco glide slope receiver, and Narco localizer receiver, respectively.

Harmonic Frequency (Hz)	Harmonic Amplitude (Volts) at Bandpass Filter Input	CDI Current (μ A)
30	0.065	-0.8
60	"	-0.7
180	"	+3.6
240	"	+0.8
270	"	+1.0
300	"	+0.6
540	0.065	+0.2
30	0.13	-0.9
60	"	-2.5
180	"	+12.6
240	"	+2.1
270	"	+1.8
300	"	+1.7
540	0.13	+0.6
30	0.26	-4.6
60	"	-10.6
180	"	+52.6
240	"	+7.8
270	"	+6.2
300	"	+5.9
540	0.26	+1.0

Apply a standard localizer centering signal at 108.1 MHz, -47 dBmW (1000 μ V), 0 DDM. The indicator sensitivity shall be $0 \pm 3 \mu$ A. At receiver bandpass filter input, 90 Hz signal amplitude equals 0.13 V_{RMS} . At receiver bandpass filter input, 150 Hz signal amplitude equals 0.13 V_{RMS} .

Table H-1a. Collins Localizer Receiver, 0 DDM.

Harmonic Frequency (Hz)	Harmonic Amplitude (Volts) at Bandpass Filter Input	CDI Current (μ A)
30	0.065	-150.1
60	"	-150.1
180	"	-144.1
240	"	-148.9
270	"	-150.2
300	"	-149.3
540	0.065	-149.3
30	0.13	-150.2
60	"	-151.6
180	"	-123.6
240	"	-146.3
270	"	-149.4
300	"	-148.5
540	0.13	-149.1
30	0.26	-151.1
60	"	-156.6
180	"	-23.1
240	"	-151.6
270	"	-143.4
300	"	-143.7
540	0.26	-148.3

Apply a standard localizer signal at 108.1 MHz, -47 dBm (1000 μ V), 0.155 DDM (90>150). The indicator should read -150 μ A. At receiver bandpass filter input, 90 Hz signal amplitude equals 0.18 V_{RMS}. At receiver bandpass filter input, 150 Hz signal amplitude equals 0.08 V_{RMS}.

Table H-1b. Collins Localizer Receiver, 0.115 DDM (90 > 150).

Harmonic Frequency (Hz)	Harmonic Amplitude (Volts) at Bandpass Filter Input	CDI Current (μ A)
30	0.065	+150.9
60	"	+150.0
180	"	+152.4
240	"	+150.5
270	"	+150.4
300	"	+150.1
540	0.065	+150.2
30	0.13	+151.7
60	"	+148.2
180	"	+159.1
240	"	+150.8
270	"	+151.3
300	"	+150.8
540	0.13	+150.1
30	0.26	+152.2
60	"	+139.6
180	"	+196.3
240	"	+154.4
270	"	+153.3
300	"	+151.3
540	0.26	+150.1

Apply a standard localizer signal at 108.1 MHz, -47 dBW (1000 μ V), 0.155 DDM (150 \times 90). The indicator should read +150 μ A. At receiver bandpass filter input, 90 Hz signal amplitude equals 0.08 V_{RMS} . At receiver bandpass filter input, 150 Hz signal amplitude equals 0.18 V_{RMS} .

Table H-1c. Collins Localizer Receiver, 0.155 DDM (150 \times 90).

Harmonic Frequency (Hz)	Harmonic Amplitude (Volts) at Bandpass Filter Input	CDI Current (μ A)
30	0.1	-2.7
60	"	-2.1
180	"	+6.1
240	"	+1.1
270	"	+3.1
300	"	+1.0
540	0.1	+0.6
30	0.2	-6.1
60	"	-6.3
180	"	+25.5
240	"	+3.0
270	"	+6.4
300	"	+3.0
540	0.2	+1.7
30	0.4	-22
60	"	-32
180	"	+123
240	"	+12
270	"	+18.8
300	"	+30.4
540	0.4	+30.4

Apply a standard glide slope centering signal at 334.7 MHz, -50 dBmW (700 μ V), 0 DDM. The indicator sensitivity shall be $0 \pm 10.7 \mu$ A. At receiver bandpass filter input, 90 Hz signal amplitude equals 0.2 V_{RMS} . At receiver bandpass filter input, 150 Hz signal amplitude equals 0.2 V_{RMS} .

Table H-2a. Collins Glide Slope Receiver, 0 DDM.

Harmonic Frequency (Hz)	Harmonic Amplitude (Volts) at Bandpass Filter Input	CDI Current (μ A)
30	0.095	-151.3
60	"	-151.2
180	"	-144.8
240	"	-150.1
270	"	-153.7
300	"	-150.2
540	0.095	-149.5
30	0.19	-151.0
60	"	-152.3
180	"	-116.5
240	"	-146.1
270	"	-153.6
300	"	-143.4
540	0.19	-148.0
30	0.38	-151.4
60	"	-147.5
180	"	-29.6
240	"	-120.1
270	"	-135.0
300	"	-144.0
540	0.38	-133.6

Apply a standard glide slope signal at 334.7 MHz, -50 dBm (700 μ V), 0.175 DDM (90 \angle 150). The indicator should read -150 μ A. At receiver bandpass filter input, 90 Hz signal amplitude equals 0.235 V_{RMS} . At receiver bandpass filter input, 150 Hz signal amplitude equals 0.145 V_{RMS} .

Table H-2b. Collins Glide Slope Receiver, 0.175 DDM (90 \angle 150).

Harmonic Frequency (Hz)	Harmonic Amplitude (Volts) at Bandpass Filter Input	CDI Current (μ A)
30	0.095	+152.8
60	"	+150.1
180	"	+154.5
240	"	+150.1
270	"	+153.5
300	"	+149.6
540	0.095	+150.2
30	0.19	+153.1
60	"	+145.3
180	"	+173.1
240	"	+149.9
270	"	+154.5
300	"	+150.2
540	0.19	+148.2
30	0.38	+143.9
60	"	+103.2
180	"	+218.7
240	"	+142.0
270	"	+146.0
300	"	+158.2
540	0.38	+135.2

Apply a standard glide slope signal at 334.7 MHz, -50 dBmW (700 μ V), 0.175 DDM (150 \angle 90). The indicator should read +150 μ A. At receiver bandpass filter input, 90 Hz signal amplitude equals 0.145 V_{RMS} . At receiver bandpass filter input, 150 Hz signal amplitude equals 0.235 V_{RMS} .

Table H-2c. Collins Glide Slope Receiver, 0.175 DDM (150 \angle 90).

Harmonic Frequency (Hz)	Harmonic Amplitude (Volts) at Bandpass Filter Input	CDI Current (μ A)
30	0.062	- 6.5
60	"	- 6.1
180	"	+ 8.6
240	"	+ 5.8
270	"	+10.5
300	"	+ 8.1
540	0.062	+ 3.6
30	0.125	-15
60	"	-29
180	"	+27
240	"	+19
270	"	+24
300	"	+19.8
540	0.125	+ 8.8
30	0.25	-36
60	"	-80
180	"	+92
240	"	+76
270	"	+68
300	"	+60.6
540	0.25	+20.8

Apply a standard localizer centering signal at 334.7 MHz, -50 dBmW (700 μ V), 0 DDM. The indicator sensitivity shall be $0 \pm 10.7 \mu$ A. At receiver bandpass filter input, 90 Hz signal amplitude equals 0.25 V_{RMS} . At receiver bandpass filter input, 150 Hz signal amplitude equals 0.25 V_{RMS} .

Table H-3a. Narco Glide Slope Receiver, 0 DDM.

Harmonic Frequency (Hz)	Harmonic Amplitude (Volts) at Bandpass Filter Input	CDI Current (μ A)
30	0.065	-158.1
60	"	-155.6
180	"	-143.2
240	"	-145.2
270	"	-150.2
300	"	-147.4
540	0.065	-149.2
30	0.13	-160.4
60	"	-159.2
180	"	-112.5
240	"	-123.2
270	"	-131.7
300	"	-131.6
540	0.13	-135.3
30	0.26	-138.6
60	"	-162.7
180	"	-186.7
240	"	- 37.9
270	"	- 68.4
300	"	- 60.7
540	0.26	- 94.2

Apply a standard glide slope signal at 334.7 MHz, -50 dBmW (700 μ V), 0.175 DDM (90>150). The indicator should read -150 μ A. At receiver bandpass filter input, 90 Hz signal amplitude equals 0.3 V_{RMS} . At receiver bandpass filter input, 150 Hz signal amplitude equals 0.19 V_{RMS} .

Table H-3b. Narco Glide Slope Receiver, 0.175 DDM (90>150).

Harmonic Frequency (Hz)	Harmonic Amplitude (Volts) at Bandpass Filter Input	CDI Current (μ A)
30	0.065	+146.4
60	"	+141.9
180	"	+145.6
240	"	+146.2
270	"	+146.6
300	"	+147.5
540	0.065	+143.5
30	0.13	+146.6
60	"	+128.6
180	"	+149.7
240	"	+149.3
270	"	+146.4
300	"	+148.2
540	0.13	+141.9
30	0.26	+113.2
60	"	+ 60.2
180	"	+173.7
240	"	+163.8
270	"	+151.6
300	"	+151.7
540	0.26	+132.2

Apply a standard glide slope signal at 334.7 MHz, -50 dBmW (700 μ V), 0.175 DDM (150 \geq 90). The indicator should read +150 μ A. At receiver bandpass filter input, 90 Hz signal amplitude equals 0.19 V_{RMS} . At receiver bandpass filter input, 150 Hz signal amplitude equals 0.3 V_{RMS} .

Table H-3c. Narco Glide Slope Receiver, 0.175 DDM (150 \geq 90).

Harmonic Frequency (Hz)	Harmonic Amplitude (Volts) at Bandpass Filter Input	CDI Current (μ A)
30	0.06	+1.5
60	"	+2.9
180	"	+1.5
240	"	-1.6
270	"	-0.6
300	"	-2.9
540	0.06	-1.1
30	0.12	+2.3
60	"	+6.6
180	"	+6.6
240	"	+9.1
270	"	+1.4
300	"	-14.2
540	0.12	+2.8
30	0.24	-10.6
60	"	+4.7
180	"	+52.7
240	"	+30.1
270	"	+9.9
300	"	-16.8
540	0.24	+8.6

Apply a standard glide slope centering signal at 108.1 MHz, -47 dBmW (1000 μ V), 0 DDM. The indicator sensitivity shall be $0 \pm 3 \mu$ A. At receiver bandpass filter input, 90 Hz signal amplitude equals 0.12 V_{RMS} . At receiver bandpass filter input, 150 Hz signal amplitude equals 0.12 V_{RMS} .

Table H-4. Narco Localizer Receiver, 0 DDM.

Harmonic Frequency (Hz)	Harmonic Amplitude (mV) at Bandpass Filter Input	CDI Current (μA)
30	0.08	-3
60	0.4	-3
180	0.42	-3
240	0.4	-3
270	13.9	-3
300	0.2	-3
450	5.4	-3
540	0.11	-3

Apply a signal at 108.1 MHz, -47 dBm (1000 μV), modulated with 90 Hz triangular wave and 150 Hz sine wave signals. The indicator should read 0±3 μA. At receiver bandpass filter input, 90 Hz signal amplitude equals 132 mV. At receiver bandpass filter input, 150 Hz signal amplitude equals 130 mV.

$$\text{Total Harmonic Distortion (THD)} = \frac{\sqrt{(\text{harmonics})^2}}{\text{fundamental}} \times 100$$

$$\text{THD} = \frac{\sqrt{222.92}}{132} \times 100$$

$$\text{THD} = 11.31\%$$

Table H-5a. Collins Localizer Receiver, 90 Hz Triangular Wave.

Harmonic Frequency (Hz)	Harmonic Amplitude (mV) at Bandpass Filter Input	CDI Current (μA)
30	0.1	-3
60	0.38	-3
180	0.15	-3
240	0.36	-3
270	1.65	-3
300	0.29	-3
450	13.6	-3
540	0.06	-3

Apply a signal at 108.1 MHz, -47 dBm (1000 μV), modulated with 90 Hz sine wave and 150 Hz triangular wave signals. The indicator should read 0±3 μA. At bandpass filter input, 90 Hz signal amplitude equals 130 mV. At bandpass filter input, 150 Hz signal amplitude equals 128 mV.

$$\text{Total Harmonic Distortion (THD)} = \frac{\sqrt{(\text{harmonics})^2}}{\text{fundamental}} \times 100$$

$$\text{THD} = \frac{\sqrt{138.0737}}{128} \times 100$$

$$\text{THD} = 10.71\%$$

Table H-5b. Collins Localizer Receiver, 150 Hz Triangular Wave.

Harmonic Frequency (Hz)	Harmonic Amplitude (mV) at Bandpass Filter Input	CDI Current (μA)
30	0.1	-10.7
60	0.3	-10.7
180	0.32	-10.7
240	0.34	-10.7
270	13.1	-10.7
300	0.15	-10.7
450	4.4	-10.7
540	0.1	-10.7

Apply a signal at 334.7 MHz, -50 dBmW (700 μV), modulated with 90 Hz triangular wave and 150 Hz sine wave signals. The indicator should read 0 ± 10.7 μA. At receiver bandpass filter input, 90 Hz signal amplitude equals 125 mV. At receiver bandpass filter input, 150 Hz signal amplitude equals 120 mV.

$$\text{Total Harmonic Distortion (THD)} = \frac{\sqrt{(\text{harmonics})^2}}{\text{fundamental}} \times 100$$

$$\text{THD} = \frac{\sqrt{191.32}}{125} \times 100$$

$$\text{THD} = 11.08\%$$

Table H-6a. Collins Glide Slope Receiver, 90 Hz Triangular Wave.

AD-A140 797

ENGINEERING AND TECHNICAL SERVICES TO IMPROVE
RELIABILITY AND MAINTAINABILITY (U) OHIO UNIV ATHENS
AVIONICS ENGINEERING CENTER J D LONGWORTH ET AL.

4/4

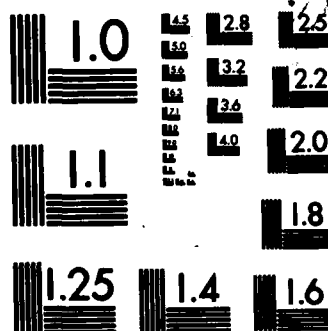
UNCLASSIFIED

JAN 83 OU/REC/EER-62-1 DOT/FAR/PM-84/7

F/G 17/7

NL





Harmonic Frequency (Hz)	Harmonic Amplitude (mV) at Bandpass Filter Input	CDI Current (μA)
30	0.1	-10.7
60	0.4	-10.7
180	0.2	-10.7
240	0.3	-10.7
270	1.4	-10.7
300	0.3	-10.7
450	12.0	-10.7
540	0.05	-10.7

Apply a signal at 334.7 MHz, -50 dBmW (700 μV), modulated with 90 Hz sine wave and 150 Hz triangular wave signals. The indicator should read 0±10.7 μA. At bandpass filter input, 90 Hz signal amplitude equals 120 mV. At bandpass filter input, 150 Hz signal amplitude equals 115 mV.

$$\text{Total Harmonic Distortion (THD)} = \frac{\sqrt{(\text{harmonics})^2}}{\text{fundamental}} \times 100$$

$$\text{THD} = \frac{\sqrt{146.25}}{115} \times 100$$

$$\text{THD} = 10.51\%$$

Table H-6b. Collins Glide Slope Receiver, 150 Hz Triangular Wave.

Harmonic Frequency (Hz)	Harmonic Amplitude (mV) at Bandpass Filter Input	CDI Current (μA)
30	0.5	-10.7
60	4.2	-10.7
180	2.5	-10.7
240	4.0	-10.7
270	13.5	-10.7
300	1.9	-10.7
450	5.0	-10.7
540	0.5	-10.7

Apply a signal at 334.7 MHz, -50 dBmV (700 μV), modulated with 90 Hz triangular wave and 150 Hz sine wave signals. The indicator should read 0 ± 10.7 μA. At bandpass filter input, 90 Hz signal amplitude equals 135 mV. At bandpass filter input, 150 Hz signal amplitude equals 130 mV.

$$\text{Total Harmonic Distortion (THD)} = \frac{\sqrt{(\text{harmonics})^2}}{\text{fundamental}} \times 100$$

$$\text{THD} = \frac{\sqrt{251.25}}{135} \times 100$$

$$\text{THD} = 11.74\%$$

Table H-7a. Narco Glide Slope Receiver, 90 Hz Triangular Wave.

Harmonic Frequency (Hz)	Harmonic Amplitude (mV) at Bandpass Filter Input	CDI Current (μA)
30	0.4	-10.7
60	4.0	-10.7
180	2.1	-10.7
240	4.2	-10.7
270	1.5	-10.7
300	2.2	-10.7
450	12.5	-10.7
540	0.1	-10.7

Apply a signal at 334.7 MHz, -50 dBmV (700 μV), modulated with 90 Hz sine wave and 150 Hz triangular wave signals. The indicator should read 0±10.7 μA. At bandpass filter input, 90 Hz signal amplitude equals 128 mV. At bandpass filter input, 150 Hz signal amplitude equals 125 mV.

$$\text{Total Harmonic Distortion (THD)} = \frac{\sqrt{(\text{harmonics})^2}}{\text{fundamental}} \times 100$$

$$\text{THD} = \frac{\sqrt{201.56}}{125} \times 100$$

$$\text{THD} = 11.35\%$$

Table H-7b. Narco Glide Slope Receiver, 150 Hz Triangular Wave.

Harmonic Frequency (Hz)	Harmonic Amplitude (mV) at Bandpass Filter Input	CDI Current (μA)
30	0.4	-3
60	0.7	-3
180	0.5	-3
240	0.8	-3
270	12.8	-3
300	0.35	-3
450	5.0	-3
540	0.2	-3

Apply a signal at 108.1 MHz, -47 dBm (1000 μV), modulated with 90 Hz triangular wave and 150 Hz sine wave signals. The indicator should read 0±3 μA. At receiver bandpass filter input, 90 Hz signal amplitude equals 118 mV. At receiver bandpass filter input, 150 Hz signal amplitude equals 128 mV.

$$\text{Total Harmonic Distortion (THD)} = \frac{\sqrt{(\text{harmonics})^2}}{\text{fundamental}} \times 100$$

$$\text{THD} = \frac{\sqrt{190.54}}{118} \times 100$$

$$\text{THD} = 11.70\%$$

Table H-8a. Narco Localizer Receiver, 90 Hz Triangular Wave.

Harmonic Frequency (Hz)	Harmonic Amplitude (mV) at Bandpass Filter Input	CDI Current (μA)
30	0.5	-3
60	0.6	-3
180	0.4	-3
240	0.82	-3
270	1.7	-3
300	4.44	-3
450	13.0	-3
540	0.25	-3

Apply a signal at 108.1 MHz, -47 dBmW (1000 μV), modulated with 90 Hz sine wave and 150 Hz triangular wave signals. The indicator should read 0±3 μA. At bandpass filter input, 90 Hz signal amplitude equals 120 mV. At bandpass filter input, 150 Hz signal amplitude equals 126 mV.

$$\text{Total Harmonic Distortion (THD)} = \frac{\sqrt{(\text{harmonics})^2}}{\text{fundamental}} \times 100$$

$$\text{THD} = \frac{\sqrt{193.09}}{126} \times 100$$

$$\text{THD} = 11.03\%$$

Table H-8b. Narco Localizer Receiver, 150 Hz Triangular Wave.

